Ca^{2+} Controls the Epithelial Cell Quiescence-Proliferation Decision through Regulating IGF Signaling

by

Yi Xin

A dissertation submitted in partial fulfillment
of the requirements for the degree of
Doctor of Philosophy
(Molecular, Cellular, and Developmental Biology)
in the University of Michigan
2020

Doctoral Committee:

Professor Cunming Duan, Chair
Professor John Kuwada
Professor Yatrick Shah
Professor Haoxing Xu

Yi Xin

xyi@umich.edu

ORCID iD: 0000-0002-4443-1342

Acknowledgements

This work would not have been possible without the support from a lot of people. First and foremost, I would like to thank my mentor Dr. Cunming Duan for his unwavering guidance and support over the past six years. Cunming has provided me with every bit of advice, assistance, encouragement, and expertise that I needed during my Ph.D. training. His enthusiasm and persistence have constantly inspired and motivated me and will continue to benefit me as I move forward in my career.

I would also like to extend my deepest gratitude to my dissertation committee members: Dr. Haoxing Xu, Dr. John Kuwada, Dr. Yatrick Shah, and Dr. Orie Shafer for their continuous encouragement and valuable suggestions on pushing forward my research project.

I am also grateful to all the Duan lab members who have worked with me. Special thanks to Dr. Chengdong Liu, who collaborated with me in the Igfbp5a project. He is such a thoughtful colleague and friend. Working with him is really a precious and enjoyable experience for me.

Last but not least, I want to thank my family for their tremendous love and support. I owe my sincerest thanks to my mom, who is extremely gentle, caring, and supportive in a non-judgmental way. And I want to thank my husband, Dr. Qifan Yang. His passion and dedication to science have truly been inspiring for me over the past ten years. And his companionship and encouragement have made me happier and more courageous than I ever thought I could be.

Table of Contents

List of Tables

List of Figures

Abstract

Epithelial tissues renew rapidly and continuously by reactivating a pool of quiescent cells. How the quiescent cells are established, maintained, and reactivated is poorly defined. Recent studies suggest that the insulin-like growth factor (IGF)-PI3 kinase-AKT-mTOR signaling pathway plays a key role in regulating epithelial cell quiescence-proliferation decision but the underlying mechanism remains unclear. In my thesis work, I use a zebrafish model to investigate the IGF action in a group of Ca^{2+}-transporting epithelial cells, known as Na^{+}-K^{+}-ATPase-rich (NaR) cells. When zebrafish are kept in normal and physiological [Ca^{2+}] embryo rearing media, NaR cells are quiescent, characterized by a very slow division rate and undetectable Akt and Tor activity. When subjected to low [Ca^{2+}] stress, the NaR cells exit the quiescent state and proliferate due to elevated IGF1 receptor-mediated Akt and Tor activity. To understand how the IGF signaling is activated exclusively in NaR cells under low [Ca^{2+}] stress, I first investigated the role of Igfbp5a, a secreted protein belonging to the IGF binding protein (IGFBP) family. Zebrafish *igfbp5a* is specifically expressed in NaR cells and genetic deletion of *igfbp5a* blunted the low Ca^{2+} stress-induce IGF-Akt-Tor activity and NaR cell reactivation. Similarly, knockdown of IGFBP5 in human colon carcinoma cells resulted in reduced IGF-stimulated cell proliferation. Re-expression of zebrafish or human Igfbp5a/IGFBP5 in NaR cells restores NaR cell proliferation. Mechanistically, Igfbp5a acts by binding to IGFs using its ligand-binding domain and promoting IGF signaling in NaR cells. These results reveal a conserved mechanism by which a locally expressed Igfbp activates IGF signaling and promoting cell

quiescence-proliferation transition under Ca^{2+}-deficient states. NaR cells are functionally equivalent to human intestinal epithelial cells, and they contain all major molecular components of the transcellular Ca^{2+} transport machinery, including the epithelial calcium channel Trpv6. Ca^{2+} is a central intracellular second messenger controlling many aspects of cell biology. I next investigated the role of Trpv6 and intracellular [Ca^{2+}]. I discovered that NaR cells are maintained in the quiescent state by Trpv6-mediated constitutive Ca^{2+} influx. Genetic deletion and pharmacological inhibition of Trpv6 promote NaR cell quiescence-proliferation transition. In zebrafish NaR cells and human colon carcinoma cells, Trpv6/TRPV6 elevated intracellular Ca^{2+} levels and activated PP2A, a group of conserved protein phosphatases, which down-regulates IGF signaling and promotes the quiescent state. Finally, chemical biology screens and genetic experiments identified CaMKK as a link between low Ca^{2+} stress and IGF signaling activation in NaR cells. Depletion of the ER Ca^{2+} store abolished NaR cell reactivation and IGF signaling. These results suggest that ER Ca^{2+} release in response to the low [Ca^{2+}] stress activates CaMKK, which in turn increases IGF signaling and NaR cell reactivation. Taken together, the results of my thesis research provide new insights into the epithelial cell proliferation-quiescence regulation and have deepened our understanding of cellular quiescence regulation. These new findings may also contribute to the future development of strategies in improving wound healing and tissue regeneration.

Chapter 1 Introduction

1.1 Background

The vast majority of cells in multicellular organisms are non-dividing cells, such as postmitotic neurons and skeletal muscle cells. Some of these cells are senescent, or terminally differentiated cells that can no longer re-enter the cell cycle to proliferate. In contrast, a subset of non-dividing cells are ‘re-activatable’. They can re-enter the active cell cycle in response to physiological growth signals, thereby these cells are called quiescent cells (Cheung and Rando, 2013). Cell quiescence protects long-lived cells by delaying cell aging through reducing DNA replication, metabolic activity, gene transcription, and mRNA translation. As all of these activities are accompanied by molecular damage. Maintaining a pool of quiescent cells that can be rapidly reactivated to expand cell population upon stimulation is critical for tissue homeostasis and repair (Cheung and Rando, 2013). The homeostatic balance between quiescence, proliferation, and differentiation is tightly controlled by integrating intrinsic and extrinsic mechanisms. Dysregulation of quiescence is linked to a wide range of hypo- and hyper-proliferative diseases like osteoporosis, cancer, autoimmune diseases and fibrosis (Fiore et al., 2018; Kitaori et al., 2009).

Historically, quiescence had been simply regarded as a passive and dormant cellular state lacking proliferative activities. Recent studies have revealed that cellular quiescence is actively maintained in the cell and it corresponds to a collection of heterogeneous states (Sun and Buttitta, 2017; Yao, 2014). Cell cycle inhibitors such as p21 and p57 (Kippin et al., 2005; Matsumoto et al., 2011), as well as, tumor suppressor genes such as Retinoblastoma (Rb) and

p53 have been identified as important regulators for quiescence maintenance (Flamini et al., 2018; Kim et al., 2017; Liu et al., 2009).

Recent studies in genetically tractable organisms have suggested that the evolutionarily ancient insulin/insulin-like growth factor (IGF)-PI3 kinase-AKT-TOR signaling pathway plays a key role in regulating cellular quiescence (Figure 1.1). Quiescent cells often exhibit reduced PI3 kinase and TOR activity (Valcourt et al., 2012). Re-activation of the IGF/PI3K/AKT/TOR signaling cascade is an evolutionally conserved mechanism that mediates quiescence exit in in various cell types across a wide range of species (Figure 1.1). Activation of the imprinted IGF2 gene also results in reactivation of HSCs from quiescence (Venkatraman et al., 2013b). Mouse genetic studies revealed that IGF2 plays a key role in reactivation adult neural stem cell and intestinal stem cells (Ferron et al., 2015; Venkatraman et al., 2013a; Ziegler et al., 2019; Ziegler et al., 2015). Genetic studies in the mouse model showed that activation of mTOR signaling by deletion of the Tsc gene in adult hematopoietic stem cells (HSCs) promotes these cells to exit quiescence and begin to proliferate (Chen et al., 2008). Conversely, inhibition of mTOR acivity by rapamycin has been shown to preserve the long-term self-renewal and hematopoietic capacity of HSCs (Chen et al., 2009). This mechanism is conserved in *Drosophila* as the long-term self-renewal capacitity of hematopoietic progenitors is also regulated by insulin-PI3K-TOR signaling (Shim et al., 2012). *Drosophila* neural stem cells are reactivated in response to dietary amino acids and this has been attributed to insulin peptide produced by neighboring glia cells (Britton and Edgar, 1998; Chell and Brand, 2010; Huang and Wang, 2018; Sousa-Nunes et al., 2011).

The regulatory role of the IGF/PI3K/AKT/TOR signal pathway in quiescence exit is not limited to adult stem cells (Chell and Brand, 2010; Gil-Ranedo et al., 2019; Hemmati et al., 2019; Sousa-Nunes et al., 2011). Naive T cells, for example, circulate in the body as non-

dividing and quiescent cells with characteristically low TOR activity. When presented with an antigen, TORC1 signaling is increased and these cells exit from the quiescent state and rapidly divide (Yang et al., 2013).

Recent studies from our lab suggested that the IGF/PI3K/AKT/TOR signaling is also crucial in regulating the proliferation-quiescence decision in a population of epithelial cells in zebrafish larval epidermis (Dai et al., 2014a; Liu et al., 2017a). These mitochondria-rich cells known as ionocytes or NaR cells take up Ca^{2+} from the surrounding aquatic habitat to maintain body Ca^{2+} homeostasis (Hwang, 2009a; Yan and Hwang, 2019a). When zebrafish are kept in media containing normal and physiological concentration of Ca^{2+}, NaR cells are most quiescent: characterized by a very slow division rate and undetectable Akt and Tor activity. When subjected to low [Ca^{2+}] stress, the NaR cells exit the quiescent state and rapidly proliferate due to elevated Akt and Tor activity (Dai et al., 2014b; Liu et al., 2017a).

The similarities among mammalian and fly adult stem cells, T cells, and fish ionocytes imply evolutionarily conserved and general mechanisms at work (Figure 1.1). However, how activity of this pathway is regulated by environmental or microenvironmental stimuli is poorly understood. A recent study in *Drosophila* intestinal stem cells indicates cytosolic Ca^{2+} can be a signal integration node in the stem cell proliferation-quiescence decision. Another recent study discovered that simply growing mouse HSCs in low Ca^{2+} culture media helps to preserve HSCs' stemness (Luchsinger et al., 2019). Ca^{2+} is also proposed as a novel guardian for mouse embryonic stem cells (mESCs) pluripotency (MacDougall et al., 2019). Reactivation of mesenchymal stem cell can be achieved through manipulation of extracellular Ca^{2+} in mice (Lee et al., 2018). Although a possible link between Ca^{2+} signaling and PI3 kinase-AKT-TOR activity (Almasi et al., 2019; Chen et al., 2010; Danciu et al., 2003; Divolis et al., 2016; Lee et al., 2017;

Vassiliadis et al., 2011; Zhang et al., 2017) has been postulated, the underlying molecular mechanisms are poorly understood.

In this thesis, I use zebrafish Ca^{2+}-transporting epithelial cells (NaR cells) as an experimental model to study how IGF/PI3K/AKT/TOR signaling is regulated by Ca^{2+} signaling. In the following sections, I will introduce more details about IGF signaling pathway, epithelial Ca^{2+} uptake, intracellular Ca^{2+} signaling, and the zebrafish NaR cell biology.

1.2 IGF/PI3K/AKT/TOR signaling cascade

1.2.1 IGF ligands and receptors

The IGF signaling axis plays fundamental roles in regulating growth, development, metabolism, and aging. The IGF system consists of two types of ligands, IGF1 and IGF2 (Laviola et al., 2007). IGF1 and IGF2 belong to the insulin family of peptide hormones that share primary and three-dimensional structures. Mature IGF1 contains 70 amino acids and IGF2 contains 67 amino acids (Denley et al., 2005). IGF ligands and insulin regulate physiology at both the whole organism level and the cellular level (Pollak, 2008a). At the cellular level, IGF signaling regulates cell proliferation, differentiation, survival, and migration (Hakuno and Takahashi, 2018).

The action of IGF1 and IGF2 is mediated by several types of receptors. The IGF1 receptor (IGF1R) binds to IGF1 with the highest affinity but also binds to IGF2 and insulin with approximately 6- and 100-fold lower affinity, respectively. IGF1R belongs to the tyrosine receptor kinase (RTK) family and functions as tetramers with two α subunits and two β subunits covalently linked. IGF1R gene encodes a single chain amino acid precursor which later gets glycosylated, dimerized and cleaved to generate α and β subunits (Ullrich et al., 1986). The α subunit contains ligand binding site while the β subunit contains the transmembrane domain and

intracellular tyrosine kinase domain (Steele-Perkins et al., 1988). The IGF1R is structurally related to insulin receptor (IR). IR exists in two isoforms (IR-A and IR-B) due to alternative splicing. While IR-B preferentially binds to insulin, IR-A binds to both insulin and IGF2 (Frasca et al., 1999). Binding of IGF ligands to IGF1R or IR-A results in activation of the receptor and downstream signaling. The IR exhibits a high degree of homology with the IGF1R, especially in their tyrosine kinase domains and can mediates similar intracellular signaling pathways. The IR and IGF1R can also form heterodimers (Pandini et al., 2002). The IGF2 receptor (IGF2R), which is structurally distinct, preferentially binds to IGF2 (Hakuno and Takahashi, 2018). The IGF2R lacks tyrosine kinase activity and has been proposed to target IGF2 to lysosome for degradation (O'Gorman et al., 2002).

The conventional view of insulin signaling and IGF signaling is that insulin signaling mediates mainly a metabolic response, whereas IGF signaling mediates growth promoting effects (Siddle et al., 2001). This is supported by the results from the IR and IGF1R knock-out mice. Mice lacking the IGF1R display pronounced growth retardation (Baker et al., 1993), whereas the IR knockout mice had only slight growth retardation. The IR knockout mice die during the first week of life from severe hyperglycemia and diabetic ketoacidosis (Accili et al., 1996; Joshi et al., 1996). Therefore, the ability of the two receptors to compensate for each other is limited and they are not interchangeable. In addition, phenotypes of the insulin knock-out mice and IGF1 knock-out mice are similar to those of IR knockout and IGF1R knockout, respectively (Duvillie et al., 1997; Powell-Braxton et al., 1993).

1.2.2. Signal transduction downstream of the IGF1R.

Upon ligand binding, the intracellular tyrosine kinase domain of IGF1R auto-phosphorylates specific tyrosine residues, which creates docking sites for adaptor proteins such

as insulin receptor substrates (IRSs) and Src homology collagen (Shc). They are subsequently activated by IGF1R through phosphorylation and then will recruit other substrates, leading to activation of different signaling cascades, including the Ras/Raf/MEK/extracellular signal-regulated kinases (ERK) pathway and the PI3K/AKT/TOR pathway, that stimulate cell proliferation and survival (Le Roith, 2003).

Growth factor receptor-bound 2 (GRB2) consists of a Src homology 2 (SH2) domain that binds to phosphorylated tyrosine in IGF1R substrate proteins (IRS1, IRS2, and Shc). The interaction between GRB2 and IGF1R substrates leads to the activation of GRB2-associated Sone of Sevenless (SOS) guanine nucleotide exchange activity, resulting in the activation of Ras small GTPase. Activated Ras interacts with and activates Raf, which in turn phosphorylates and activates MEK, then activates ERK. Activated ERK is shown to be required for the IGF-induced DNA synthesis and cell survival in various cell types (McCubrey et al., 2007).

The other major intracellular signaling pathway downstream of IGF1R activation is the PI3K/AKT/TOR pathway. Class I phosphoinositide 3-kinases (PI3Ks) comprise one catalytic subunits (p110) and a regulatory subunit of variable sizes (Jean and Kiger, 2014; Thorpe et al., 2015). RTKs primarily activate one subset within this group, Class 1A PI3K, which are comprised of a heterodimer of one p110α, β, or γ catalytic subunit and one p85α (or its splice variants p50α and p55α), p85β or other regulatory subunits. Class 1B PI3Ks consist of the p110γ catalytic subunit and the p101 and p87 regulatory subunits and they are mainly activated by G-protein coupled receptor (GPCR) signaling instead (Vadas et al., 2013). For Class IA PI3Ks, the interaction of regulatory and catalytic subunits is constitutive in the absence of signals and suppresses the activity of catalytic subunits (Miled et al., 2007; Vadas et al., 2011). Binding of

the regulatory subunit to specific motifs harboring phosphorylated tyrosine residues via its SH2 domains relieves the inhibition of p110 subunits.

Activated PI3K leads to increased level of phosphatidylinositol 3,4,5-trisphosphate (PI(3,4,5)P3) and PI(3,4)P2 in the membrane, which recruits the critical downstream kinase AKT to the plasma membrane through the binding of its pleckstrin homology (PH) domain to PIP3. AKT is a serine/threonine-specific protein kinase playing a fundamental role in numerous cellular processes (Manning and Toker, 2017). AKT is activated through phosphorylation at its Thr308 and Ser473 residues by phosphoinositide dependent protein kinase 1 (PDK1) and TOR complex 2 (TORC2), respectively (Moore et al., 2011). Normally, phosphorylation of Ser473 promotes phosphorylation of Thr308, stabilizing the activated form of AKT. However, AKT lacking Ser 473 phosphorylation can still be active, but with greatly lowered capacity (Alessi et al., 1996). A third, constitutively phosphorylated site at Thr450 in the turn motif of AKT is essential for its folding and stability (Facchinetti et al., 2008). Fully-activated AKT can be observed within seconds to minutes after growth factor stimulation. The down-regulation of AKT phosphorylation is achieved through phosphatase and tensin homolog (PTEN), which dephosphorylates PIP3 to PIP2, limiting AKT binding to the membrane, therefore decreasing its activity. Additionally, protein phosphatase 2A (PP2A) and the PH domain leucine-rich repeat protein phosphatases (PHLPP1 and PHLPP2) can dephosphorylate AKT at Thr308 and Ser473 sites, respectively (Andjelkovic et al., 1996; Gao et al., 2005).

A recent study suggested that the PH domain within the SIN1 component of TORC2 binds to PIP3, relieving the autoinhibition of TOR kinase activity (Liu et al., 2015). PIP3 binding therefore has dual functions of re-localizing TORC2 to membranes (where AKT is also recruited) and relieving conformational constraints on the TOR kinase, allowing AKT

phosphorylation. Another study using intracellular compartment-specific reporters, however, concluded that PI3K activation is dispensable for TORC2 activity (Ebner et al., 2017b).

The conventional model for AKT signaling suggests that activated AKT dissociates from the membrane and freely diffuses through the cytosol in a “locked” active state, phosphorylating substrates in other subcellular compartments. This model has been challenged by recent publications which have demonstrated active AKT is primarily associated with cellular membranes (Ebner et al., 2017a). Binding of AKT to PIP3 results in a conformational change in AKT that relieves the steric block against substrate binding. This is followed by phosphorylation of its hydrophobic motif, resulting in high-affinity substrate binding and activation (Lucic et al., 2018). Although earlier studies suggested that PIP3 is exclusively localized to the plasma membrane, more recent reports have provided evidence for endomembrane pools of PIP3 and PI(3,4)P2 that directly contribute to AKT activation (Jethwa et al., 2015; Liu et al., 2018b; Siess and Leonard, 2019). Activated AKT can phosphorylate up to 200 substrates. Restriction of AKT activity to subcellular membrane compartments helps define the specificity of AKT signaling by targeting the kinase to a particular set of substrates. Knockdown of the endosomal protein Appl1 in zebrafish resulted in decreased phosphorylation of the Akt substrate glycogen synthase kinase (Gsk) 3β, but not tuberous sclerosis complex 2 (Tsc2) (Schenck et al., 2008), demonstrating that Akt localization to early endosomes restricts Akt substrate specificity to Gsk3β. Phosphorylation of another AKT substrate TSC2 appears to be restricted to lysosomes (Demetriades et al., 2014; Menon et al., 2014), although whether lysosomal localization of AKT is sufficient for TSC2 phosphorylation is currently unknown.

AKT phosphorylation of TSC2 releases TSC’s inhibition of the Ras homolog enriched in brain (RHEB). GTP-binding RHEB directly activates the mechanistic target of rapamycin

Complex 1 (mTORC1 or TORC1). TORC1 has three core components: TOR kinase, the regulatory-associated protein of TOR (Raptor), and mammalian lethal with SEC13 protein8 (mLST8) (Kim et al., 2002). Additionally, AKT can phosphorylate PRAS40, a non-core component of TOC1. PRAS40 functions as a negative regulator of TORC1 and its phosphorylation mediated by AKT results in its disassociation from TORC1 and relieve its inhibition (Sancak et al., 2007; Vander Haar et al., 2007). TORC1 is a highly conserved regulator of cell growth and is one of the most highly integrated signaling nodes present in all cells (Beauchamp and Platanias, 2013; Dibble and Manning, 2013; Laplante and Sabatini, 2012). It plays a central role in regulating the production of proteins, lipids, and nucleotides for cell division while also suppressing catabolic pathways such as autophagy and therefore controls the balance between anabolism and catabolism in response to environmental conditions (Howell et al., 2013; Saxton and Sabatini, 2017).

1.2.3 IGFBP5

The bioavailability and biological activity of IGFs also is further regulated by a family of secreted IGF binding proteins (IGFBPs) of which there are six distinct types in most vertebrates (Allard and Duan 2018). These IGFBPs share significant sequence homology and they are capable of binding IGFs with equal or greater affinity than the IGF1R. They regulate IGF signaling both globally and locally. Because IGFBPs do not bind to insulin, these proteins can prevent potential cross-binding of IGFs to the IR (Clemmons, 1993).

The precursor forms of all six IGFBPs contain a signal peptide ranging from 20 to 39 amino acids. The mature proteins are found in the extracellular space. They share a highly conserved structure that consists of three domains: an N-terminal highly cysteine rich region (N-domain), a C-terminal cysteine rich region (C-domain), and a linker region (L-domain). The N-

terminal and C-terminal regions contribute to IGF binding and are highly conserved among the IGFBPs and across species. The L-domain is variable and contain sites of post-translational modification such as glycosylation, serine/threonine phosphorylation and proteolysis (Jones and Clemmons, 1995).

IGFBP5 is the most highly conserved members of the IGFBP family (Baxter and Twigg, 2009; Duan and Xu, 2005). Similar to other IGFBPs, human IGFBP-5 has a secretory signal peptide of 20 amino acids and the mature protein contains 252 amino acids (Wetterau et al., 1999). The primary IGF binding site is located in the N-domain (Kalus et al., 1998). Mutations of five residues (K68N/P69Q/L70Q/L73Q/ L74Q) in the N-domain caused a 1,000-fold reduction in its affinity for IGF1 (Imai et al., 2000). The N-domain also contains several acidic residues and prolines that are critical for transcriptional activation activity (Zhao et al., 2006b). The C-domain of IGFBP5 has a stretch of basic amino acids (R201-R218) that are involved in nuclear localization (Xu et al., 2004), acid-labile subunit (ALS) binding (Firth et al., 2001), and extracellular matrix (ECM) binding (Zheng et al., 1998b). In the blood, IGFBP5 forms a complex with IGF and ALS (Baxter et al., 1989; Twigg and Baxter, 1998), which can prolong the half-life of IGFs and prevent the potential hypoglycemic effect of IGFs (Binoux and Hossenlopp, 1988; Daughaday and Kapadia, 1989; Lewitt et al., 1994; Ueki et al., 2000). Studies with cultured human fetal fibroblasts suggest that binding to ECM can protect IGFBP5 from degradation and potentiate the biological actions of IGF1 (Jones et al., 1993).

1.2.4 IGF signaling in human diseases

IGF1 and IGF2 are both strong mitogens in a wide variety of cancer cell lines. High circulating levels of IGF1 have been associated with increased risks for breast, prostate, and colon cancers (Pollak, 2008b). IGF2 is maternally imprinted, and loss of this imprinting results

in increased IGF2 production. This process was first described in Wilms tumor, a childhood nephroblastoma, and has been subsequently identified in adult tumors. Increased IGF2 production is also commonly associated with an increased risk of colon cancer (Cui et al., 2003). It has been shown that IGF2 is the single most overexpressed gene in colorectal neoplasia relative to normal colorectal mucosa (Zhang et al., 1997). IGF1R is ubiquitously expressed in normal tissues and plays an important role in growth and various physiological functions. Increases in IGF1R have been shown in different types of cancers, such as melanomas, and carcinomas. The IGF signaling has been implicated with the transformation of normal cells to malignant cells, and also with cancer cell proliferation, growth, survival, and metastasis. Therefore, it has been an attractive therapeutic target (Denduluri et al., 2015; Laviola et al., 2007; Siddle, 2012; Weroha and Haluska, 2012).

There are three major classes of IGF/IGF1R inhibitors developed and clinically tested (Chen and Sharon, 2013): 1) IGF1R targeting monoclonal antibodies, 2) IGF1 and IGF2 neutralizing monoclonal antibodies, and 3) small molecule tyrosine kinase inhibitors. Early trials of these IGF1R inhibitors have clearly shown therapeutic benefit by slowing disease progression. However, these results were not replicable in larger phase III randomized trials. Another potential drawback of such approaches is the negative side effects or toxicities due to the interference with the insulin signaling pathway. Instead, IGFBPs could potentially serve as better therapeutic targets as these proteins do not bind insulin and thus do not interfere with insulin-insulin receptor interactions (Brahmkhatri et al., 2015).

The action of IGFBP5 on IGF signaling has been intensively studied in mammalian cells. In vitro studies suggested that IGFBP5 can both potentiate and/or inhibit IGF signaling (Conover and Kiefer, 1993; Dai et al., 2010; Ding et al., 2016; Kiefer et al., 1992; Schneider et al., 2001).

IGFBP5 has been associated with metastasis and poor prognosis in breast cancer cells (Mita et al., 2007; Wang et al., 2008). However, forced-overexpression of IGFBP5 in breast cancer cell lines has been shown to inhibit cell growth (Butt et al., 2003). Further studies suggested that the subcellular localization of IGFBP5 influences its biological effect. Cytoplasmic IGFBP5 promoted cell proliferation and motility while nuclear IGFBP5 did not (Akkiprik et al., 2009). IGF-independent activity for IGFBP5 is thought to involve the AKT pathway with effects on ovarian cancer angiogenesis (Tripathi et al., 2009).

1.3 Epithelial Ca^{2+}-transporting cells

1.3.1 NaR cells are conserved from fish to human

NaR cells belong to a large family of specialized epithelial cells known as ionocytes that are responsible for ion homeostasis regulation in different species. Ionocytes, formerly known as chloride cells, were originally described in the gills of seawater acclimated European eel (*Anguilla anguilla*) (Keys and Willmer, 1932). They were so named because they secret excess sodium and chloride. The secretory mechanism in these teleost ionocytes is functionally comparable to that in the intercalated cells in mammalian kidney collecting duct (Haas and Forbush, 2000). Recently, this term has also been adopted to describe a new lung cell type that express high levels of cystic fibrosis transmembrane conductance regulator (*CFTR*) (Montoro et al., 2018; Plasschaert et al., 2018). Mutation of *CFTR* disrupts airway fluid and mucus physiology, resulting in cystic fibrosis (De Boeck and Amaral, 2016).

In addition to the renal and airway epithelium, ionocytes are also known to exist in the human epididymis (Palacios et al., 1991), ciliary epithelium, retinal pigment epithelium of the eye, and liver epithelium (Marshall, 2011). These cells contain elaborate basolateral infoldings

that produce an extensive intracellular tubular system associated with the ion-transporting enzyme Na^+, K^+-ATPase (Karnaky et al., 1976) and numerous mitochondria.

Ionocyte cell specification and development are most extensively studied in zebrafish (Figure 1.3). All types of ionocytes originate from a population of epidermal stem cells that express ΔNp63 (an isoform of transcription factor p63, a member of p53) (Lee and Kimelman, 2002). p63 induces the specification of epidermal ectoderm and inhibits the neural ectoderm formation during early gastrulation (Aberdam et al., 2007; Bakkers et al., 2002). After gastrulation, p63-positive epidermal stem cells differentiate into Forkhead-box I transcription factor 3a (Foxi3a) -activated ionocyte progenitors and Foxi3a-inactive Keratinocyte progenitors by a Notch signaling-mediated lateral inhibition mechanism (Hsiao et al., 2007). Kruppel-like factor 4 (Klf4) has recently been shown to play a crucial role in maintaining the ionocyte progenitor cell pool by stimulating epidermal cell stem proliferation (Chen et al., 2019).

The ionocyte progenitors then give rise to different types of ionocytes, expressing respective unique sets of transporters and enzymes, through complicated transcriptional networks mediated by Foxi3a/b, Foxi1, and Glial cell missing 2 (Gcm2) (Chang et al., 2009; Esaki et al., 2009). The detailed regulatory mechanisms controlling the specification of ionocyte subtypes are not fully understood and need to be further elucidated. Five subtypes of ionocytes have been identified to date: Na^+-K^+-ATPase rich (NaR) cells, H^+-ATPase-rich (HR) cells, Na^+-Cl^- cotransporter (NCC) expressing cells, K^+-secreting (KS) cells and solute carrier 26-expressing (SLC26) cells (Abbas et al., 2011; Bayaa et al., 2009; Lin et al., 2006; Wang et al., 2009). These different ionocytes are required to deal with diverse ionic changes in varied hypotonic milieus (Hwang and Chou, 2013).

Among the five types of ionocytes, NaR cells are specialized for Ca^{2+} uptake. Zebrafish are freshwater fish and must be able to maintain normal blood Ca^{2+} levels. Active uptake of Ca^{2+} is therefore a requisite for them to live and grow. As early as 1981, physiological studies in freshwater teleosts have speculated that ionocytes are responsible for calcium uptake (Payan et al., 1981). The need of Ca^{2+} uptake is not unique to aquatic habitants. Terrestrial animals like humans also uptake Ca^{2+} transportation in the intestine and kidney . On a daily basis, around 80% Ca^{2+} filtered at the glomerulus will be reabsorbed and 20% is via an active transcellular Ca^{2+} transport route in the distal part of the nephron. During pregnancy and lactation, Ca^{2+} transport from mother to the fetus and Ca^{2+} secretion to the milk both require active Ca^{2+} transportation against the chemical gradient (Lee et al., 2009). Therefore, Ca^{2+} -transporting epithelial cells exist in epithelium in the human gastrointestinal tract, bone, kidney, and placenta (Hoenderop et al., 2005).

In early developmental stages of zebrafish, before the gills are fully developed and functional, NaR cells are located in the epithelia covering the yolk. These extra-branchial NaR cells are considered to be the major site of ionic regulation in embryonic and larval zebrafish (Hwang and Chou, 2013). The transparency of zebrafish embryos and larvae as well as their *ex utero* development allows for noninvasive real-time imaging to monitor biological events in vivo (Lawson and Weinstein, 2002). Epithelia of zebrafish embryos or larvae are therefore an excellent model to study the functions of vertebrate Ca^{2+}-transporting epithelia.

Early studies in rainbow trout (*Oncorhynchus mykiss*) and Nile tilapia (*Oreochromis niloticus*) demonstrated that low Ca^{2+} adaptation increases the density of NaR cell-like Ca^{2+}-transporting cells in parallel with Ca^{2+} transport capacity (McCormick et al., 1992). Studies about the hormonal regulation in low Ca^{2+} adaptation in zebrafish revealed that a set of

hormones (e.g., parathyroid hormones, stanniocalcin, cortisol, isotocin) are responsible for regulating NaR cell number through controlling NaR cell differentiation from epidermal stem cells (Lin and Hwang, 2016). Studies from our group demonstrated that the increased NaR cells in zebrafish larvae under low Ca^{2+} adaptation are mainly due to the elevated proliferation of pre-existing NaR cells (Dai et al., 2014a; Liu et al., 2017a). Similarly, dietary Ca^{2+} levels have been inversely associated with colon cancer risk for a long time (Han et al., 2015; Lamprecht and Lipkin, 2003; Peterlik and Cross, 2005). Presumably, epithelial cells in the colon epithelium can undergo an aberrant reactivation and contribute to the hyperactivity of cell proliferation in colon cancer initiation and progression. Mitochondrion-rich phenotype is also strongly associated with poor prognosis of ERG negative prostate cancers (Grupp et al., 2013). After acute kidney injury, resident differentiated tubule cells are known to be self-renew and produce differentiated offsprings This proliferation capacity is required for the tissue repair (Feng et al., 2015; Vogetseder et al., 2007; Vogetseder et al., 2008). Intercalated cells in the mammalian kidney epithelium were also thought to be terminally differentiated and unable to further proliferate. However, proliferation of these intercalated cells has been shown during acidosis in mouse and rat kidney (Duong Van Huyen et al., 2008; Welsh-Bacic et al., 2011). This elevated proliferation of intercalated cells may contribute to the adaptive re-modelling of the collecting duct. In addition, unrestrained intercalated cell proliferation was linked to chromophobe renal cell carcinomas and oncocytomas of the kidney (Storkel et al., 1989). IGF/PI3K/AKT/TOR pathway seems to play a decisive role in chromophobe renal cell carcinoma in preclinical models (Shuch et al., 2012). Therefore, studying the activation mechanism of IGF/PI3K/AKT/TOR signaling cascade in fish NaR cells can contribute to the general understanding of the quiescence to proliferation state switch of ionocytes. In addition to the potential indication in cancer therapy,

IGFPB5 might also be a conserved regulator for fish osmoregulation. Recently, transcriptome analysis of different ecotypes of stickleback identified *igfbp5* as a potential regulator for salinity adaptation as it is differentially expressed in marine and freshwater sticklebacks (Kusakabe et al., 2017). *Igfbp5* is also found to be highly expressed in another anadromous fish, the Atlantic salmon (Breves et al., 2017). Therefore, elucidating role of *igfbp5* in the adaptive proliferation of NaR cells under low Ca^{2+} stress can shed light on our limited knowledge of Igfbp5 in the fish homeostasis regulation as well.

1.3.2 Epithelial Ca^{2+} channel TRPV6

The transcellular Ca^{2+} transportation pathway in epithelial cells is a multistep process, consisting of Ca^{2+} entry through the apical membrane of epithelial cells, Ca^{2+} transportation from the entry point to the basolateral membrane, and Ca^{2+} extrusion into the circulatory system (Hoenderop et al., 2005). The molecular identity of the apical Ca^{2+} influx protein in intestinal epithelia was unraveled by functional expression cloning of RNA isolated from the duodenum of rats fed with a Ca^{2+} -deficient diet. The epithelial Ca^{2+} channel (ECaC, later known as Trpv6) transcript expression was enriched in rat small intestine and colon (Peng et al., 1999). In mice, significant Trpv6 expression was shown in duodenum, cecum, and distal colon (Rievaj et al., 2013). Immunohistochemistry has shown TRPV6 localizes in the apical membrane of villous cells in human intestine (Zhuang et al., 2002).

TRPV6 belongs to transient receptor potential (TRP) channel superfamily. The *trp* gene was initially discovered in *Drosophila* as a phototransduction channel in late 1960s (Cosens and Manning, 1969). Since then, more then 100 TRP genes have been identified based on a common structure feature. They act as cellular sensors and can be activated by a plethora of extracellular and intracellular stimuli including temperature changes, chemicals, mechanical force, and light

(Nilius and Flockerzi, 2014). Most TRP channels are permeable to Ca^{2+}, but only two, TRPV5 (synonyms ECaC1, CaT2) and TRPV6 (synonyms ECaC2, CaT1, CaT-like) are highly Ca^{2+}-selective with PCa/PNa ratios > 100 (Vennekens et al., 2000). Compared to TRPV6, TRPV5 is mainly expressed in the kidney epithelium. TRPV5 and TRPV6 are juxtaposed on the human chromosome 7 with a distance of only 22kb, suggesting an evolutionary gene duplication event. In the zebrafish genome, only one orthologue of TRPV5/6 is present (Vanoevelen et al., 2011). Zebrafish Trpv6 was cloned in 2005 (Pan et al., 2005).

Functional analysis indicates TRPV6 constitutes the rate-limiting step in the tricellular Ca^{2+} transport pathway in intestinal epithelia (Hoenderop et al., 2005). Two Trpv6-deficient mice mutants generated independently both exhibited decreased intestinal Ca^{2+} absorption under Ca^{2+}-restricted diets (Bianco et al., 2007; Lieben et al., 2010; Weissgerber et al., 2011), demonstrating a critical role of TRPV6 in Ca^{2+} absorption, especially under conditions of limited Ca^{2+} supplies. This function is conserved in zebrafish. Zebrafish *trpv6* expression in NaR cells is elevated in response to low environmental Ca^{2+} levels (Liao et al., 2007). Zebrafish *trpv6* mutants display a severe Ca^{2+} deficiency in calcified structures from early larval stage and are lethal around 7-9 dpf (Vanoevelen et al., 2011).

In addition to the intestine and kidney, maternal-fetal transport of Ca^{2+} also requires an transcellular transport mechanism, as the serum Ca^{2+} is higher in fetuses than in mothers (Schauberger and Pitkin, 1979). Recent studies have reported that patients with *TRPV6* mutations have transient neonatal hyperparathyroidism (TNHP) and severe skeletal under-mineralization, most likely due to a defect in the maternal-fetal calcium transport through the placenta (Burren et al., 2018; Suzuki et al., 2018; Yamashita et al., 2019).

Ca^{2+}-dependent feedback regulation of TRPV6 has been demonstrated by whole cell patch clamp experiments in HEK293 cells as well as structural analysis using cryo-electron microscopy (Bate et al., 2018; Singh et al., 2018a). Calmodulin have been shown to directly interact with TRPV6 (Kovalevskaya et al., 2012; Lambers et al., 2004) and TRPV6 channel inactivation was proposed to occur via a CaM-dependent manner (Lambers et al., 2004). Mutation of TRPV6 CaM-binding sites significantly increased the intracellular Ca^{2+} concentration in HEK293 cells (Cao et al., 2013).

It is possible TRPV6 has functions beyond as a Ca^{2+} channel. TRPV6 channel permeability is estimated to be about 100 times more selective for Ca^{2+} than for Na^{+}, and a single aspartate residue (D542 in human, D541 in mice and D539 in zebrafish) in the pore-forming region between the 5^{th} and the 6^{th} transmembrane domain of TRPV6 determines such selectivity (Voets et al., 2004). Under physiological conditions, TRPV6 mainly conducts Ca^{2+} ions. However, in the absence of divalent cations, the channel conducts monovalent ions such as Na^{+}. An increase in Ca^{2+} concentration leads to an increase of Ca^{2+} current but a reduction of Na^{+} current or whole cell current. As Ca^{2+} continues to increase, the Ca^{2+} current becomes dominant again and the channel is highly Ca^{2+}-selective. When HEK293 cells overexpressing TRPV6 were exposed to divalent-free (DVF) solutions, currents induced by voltage ramps/steps increased markedly compared to that in 10 mM Ca^{2+} containing solution (Yue et al., 2001).

This conversion to non-selectivity in the absence of Ca^{2+} is referred as anomalous mole fraction effect (AMFE) and has also been observed in TRPV5 and L-type voltage-gated Ca^{2+} channels. AMFE is generally accepted as evidence for a channel pore containing multiple binding sites occupied by permeant ions moving in single file through the channel (Hille, 1978).

Crystal structures of TRPV6 were resolved recently through Cryo-EM and further support the kinetic model proposed for ion permeation through TRPV6 pore region (McGoldrick et al., 2018; Saotome et al., 2016). Consistent with the physiological studies, non-equilibrium simulations based on the crystal structure suggest a "knock-off" Ca^{2+} permission mechanism: the high affinity of D541 side chain to Ca^{2+} makes the absence of a bound Ca^{2+} energetically unfavorable. Removal of Ca^{2+} from D541 aspartate ring requires an immediate replacement of another Ca^{2+} ion and therefore a substantially high local Ca^{2+} would be necessary for the Ca^{2+} permission to proceed (Sakipov et al., 2018). On the other side, Na^{+} permeation through TRPV6 is completely different. Many Na^{+} ions can occupy the selectivity filter and the permission of Na^{+} is completely independent of the approaching Na^{+} from the above. TRPV6 has been known to be subjected to Ca^{2+}-dependent feedback inhibition through interaction with calmodulin in the intracellular domain (Bate et al., 2018; Cao et al., 2013; Lambers et al., 2004; Singh et al., 2018a). In contrast, Na^{+} current do not inactivate TRPV6 channel (Nilius et al., 2002; Vennekens et al., 2000). Naturally, inactivated Na^{+} influx might result in a change of the membrane potential and thus contribute to the cell status change.

1.3.3 Implication of TRPV6 in cell cycle regulation

TRPV6 has been implicated in malignancies and its oncogenic potential has been suggested by in vitro studies (Lehen'kyi et al., 2012; Santoni et al., 2011). Clinically, TRPV6 expression correlates with Gleason scores in prostate cancer and with poor prognosis in breast cancer (Peng et al., 2000; Peters et al., 2012). Elevated expression of TRPV6 mRNA was detected in human prostate cancer cell lines (LNCaP and PC-3) in comparison to normal and benign cells (PrEC, BPH1) (Peng et al., 2001). Immunohistochemistry has shown substantial

increase of TRPV6 proteins in carcinomas of prostate, colon, breast, thyroid cancers compared to normal tissue (Zhuang et al., 2002).

Different results have been reported for TRPV6 action. Silencing TRPV6 expression attenuated cell proliferation and increased apoptosis in prostate, colon, breast, and pancreatic cancer cell lines (Lehen'Kyi et al., 2007; Peleg et al., 2010; Peters et al., 2012; Skrzypski et al., 2016b), presumably because of diminished activity of the Ca^{2+}/NFAT-dependent pathway. Soricidin-derived TRPV6-antagonistic peptides (SOR-C13 and SOR-C27) was found to effectively inhibit tumor growth in mice bearing xenografted ovarian tumors (Xue et al., 2018). In a recent Phase I clinical trial, two of four patients showed stable decease of tumor size after two cycles of treatment of SOR-C13 (Fu et al., 2017). On the contrary, other studies suggested that TRPV6 may act as a tumor suppressor. Curcumin, a ligand of 1,25-vitamine-D3 receptor, exerts chemoprevention effects in colon cancer cells through promoting Ca^{2+} uptake by up-regulation of TRPV6 expression (Bartik et al., 2010). Capsaicin, which is normally considered to be a TRPV1 agonist, induce cell apoptosis in gastric cancer cells and small cell lung cancers and such effects were dependent on TRPV6 activity (Allard and Duan, 2018; Chow et al., 2007; Lau et al., 2014). Dietary calcium intake has been associated negatively with colon cancer risk for a long time (Han et al., 2015; Meng et al., 2018b; Peterlik et al., 2009). High calcium diet abrogated hyperplasia in a citrobacter rodentium-induced transmissible murine colonic hyperplasia (TMCH) model (Peleg et al., 2010).

These discrepancies can partially be explained by the different stages or type of cancer cells/tumor tissues used in different studies. However, as all the studies by far were carried out in cancer cell lines or tumor tissues which are already advanced in cancer progression. it remains

unclear whether TRPV6-mediated Ca^{2+} influx or ion-independent function of TRPV6 is involved in cell proliferation and whether it has an oncogenic potential in vivo.

1.3.4 Other Ca^{2+} signaling machinery in NaR cells

In epithelial cells responsible for active Ca^{2+} uptake, Ca^{2+} buffer proteins are crucial (Feher and Wasserman, 1979). In the mammalian kidney epithelium, calbindin-D9k and -D28k are known to play important roles in facilitating cytosolic Ca^{2+} diffusion between the apical and basolateral surfaces of the cell to achieve transcellular Ca^{2+} transport (Feher et al., 1992). Calbindin-D28k knockout mice exhibited a two times higher urinary Ca^{2+} excretion compared with their wild-type littermates, but no significant differences in serum Ca^{2+}, PTH, or in serum and urinary Mg^{2+} and phosphate were observed (Sooy et al., 2000). Calbindin-D9k are also known to be expressed and localized in the bovine uterus and placenta during pregnancy together with TRPV6 (Sprekeler et al., 2012). Additionally, it is proposed that Ca^{2+}-enriched vesicles and lysosome can be used in those Ca^{2+}-transporting cells to sequester Ca^{2+} and facilitate its movement to the basolateral membrane (Larsson and Nemere, 2002).

S100A10, which belong to the S100 EF-hand Ca^{2+} binding protein family, has been shown to be associated with TRPV5 and TRPV6 and regulate their activity (van de Graaf et al., 2003). However, S100A10 is the only S100 member that does not bind Ca^{2+}. Both Ca^{2+}-binding sites in S100A10 are missing and the function of S100A10 is suggested to be Ca^{2+}-independent (Zimmer et al., 2003). Interestingly, zebrafish *s100a11* exhibits a salt-and-pepper expression pattern in zebrafish embryonic skin (Kraemer et al., 2008). S100A11 expression is increased in various tumors, and is associated with tumor metastasis as well as poor prognosis in pancreatic, lung and colon cancers (Cross et al., 2005; Melle et al., 2006).

In zebrafish, six plasma membrane Ca^{2+} -ATPases (PMCA) and seven isoforms of Na^{+}/ Ca^{2+} exchanger (NCX1) have been identified, of which only PMCA2 and NCX1b were found in NaR cells, as determined by triple *in situ* hybridization and immunocytochemistry (Liao et al., 2007). While all *trpv6*-expressing cells co-expressed *ncx1b*, only half of the *trpv6*-expressing cells co-expressed *pmca2*, indicating the possible existence of sub-populations within NaR cells. The NCX has low Ca^{2+} affinity but high capacity for Ca^{2+} transport, whereas the PMCA has a high Ca^{2+} affinity but low transport capacity. Thus, traditionally, the PMCA pump has been attributed a housekeeping role in maintaining cytosolic Ca^{2+}, and the NCX the dynamic role of counteracting large cytosolic Ca^{2+} variations (Brini and Carafoli, 2011). NCX, like other secondary active transporters, utilizes the electrochemical gradient of Na^{+} across the membrane, which is generated by the primary active transporter, the Na^{+}-K^{+}-ATPase. Na^{+}-K^{+}-ATPase, a heterodimeric integral membrane protein composed of a catalytic subunit and a smaller glycosylated subunit, enables ion transport directly through movement of ions across epithelial membranes. Moreover, of the six NKAα1 subunit genes, only *atp1a1a.1* was expressed in NaR cells (Liao et al., 2009).

In mammals, PMCA2 was found to be expressed in the hair cell hair bundle in the inner ear, suggesting that it may be responsible for endolymph Ca^{2+} homeostasis (Shull, 2000). Mammalian PMCA1 was found to be a major Ca^{2+} extrusion transporter for Ca^{2+} absorption in intestine and kidney (Armbrecht et al., 1999). However, the opposite is true in zebrafish as zebrafish *pmca2* is expressed in a housekeeping. Zebrafish *pmca1a* on the other hand, showed an expression pattern in hair cells during embryonic stages (Liao et al., 2007).

In zebrafish, the NCX1b isoform is required for Ca^{2+} extrusion in gill/skin ionocytes, while its paralogue NCX1a is expressed specifically in the heart where mutant forms cause

cardiac fibrillations (Langenbacher et al., 2005). Conversely, a single NCX1 performs the roles of both NCX1a and NCX1b in mammals (Cho et al., 2003).

1.3.5 Intracellular Ca^{2+} signaling

Ca^{2+} signaling is crucial for many cell behaviors, including muscle contraction, secretion, fertilization of oocytes, embryonic pattern formation, cell proliferation, differentiation, and cell death. Starting from 1970s, evidence began to emerge suggesting that cytosolic Ca^{2+} levels are involved in the regulation of cell proliferation (Balk, 1971; Durham and Walton, 1982). It was observed that while tumor cells can proliferate in Ca^{2+}-depleted medium, normal cells cannot, suggesting normal cells probably have higher intracellular Ca^{2+} storage (Boynton and Whitfield, 1976). Indeed, tumor cells are reported to have several folds higher intracellular Ca^{2+} concentration ($[Ca^{2+}]_i$) level compared to normal cells (Mignen et al., 2017).

The level of free Ca^{2+} in the extracellular fluids ($[Ca^{2+}]_e \approx 1$ mM) is approximately 10,000 times higher than the level of resting Ca^{2+} in the cytosol ($[Ca^{2+}]_i \approx 100$ nM). Correlation of Ca^{2+} signals and T cell proliferation revealed that an average rise of $[Ca^{2+}]_i$ from 40 nM to 220 nM is sufficient to induce maximal proliferation (Schwarz et al., 2007). However, increased global or local Ca^{2+} level is not always pro-proliferative. Pharmacological activation of TRPV4 channels reduces proliferation of tumor endothelial cells (Thoppil et al., 2015), suggesting the role of $[Ca^{2+}]_i$ in cell cycle regulation is context dependent.

Unlike many other intracellular signals, Ca^{2+} cannot be created from an enzymatic reaction or converted into an inactive metabolite. Source of Ca^{2+} signals is either from the external medium or the from internal Ca^{2+} stores. External Ca^{2+} entry is mediated by the opening of plasma membrane Ca^{2+} -permeable ion channels such as voltage-gated (classified through electrophysiological properties into L-type, T-type, P/Q-type, R-type and N-type), or members of

the transient receptor potential (TRP) family (Deliot and Constantin, 2015). $[Ca^{2+}]_i$ levels can also be increased through Ca^{2+} release from internal Ca^{2+} stores, such as inositol 1,4,5-triphosphate (IP3), which activates the IP3 receptors (IP3Rs) in the endoplasmic reticulum (ER). IP3 can be generated through the stimulation of GPCRs or RTKs, through activation of phospholipase C (PLC) (Nixon et al., 1994; Taylor and Machaca, 2018). Ca^{2+} release from ER can also mediated by ryanodine receptors (RyRs). RyRs are the largest known ion channels and bind to the plant alkaloid ryanodine (Lanner et al., 2010; Otsu et al., 1990). Several TRP channels, in addition to their roles in the plasma membrane, may also mediate release of Ca^{2+} from intracellular stores (Gees et al., 2010). ER-localized TRPV channels have been recently demonstrated to be responsible for ER Ca^{2+} release and are required for glucose starvation-induced AMPK activation (Li et al., 2019). The depletion of the ER Ca^{2+} store can be detected by the ER Ca^{2+} sensor stromal interaction molecule 1 (STIM1). STIM1 proteins are redistributed upon Ca^{2+} store depletion and subsequently interact with plasma membrane ORAI1 proteins and lead to store-operated Ca^{2+} entry (SOCE) (Hogan and Rao, 2015).

Due to the spatial distribution and temporal kinetics of different Ca^{2+} permeable molecules, the actual elevation of intracellular Ca^{2+} can vary widely between different cell types and sub-cellular compartments, and local concentrations have been estimated to reach levels as high as 10-100 μM during an induced Ca^{2+} influx from the plasma membrane or Ca^{2+} release from ER Ca^{2+} store (Berridge, 2006; Matthews et al., 2013).

Once $[Ca^{2+}]_i$ or local Ca^{2+} concentration increases, Ca^{2+}-sensitive proteins propagate the signal and many of these signal transduction events are mediated by members of the EF-hand family of calcium binding proteins via interaction with target proteins in a Ca^{2+}-dependent

manner. The EF-hand calcium-binding protein family can further be classified as sensor or buffer proteins based on their function (Ikura, 1996).

Another mechanism to tightly control cytosolic Ca^{2+} level is through Ca^{2+} uptake into the intracellular ER Ca^{2+} store mediated by sarco/endoplasmic reticulum Ca^{2+}-ATPase (SERCA), which is widely distributed in the endoplasmic reticulum of most cells. ER is the major intracellular Ca^{2+} reservoir and it is also responsible for protein synthesis and post-translational modifications (Humeau et al., 2018). The maintenance of high intraluminal Ca^{2+} is essential for these processes. Therefore, alterations in Ca^{2+} concentration within the endoplasmic reticulum ($[Ca^{2+}]_{ER}$) may destabilize the physiological balance of the endoplasmic reticulum lumen, and hence inhibit cell growth (Humeau et al., 2018).

It has been well described that exposing cells to SERCA blocker thapsigargin results in depletion of Ca^{2+} pools and inhibition of cell proliferation, suggesting a potential role of SERCA proteins in regulating cell growth (Short et al., 1993). However, current data concerning the role of ER Ca^{2+} level and SERCA activity in cell growth are rather contradictory. In some model systems inhibition of ER Ca^{2+} uptake through SERCA by thapsigargin induces cell cycle arrest (Furuya and Isaacs, 1994), whereas in other systems, it stimulates cell proliferation (Charlesworth and Rozengurt, 1994; Legrand et al., 2001).

Lately, thapsigargin-induced depletion of the ER Ca^{2+} store has been more and more recognized as a signal to trigger store-operated Ca^{2+} entry (SOCE). The molecular basis for this pervasive signaling pathway was not resolved until large scale genomic screens revealed the two fundamental players: STIM proteins that sense Ca^{2+} levels in the endoplasmic reticulum, and Orai proteins that constitute the basic pore-forming subunits of the store-operated channels (Feske et al., 2006; Liou et al., 2005). Depletion of ER Ca^{2+} stores results in loss of Ca^{2+} from EF

hand domain of STIM and eventually causes oligomerization of STIM into large puncta that are readily visible by light microscopy (Liou et al., 2007). These puncta are stabilized in a subplasma membrane ER that localizes within 10-20 nm of the cell membrane, where they physically recruit Orai1 into coincident puncta at the cell membrane, leading to Orai1 opening and Ca^{2+} influx (Yeromin et al., 2006).

Mammalian genomes contain two STIM homologues, STIM1 and STIM2. STIM1 has been shown to be essential for SOCE, whereas STIM2 appears to be primarily involved in maintaining Ca^{2+} homeostasis (Cahalan, 2009). Expression of the STIM1 cytoplasmic domain alone produces constitutively active SOCE (Huang et al., 2006). The Orai family has three homologs, Orai1, 2, and 3 wherein Orai3 is exclusively present in mammals (Cai, 2007). Zebrafish has three Orai genes (*orai1a, orai1b* and *orai2)* and four STIM1 paralogues (*stim1a, stim1b, stim2a, stim2b*) (Wasilewska et al., 2019). Knockdown of Orai1b by morpholino has been shown to lead to heart failure and skeletal myopathy in zebrafish (Volkers et al., 2012). Zebrafish STIM1a morphants have substantially reduced number of the pigmented black-colored melanophores (Motiani et al., 2018).

A critical role for STIM and Orai proteins in promoting tumorigenesis has emerged with increasing studies supporting the idea that STIM and Orai proteins could be therapeutically targeted for better management of cancers. SOCE-mediated Ca^{2+} influx is essential for breast cancer cell migration (Yang et al., 2009). In colorectal cancers, higher STIM1 expression correlated with increased tumor size, tumor invasion, and metastasis (Wang et al., 2015a). Increase in SOCE was suggested to be associated with increased proliferation, invasion, and cell survival of colorectal carcinoma cells (Sobradillo et al., 2014).

The role of TRP channels in SOCE was controversial as they were later found to behave in a non-store-operated manner (Acharya et al., 1997). However, with studies of TRP homologues in mammals, increasing evidence has suggested a role for TRP channels in the conduction of SOCE, especially the transient receptor potential canonical (TRPC) subfamily members, which can be activated in response to stimuli, and result in PIP2 hydrolysis (Venkatachalam and Montell, 2007). Inhibition of TRPC1 and TRPC3 channels in HEK cells reduced Ca^{2+} influx after the depletion of Ca^{2+} stores and the knockdown of other TRPC channels such as TRPC4 inhibited SOCE in human corneal epithelial cells (Cheng et al., 2013). TRPV6 has been found to function as a component of store-operated Ca^{2+} entry (SOCE) in prostate cancer cells and facilitates Ca^{2+} entry (Raphael et al., 2014). SOCE inhibitor 2-aminoethoxydiphenyl borate (2-APB) has been shown to inhibit Ca^{2+} influx mediated by TRPV6 (Kovacs et al., 2012; Singh et al., 2018b).

The third way to remove excessive cytosolic Ca^{2+} is mediated by passive Ca^{2+} uptake through mitochondria Ca^{2+} uniporter (MCU) into mitochondria matrix. One major feature of ionocytes is that they possess many mitochondria, occupying approximately 28% of the cytoplasmic volume, and are therefore also named mitochondria-rich (MR) cells (Becerra and Anadon, 1993). Mitochondria are dynamic organelles involved in numerous physiological functions. They can localize at specific positions throughout the cell and shape the cellular Ca^{2+} responses and play a key role in the buffering of cytosolic Ca^{2+} (Wacquier et al., 2019). As mitochondria are the central metabolic and energetic hub in cells controlling ATP production, redox balancing and cellular metabolism, Ca^{2+} transported into the matrix also regulates mitochondrial function. Therefore, mitochondria function both as regulators and decoders of Ca^{2+} input (Giorgi et al., 2018).

MCU activity is heavily depending on the surrounding cytosolic Ca^{2+} concentration (Moreau et al., 2006). The affinity of MCU for Ca^{2+} is relatively low (Kd ≈ 10 μM), so the basal Ca^{2+} concentration in the cytosol is not sufficient to allow for an efficient mitochondrial uptake. However, mitochondria located near plasma membrane or ER Ca^{2+} channels can be exposed to large concentrations of Ca^{2+} (or Ca^{2+} microdomains) and take up considerable amounts of Ca^{2+} (Nunez et al., 2006; Villalobos et al., 2001). It is now well-established that one of the main functions of mitochondria-ER contact sites is to generate highly localized and concentrated Ca^{2+} microdomains facilitating Ca^{2+} transport into mitochondria (Giacomello and Pellegrini, 2016). It has also been proposed that mitochondria re-localize to the plasma membrane to directly buffer Ca^{2+} entry and inhibit the Ca^{2+}-dependent inactivation of the Orai1 channels during store-operated Ca^{2+} entry (Schwindling et al., 2010). The ability of surrounding mitochondria to remove or dampen Ca^{2+} microdomains determines the extent and duration of SOCE (Malli and Graier, 2017).

Studies have shown that mitochondrial Ca^{2+} uptake is dependent on the steep mitochondrial membrane potential ($\Delta\psi \approx -180mV$) and was inhibited by the drug Ruthenium Red or its analog Ruthenium 360 (Pathak and Trebak, 2018). In and Jurkat T lymphocytes and HT29 human colon carcinoma cells, studies have demonstrated that disruption of mitochondria Ca^{2+} uptake through mitochondrial depolarization by mitochondrial un-couplers prevent mitochondrial Ca^{2+} uptake, and therefore hinder SOCE and cell proliferation in a dose-dependent manner (Nunez et al., 2006; Valero et al., 2008). Induction of mitochondrial stress by depletion of mitochondrial DNA results in rise in cytosolic Ca^{2+} that in turn stimulates pro-survival and invasive pathways in human pulmonary carcinoma cells (A549) (Berra-Romani et al., 2008).

Prolonged increase in $[Ca^{2+}]_{mito}$ leads to the opening of the mitochondrial permeability transition pore (mPTP), a critical event driving to cell death by apoptosis (Giorgi et al., 2008).

AKT and its activator TORC2 have been known to localize to mitochondria-ER contact sites, phosphorylating IP3R and blocking the IP3R-mediated Ca^{2+} flow from ER to mitochondria (Betz et al., 2013; Marchi et al., 2012; Marchi et al., 2008). Additionally, AKT has been recently shown to be responsible for phosphorylating the MCU regulatory subunit MICU1 and impairing MICU1 stability, resulting in aberrant mitochondrial Ca^{2+} levels and tumor progression (Marchi et al., 2019).

However, compared to our increasing knowledge about the PI3K/AKT/TOR pathway in the regulation Ca^{2+} transfer in intracellular organelles (Rimessi et al., 2019), little is known for how intracellular Ca^{2+} signaling can regulate PI3K/AKT/TOR activity. The mitochondrial GTPase mitofusin-2 (MFN2), which is essential for mitochondria fission and tethering ER-mitochondria membranes, has been identified to negatively regulate cancer cell proliferation through inhibiting TORC2-AKT activity (Xu et al., 2017). MFN2 silencing drives quiescence exit of embryonic stem cells and promotes neural differentiation via regulating AKT signaling (Yi et al., 2019). Moreover, studies in human $CD8^+$ T cells have shown TORC2-AKT activity is regulated by Ca^{2+} flow from ER to mitochondria but the underlying mechanism remains unclear (Bantug et al., 2018).

1.5 Project summary

Both IGF signaling and Ca^{2+} signaling have been implicated in the quiescence-proliferation decision in several cell types across species. However, how these two signaling pathways crosstalk is still poorly understood. Zebrafish NaR cells offer an excellent *in vivo* model to address this question because 1) NaR cells are directly in contact with external

environment and readily accessible for experimental manipulations and observations, 2) there is only one copy of epithelial Ca^{2+} channel in zebrafish and therefore ruling out functionally redundancy and compensation existing in mammalians, and 3) Akt phosphorylation is strongly and exclusively elevated in NaR cells while not in the surrounding epithelial cells under low Ca^{2+} stress, providing an easy readout of IGF signaling activity.

In chapter 2, I tested the hypothesis that local IGF binding proteins are important in the cell specific activation of IGF signaling. I report that loss of Igfbp5a impairs Akt and Tor signaling activation and diminishes the quiescence-proliferation transition in NaR cells under low Ca^{2+}stress. Mechanistically,Igfbp5 functions through its ability to bind IGF ligands. In chapter 3, I report a crucial role of Trpv6 in suppressing IGF signaling and in promoting NaR cell quiescent state. Through constructing a NaR cell-specific Ca^{2+} reporter fish, I found Trpv6 constitutively transports Ca^{2+} into NaR cells and maintains the intracellular Ca^{2+} concentration ($[Ca^{2+}]_i$). Pharmacological blockage or genetic knockout of Trpv6 resulted in reduced $[Ca^{2+}]_i$, elevated IGF signaling, and increased NaR cell quiescence exit. Chemical biology screen reveals protein phosphatase 2A (PP2A) as a possible Ca^{2+} -sensing molecule mediating the Tprv6-mediated Ca^{2+} influx to the suppression of IGF signaling. In chapter 4, I provide preliminary results indicating that the Ca^{2+}/calmodulin-dependent kinase kinase (CaMKK) is required for low $[Ca^{2+}]_i$-triggered NaR cell reactivation. I propose local Ca^{2+} microdomains mediated by Ca^{2+} release from the ER Ca^{2+} store can is underlying the regulation of CaMKK activity. In agreement with this proposed mechanism, depletion of ER Ca^{2+} store blocks Akt phosphorylation and NaR cell quiescence exit under low $[Ca^{2+}]_i$.

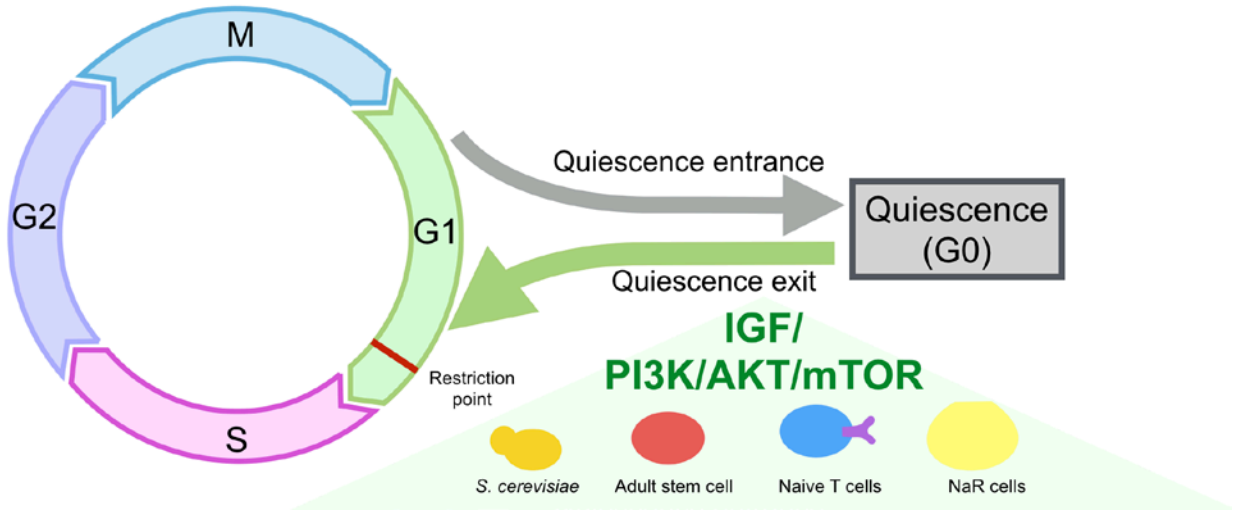

Figure 1.1 Role IGF/PI3K/AKT/TOR pathway in regulating quiescence exit

Cell cycle consists of G1 phase, S phase, G2 phase and M phase. Cells that pass the restriction point in the G1 phase will progress through the cell cycle and divide. By contrast, non-dividing cells can enter the G0 phase and become quiescent. Insulin/insulin-like growth factor (IGF)-PI3 kinase-AKT-TOR signaling pathway activation is an evolutionary conserved mechanism for quiescence exit in yeast, adult stem cells, naïve T cells. Recently, it is shown that IGF/PI3K/AKT/TOR pathway is exclusively activated in zebrafish Ca^{2+}-transporting epithelial cells or NaR cells and is required for quiescence exit in those cells.

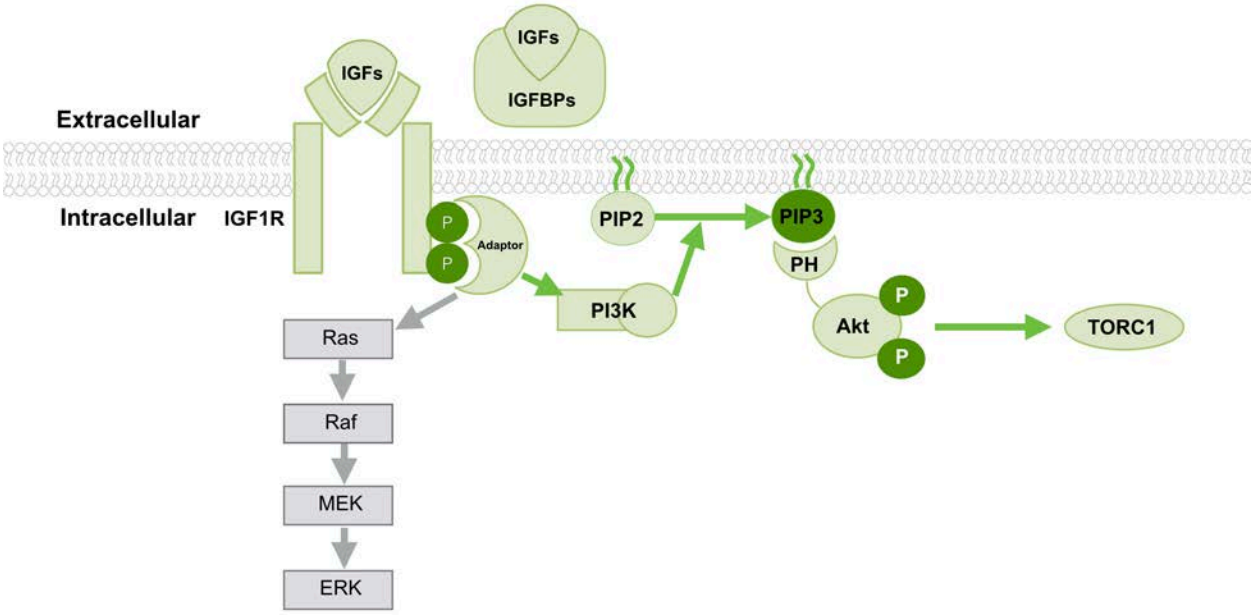

Figure 1.2 The IGF/PI3K/AKT/TOR signaling cascade

Insulin-like growth factors (IGFs) bind to the IGF1 receptor and induce autophosphorylation of the receptor via its tyrosine kinase domain, providing docking sites for adaptors. Activated adaptors phosphorylates phosphatidylinositol 3-kinases (PI3Ks), which subsequently turns phosphatidylinositol 4,5-trisphosphate (PIP2) to phosphatidylinositol 3,4,5-trisphosphate (PIP3). PIP3 recruits AKT to the membrane through interaction with its pleckstrin homology (PH) domain. AKT is then phosphorylated by phosphoinositol-dependent kinase 1 (PDK1) at Thr 308 site and TOR complex 2 (TORC2) at Ser 473 site. Activated AKT phosphorylates a wide range of substrates and activates TOR complex 1 (TORC1). IGF binding proteins (IGFBPs) are a group of secreted protein known to bind IGF ligands with high affinity. IGFBPs serve as critical regulator of IGF signaling both in circulation and local tissues.

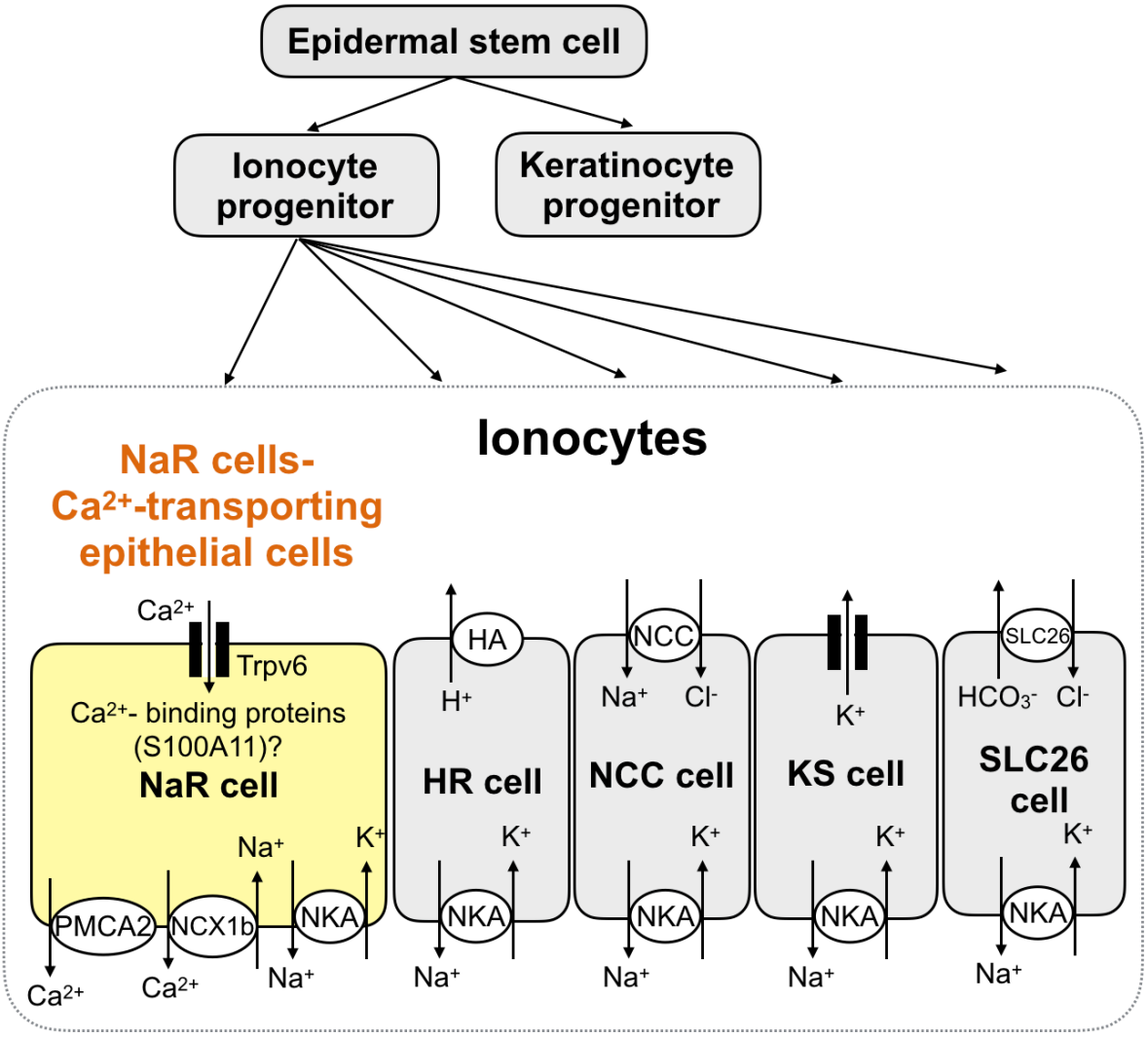

Figure 1.3 Developmental origin and Ca^{2+}-transporting machinery of NaR cells

Ionocytes are originated from epidermal stem cells. Various types of ionocytes are responsible for transport of different ions using distinct set of ion transporters. In NaR cells, Ca^{2+} entry in the apical membrane is mediated by epithelial Ca^{2+} channel Trpv6. Intracellular Ca^{2+} transportation is proposed to be mediated by Ca^{2+}-binding proteins. At the basolateral membrane, Ca^{2+} extrusion to the circulation system is mediated by plasma membrane Ca^{2+}-ATPase 2 (PMCA2) and Na^{+}- Ca^{2+} exchanger 1b (NCX1b) (modified from (Guh et al., 2015)).

Chapter 2 Ca^{2+} Concentration-dependent Premature Death of *igfbp5a*$^{-/-}$ Fish Reveals a Critical Role of IGF Signaling in Adaptive Epithelial Growth[1]

2.1 Abstract

The phenotype gap is a major challenge to genetic dissection of the highly redundant endocrine signaling network. A notable example is the insulin-like growth factor binding protein (IGFBP) family, of which six distinct types exist. Gain-of-function studies have demonstrated that IGFBPs can inhibit, potentiate IGF actions or have IGF-independent actions. However, mutant mice lacking IGFBP-encoding genes do not exhibit major phenotypes. Here we report that although deletion of zebrafish *igfbp5a* did not result in notable phenotypes when raised in Ca^{2+} rich solutions, mutant fish died prematurely in low Ca^{2+} conditions. The *igfbp5a* gene is expressed in a group of epithelial cells, which take up Ca^{2+} to maintain constant body Ca^{2+} levels. When the environmental Ca^{2+} levels are low, these cells undergo proliferation due to an activation of IGF1R-PI3K-Akt-Tor signaling. Deletion of *igfbp5a* blunted the low Ca^{2+} stress-induced IGF signaling and impaired the adaptive proliferation. Reintroducing zebrafish Igfbp5a, but not its ligand binding deficient mutant, restored the adaptive cell proliferation. Likewise, constitutive activation of Akt was sufficient to restore NaR cell proliferation. Expression of human IGFBP5, but not two cancer-associated IGFBP5 mutants, had similar effect. Knockdown

[1] This chapter is published in *Sci Signal*. 2018 Sep 18;11(548), with authors listed as: Chengdong Liu*, Yi Xin*, Yan Bai, Grant Lewin, Gen He, Kangsen Mai, and Cunming Duan. * These authors contributed equally to this work.

of IGFBP5 in human colon carcinoma cells resulted in a similar reduction in IGF-stimulated cell proliferation. These results reveal a conserved mechanism by which a locally expressed Igfbp regulates organismal Ca^{2+} homeostasis and survival by activating IGF signaling in epithelial cells and promoting their proliferation under Ca^{2+} deficient states. These findings underscore the importance of physiological context when analyzing loss-of-function phenotypes of endocrine factors.

2.2 Introduction

Zebrafish live in hypo-osmotic environments and continuously lose Ca^{2+} and other ions into the surrounding water. They constantly take up Ca^{2+} from the aquatic habitat to maintain body Ca^{2+} homeostasis. This vital task is accomplished by a group of epithelial cells called Na^{+}-K^{+}-ATPase-rich (NaR) cells in zebrafish (Hwang, 2009b). NaR cells are functionally equivalent to human intestinal epithelial cells and they contain all major molecular components of the transcellular Ca^{2+} transport machinery, including the epithelial Ca^{2+} channel Trpv5/6 (Flik et al., 1995; Hwang, 2009b). Although distributed in the adult intestine and gills (a major osmoregulatory organ in fish), NaR cells are located on the yolk sac skin during the embryonic and larval stages, making them easily accessible for experimental manipulation and observation (Flik et al., 1995; Hwang, 2009b). When faced with low [Ca^{2+}] challenge, preexisting NaR cells re-enter the cell cycle to yield more cells (Dai et al., 2014a; Liu et al., 2017a). This is considered to be an adaptive response that allows fish to acquire adequate Ca^{2+} to maintain their body Ca^{2+} constant to survive under low [Ca^{2+}] environments (Dai et al., 2014a; Liu et al., 2017a). Ca^{2+} deficiency also stimulates mammalian and human intestinal epithelial cell proliferation (Beaty et al., 1993; Lamprecht and Lipkin, 2003; Mokady et al., 2000; Tu et al., 2004), suggesting an evolutionarily conserved mechanism at work. We have shown that low [Ca^{2+}] stress activates

insulin-like growth factor (IGF) receptor (IGF1R)-mediated PI3 kinase-Akt-Tor signaling in NaR cells exclusively and the increased IGF signaling promotes NaR cells to re-enter the cell cycle and proliferate (Dai et al., 2014a; Liu et al., 2017a). How the IGF signaling is activated specifically in NaR cells under low [Ca^{2+}] stress is not clearly understood.

IGFs are evolutionarily ancient polypeptides structurally related to insulin. IGF binds to and activates the IGF1R, a receptor tyrosine kinase structurally related to the insulin receptor. Unlike insulin, however, IGFs are bound to one of six types of IGF binding proteins (IGFBPs) in extracellular fluids. Binding to an IGFBP increases IGF half-life in the circulation and prevents the potential interaction of IGFs to the insulin receptor (Baxter, 2014; Clemmons, 2016). In addition to these endocrine roles, gain-of-function studies have suggested that IGFBPs can also act locally, both negatively and positively modulating IGF action in target tissues and some IGFBPs have IGF-independent biological activities (Baxter, 2014; Baxter and Twigg, 2009; Clemmons, 2016; Duan and Xu, 2005). Some IGFBPs have been shown to be present in the nucleus and possess nuclear activity (Baxter and Twigg, 2009; Duan and Xu, 2005). Unexpectedly, mice lacking IGFBP-encoding genes do not exhibit major phenotypes. *IGFBP2* knockout mice are phenotypically normal with the exception of minor gender specific changes in bone structure and minor changes in the spleen and liver in adult males (DeMambro et al., 2008; Wood et al., 2000). *IGFBP3* knockout mice are normal in size (Zhao et al., 2006a). Deletion of the *IGFBP4* gene in mice results in a mild 10-15% reduction in prenatal growth, which is somewhat paradoxical given that overexpression of IGFBP4 also reduces growth (Zhao et al., 2006a). *IGFBP5* knockout mice are phenotypically normal (Zhao et al., 2006a). The *IGFBP3*, *4*, and *5* triple knockout mice are viable and only show a 25% reduction in body growth (Zhao et

al., 2006a). Although it was postulated that genetic redundancy and possible changes in other IGFBPs may be responsible for the lack of phenotypes, the underlying mechanism(s) is not clear.

We have previously reported that one of the zebrafish *igfbp* genes, *igfbp5a*, is specifically expressed in NaR cells (Dai et al., 2014a). Knockdown of Igfbp5a using antisense morpholinos decreases the low [Ca^{2+}] stress-induced Akt signaling, suggesting that locally expressed Igfbp5a may be important (Dai et al., 2014a). Because morpholinos only knock down target genes transiently, this approach could not be used to investigate the possible role of Igfbp5a in adaptive NaR cell proliferation nor the long-term biological consequence. More importantly, we now understand that morpholinos have many limitations, including high toxicity and "off-target" effects (El-Brolosy and Stainier, 2017). In this study, we sought to investigate the functional role of Igfbp5a in NaR cells and its long-term functional significance by deletion Igfbp5a using TALEN and CRISPR-Cas9 technology. The *igfbp5a*$^{-/-}$ mutant fish appeared indistinguishable from their wild type siblings when raised in Ca^{2+} rich embryo solutions. When raised in regular water or low Ca^{2+} solutions, however, they died prematurely. Further analyses showed that deletion of Igfbp5a impaired the low [Ca^{2+}] stress-induced NaR cell proliferation and diminished IGF signaling. The diminished IGF signaling and NaR cell proliferation were restored by reintroducing Igfbp5a or human IGFBP5. Further mechanistic analyses suggested that Igfbp5a acts by binding to IGF ligand and activating Akt-Tor signaling in epithelial cells under Ca^{2+} deficient states and this action is conserved in human colon carcinoma cells.

2.3 Results

2.3.1 Deletion of Igfbp5a leads to premature death

Two independent F1 lines were obtained using a TALEN-based approach (Figure 2.1 and Figure 2.2A). Both are predicted to be null alleles. The *igfbp5aΔ4* line harbors a 4 bp deletion allele that introduces a 23-amino acid sequence shortly after the signal peptide. The *igfbp5aΔ11* line contains an 11 bp deletion allele, which truncates Igfbp5a after the signal peptide. F2 progeny from these lines were raised in the standard embryo solution (containing 0.33 mM [Ca^{2+}] and referred as E3 solution hereafter) to 5 days post fertilization (dpf), and transferred to the standard fish system water. Genotyping of adults showed a complete lack of homozygous adult fish in both lines. To determine whether the mutant fish died prematurely, we intercrossed each of the two F1 lines and randomly genotyped their F2 progeny at the larval and adult stages. While 27% of larvae (5 dpf) in the *igfbp5aΔ4* group were homozygous, adult progeny were either heterozygous or wild type (Figure 2.2B). Likewise, none of homozygous *igfbp5aΔ11* fish (20% detected in 3 dpf) survived to 3 months (Figure 2.2B). Among the survived *igfbp5aΔ11* adult fish, 43% were heterozygous (Figure 2.2B). This lower percentage may be related to the fact that the heterozygous fish had a lightly higher mortality rate (See Figure 2.6A).

2.3.2 *igfbp5a*$^{-/-}$ mutant fish develop and grow normally in Ca^{2+}-rich solutions

Because *igfbp5a* mRNA is specifically expressed in NaR cells, which are crucial for Ca^{2+} uptake, we speculated that the mutant fish died due to the deficiency of this essential ion. If this were correct, then raising the progeny in embryo solutions containing high [Ca^{2+}] should rescue the mutant fish because Ca^{2+} can enter through paracellular transport in Ca^{2+} rich solutions. Indeed, when progeny of *igfbp5aΔ4* intercrosses and *igfbp5aΔ11* intercrosses were raised in the 5PPT solution (containing 1.6 mM [Ca^{2+}] and referred as high [Ca^{2+}] solution hereafter), many

mutant fish grew to adulthood (Figure 2.2C). The adult mutant fish in both lines were fertile and morphologically indistinguishable from their siblings. There was no notable difference in the growth rate or speed of development (Figure 2.3A-D). The *igfbp5aΔ11* line, referred as *igfbp5a*$^{-/-}$ mutant fish hereafter, were used in subsequent studies unless otherwise stated.

2.3.3 Deletion of Igfbp5a increases mortality and impairs adaptive NaR cell proliferation

To investigate whether Igfbp5a plays a local role in NaR cell development, we randomly sampled progeny from an *igfbp5a*$^{+/-}$ intercross at various stages. NaR cells were visualized, quantified, and then each fish genotyped individually. There was no difference in the NaR cell number between the *igfbp5a*$^{-/-}$ mutants and their siblings at all stages examined (Figure 2.3E). The expression of *igfbp5aΔ11* mRNA was confirmed (Figure 2.4A). Because of genetic redundancy, genetic compensation and/or transcriptional adaptation can mask what would otherwise be more obvious phenotypes (El-Brolosy and Stainier, 2017), we measured the expression of *igfbp5a*, but found no differences between *igfbp5a*$^{-/-}$ mutant fish and their siblings (Figure 2.4B). No difference was detected in the expression pattern or levels of the paralogous *igfbp5b* between wild-type and *igfbp5a*$^{-/-}$ mutant fish, either (Figure 2.5A and B).

To confirm that *igfbp5a*$^{-/-}$ fish were prone to premature death, we performed a blind, low [Ca^{2+}] challenge test with 5 dpf larvae obtained from an *igfbp5a*$^{+/-}$ intercross. *igfbp5a*$^{-/-}$ mutant fish died earlier and at a significantly greater rate (Figure 2.6A). On 2 and 3 days post low [Ca^{2+}] challenge, *igfbp5a*$^{-/-}$ mutants comprised 66% and 38% of the dead larvae. These values were much greater than the expected 25% according to Mendelian ratio. Similarly, *igfbp5aΔ4* mutant fish died at a significantly greater rate under the low [Ca^{2+}] challenge (Figure 2.7). We hypothesized that the premature death of *igfbp5a*$^{-/-}$ fish was due to Ca^{2+} deficiency in the body. Indeed, Alizarin red staining showed that calcified bone mass in the mutant fish raised in a

solution containing 0.2 mM [Ca^{2+}] (referred as regular [Ca^{2+}] solution because its [Ca^{2+}] is similar to fish system water) was comparable to that of those wild-type fish raised in a solution with 10 folds lower Ca^{2+} levels (Figure 2.6B). Calcified bone mass in *igfbp5a*$^{-/-}$ fish was further reduced by exposure to the lower [Ca^{2+}] solution (Figure 2.6B-C). Increased *trpv5/6* expression is an indication of a Ca^{2+} deficient state in the body (Hwang, 2009b; Liu et al., 2017a). The *igfbp5a*$^{-/-}$ group showed increased *trpv5/6* expression in NaR cells under regular [Ca^{2+}] solution (Figure 2.6D). Low [Ca^{2+}] challenge treatment increased *trpv5/6* mRNA levels in both wild type and *igfbp5a*$^{-/-}$, but the magnitude of increase was significantly greater in the *igfbp5a*$^{-/-}$ group. These results suggest that deletion of Igfbp5a leads to body Ca^{2+} deficiency and low [Ca^{2+}] treatment further exacerbates the Ca^{2+} deficiency.

When acclimated to low [Ca^{2+}] environments, NaR cells undergo proliferation to yield more NaR cells in order to take up sufficient Ca^{2+} for survival (Dai et al., 2014a; Liu et al., 2017a). We tested whether deletion of Igfbp5a impaired this adaptive proliferation response. Visualization of NaR cells by in situ hybridization using a *trpv5/6* probe showed that 48 h low [Ca^{2+}] treatment significantly increased the NaR cell number in the wild type and heterozygous larvae. This increase was blunted in the *igfbp5a*$^{-/-}$ larvae (Figure 2.6E). We next crossed *igfbp5a*$^{-/-}$ fish with *Tg(igfbp5a:GFP)* fish, a transgenic line in which NaR cells are labeled by GFP expression, allowing real-time visualization and quantification of NaR cell division (Liu et al., 2017a). Low [Ca^{2+}] treatment resulted in significant increases in NaR cells in *Tg(igfbp5a:GFP)* larvae at 96, 104, and 120 hpf (Figure 2.6F). This increase was significantly reduced in *igfbp5a*$^{-/-}$*;Tg(igfbp5a:GFP)* larvae (Figure 2.6F). Next, we performed transient knockout experiments in *Tg(igfbp5a:GFP)* fish using a CRISPR/Cas9-based approach (Figure 2.8A). Transient deletion of Igfbp5a using two different sgRNAs significantly decreased NaR cell proliferation under low

[Ca^{2+}], but had no effect under normal [Ca^{2+}] (Figure 2.8B). Therefore, either permanent or transient deletion of Igfbp5a impairs the adaptive proliferation response of NaR cells.

RNA expression analysis showed that among members of the IGF and insulin gene family, *igf2b* is most abundantly expressed in NaR cells followed by *igf2a* (Figure 2.9A). The expression of *igf1*, *insulin a* and *insulin b* was minimal (Figure 2.9A). The strong expression of *igf2b* mRNA in NaR cells was confirmed by double label staining (Figure 2.9B). The two *igf1r* genes and two *insr* genes were all expressed in NaR cells with *igf1ra* being the most abundant one (Figure 2.9A). Low [Ca^{2+}] treatment did not alter the expression of any of the above genes (Figure 2.9A and B).

2.3.4 Deletion of Igfbp5a but not its paralog Igfbp5b impairs low-[Ca^{2+}] stress-induced Akt-Tor signaling in NaR cells

Our previous studies using double label staining have shown that low [Ca^{2+}] treatment induces phosphorylated Akt signaling in NaR cells exclusively (Dai et al., 2014a; Liu et al., 2017a). In agreement with these previous reports, immunostaining analysis revealed that there were few phosphorylated Akt-positive NaR cells on the yolk sac in wild-type larvae under regular [Ca^{2+}] conditions. Low [Ca^{2+}] treatment resulted in a robust increase in NaR cells positive for phosphorylated Akt (Figure 2.10A and B). In comparison, low [Ca^{2+}] treatment resulted in a significantly lower number of NaR cells positive for phosphorylated Akt in *igfbp5a*$^{-/-}$ larvae (Figure 2.10A and B), indicating that deletion of Igfbp5a impairs Akt signaling. Similar results were observed with the phosphorylated S6, an indicator of Tor signaling, although the basal phosphorylated S6 levels were higher (Figure 2.10C and D). In contrast, phosphorylated Erk levels were similar between wild-type and *igfbp5a*$^{-/-}$ larvae under both regular and low [Ca^{2+}] conditions (Figure 2.10E and Figure 2.11). The phosphorylated Erk signal was authentic

because it was abolished by MEK inhibitor treatment (Figure 2.10E and Figure 2.11). As another control, we knocked out the paralogous *igfbp5b* gene using CRISPR-Cas9. Deletion of Igfbp5b did not change the induction of phosphorylated Akt in NaR cells by low [Ca^{2+}] treatment (Figure 2.10F).

2.3.5 Reintroduction of Igfbp5a or constitutively active Akt in NaR cells restores adaptive proliferation

To test whether expression of Igfbp5a was sufficient to activate IGF signaling in NaR cells, zebrafish Igfbp5a, its ligand binding domain (LBD), or nuclear localization signal (NLS) mutants was randomly expressed in NaR cells in *igfbp5a*$^{-/-}$*;Tg(igfbp5a:GFP)* larvae using a Tol2 transposon BAC-mediated genetic mosaic assay (Figure 2.12A and B). NaR cells expressed Igfbp5a were able to proliferate under low [Ca^{2+}] stress and stained positive for phosphorylated Akt (Figure 2.12C and D). NaR cell proliferation in *igfbp5a*$^{-/-}$*;Tg(igfbp5a:GFP)* larvae under low [Ca^{2+}] stress was also restored by the expression of the Igfbp5a NLS mutant, but not by that of the LBD mutant (Figure 2.12C), suggesting that Igfbp5a acts in an IGF-binding dependent manner. If Igfbp5a indeed stimulates NaR cell proliferation by binding to IGFs and activating Akt signaling, then expression of a constitutively active Akt should rescue the defective NaR cell proliferation in *igfbp5a*$^{-/-}$ larvae. Indeed, expression of myr-Akt restored NaR cell proliferation in response to low [Ca^{2+}] stress (Figure 2.12E). Because the Tol2 transposon BAC-mediated genetic mosaic assay only targets the expression of Igfbp5a in a small number of NaR cells randomly, this approach cannot be used to rescue the lethality phenotype.

To test whether IGFBP5 acts in a similar manner in human epithelial cells, human colon carcinoma (LoVo) cells were transfected with a validated siRNA plasmid (pSuperBP5) targeting human IGFBP5 L-domain (Yin et al., 2004). The effect of IGFBP5 knockdown on IGF2-induced

cell proliferation was analyzed by FACS analysis as reported (Dai et al., 2014a). In cells transfected with the empty pSuper plasmid, IGF2 treatment resulted in a significant increase in the percentage of S-phase cells. This increase was abolished in the pSuperBP5 transfected cells (Figure 2.13A), suggesting the endogenous IGFBP5 is required in the proliferative response of these human cells to IGF2 stimulation. To demonstrate the specificity of the siRNA knockdown effect and the sufficiency of IGFBP5, we co-transfected LoVo cells with pSuperBP5 and IGFBP545. The latter contains IGFBP5 N- and C-domain but the L-domain from IGFBP4 and therefore resistant to pSuperBP5 (Yin et al., 2004). The results showed expression of IGFBP545 restored the proliferation response to IGF2 stimulation (Figure 2.13A). To further investigate the function of human IGFBP5 and its mechanism of action in an in vivo setting, we expressed human IGFBP5 and two mutants (G223R and W242*) in NaR cells in *igfbp5a*$^{-/-}$*;Tg(igfbp5a:GFP)* embryos using the genetic mosaic assay (Figure 2.13B). G223R and W242* are two cancer-associated mutations that were speculated to have lost IGF binding ability (Ding et al., 2016). Ectopic expression of wild-type human IGFBP5, but not these mutants, significantly increased NaR cell proliferation under low [Ca^{2+}] stress (Figure 2.12D). These results suggest that human IGFBP5 acts by binding to the IGF ligand and promoting IGF action in human LoVo cells.

2.4 Discussion

IGFBP5 is the most conserved member of the IGFBP family (Baxter and Twigg, 2009; Duan and Xu, 2005). There is a host of in vitro and overexpression studies in the literature indicating its action in inhibiting, potentiating IGF actions, or acting as a growth factor by itself in mammalian cells (Baxter, 2014; Baxter and Twigg, 2009; Clemmons, 2016; Duan and Xu, 2005). In spite of these findings, *IGFBP5* deficient mice do not have overt phenotypes (Ning et

al., 2007). In this study, we showed that genetic deletion of zebrafish Igfbp5a causes body Ca^{2+} deficiency and premature death under regular laboratory conditions. The *igfbp5a*$^{-/-}$ mutant larvae exhibited clear and specific defects in NaR cell adaptive proliferation under Ca^{2+} deficient conditions. These results reveal a critical role of Igfbp5a in regulating organismal survival and Ca^{2+} balance by promoting NaR cell proliferation under low Ca^{2+} states.

It was postulated that the lack of phenotype in *IGFBP5* null or other *IGFBP* null mice might be due to the greater genetic redundancy in the mouse model (Duan and Xu, 2005). We now realize that the phenotype gap is widely present among a wide range of organisms, including zebrafish. Recent advances in CRISPR-Cas9 and TALEN make deleting and editing genes increasingly easy and versatile. While great progress has been made, many cases have been reported in which permanent deletion of gene(s)-encoding various hormones and growth factors, including many that were previously thought to be critical or even essential, show no notable phenotypic changes (Allard and Duan, 2018; El-Brolosy and Stainier, 2017; Ewen-Campen et al., 2017; Liu et al., 2017b; Tang et al., 2015). Genetic studies in zebrafish have also found major discrepancies in phenotypes between permanent genetic knockout and transient knockdowns (Anderson et al., 2017; Kok et al., 2015; Rossi et al., 2015; Zhang et al., 2016). Several additional mechanisms, including genetic compensation, transcriptional adaptation, and altered mRNA processing, have been proposed to account for the lack of phenotypes in permanent genetic mutants (Anderson et al., 2017; El-Brolosy and Stainier, 2017). These mechanisms cannot fully explain the findings of this study. The zebrafish genome contains 9 *igfbp* genes due to a teleost-specific genome wide duplication event (Daza et al., 2011). One could argue that zebrafish may have a greater genetic redundancy than mice. For example, there are two *igfbp5* genes, *igfbp5a* and *igfbp5b* in zebrafish compared to a single *IGFBP5* gene in

mice and humans (Dai et al., 2010). Nevertheless, our genetic data showed that permanent deletion of Igfbp5a compromised the adaptive NaR cell proliferation response and led to low body Ca^{2+} contents and premature death. We did not detect any sign of non-sense-mediated mRNA decay of *igfbp5a* mRNA nor observe compensatory increases in the paralogous *igfbp5b* expression in the *igfbp5a*$^{-/-}$ mutant fish. We showed that transient deletion of Igfbp5a resulted in similar defects in NaR cells. A key and interesting finding made in this study is that the phenotypes of the *igfbp5a*$^{-/-}$ mutant fish were context-dependent. When raised in [Ca^{2+}] rich solutions, however, *igfbp5a*$^{-/-}$ mutant fish grew to the adult stage and appeared indistinguishable from their siblings. When raised in low [Ca^{2+}] solutions, they showed specific defects in adaptive NaR cell proliferation and died prematurely. These context-dependent phenotypes were specific because no such changes were found in the *igfbp5b*$^{-/-}$ mutant fish. Our findings underscore the importance of physiological context in genetic dissection of the highly redundant endocrine signaling network.

The role of IGF signaling in regulating global growth and development is well established (Baker et al., 1993; Liu et al., 1993). IGF signaling also exerts many cell type-specific and context-dependent actions (Clemmons, 2016). How the IGF signaling system exerts these cell-type specific and context-dependent actions is not well understood. In this study, we showed that genetic deletion of Igfbp5a, but not the closely related Igfbp5b, reduced IGF1R-mediated Akt and Tor signaling in NaR cells specifically and in a Ca^{2+} concentration-dependent manner. Re-introducing Igfbp5a was sufficient to activate Akt signaling in the mutant NaR cells and restore their proliferation. Importantly, knockdown of IGFBP5 abolished the human LoVo cell proliferation response to IGF2 stimulation. Re-expression of a siRNA resistant form of IGFBP5 restored the mitotic response to IGF2 stimulation. These results reveal a conserved

mechanism by which a locally expressed IGFBP activates the IGF signaling in a cell-type specific and context-dependent manner.

Mammalian cell culture studies suggest that IGFBP5 has several modes of actions. When added to cultured human or rodent cells together with IGF1 or IGF2, IGFBP5 inhibits IGF-induced cell proliferation and/or differentiation (Conover and Kiefer, 1993; Dai et al., 2010; Ding et al., 2016; Kiefer et al., 1992; Schneider et al., 2001). IGFBP5 can also potentiate IGF-induced cell proliferation and/or survival (Andress and Birnbaum, 1991; Bautista et al., 1991; Duan and Clemmons, 1998; Mohan et al., 1995; Ren et al., 2008). IGFBP5 has also been shown to possess IGF-independent activities (Baxter, 2014; Baxter and Twigg, 2009; Clemmons, 2016; Duan and Xu, 2005). Mammalian IGFBP5 is detected in the nucleus and has nuclear activity (Xu et al., 2004; Zhao et al., 2006b). The nuclear localization and action is also observed in zebrafish (Dai et al., 2010). How IGFBP5 acts in vivo under a physiological context has not been reported. In this study, we elucidated the mechanism of Igfbp5a action using genetic mosaic assays. The results showed that Igfbp5a acts by binding to IGF ligand and activating Akt-Tor signaling in NaR cells because the LBD mutant lacked the activity to stimulate NaR cell proliferation. Mutation of the NLS of Igfbp5a had no effect on its ability, suggesting the nuclear presence is not important for this action of Igfbp5a. The conclusion that Igfbp5a acts through binding to IGFs in NaR cells is further supported by the gene expression analysis results. In the zebrafish genome, there are four IGF ligand genes (*igf1, igf2a, igf2b, and igf3* (also known as *igf1b*) and two *igf1r* genes due to a teleost linage-specific genome duplication (Maures et al., 2002; Schlueter et al., 2006; Zou et al., 2009). Both *igf1r* genes were detected in NaR cells with *igf1ra* more abundant. Future studies will be needed to determine whether Igfbp5 acts by binding to Igf2b to activate Igf1ra and/or Igf1rb in NaR cells. Mammalian cell culture and biochemical

studies suggest that IGFBP5 can potentiate IGF action by bringing IGF ligand to the IGF1R through the proteolysis of IGFBP5 or association with the cellular membrane or extracellular matrix proteins (Conover and Oxvig, 2017; Mohan et al., 1995; Schmid et al., 1996). Whether these mechanisms are involved in Igfbp5a action in NaR cells need to be elucidated in the future.

Aberrant regulation or mutations of key components in the IGF-PI3 kinase-AKT-TOR signaling pathway have been linked to major human diseases including cancers (Manning and Toker, 2017). In colon cancers, for example, several genes belonging to this pathway are mutated (Massoner et al., 2010). These mutations result in increased *IGF2* gene expression, increased PIK3CA and PIK3R1 activity, reduced *PTEN* expression or activity (Sood et al., 2012). Ding et al. (Ding et al., 2016) has identified over 20 non-synonymous mutations for IGFBP5 in cancer, including several frame-shift and non-sense mutations. While some of these mutations were evaluate in culture human cells, none was tested in an in vivo setting. Because the IGF-PI3K-Akt-Tor pathway is highly conserved and activation of this pathway is both required and sufficient for NaR cell proliferation, the zebrafish larvae-NaR cell system provides an excellent in vivo platform for functional analysis of these cancer-associated mutations. As a proof-of principle experiment, we compared the activities of two cancer-associated IGFBP5 mutations G223R and W242* with wild-type IGFBP5. While IGFBP5 was able to stimulate NaR cell proliferation in vivo, both mutants lost this biological activity. These results provided in vivo evidence supporting the idea that IGFBP5 G223R and W242* have lost IGF binding ability (Ding et al., 2016).

In summary, the findings in this study reveal a conserved mechanism by which a locally expressed Igfbp regulates organismal Ca^{2+} homeostasis and survival by activating IGF signaling in epithelial cells and promoting their proliferation under Ca^{2+} deficient states. This type of

regulatory mechanism may not be limited to zebrafish or IGFBP5. Although IGFBP5 knockout mice exhibit normal mammary gland development under standard lab conditions, these animals show delayed mammary gland involution and enhanced alveolar bud formation after ovariectomy followed by estrogen treatment (Ning et al., 2007). In breast cancer cells, doxorubicin-induced senescence increases IGFBP3 expression and cleavage of IGFBP3 prevents cell senescence (Baxter, 2014). In human vascular endothelial cells, hypoxia induced the expression of IGFBP6. The elevated IGFBP6 in turn suppresses angiogenesis as a negative feedback during tumor growth (Zhang et al., 2012). Future studies are needed to identify additional stressful or disease conditions that different IGFBPs respond to and to determine whether regulation of IGF signaling locally by IGFBPs is a widespread mechanism.

2.5 Materials and methods

Ethics statement

All experiments were conducted in accordance with the guidelines approved by the Institutional Committee on the Use and Care of Animals, University of Michigan.

Zebrafish husbandry and embryo rearing media with different Ca^{2+} concentrations

All zebrafish lines were raised and crossed according to zebrafish husbandry guidelines (61). Embryos were obtained by natural cross and staged following Kimmel et al. (Kimmel et al., 1995a). Several embryo rearing media were used. A standard solution containing 0.33 mM [Ca2+], referred as E3 solution, was prepared as described in Zebrafish Book (Westerfield, 2000b). A solution containing high centration of Ca2+ (1.6 mM [Ca2+]), referred as 5PPT high [Ca2+] solution, was prepared by dissolving 5 g Instant Ocean® salt in 1000 ml distilled water.

Two embryo rearing solutions containing either 0.2 mM [Ca2+] (referred to as regular [Ca2+] solution) or 0.001 mM [Ca2+] (referred to as low [Ca2+] solution) were prepared as previously reported (Dai et al., 2014a). To inhibit pigmentation, 0.003% (w/v) N-phenylthiourea (PTU) was added to these solutions.

Chemicals and reagents

Reagents were purchased from Fisher Scientific (Pittsburgh, PA, USA) unless stated otherwise. The MEK inhibitors (U0126 and PD98059), Phospho-Akt, Phospho-S6, and Phospho-Erk antibodies were purchased from Cell Signaling Technology (Danvers, MA, USA). Restriction enzymes were bought from New England BioLabs (Ipswich, MA, USA). Primers, cell culture media and supplements, the TRIzol reagent, M-MLV reverse transcriptase, and Alexa Fluor 488 Tyramide SuperBoost Kit were bought from Invitrogen (Carlsbad, CA, USA). Cas9 protein was purchased from ToolGen (Seoul, South Korea). Calcein and Alizarin Red S was purchased from Sigma (St. Louis, MO, USA). Anti-Digoxigenin-POD and Anti-Digoxigenin-AP were purchased from Roche (Basel, Switzerland).

Generation of *igfbp5a* mutant line using TALEN

TALEN target sites were designed following published criteria (Bedell et al., 2012) and shown in Supplemental Fig. 1A. TALEN constructs were assembled using a Golden Gate cloning strategy following a published protocol (Cermak et al., 2011). The assembled plasmids were determined by StuI and AflII digestion and confirmed by DNA sequencing.

TALEN capped mRNA was synthesized by in vitro transcription using T3 polymerase (Ambion mMessage mMachine kit, Austin, TX) and injected into embryos at the 1-cell stage.

After confirming indels using T7E1 assays in a subset of pooled F0 embryos, the remaining F0 embryos were raised to adulthood and crossed with wild type fish. F1 fish were raised and caudal fin was severed and genotyped as described below. Positive F1 fish were subjected to DNA sequencing. The F1 adult fish were intercrossed and the progeny were raised and genotyped as described below. To obtain the viable homozygous fish, progeny from the F1 intercrosses were raised in the 5PPT high [Ca^{2+}] solution in the first month and then transferred into the fish system.

Transient and stable knockout of *igfbp5a* and *5b* genes using CRISPR/Cas9

Two sgRNAs targeting *igfbp5a* exon 1 and 2 sgRNAs targeting *igfbp5b* exon 1 were designed using the online tool ZiFiT Targeter V4.2 (http://zifit.partners.org/ZiFiT). Their sequences are: *igfbp5a*-sgRNA-1, 5'-GGTGCGGAACGGGTGTCAGGTGG-3' (sense strand, +114 - +136), *igfbp5a*-sgRNA-2, 5'-GTTCCGCACCGGAGGACACATGG-3' (anti-sense strand, +123 - +101), *igfbp5b*-sgRNA-1, 5'-GGTGGGCTGTCAGCTAGTGAAGG-3' (sense strand, +114 - +136), *igfbp5b*-sgRNA-2, 5'-GTGCGAGCCGTGCGATCAGAAGG-3' (sense strand, +66 - +88). These sgRNAs were synthesized by in vitro transcription following a published method (Shao et al., 2014). sgRNAs (30 ng/μl) were mixed with Cas9 protein (700 ng/μl) or mRNA (250 ng/μl) and co-injected into *Tg(igfbp5a:GFP)* or wild type embryos at the 1-cell stage. The injected embryos were raised in E3 solution until 72 hpf and transferred to either the regular or low [Ca^{2+}] solution. NaR cells were quantified at 120 hpf as previously reported (Liu et al., 2017a). To generate the *igfbp5b* mutant line, F0 fish were screened using T7E1 assays with the following primers, *igfbp5b*-gt-F, 5'-AACCCCAACCTGTGTTTTCA-3',

igfbp5b-gt-R, 5’-GATACAAACCACCGCACCCA-3’. *igfbp5b* homozygous mutants were obtained following the cross strategy described above.

Genotyping

To isolate genomic DNA, pooled embryos or individual adult caudal fin were incubated in 50 μl NaOH (50 mM) at 95 °C for 10 min and neutralized by adding 5 μl 1M Tris-HCl (pH 8.0). T7E1 assay and heteroduplex motility assay (HMA) were carried out as reported (Zhu et al., 2014). For T7E1 assays, PCR was performed using following primers: *igfbp5a*-TAL-nF, 5’-GAACGCTGTTCGCTTGAT-3’, *igfbp5a*-TAL-nR, 5’-CGCAGTCCTCGTCCACAT-3’. For HMA assays, PCR was performed using following primers: *igfbp5a*-HRMA1-F, 5’-GTGGCATTTGTATGGGGACT-3’, *igfbp5a*-HRMA2-R: 5’-AGGTCAAGCAGCATCCGCA-3’.

Individual genotyping was carried out as previously reported (Dai et al., 2014a). Briefly, after immunostaining or in situ hybridization analysis, each embryo/larva was washed with 1xPBST twice and methanol 3 times. They were air-dried overnight. Then, each embryo/larva was digested in 100 μl SZL buffer (50mM KCl, 2.5mM $MgCl_2$, 10mM Tris-HCl pH 8.3, 0.45% NP-40, 0.45% Tween-20, 0.01% Gelatine) containing 100 μg/ml proteinase K for 1h at 60°C. The reaction was stopped by 15 min heat treatment (95°C). After spinning at 10,000 rpm for 1 min, the supernatant was used as template for PCR followed by HMA assay as reported (Zhu et al., 2014).

Zebrafish larva survival experiments

For survival experiments, embryos/larvae of different genotypes were raised in E3 solution to 72 or 120 hpf. They were then transferred to the low [Ca^{2+}] solution. Dead larvae were collected daily and genotyped individually.

Morphology analysis

Body length is defined as the curvilinear distance from the head to the end of caudal tail. Somite number and head-trunk angles were measured manually (Kamei et al., 2011; Liu et al., 2014). To visualize the bone morphology, calcein and Alizarin red staining were performed following a published protocol (Du et al., 2001). For calcein staining, juvenile fish were immersed in the calcein staining solution for 10 min. Then, they were washed 3 times in E3 solution to remove residual calcein. Images were captured with a stereomicroscope (Leica MZ16F, Leica, Wetzlar, Germany) equipped with a QImaging QICAM camera (QImaging, Surrey, BC, Canada).

qPCR, whole-mount in situ hybridization, and immunostaining

Total RNA was isolated using TRIzol reagent (Invitrogen). RNA samples were treated with DNase I to remove DNA. One microgram of RNA was reverse transcribed to single-strand cDNA using M-MLV (Promega, Madison, WI) and oligo$(dT)_{18}$ primer. RT-PCR was performed using Taq DNA polymerase (New England Biolabs). qPCR was carried out using SYBR Green (Bio-Rad, Hercules, CA) on a StepONE PLUS real-time thermocycler (Applied Biosystems, Foster City, CA). Primers for qPCR used in this study are shown below. *igfbp5a*: 5'-GCTGCACGCTCTGCTTTAC-3' and 5'-AATGGAACCTTGGCCTGAG-3'; *igfbp5b:* 5′-GGGAGTGTGTACGAACGAGAA-3′ and 5′-TCCTGTCACAGTTAGGCAGGTA-3′; *trpv5/6*:

5'- GGACCCTACGTCATTGTGATAC-3' and 5'- GGTACTGCGGAAGTGCTAAG-3'; *β-actin*: 5'-GATCTGGCATCACACCTTCTAC-3' and 5'-CCTGGATGGCCACATACAT-3'.

Whole-mount in situ hybridization and immunostaining were performed as previously reported (Dai et al., 2014a). For double staining of in situ hybridization and immunostaining, *mCherry* or *igfbp2b* mRNA were detected using digoxigenin (DIG)-labeled antisense riboprobes (Zou et al., 2009). The *mCherry* signal was detected using anti-DIG-POD antibody (Roche), followed by Alexa 488 Tyramide Signal Amplification (Invitrogen). The *igfbp2b* signal was detected using anti-DIG-AP antibody (Roche), followed by NBT/BCIP staining. After in situ hybridization analysis, the stained larvae were washed in 1xPBST and incubated with pAkt or GFP antibody overnight at 4 °C. Next, they were stained with a Cy3 conjugated Goat anti-Rabbit IgG antibody (Jackson ImmunoResearch, West Grove, PA). Fluorescent images were acquired using a Nikon Eclipse E600 Fluorescence Microscope with PMCapture Pro 6 software.

Plasmid and BAC constructs

The construction of the Igfbp5a expression plasmid has been reported (Dai et al., 2014a). This plasmid was used as a template to generate Igfbp5a nuclear localization signal (NLS) and ligand binding domain (LBD) mutants. For the NLS mutant, the ^{236}KGRK^{239} motif in Igfbp5a C-domain was changed to LDGQ, the corresponding sequence of zebrafish Igfbp1a (Maures and Duan, 2002) by site-directed mutagenesis (Supplemental Table 1). For the LBD mutant, the sequence ^{86}KPLLL^{92} in Igfbp5a was mutated to NQQQQ (Zhong et al., 2011). Next, human IGFBP5 G223R and IGFBP5 W242*, two cancer-associated IGFBP5 mutations (Ding et al., 2016), were generated by site-direct mutagenesis (Supplemental Table 1). The resulting Igfbp5a/IGFBP5 DNAs were cloned into the pIRES2-mCherry using the EcoR1 and BamH1

sites. The pIRES2-mCherry plasmid was engineered by replacing the DsRed-Express2 cassette in the pIRES2-DsRed-Express2 plasmid with mCherry using the BstX1 and Not1 sites. The Igfbp5a/IGFBP5-IRES2-mCherry-KanR cassette DNAs were amplified by PCR using primers listed in Supplemental Table 1. They were inserted into the *igfbp5a BAC* construct (Liu et al., 2017a) to replace the *igfbp5a* sequence from the start codon to the end of the first exon through homologous recombination. The resulting BAC DNA was validated by DNA sequencing using primers shown in Supplemental Table 1. The validated *BAC(igfbp5a:Igfbp5a/IGFBP5-mCherry*) DNA constructs were injected into *igfbp5a*$^{-/-}$*;Tg(igfbp5a:GFP)* embryos at the 1-cell stage. The embryos were raised in the E3 solution until 72 hpf and then subjected to the low [Ca^{2+}] challenge test by transferring into low [Ca^{2+}] solution. Cells co-expressing mCherry and GFP were defined as *igfbp5a/IGFBP5*-expressing NaR cells. They were scored using the scoring system shown in Fig. 5B. A similar cloning strategy was used to generate *BAC(igfbp5a:myr-Akt-mCherry)* plasmids. All these constructs were confirmed by DNA sequencing at the University of Michigan DNA Sequencing Core Facility.

Cell culture, transfection, and flow cytometry analysis

Human colorectal carcinoma (LoVo) cells were purchased from ATCC (Manassas, VA), and cultured in DMEM/F-12 supplemented with 10% FBS, penicillin, and streptomycin in a humidified-air atmosphere incubator containing 5% CO2 at 37°C. LoVo cells were seeded in 6-well plates (Falcon, Corning, NY), and transfected with 2 µg pSuperBP5 or pSuper and 2 µg pCMV-BP545 or pCMV plasmids using Lipofectamine 2000 (Invitrogen). 24 hours post transfection, the cells were washed and incubated with fresh serum-free medium for 8 hours. 400 ng/ml IGF2 was then added. Cells were collected after 3 days of IGF2 treatment. Cell cycle

analysis was carried out using an Attune Acoustic Focusing Cytometer (Applied Biosystems, Life Technologies, Carlsbad, CA) as previously described (Liu et al., 2017a). Briefly, a two-parameter dot-plot of forward scatter (FSC) versus side scatter (SSC) was constructed along with a two-parameter dot-plot of FL2 (PI) area versus FSC area. In addition, a single-parameter FL2 (PI) area histogram was constructed to illustrate relative DNA content in each cell cycle phase.

Statistical analysis

Values are shown as mean ± standard error of the mean (SEM). Statistical significance among experimental groups was determined using unpaired two-tailed t test, one-way ANOVA followed by Tukey's multiple comparison test, Logrank test, or Chi-square test. Statistical significances were accepted at $P < 0.05$ or greater.

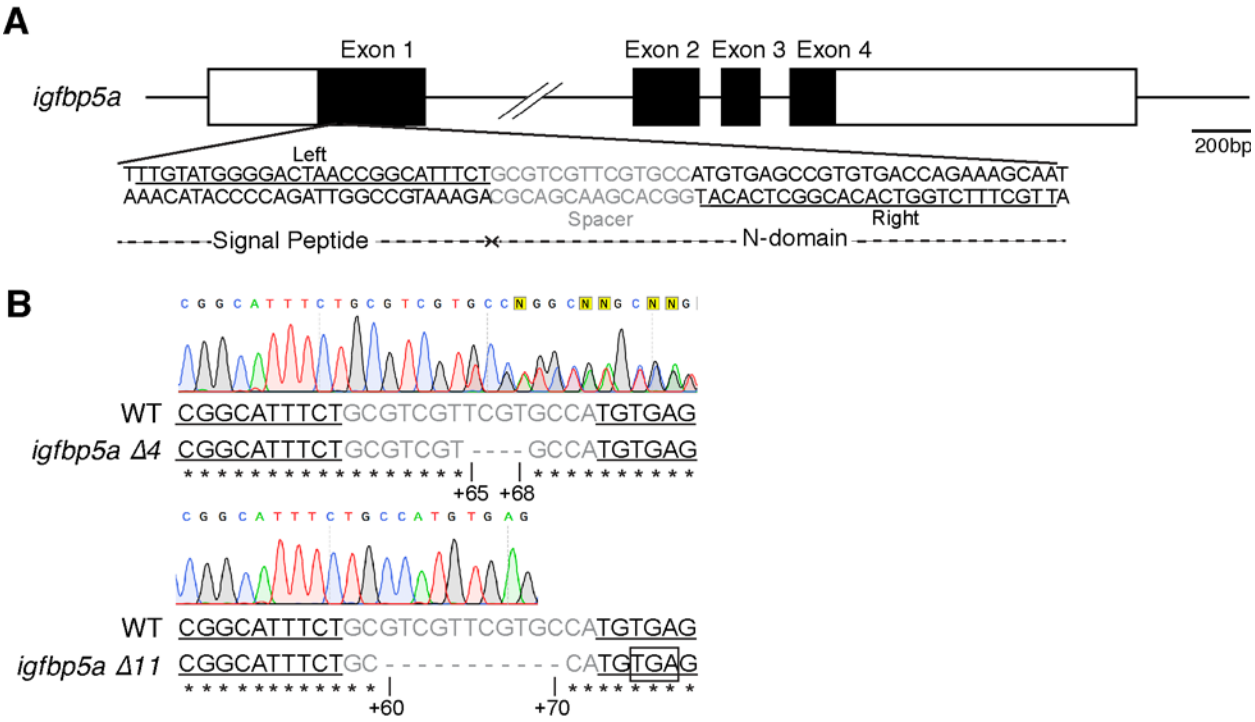

Figure 2.1 Generation of *igfbp5a* mutant fish

(A) Schematic diagram of the *igfbp5a* gene and the TALEN targeting sites. Exons are shown as boxes and introns as lines. Open and filled boxes represent untranslated and protein coding regions, respectively. The TALEN targeting sites are underlined. The spacer sequence is indicated in grey letters. (B) DNA sequence of the indicated zebrafish mutants. Open box indicates premature stop codon.

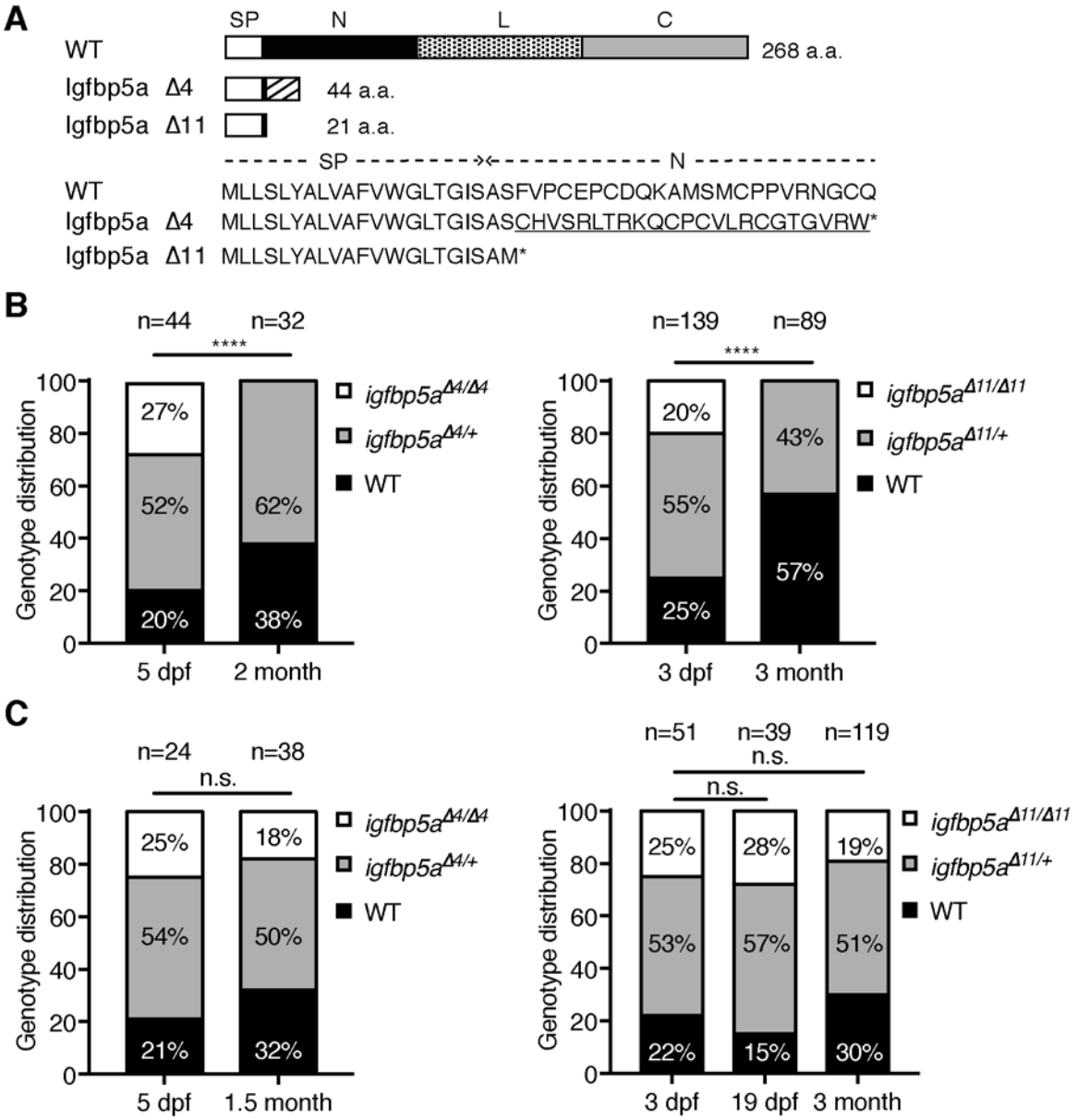

Figure 2.2 Deletion of Igfbp5a leads to premature death

(A) Structure of wild type Igfbp5a (WT), Igfbp5aΔ4, and Igfbp5aΔ11. SP, N, L, and C indicate the signal peptide, N-, Linker-, and C-domain of Igfbp5a. a.a. indicates amino acids and * indicates a stop codon. The underlined amino acids were introduced by a frameshift. (B-C) F2 progeny of *igfbp5a Δ4*$^{+/-}$ intercrosses (left panel) and *igfbp5a Δ11*$^{+/-}$ (right panel) intercrosses were raised in E3 solution until 3 or 5 days post fertilization (dpf) and transferred into either fish

system water (B) or 5PPT high [Ca^{2+}] solution (C). The fish were sampled randomly and genotyped at the indicated stages. The genotype distributions are shown. ****, $P<0.0001$ by chi-square test, n.s., not statistically significant, total number of fish in each group is shown above the bar.

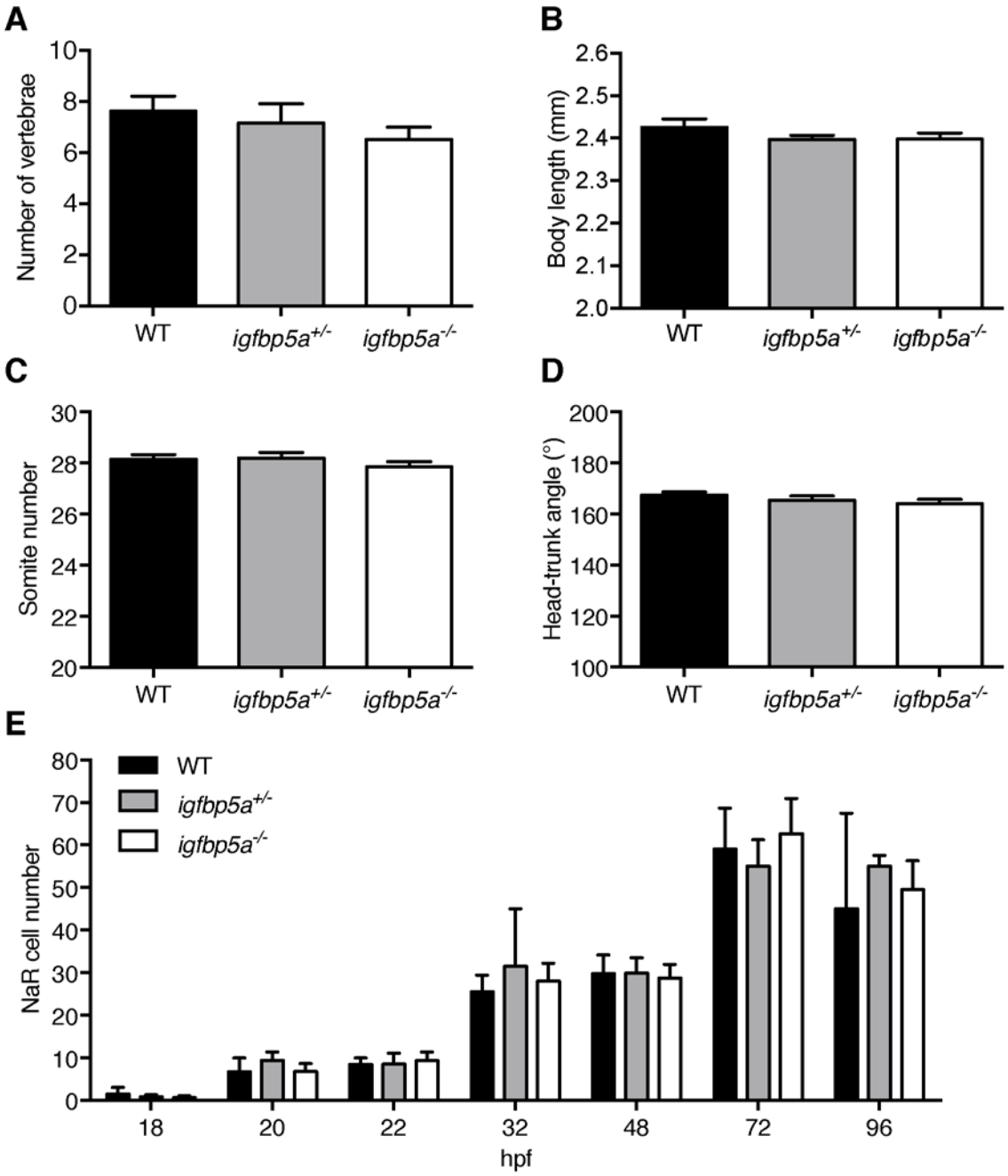

Figure 2.3 The *igfbp5a*$^{-/-}$ mutant fish develop and grow normally in Ca^{2+} rich solutions

(A) Progeny of *igfbp5a*$^{+/-}$ intercrosses were raised in E3 solution until 5 dpf and transferred into high [Ca^{2+}] 5PPT solution. The vertebrate columns of 12 dpf larvae were visualized by calcein staining and quantified. Data shown are means ± SEM. n = 18~19 fish/group. No statistical significance was found among the groups using one-way ANOVA followed by Tukey's multiple

comparison test. (B, C, and D) Embryos of the indicated genotypes were raised in E3 solution. Their body length (B) and somite number (C) was measured at 24 hpf and head-trunk angle (D) measured at 72 hpf. Data shown are means ± SEM. n = 12~73 fish/group. No statistical significance was found using one-way ANOVA followed by Tukey's multiple comparison test. (E) Progeny of *igfbp5a*$^{+/-}$ intercrosses were sampled at the indicated stages. After NaR cells were visualized by in situ hybridization using a *trpv5/6* cRNA probe and quantified, the fish were genotyped individually. Data shown are means ± SEM. n = 6~14 fish/group. No statistical significance was found by one-way ANOVA followed by Tukey's multiple comparison test.

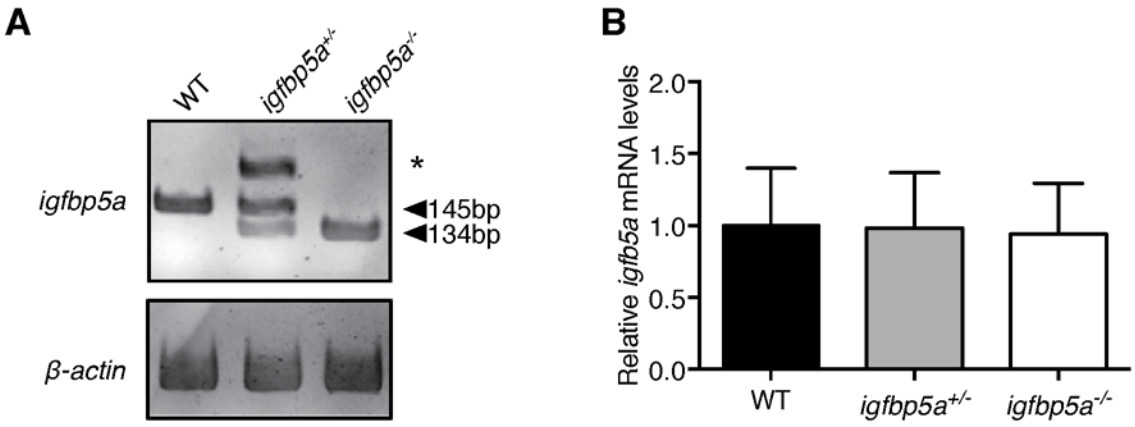

Figure 2.4 *igfbp5a* mRNA levels in mutant fish

(A) Heteroduplex mobility assay (HMA) results are shown. Upper and lower arrowheads indicate the wild-type and mutant homoduplex, respectively. Asterisk indicates the heteroduplex. RNA from 48 hpf embryos of indicated genotype was reversed transcribed to cDNA and used as template. (B) The expression of igfbp5a mRNA in 48 hpf embryos of the indicated genotypes were analyzed by qPCR and normalized by β-actin mRNA levels. Values are means ± SEM of 3 independent experiments, each containing RNA isolated from a pool of 10-15 embryos. No statistical difference was detected by one-way ANOVA followed by Tukey's multiple comparison test.

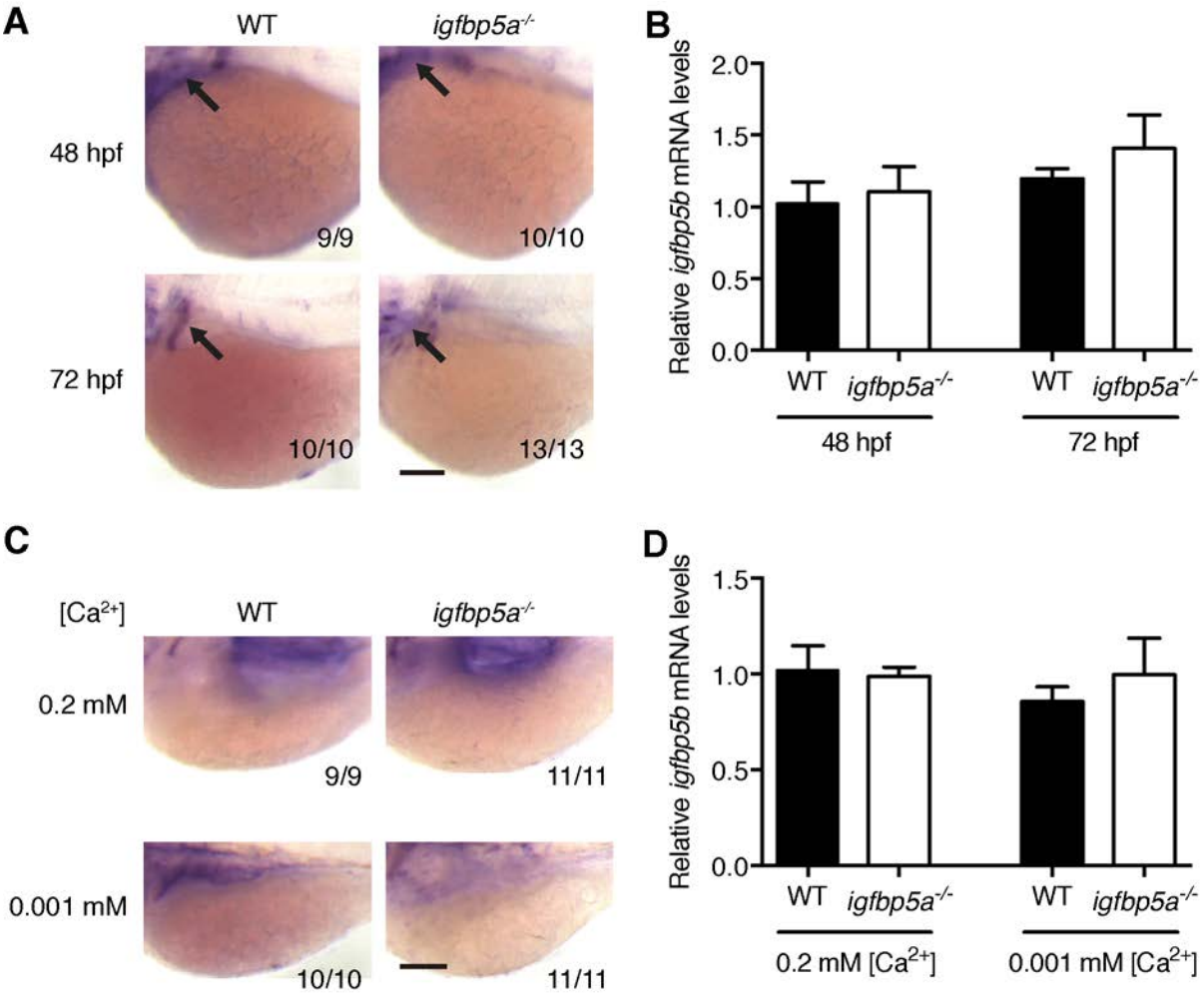

Figure 2.5 Deletion of Igfbp5a does not alter igfbp5b expression

(A) *In situ* hybridization analysis of *igfbp5b* in wild-type and *igfbp5a*$^{-/-}$ mutant larvae at the indicated stages. Arrows, arrowheads, and asterisk indicate signals in the neural tissues, pharyngeal arches, and pectoral fin, respectively. Scale bar = 0.1 mm. The frequency of larvae with the indicated expression patterns is shown in the bottom right corner in each panel. (B) No *igfbp5b* expression is detected in the yolk sac region in either wild-type or *igfbp5a*$^{-/-}$ mutant larvae. Arrowheads point to signals in the pharyngeal arches. Scale bar=0.1mm. (C) The expression of igfbp5b in fish of the indicated genotypes and stages was analyzed by qPCR and normalized by the β-actin levels. Values are means ± SEM of 3 independent experiments, each

containing RNA isolated from a pool of 20 embryos. No statistical difference was found by one-way ANOVA followed by Tukey's multiple comparison test. (D) Wild-type and *igfbp5a*$^{-/-}$ mutant embryos were raised in E3 solution to 72 hpf and transferred to the solutions with the indicated Ca^{2+} concentrations. After 48 hours, they were analyzed by qPCR analysis. The igfbp5b mRNA levels were normalized to β-actin mRNA levels. Values are means ± SEM of 3 independent experiments, each containing RNA isolated from a pool of 20 larvae. No statistical difference was found by one-way ANOVA followed by Tukey's multiple comparison test.

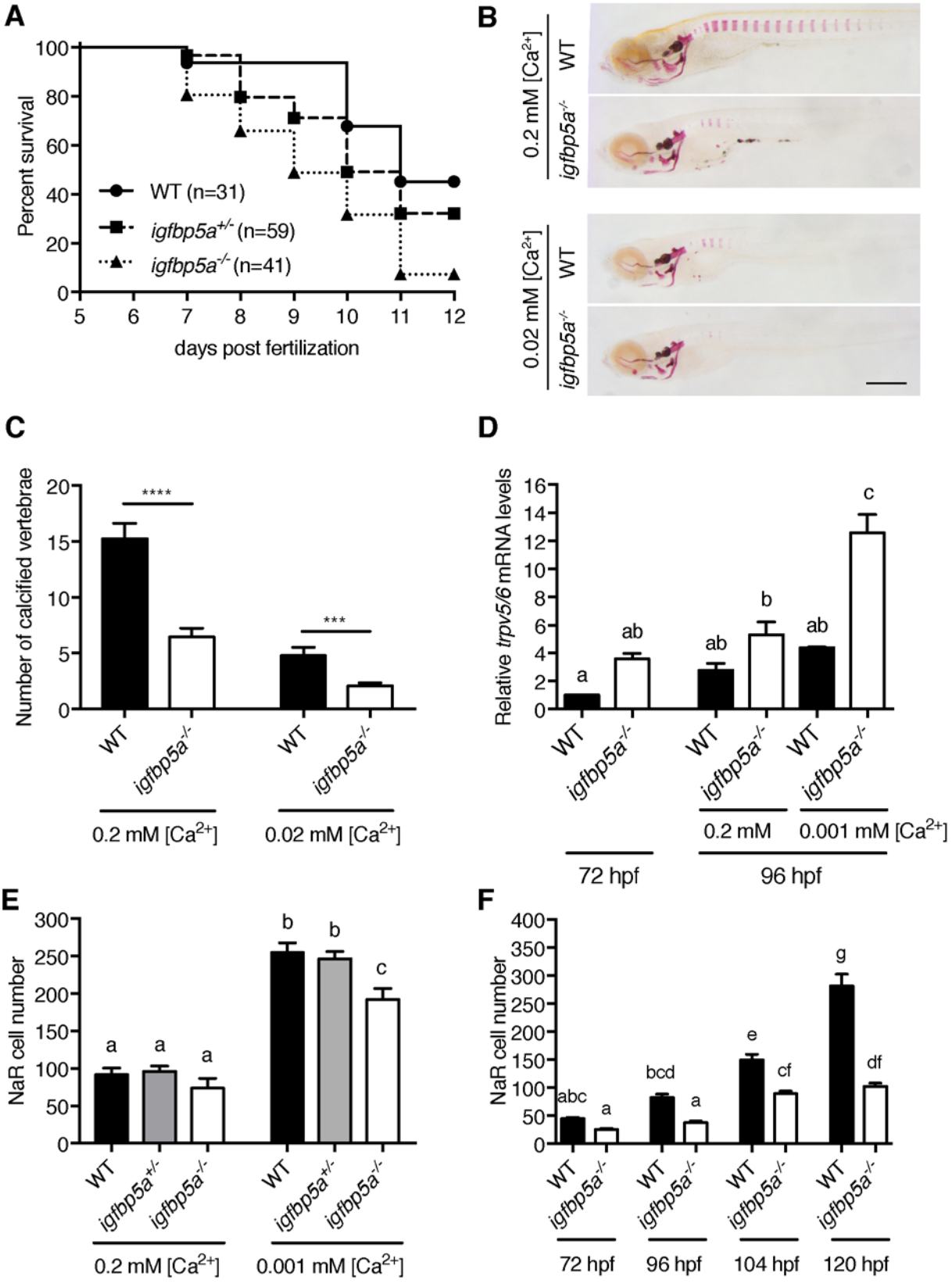

Figure 2.6 Deletion of Igfbp5a increases mortality and impairs adaptive NaR cell proliferation

(A) Progeny of *igfbp5a*$^{+/-}$ intercrosses were raised in E3 solution until 5 dpf and transferred into low [Ca^{2+}] solution. Dead larvae were collected daily and genotyped. The survival curve is shown and the numbers of fish are indicated. P<0.0001 by Logrank test. (B and C) Fish of the indicated genotypes were raised in solutions containing the indicated Ca^{2+} concentration to 11 dpf and stained by Alizarin red. Representative images are shown in (B) and the average number of calcified vertebral columns shown in (C). n = 19~29 fish/group, ***, P<0.001. ****, P<0.0001, unpaired two-tailed t test. Scale bar = 0.5 mm. (D) Embryos of the indicated genotypes were raised in E3 solution till 72 hpf and transferred to solutions containing the indicated Ca^{2+} concentration. The expression of *trpv5/6* mRNA was measured by qPCR and normalized to the NaR cell number at the corresponding time point and treatment. Values are means ± SEM of 3 independent experiments, each containing RNA isolated from a pool of 20 larvae of the indicated stages. Different letters indicated statistically significant differences (P < 0.05, one-way ANOVA followed by Tukey's multiple comparison test). (E) Progeny of *igfbp5a*$^{+/-}$ intercrosses were raised in E3 solution to 72 hpf and transferred to solutions containing the indicated Ca^{2+} concentration. The fish were sampled at 120 hpf. NaR cells were visualized by in situ hybridization using the *trpv5/6* cRNA probe and quantified. Each larva was genotyped afterwards. Data shown are mean ± SEM, n = 13~40 fish/group. Different letters indicated statistically significant differences (P < 0.05, one-way ANOVA followed by Tukey's multiple comparison test). (F) *Tg(igfbp5a:GFP)* of the indicated genotypes were raised in E3 solution till 72 hpf and transferred to low [Ca^{2+}] solution. The number of GFP-labeled NaR cells was quantified at 72, 96, 104, and 120 hpf. Data shown are mean ± SEM, n = 7~36 fish/group. Different letters indicate significant differences (P < 0.05, one-way ANOVA followed by Tukey's multiple comparison test).

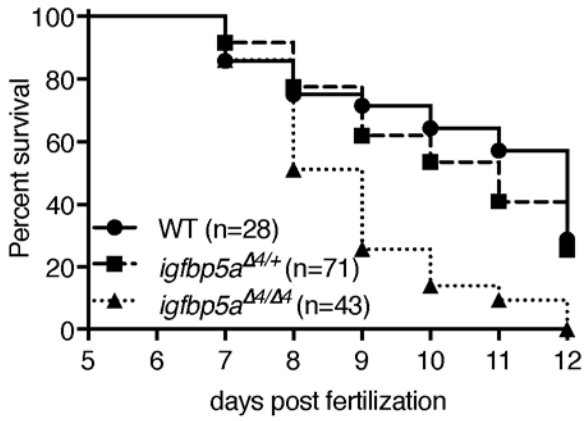

Figure 2.7 *igfbp5a Δ4* mutant fish are prone to dying under low Ca^{2+} stress

Progeny of *igfbp5a*$\Delta 4^{+/-}$ intercrosses were raised in E3 solution until 5 dpf and transferred into the low [Ca^{2+}] solution. Dead larvae were collected daily and genotyped. The survival curve is shown and the total numbers of fish for each genotype are indicated. The *igfbp5a*$\Delta 4^{-/-}$ group was significantly different from the WT and *igfbp5a*$\Delta 4^{+/-}$ groups, $P<0.0001$, Logrank test.

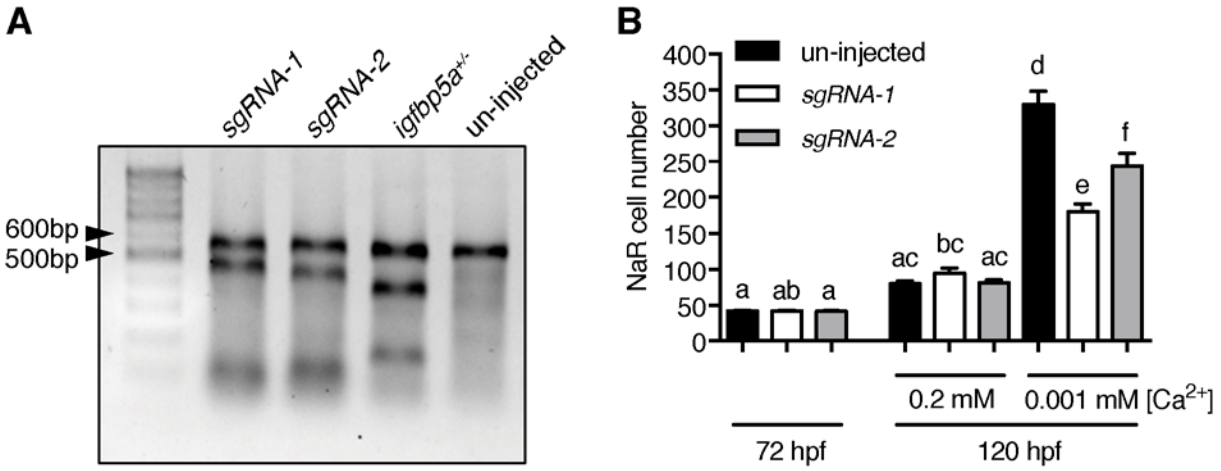

Figure 2.8 CRISPR/Cas9-mediated transient deletion of Igfbp5a impairs adaptive NaR cell proliferation

(A) The *igfbp5a*-targeting sgRNA-1 or -2 were co-injected with Cas9 protein into *Tg(igfbp5a:GFP)* embryos at the 1-cell stage. The injected embryos were raised until 5 dpf in E3 solution and subjected to a T7E1 endonuclease assay. Cleaved bands were observed in sgRNA-1 and sgRNA-2 injected larvae but not the uninjected larvae. Heterozygous *igfbp5a*$^{+/-}$ larvae were used as a positive control. (B) The injected embryos described in (A) were raised in E3 solution until 72hpf and transferred to solutions with the indicated Ca^{2+} concentrations. After 48 hours, GFP-expressing NaR cells were quantified in each fish. Values are means ± SEM. n= 15~41 fish per group. Different letters indicate significant differences among groups ($P < 0.05$). One-way ANOVA followed by Tukey's multiple comparison test.

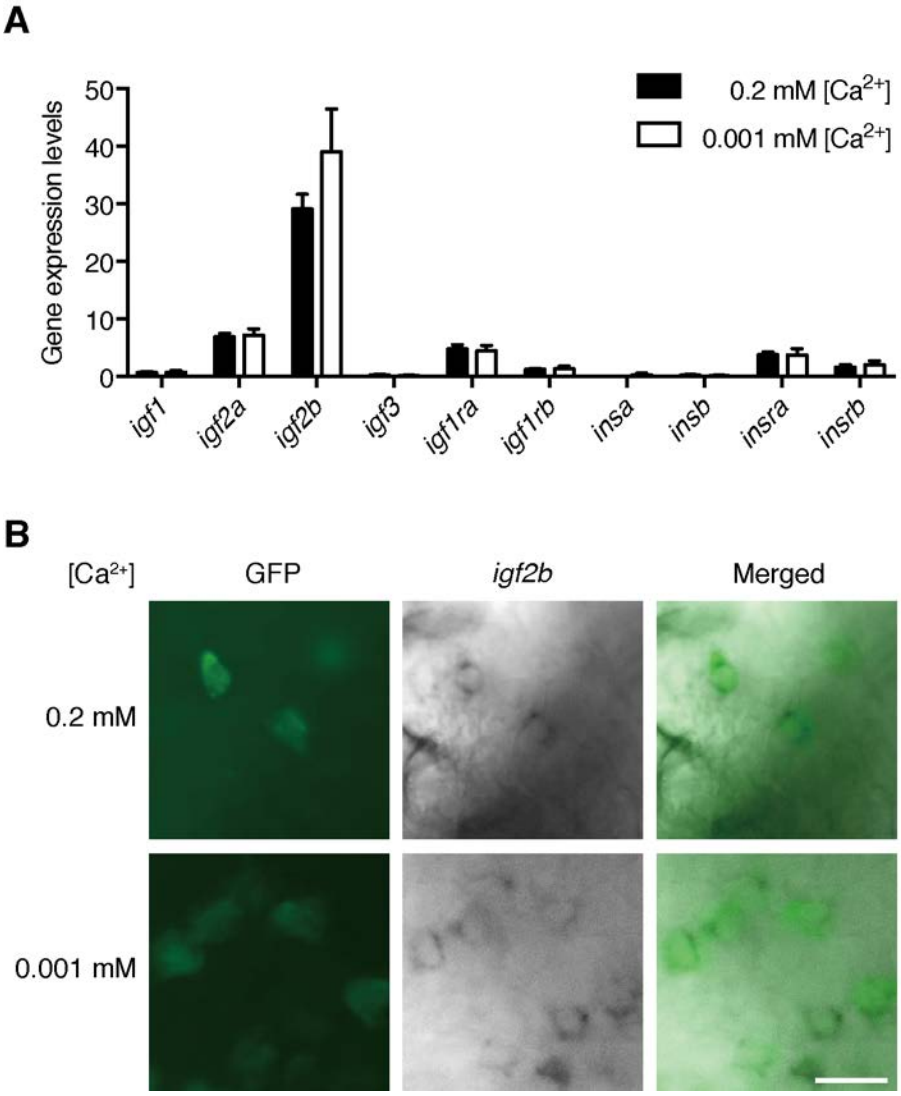

Figure 2.9 Expression of IGF and insulin ligand and receptor genes in NaR cells

(A) *Tg(igfbp5a:GFP)* embryos were raised in E3 solution to 72 hpf and transferred to solutions with the indicated Ca^{2+} concentrations. After 18 hours, NaR cells were sorted by FACS and mRNA levels of the indicated genes were measured. Values are mean ± SEM, n= 4 independent experiments, each containing RNA isolated from FACS-sorted GFP-expressing NaR cells from a pool of more than two hundred embryos. (B) *Tg(igfbp5a:GFP)* larvae (72hpf) were transferred to solutions with the indicated Ca^{2+} concentrations. After 48 hours, they were analyzed by GFP immunostaining (left panel) and in situ hybridization for *igf2b* mRNA (middle panels). Merged

views are shown in the right panels. Representative of 7-12 larvae/group. Scale bar = 20 μm.

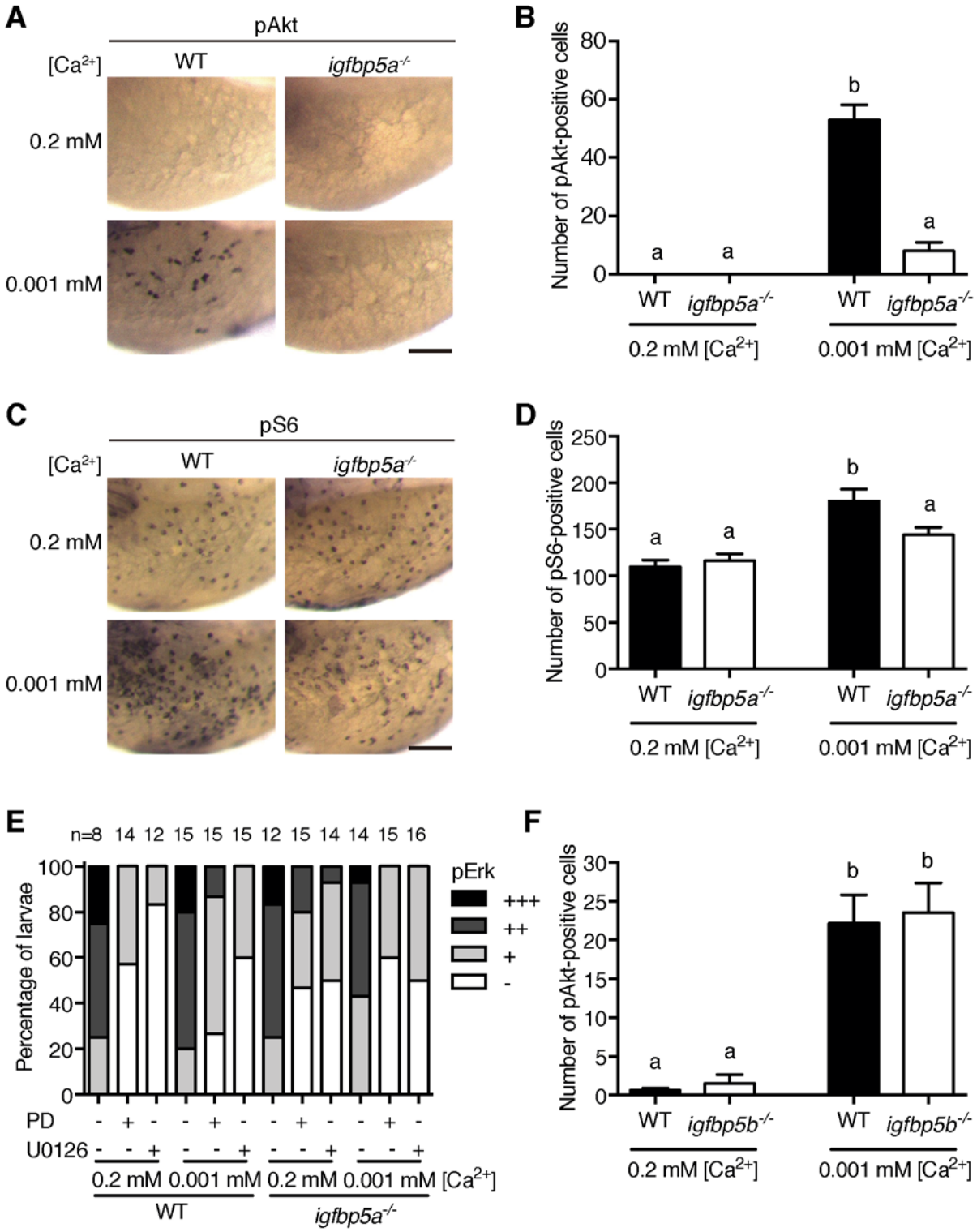
A
pAkt
[Ca2+]
WT
igfbp5a-/-
0.2 mM
0.001 mM
B
Number of pAkt-positive cells
a
a
b
a
WT
igfbp5a-/-
WT
igfbp5a-/-
0.2 mM [Ca2+]
0.001 mM [Ca2+]
C
pS6
[Ca2+]
WT
igfbp5a-/-
0.2 mM
0.001 mM
D
Number of pS6-positive cells
a
a
b
a
WT
igfbp5a-/-
WT
igfbp5a-/-
0.2 mM [Ca2+]
0.001 mM [Ca2+]
E
n=8 14 12 15 15 15 12 15 14 14 15 16
Percentage of larvae
pErk
+++
++
+
-
PD
U0126
0.2 mM 0.001 mM 0.2 mM 0.001 mM [Ca2+]
WT
igfbp5a-/-
F
Number of pAkt-positive cells
a
a
b
b
WT
igfbp5b-/-
WT
igfbp5b-/-
0.2 mM [Ca2+]
0.001 mM [Ca2+]

Figure 2.10 Deletion of Igfbp5a but not its paralog Igfbp5b impairs low [Ca^{2+}] stress-induced Akt-Tor signaling in NaR cells

(A-D). Fish of the indicated genotypes raised in the E3 solution were transferred to solutions containing the indicated Ca^{2+} concentration at 72 hpf. After 24 hours, they were stained for phosphorylated Akt (A and B) or phosphorylated S6 (C and D). Representative images are shown in (A and C). The numbers of cells positive for pAkt or pS6 in each fish were quantified and the quantitative results are shown in (B and D). Values are means ± SEM, n = 6~12 fish/group. Different letters indicate significant differences between groups ($P < 0.05$, one-way ANOVA followed by Tukey's multiple comparison test). (E) Fish of the indicated genotypes were raised in E3 solution to 72 hpf and transferred to solutions containing the indicated [Ca^{2+}] with or without U0126 (10 μM) or PD98059 (10 μM). After 8 hours, they were stained for phosphorylated Erk. The pErk signal was scored following a previously published scoring system (Dai et al., 2014a). Total numbers of fish are shown above the bar. (F) Deletion of Igfbp5b has no effect on Akt signaling. Larvae of the indicated genotypes were raised in E3 solution to 72 hpf and transferred to solutions containing the indicated Ca^{2+} concentration. After 8 hours, they were stained for phosphorylated Akt. The number of cells positive for pAkt was quantified. Values are means ± SEM, n = 13~18 fish/group. Different letters indicate significant differences ($P < 0.05$, one-way ANOVA followed by Tukey's multiple comparison test).

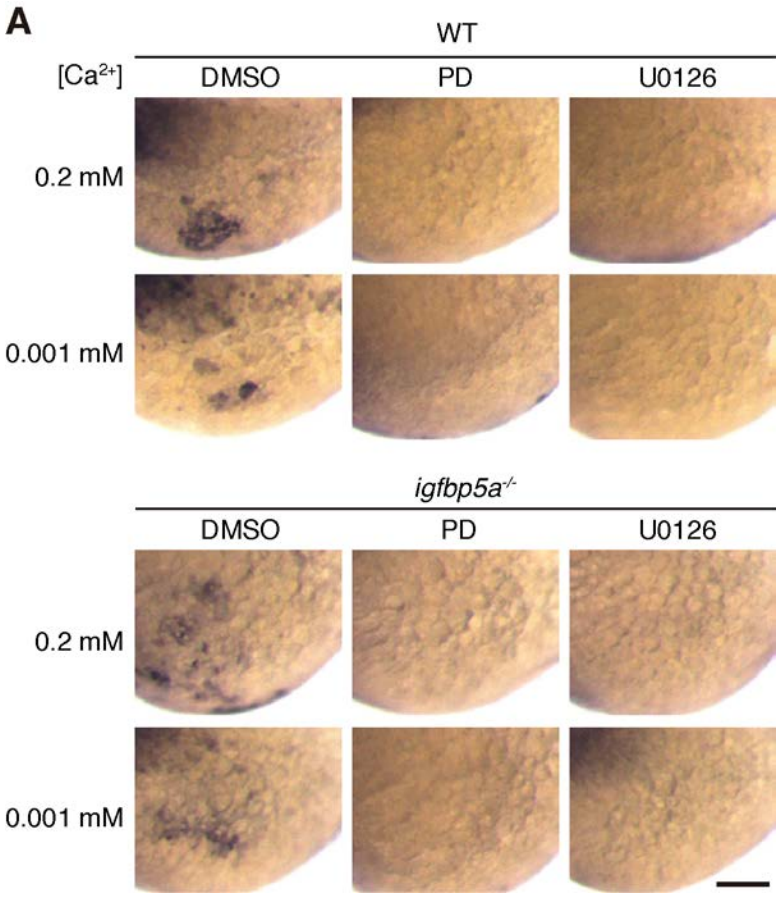

Figure 2.11 Deletion of Igfbp5a has no effect on phosphorylated Erk signaling

Wild-type and *igfbp5a* mutant fish were raised in E3 solution to 72 hpf and transferred to embryo solutions containing the indicated [Ca^{2+}] with or without PD98059 (10 μM) or U0126 (10 μM). After 8 hours, they were stained for pErk. Representative views are shown. The quantified data are shown in Fig. 4E. Scale bar = 0.1 mm.

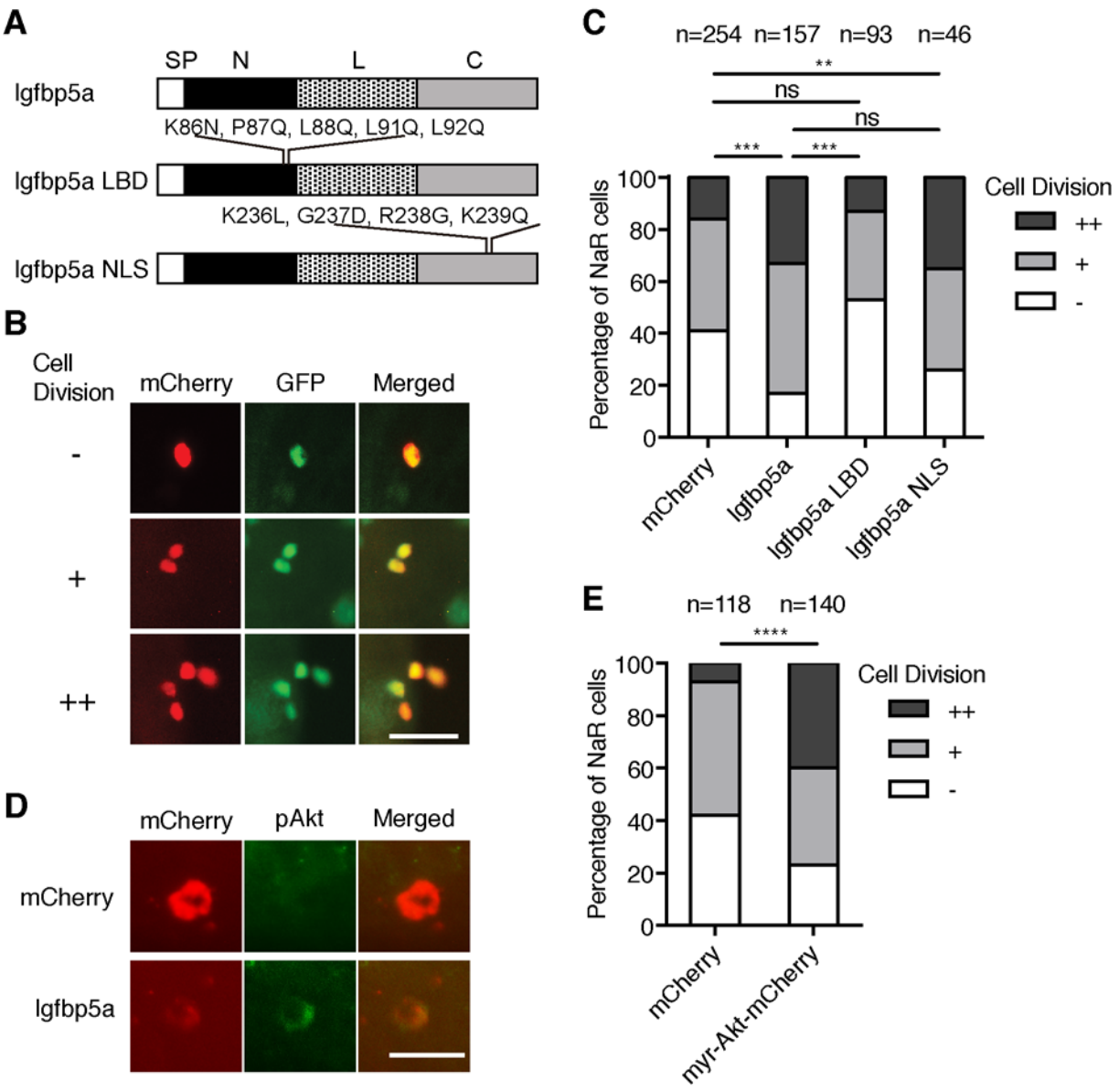

Figure 2.12 Re-introduction of Igfbp5a or constitutively active Akt in NaR cells restores the adaptive proliferation

(A) Structure of zebrafish Igfbp5a and its mutants. SP, N, L, and C domains are indicated. Mutated residues are shown. (B and C) The NaR division scoring system. Zebrafish *igfbp5a*$^{-/-}$*;Tg(igfbp5a:GFP)* embryos injected with the *igfbp5a-IRES-mCherry* BAC constructs containing the indicated genes were raised in E3 solution until 72 hpf and transferred to low [Ca^{2+}] solutions. Igfbp5a expressing NaR cells are labeled by both GFP and mCherry. The NaR

division scoring system is shown in (B). During the 48 hour treatment period, NaR cells that divide 0, 1, or 2 times are scored as -, +, and ++. Scale bar = 0.05 mm. The quantified data is shown in (C). Chi-square test was used for statistical analysis. **, and ***, P< 0.01 and 0.001, n.s. not statistically significant, total numbers of cells are shown above the bar. (D) The larvae described in (B and C) were collected after 24 hours in low [Ca^{2+}] solution and stained for phosphorylated Akt and mCherry in situ hybridization. Scale bar = 0.02 mm. (E) The experiment procedure was the same as in (B and C) except myr-Akt-mCherry BAC DNA was injected into *igfbp5a*$^{-/-}$*;Tg(igfbp5a:GFP)* embryos. Chi-square test was used for statistical analysis. ****, *P*< 0.0001, total numbers of cells are shown above the bar.

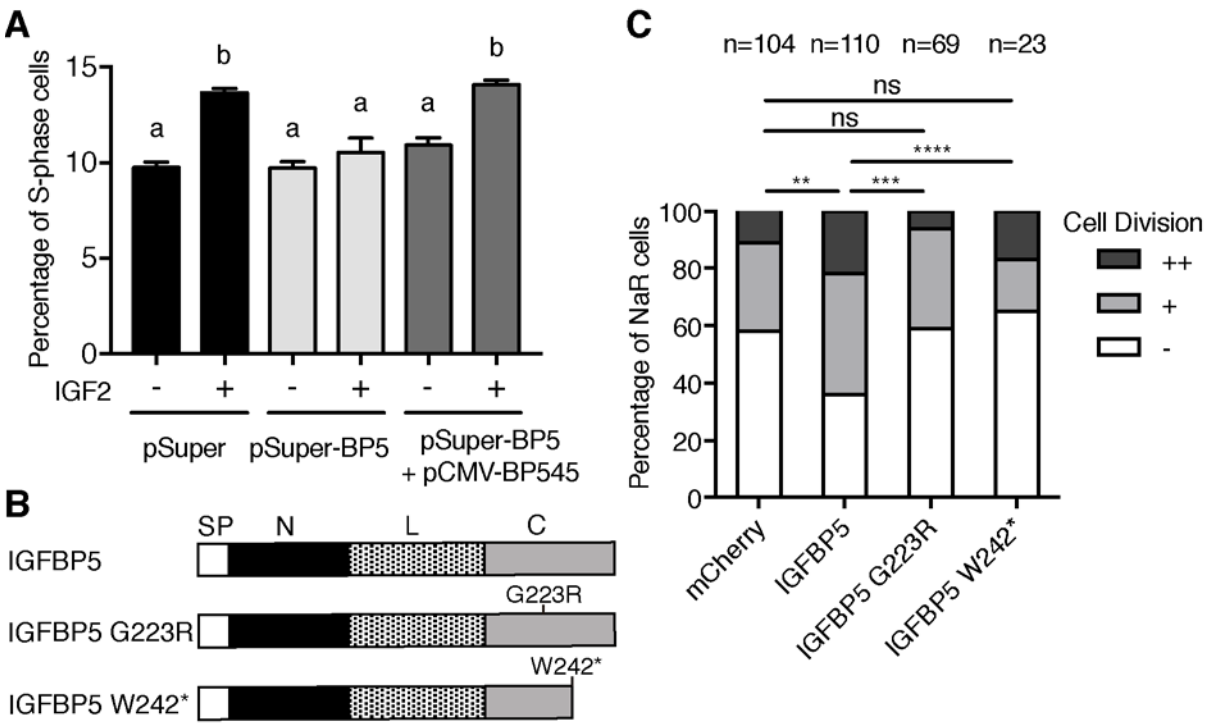

Figure 2.13 IGFBP5 but not two cancer-associated IGFBP5 mutants promotes the mitotic response of human epithelial cells to IGF stimulation

(A) Human LoVo epithelial cells were transfected with the indicated siRNA construct with or without pCMV-BP545. After 24 hours, they were treated with 400 ng/ml human IGF2 for 96 hours and analyzed by flow cytometry. The percentage of S-phase cells is shown. Values shown are mean ± S.E.M., n = 3. Groups labeled with different letters are significantly different from each other (P<0.05, one-way ANOVA followed by Tukey's multiple comparison test). (B) Structure of human IGFBP5 and its two cancer-associated mutants. SP, N, L, and C domains are indicated. Mutated residues are shown. * indicates stop codon. (C) Zebrafish *igfbp5a*$^{-/-}$*;Tg(igfbp5a:GFP)* embryos injected with the indicated human IGFBP5 were raised in E3 solution until 72 hpf and transferred to low [Ca^{2+}] solution. 48 hours later, GFP and mCherry double positive cells were quantified using the score system shown in Fig. 5B. Chi-square test

was used for statistical analysis. **, ***, and **** indicate $P< 0.01$, 0.001, and 0.001, n.s. not statistically significant, total numbers of cells are shown above the bar.

Table 2-1 Primers for cloning and sequencing of Igfbp5a, IGFBP5, and their mutants

	Primer name	**Sequence (5'-3')**
igfbp5a genotyping	*igfbp5a*-TAL-nF	GAACGCTGTTCGCTTGAT
	igfbp5a-TAL-nR	CGCAGTCCTCGTCCACAT
	igfbp5a-HRMA1-F	GTGGCATTTGTATGGGGACT
	igfbp5a-HRMA2-R	AGGTCAAGCAGCATCCGCA
qPCR	*igfbp5a*-qPCR-F	GCTGCACGCTCTGCTTTAC
	igfbp5a-qPCR-R	AATGGAACCTTGGCCTGAG
	β-actin-qPCR-F	GATCTGGCATCACACCTTCTAC
	β-actin-qPCR-R	CCTGGATGGCCACATACAT
Igfpb5a LBD	Igfbp5a-LBD-F	GATTGGGGAGGAAAACCAGCAGCACGCTCAG CAGTACGGCAAAGGAG
	Igfbp5a-LBD-R	CTCCTTTGCCGTACTGCTGAGCGTGCTGCTGG TTTTCCTCCCCAATC
Igfpb5a NLS	Igfbp5a-NLS-F	GTGTAAGCCCTCTCTGGACGGCCAGCGGGGC ATCTGCTGG
	Igfbp5a-NLS-R	CCAGCAGATGCCCCGCTGGCCGTCCAGAGAG GGCTTACAC
IGFBP5 G223R	IGFBP5-G223R-F	GTGACCGCAAAAGATTCTACAAG
	IGFBP5-G223R-R	CTTGTAGAATCTTTTGCGGTCAC
IGFBP5 W242*	IGFBP5-W242stop-F	GGCATCTGCTGATGCGTGGACAAG
	IGFBP5-W242stop-R	CTTGTCCACGCATCAGCAGATGCC
BAC cloning	*igfbp5a*-ORF-F	GTTTTGCCATTTCAAAGCTGGTGAAATAGGTG TTCTACAGTAGGACGATGCTGCTAAGTTTGTA TGCTCTGGTG
	igfbp5a-pEGFP-C3–kan-R	GTTTACTTTTGTCCCATATAAAACAAATACTA CAAGTCAATAAAACATACAGAACTCCAGCAT GAGATCCCCGC
BAC sequencing	*igfbp5a*-5UTR-F	GAACGCTGTTCGCTTGAT
	igfbp5a-stop-BamHI-R	CGCGGATCCTCATTCGTTGTTGTTG

Chapter 3 Cell-autonomous Regulation of Epithelial Cell Quiescence by Calcium Channel Trpv6 [2]

3.1 Abstract

Epithelial homeostasis and regeneration require a pool of quiescent cells. How the quiescent cells are established and maintained is poorly understood. Here we report that Trpv6, a cation channel responsible for epithelial Ca^{2+} absorption, functions as a key regulator of cellular quiescence. Genetic deletion and pharmacological blockade of Trpv6 promoted zebrafish epithelial cells to exit from quiescence and re-enter the cell cycle. Reintroducing Trpv6, but not its channel dead mutant, restored the quiescent state. Ca^{2+} imaging showed that Trpv6 is constitutively open in vivo. Mechanistically, Trpv6-mediated Ca^{2+} influx maintained the quiescent state by suppressing insulin-like growth factor (IGF)-mediated Akt-Tor and Erk signaling. In zebrafish epithelia and human colon carcinoma cells, Trpv6/TRPV6 elevated intracellular Ca^{2+} levels and activated PP2A, which down-regulated IGF signaling and promoted the quiescent state. Our findings suggest that Trpv6 mediates constitutive Ca^{2+} influx into epithelial cells to continuously suppress growth factor signaling and maintain the quiescent state.

[2] This chapter is published *Elife*. 2019 Sep 17;8, with authors listed as: Yi Xin, Allison Malick, Meiqin Hu, Chengdong Liu, Heya Batah, Haoxing Xu, and Cunming Duan.

3.2 Introduction

Quiescence is a non-proliferative cellular state found in many cell types in the body. While non-proliferative, these cells retain the ability to re-enter the cell cycle in response to appropriate cell-intrinsic and extrinsic signals (Matson and Cook, 2017; Sun and Buttitta, 2015; Yao, 2014). Quiescence protects long-lived cells, such as adult stem cells against the accumulation of genomic aberrations and stress. Maintaining a pool of quiescent cells is critical for tissue repair, wound healing, and regeneration (Cheung and Rando, 2013). This is particularly important for epithelia which are rapidly and continuously renewed throughout life. The intestinal epithelial cells, for example, are renewed every 4 to 5 days (van der Flier and Clevers, 2009). By synchronizing cultured mammalian cells in G0 via serum starvation followed with serum re-stimulation, Yao et al. (2008) showed that the Rb proteins (pRb, p107, and p130) and their interactions with E2F proteins are critical in regulating the proliferation-quiescence decision (Yao et al., 2008). Acting downstream, a bifurcation mechanism controlled by CDK2 activity and p21 regulating the proliferation-quiescence decision has also been demonstrated in cultured mammalian cells (Spencer et al., 2013). While important insights have been learnt from in vitro studies, how the quiescent cell pools are established during development and maintained in vivo is not well understood. The exceptionally high turnover rate implies that cell type-specific mechanism(s) must exist.

The transient receptor potential cation channel subfamily V member 6 (TRPV6) is expressed in mammalian intestinal epithelial cells (Hoenderop et al., 2005). TRPV6 is a conserved calcium channel that constitutes the first and rate-limiting step in the transcellular Ca^{2+} transport pathway (Hoenderop et al., 2005; Peng et al., 1999; Peng et al., 2000; Wissenbach et al., 2001). In zebrafish, *trpv6* is specifically expressed in a population of epithelial cells

known as ionocytes or NaR cells (Dai et al., 2014a; Pan et al., 2005). NaR cells take up Ca^{2+} from the surrounding habitats into the body to maintain body Ca^{2+} homeostasis (Liao et al., 2009; Yan and Hwang, 2019b). NaR cells are polarized cells that functionally and molecularly similar to human intestinal epithelial cells. While located in the gill filaments and the intestine in the adult stages, these cells are distributed in the yolk sac skin during the embryonic and larval stages, making these easily accessible for experimental observation and perturbations (Dai et al., 2014a; Pan et al., 2005). When zebrafish are grown in homeostatic normal [Ca^{2+}] conditions, NaR cells are maintained in a quiescent state and the Akt-Tor activity is regulated at low levels. Low [Ca^{2+}] stress increases Akt-Tor activity in these cells and promotes their re-entry into the cell cycle (Dai et al., 2014; Liu et al., 2017). This is similar to the proposed role of TOR signaling in adult stem cells (Chen et al., 2002; Kim and Guan, 2019; Meng et al., 2018a), suggesting an evolutionarily conserved mechanism(s) at work. More recent studies suggest that insulin-like growth factor binding protein 5a (Igfbp5a), a secreted protein that binds IGF with high-affinity, plays a critical role in activating Akt-Tor signaling in these cells via the IGF1 receptor under calcium deficient states (Liu et al., 2018a). The mechanism controlling the quiescent state under normal [Ca^{2+}] condition is currently unknown. In a previous study, we found that zebrafish *mus* mutant larvae, a loss-of-function Trpv6 mutant fish line obtained from an ENU mutagenesis screen (Vanoevelen et al., 2011), had many proliferating NaR cells and elevated Akt-Tor signaling, suggesting Trpv6 may play a negative role in regulating NaR cell proliferation (Dai et al., 2014a). How does Trpv6 act to inhibit Akt-Tor signaling and whether it involves in cell quiescence regulation are unknown. Because TRPV6/Trpv6 is the primary Ca^{2+} channel responsible for epithelial Ca^{2+} uptake and since Ca^{2+} is a major second messenger involved in cell proliferation and differentiation in many cell types (Clapham, 2007; Hoenderop

et al., 2005), we hypothesized that Trpv6 regulates the quiescent state by conducting Ca^{2+} influx into epithelial cells and suppressing IGF1 receptor mediated signaling. The objective of this study was to test this hypothesis and to elucidate the underlying mechanisms of Trpv6 action.

3.3 Results

3.3.1 Trpv6 is crucial for epithelial Ca^{2+} uptake in zebrafish

Three *trpv6* mutant fish lines were generated using CRISPR/Cas9 (Figure 3.1A). All three Trpv6 mutant proteins lack the 6 transmembrane domains and the critical ion pore region and are predicted to be null mutations (Figure 3.1B). The *trpv6Δ7* and *trpv6Δ8* lines were made in the *Tg(igfbp5a:GFP)* fish background. *Tg(igfbp5a:GFP)* is a transgenic fish line expressing EGFP in the *trpv6*-expressing NaR cells (Liu et al., 2017a), allowing real-time analysis of NaR cell proliferation. The *trpv6Δ8-2* line was in a non-transgenic fish background and used in Ca^{2+} imaging analysis described later. The gross morphology and body size of the mutant fish were similar to their siblings (Figure 3.2). All mutant fish died within 2 weeks (Figure 3.1C and D). Alizarin red staining indicated a marked reduction in the calcified bone mass in the *trpv6*$^{-/-}$ mutant fish (Figure 3.1E), indicating body calcium deficiency. Fura-2 Ca^{2+} imaging experiments in HEK293 cells transfected with zebrafish Trpv6 and human TRPV6 were performed. The Trpv6-mediated $[Ca^{2+}]_i$ change was similar to that of TRPV6 (Figure 3.1F). D542 in mammalian TRPV6 occupies a critical position in the ion pore region and mutation of this residue abolishes its Ca^{2+} permeability (McGoldrick et al., 2018; Sakipov et al., 2018). This residue is conserved in zebrafish Trpv6 at position 539 (Figure 3.3). We generated and tested Trpv6D539A mutant. The $[Ca^{2+}]_i$ levels in Trpv6D539A mutant transfected cells were low and did not respond to changes in extracellular $[Ca^{2+}]$ (Figure 3.1F). The maximal Ca^{2+} influx rate was reduced to a negligible level in Trpv6D539A transfected cells (Figure 3.1G). Whole-cell patch clamp experiments

confirmed that the Trpv6 mediated Ca^{2+} current and this activity was abolished in the Trpv6D539A mutant (Figure 3.1H). These findings support the notion that Trpv6 plays an indispensable role in epithelial Ca^{2+} uptake and maintaining body Ca^{2+} balance and provided critical reagents for subsequent experiments.

3.1.2 Trpv6 regulates the quiescence-proliferation decision in epithelial cells

To determine the possible role of Trpv6 in NaR cells, double-blind tests were performed (Figure 3.4A). In agreement with previous studies (Dai et al., 2014; Liu et al., 2017), NaR cells in the wild-type and heterozygous siblings were distributed in the yolk sac region as single cells in a salt-and-pepper pattern (Figure 3.4B). NaR cells in the *trpv6Δ8* mutant larvae were often observed in clusters of newly divided cells (Figure 3.4B). These proliferating NaR cells had enlarged apical opening (Figure 3.5). The NaR cell proliferation rate was significantly elevated in the mutant fish in all stages examined (Figure 3.4C). At 5 dpf, the *trpv6Δ8* mutant fish had 3-time more NaR cells (Figure 3.4C). Essentially same data were obtained with the *trpv6Δ7* fish (Figure 3.4D). $GdCl_3$, a Trpv6 inhibitor, was used to further test the role of Trpv6. $GdCl_3$ treatment increased NaR cell proliferation in the wild-type and heterozygous fish, while it did not further increase NaR cell proliferation in the mutant fish (Figure 3.4E and Figure 3.6). Ruthenium red, another Trpv6 inhibitor, had similar effects (Figure 3.6). Next, Trpv6 and Trpv6D539A were randomly expressed in NaR cells in *trpv6Δ8*$^{-/-}$; *Tg(igfbp5a:GFP)* fish using a Tol2 transposon BAC-mediated genetic mosaic assay (Liu et al., 2018a). Reintroduction of Trpv6 reversed the quiescence to proliferation transition (Figure 3.4F) and reduced the apical opening site to the control levels (Figure 3.5). Trpv6D539A, however, had no such effect (Figure 3.4F). These data showed that Trpv6 functions as a major barrier in the quiescence to proliferation transition and this action requires its Ca^{2+} permeability.

3.3.3 Trpv6 controls the quiescence-proliferation decision via regulating IGF signaling

Previous studies showed that pre-exiting NaR cells in wild-type fish re-enter the cell cycle in response to low [Ca^{2+}] treatment (Dai et al., 2014a; Liu et al., 2017a). To determine whether this effect is related to Trpv6, 3 dpf *trpv6Δ7*$^{-/-}$*;Tg(igfbp5a:GFP)* larvae and siblings were subjected to low [Ca^{2+}] challenge test. Low [Ca^{2+}] treatment resulted in a 3-fold increase in proliferating NaR cells in the wild-type and heterozygous fish (Figure 3.7A). This value was comparable to that of *trpv6Δ7*$^{-/-}$ larvae kept in normal [Ca^{2+}] media (Figure 3.7A). Low [Ca^{2+}] treatment did not further increase NaR cell number in the mutant larvae (Figure 3.7A). Low [Ca^{2+}] treatment also significantly increased *trpv6* mRNA level in wild-type fish and heterozygous fish, an adaptive response in Ca^{2+} homeostasis reported previously (Liu et al., 2017a). This increase, however, was abolished in *trpv6*$^{-/-}$ mutant (Figure 3.8A), likely due to non-sense mRNA decay of mutant *trpv6* mRNA.

Low [Ca^{2+}] stress induces NaR cell proliferation and this has been attributed to the activation of IGF1 receptor-mediated PI3 kinase-Akt-Tor signaling (Dai et al., 2014a; Liu et al., 2017a; Liu et al., 2018a). Gene expression analysis results showed that the *igfr1a* and *igfr1b* mRNA levels were comparable between *trpv6Δ7*$^{-/-}$ larvae and siblings (Figure 3.8B and C). Immunostaining results showed significant increases in the number of phosphorylated Akt-positive NaR cells in *trpv6Δ7*$^{-/-}$ and *trpv6Δ8*$^{-/-}$ larvae kept in the normal [Ca^{2+}] embryo medium (Figure 3.7B and Figure 3.9A). The levels of phospho-Akt in the siblings were minimal. Re-expression of Trpv6 in mutant fish inhibited Akt phosphorylation in NaR cells (Figure 3.7D), indicating that Trp6 is both required and sufficient in suppressing Akt signaling. Tor signaling activity was also significantly elevated in the *trpv6Δ7*$^{-/-}$ and *trpv6Δ8*$^{-/-}$ mutant larvae (Figure 3.7C and Figure 3.9B). Blocking Trpv6 channel activity using $GdCl_3$ and Ruthenium red increased

phospho-Akt levels and NaR cell proliferation in the wild-type fish (Figure 3.10). Mitogen-activated kinase (MAPK) pathway is another major signaling pathway downstream of the IGF1 receptor (Duan et al., 2010). Immunostaining results pErk signaling activity was significantly increased in *trpv6*$^{-/-}$ mutant larvae (Figure 3.7E and Figure 3.11). These data show that loss of Trpv6 expression or activity results in elevated IGF signaling in NaR cells.

If Trvp6 regulates the quiescence-proliferation decision by suppressing the IGF1 receptor-mediated signaling, then blockade of IGF1 receptor and key downstream signaling molecules should inhibit the quiescent to proliferation transition. Indeed, treatment of *trpv6*$^{-/-}$ mutant fish with BMS-754807, an IGF1 receptor inhibitor, abolished the quiescence to proliferation transition in mutant larvae (Figure 3.7F). However, IGF1 receptor inhibition did not show any significant effect on NaR cell proliferation in wild-type and heterozygous siblings (Figure 3.7F). Treatment of *trpv6*$^{-/-}$ mutant fish with PI3 kinase inhibitor Wortmannin, Tor inhibitor Rapamycin, and Mek inhibitor U0126 had similar effects (Figure 3.7G-I).

3.3.4 Trpv6 constitutively conducts Ca^{2+} into epithelial cells and regulates the $[Ca^{2+}]_i$ levels in vivo

To investigate Trvp6-mediated Ca^{2+} influx in NaR cells in vivo, we generated the *Tg(igfbp5a:GCaMP7a)* fish, a stable reporter fish line expressing GCaMP7a in NaR cells (Figure 3.12). After validating the effectiveness of GCaMP7a in reporting intracellular Ca^{2+} levels ($[Ca^{2+}]_i$) (Figure 3.13), *trpv6Δ8-2*$^{+/-}$;*Tg(igfbp5a:GCaMP7a)*$^{+/-}$ fish were crossed with *trpv6Δ8-2*$^{+/-}$ fish and their offspring were screened at 3 dpf and subsequently genotyped individually. While GCaMP7a-positive cells were observed in ~50% of the siblings as expected, none of the *trpv6Δ8-2*$^{-/-}$ mutant larvae had any GCaMP7a-positive cells (Figure 3.14A). Addition of the Ca^{2+} ionophore ionomycin restored GCaMP7a signal in the mutant fish to a level

comparable to their siblings (Figure 3.14B and C), thus ruling out the possibility that GCaMP7a expression is altered in the mutant fish. Next, Trpv6 was randomly expressed in NaR cells in the *trpv6 Δ8-2*$^{-/-}$; *Tg(igfbp5a:GCaMP7a)* fish using the genetic mosaic assay. Reinduction of Trpv6 significantly increased GCaMP7a signal levels (Figure 3.14D). Ionomycin treatment did not result in further increase (Figure 3.14D). These genetic and in vivo imaging data argue strongly that Trpv6 is not only critical in conducting Ca^{2+} into NaR cells, but also in maintaining the high $[Ca^{2+}]_i$ levels in these cells. We next used Trpv6 inhibitors to block Trpv6 activity in *Tg(igfbp5a:GCaMP7a)* fish. Within 8 min after the $GdCl_3$ treatment, the $[Ca^{2+}]_i$ levels became significantly lower and the reduction became more pronounced in 12 and 16 min (Figure 3.14E and G). When $GdCl_3$ was washed out, the $[Ca^{2+}]_i$ levels gradually increased and returned to normal levels after 12 min (Figure 3.14F and G). Similar results were obtained with Ruthenium red (Figures 3.15). Addition of the IGF1 receptor inhibitor BMS-754807 did not change the $[Ca^{2+}]_i$ levels in NaR cells (Figures 3.16). Therefore, Trpv6 constitutively conducts Ca^{2+} into epithelial cells and continuously maintains high $[Ca^{2+}]_i$ levels in vivo.

3.3.5 Trpv6 inhibits IGF signaling and epithelial cell proliferation by regulating $[Ca^{2+}]_i$ and PP2A is a downstream effector

The observation that $[Ca^{2+}]_i$ in NaR cells are continuously maintained at high levels was surprising and intriguing. To determine whether the observed high $[Ca^{2+}]_i$ levels have any functional significance, *Tg(igfbp5a:GFP*) larvae were treated with the intracellular Ca^{2+} chelator BAPTA-AM. BAPTA-AM treatment resulted in a significant increase in NaR cell proliferation (Figure 3.14H) and in phospho-Akt signaling levels (Figure 3.14I). These data indicate that the high $[Ca^{2+}]_i$ levels are critical in maintaining the quiescent state. To identify the downstream effector(s) of $[Ca^{2+}]_i$, a collection of small molecule inhibitors with known protein targets were

screened using *Tg(igfbp5a:GFP*) larvae. Okadaic acid and Calyculin, two inhibitors of the conserved protein phosphatase 2A (PP2A), were among the strongest hits. Treatment of *Tg(igfbp5a:GFP*) larvae with either drug significantly increased NaR cell proliferation (Figure 3.16A and B). This effect is specific because the drug treatment had no such effect in PP2A deficient zebrafish (Figure 3.18). Importantly, the Okadaic acid and Calyculin treatment-induced NaR cell proliferation was abolished by the IGF1 receptor inhibitor BMS-754807, PI3K inhibitor Wortmannin, Tor inhibitor Rapamycin, and Mek inhibitor U0126 (Figure 3.17A-C). Okadaic acid or Calyculin treatment also resulted in significant increases in the phosphorylated-Akt levels in an IGF1 receptor-dependent manner (Figure 3.17D). However, Okadaic acid or Calyculin treatment did not change the $[Ca^{2+}]_i$ levels (Figure 3.19), indicating that PP2A acts downstream of the $[Ca^{2+}]_i$.

PP2A are a family of conserved protein phosphatases that dephosphorylate Akt and many other proteins (Perrotti and Neviani, 2013; Seshacharyulu et al., 2013). PP2A holoenzymes are heterotrimers. The core enzyme is made by a catalytic C subunit (Cα and Cβ isoform), a scaffold A subunit (Aα and Aβ), and many regulatory B subunits (Virshup and Shenolikar, 2009). The combination of these subunits results in a very large number of different holoenzyme complexes. Our database search suggests that the zebrafish genome contains 3 C subunit genes (*ppp2*ca, cb, and cc). We used CRISPR/Cas9 to transiently knockdown the *ppp2c* genes because stable knockout is likely embryonic lethal. The effectiveness of the targeting guide RNAs was validated (Figure 3.18). Transient knockdown of *ppp2cs* resulted in significant increases in the number of proliferating NaR cells (Figure 3.17E) and in phospho-Akt levels (Figure 3.17F), suggesting that PP2A mediates the action of Trpv6-mediated Ca^{2+} influx in zebrafish epithelia.

To determine whether this signaling mechanism is functional in human cells, TRPV6 knockdown experiments were performed in human LoVo colon carcinoma cells using validated siRNA (Lallet-Daher et al., 2009). These cells were synchronized by serum starvation followed by serum re-stimulation. Knockdown of TRPV6 resulted in a significant increase in LoVo cell proliferation (Figure 3.20A and Figure 3.21). Treatment of LoVo cells with Ruthenium red, $GdCl_3$, BAPTA-AM, and Okadaic acid all significantly increased cell proliferation (Figure 3.20B and Figure 3.22). MTT assay results showed little changes in cell viability in $GdCl_3$, BAPTA-AM, and Okadaic acid treated cells. Ruthenium red treatment resulted in a modest but statistically significance decrease in cell viability (Figure 3.23). Finally, LoVo cells were transfected with PP2A-$C\alpha^{L199P}$ and PP2A-$C\alpha^{H118N}$, two dominant-negative forms of catalytic subunit Cα of PP2A (Katsiari et al., 2005). Expression of PP2A-$C\alpha^{L199P}$ and PP2A-$C\alpha^{H118N}$ both significantly increased LoVo cell proliferation (Figures 3.20C and 3.24).

3.4 Discussion

In this study, we uncover a previously unrecognized role of Trpv6 and delineates a Trpv6-mediated and evolutionarily conserved Ca^{2+} signaling pathway controlling cell quiescence. We showed that genetic deletion of Trpv6 not only impaired Ca^{2+} uptake and reduced body Ca^{2+} content, but also promoted epithelial cells to exit quiescence and proliferate. Likewise, pharmacological inhibition of Trpv6 increased epithelial cell quiescence-proliferation transition. While low [Ca^{2+}] treatment increased epithelial cell proliferation in the siblings, it had no such effect in *trpv6*$^{-/-}$ larvae, supporting the notion that Trpv6 functions as a major regulator of the quiescent state. Our genetic mosaic analysis results showed that the quiescent state is regulated by Trpv6 in a cell autonomous manner. Reintroduction of Trpv6 in the *trpv6*$^{-/-}$ mutant fish was sufficient to restore the $[Ca^{2+}]_i$ levels, suppress IGF signaling, and reverse the cells back

to the quiescent state. The $Trpv6_{D539A}$ mutant had no such activity, suggesting that this action of Trpv6 requires its Ca^{2+} conductance activity.

The impaired Ca^{2+} uptake, reduced body Ca^{2+} content, and premature death observed in *trpv6Δ7* and *trpv6Δ8* mutant fish are in good agreement with a previous study by Vanoevelen et al. (2011) using the *mus* mutant fish, but differ considerable from findings made in the mouse model. Bianco et al. reported that *Trpv6* knockout mice were viable but had reduced intestinal Ca^{2+} uptake, increased urinary Ca^{2+} excretion, decreased bone mineral density, and decreased growth and fertility (Bianco et al., 2007). Another $Trpv6^{-/-}$ mutant mouse line reported by Chen et al., however, had normal blood Ca^{2+} concentration and normal bone formation, but with an increased number of osteoclasts (Chen et al., 2014). A third $Trpv6^{-/-}$ mutant mouse model showed reduced fertility in male only (Weissgerber et al., 2012). The reason(s) of these discrepancies among these mouse studies is not fully understood, but factors such as dietary Ca^{2+} contents may have been critical (Van der Eerden et al., 2012). Zebrafish embryos continuously lose Ca^{2+} and other ions into the surrounding hypo-osmotic environments and must constantly take up Ca^{2+} from the habitat to survive (Liu et al., 2018a). This may also contribute to the premature phenotypes found in the zebrafish mutants. Another factor to take into consideration is genetic redundancy. In mammals, there is another closely related TRPV sub-family member, TRPV5. TRPV5 plays similar roles in the transcellular Ca^{2+} transport pathway, although it is mainly expressed in the kidney (Hoenderop et al., 2005). It has been shown that TRPV5 expression in the intestine is elevated in *Trpv6* mutant mice (Woudenberg-Vrenken et al., 2012). In comparison, zebrafish genome has a single trpv6 gene and lacks this genetic redundancy (Vanoevelen et al., 2011).

An important finding made in this study is that TRPV6 mediates constitutive Ca^{2+} influx into epithelial cells in vivo. The notion that TRPV6 is the primary epithelial Ca^{2+} channel is supported by in vitro findings made in mammalian cells over-expressing TRPV6 (Fecher-Trost et al., 2017) and by measuring endogenous TRPV6-mediated Ca^{2+} influx in cultured Jurkat T cells and rat cauda epidermal principle cells (Gao da et al., 2016; Kever et al., 2019). Fura-2 Ca^{2+} imaging studies in cultured mammalian cells transfected with TRPV6 indicated that this channel may be constitutively open (Vennekens et al., 2000). Although another study reported that patch-clamp recording of mammalian cells transfected with TRPV6 failed to detect spontaneous channel activity (Bodding and Flockerzi, 2004), a recent study has provided structural and functional evidence that TRPV6 is constitutively active (McGoldrick et al., 2018). Other studies have reported that TRPV6 activity is activated by a reduction in $[Ca^{2+}]_i$ concentration, and inactivated by higher $[Ca^{2+}]_i$ in mammalian cells (Nilius et al., 2000; Yue et al., 2001). How TRPV6/Trpv6 channel activity is regulated in vivo is less clear. In this study, we generated a reporter fish line using the high-performance genetic calcium reporter GCaMP7a to measure intracellular Ca^{2+} activity in vivo. GCaMPs has been used for imaging intracellular Ca^{2+} activity in zebrafish neurons (Muto and Kawakami, 2013). This approach has alleviated the concern associated with Fura-2 and cell culture systems. Our in vivo Ca^{2+} imaging results showed that the Trpv6 channel is constitutively open in NaR cells in vivo. This conclusion is supported by the facts that genetic deletion of *trpv6* reduced the $[Ca^{2+}]_i$ to undetectable levels and re-expression of Trpv6 restored the $[Ca^{2+}]_i$ levels in NaR cells. Addition of ionomycin did not result in further increase, indicating the endogenous $[Ca^{2+}]_i$ levels are high in these cells. More direct evidence came from the $[Ca^{2+}]_i$ dynamics analysis results. Within minutes after the addition of Trpv6 blockers $GdCl_3$ or Ruthenium red, the levels of $[Ca^{2+}]_i$ were

significantly reduced. When these drugs were washed out, the $[Ca^{2+}]_i$ signal levels returned to normal levels. It was thought that Ca^{2+} transporting epithelial cells, being continuously challenged by Ca^{2+} traffic from the apical side, maintain low levels of $[Ca^{2+}]_i$ using the cytosolic Ca^{2+} binding protein (Hoenderop et al., 2005). The in vivo imaging findings made in this study challenge this conventional view. We postulate that maintaining high $[Ca^{2+}]_i$ levels in these Ca^{2+} transporting cells is likely beneficial to the organism because it keeps these cells in differentiated state and functioning as Ca^{2+} transporting units. This idea is supported by the fact that treatment of zebrafish with the intracellular Ca^{2+} chelator BAPTA-AM promoted quiescent epithelial cells to proliferate.

Mechanistically, Trpv6 regulates the quiescent state by mediating constitutive Ca^{2+} influx to continuously down-regulating IGF1 receptor-mediated Akt-Tor and Erk signaling. This is supported by the findings that 1) genetic deletion of Trpv6 or pharmacological inhibition of Trpv6-mediated Ca^{2+} uptake increased Akt-Tor and pErk signaling activity in an IGF1 receptor-dependent manner; 2) re-expression of Trpv6 in the mutant cells suppressed Akt signaling; and 3) inhibition of the IGF1 receptor, PI3 kinase, Tor, and Mek activity abolished or inhibited NaR cell proliferation in *trpv6*$^{-/-}$ mutant fish. This conclusion is consistent with previous reports that up-regulating of IGF signaling promotes NaR cells to exit the quiescence and re-enter the cell cycle (Liu et al., 2017a; Liu et al., 2018a). NaR cells are one of the five types of ionocytes originated from a population of epidermal stem cells, which are specified by the expression of p63 (ΔNp63), a direct target of BMP signaling (Bakkers et al., 2002; Janicke et al., 2007; Lee and Kimelman, 2002). These epidermal stem cells further develop into Foxi3a/b-activated ionocyte progenitor cells and keratinocyte progenitor cells with low Foxi3a/b expression (Hsiao et al., 2007). Krüppel-like factor 4 (Klf4) plays an important role in maintaining the ionocyte

progenitor cell pool by stimulating epidermal cell stem proliferation (Chen et al., 2019). In addition, several hormones, including isotocin, cortisol and stanniocalcin 1, have been implicated in the regulation of the ionocyte progenitor cell pool (Chou et al., 2011; Chou et al., 2015; Yan and Hwang, 2019b). Fox3a/3b form a positive regulatory loop and this loop is critical in specifying ionocyte progenitors to give rise to the 5 types of ionocytes (Chang et al., 2009; Hsiao et al., 2007; Yan and Hwang, 2019b). A hallmark of NaR cells is the expression of Trpv6 (Liu et al., 2017a; Pan et al., 2005). The role of Trpv6 and IGF signaling in NaR cell quiescence regulation unraveled in this study differs from the mechanisms acting in epidermal stem cells and ionocyte progenitor cells, and provides novel insights into the regulation of NaR cell development and function.

Our chemical biology screens and genetic studies identified PP2A as a key effector downstream of TRPV6/Trvp6. Inhibition of PP2A by two distinct inhibitors led to elevated Akt signaling and increased epithelial cell proliferation. Importantly, an IGF1 receptor inhibitor abolished these changes. Likewise, CRISPR/Cas9-mediated transient knockdown of PP2A catalytic subunits increased epithelial cell proliferation and Akt signaling. PP2A can activate Akt and Erk signaling at multiple sites in the IGF signaling pathway (O'Connor, 2003). Numerous biochemical studies showing that PP2A can dephosphorylate Akt (Perrotti and Neviani, 2013; Seshacharyulu et al., 2013). In several human cancer cell lines, PP2A regulates Shc phosphorylation state and up-regulates ERK signaling activity in the IGF1-induced signaling pathway (Yumoto et al., 2006). Our in vivo findings, together with the in vitro findings indicate that a $[Ca^{2+}]_i$-regulated PP2A isoform(s) likely acts downstream of TRPV6/Trpv6 and regulates the quiescent state in epithelial cells. This is in good agreement with a recent study showing that compromising PP2A activity delays cell cycle exit in Drosophila (Sun and Buttitta, 2015). The

TRPV6-$[Ca^{2+}]_i$-PP2A signaling axis appears to be conserved in human colon carcinoma cells because siRNA-mediated knockdown or inhibition of TRPV6 increased LoVo cell proliferation. Likewise, chelating intracellular Ca^{2+}, genetic and pharmacological inhibition of PP2A activity resulted in elevated cell proliferation of LoVo cells. The B regulatory subunits control substrate specificity and intracellular distribution of the PP2A holoenzymes and are encoded by a large set of genes classified into four families, i.e., B, B′, B″, and B‴ (Virshup and Shenolikar, 2009). Recent studies suggest that PR72/130 and PR70, 2 members of the B" family, possess 2 conserved EF hand motifs (termed EF1 and EF2) and increasing $[Ca^{2+}]_i$ increased the holoenzyme assembly and phosphatase activity (Kurimchak et al., 2013; Magenta et al., 2008). Another mechanism involves the action of $[Ca^{2+}]_i$-dependent m-calpain: m-calpain degrades PR72 and PR130 into a 45 kDa fragment (Janssens et al., 2009). This fragment, termed as PR45, is resistant to further degradation and exhibits enhanced PP2A activity. These two mechanisms may be related because the calpain-mediated proteolytic activation of PP2A depends on the EF hand integrity (Janssens et al., 2009). Future studies are needed to determine whether these mechanisms mediate TRPV6/Trpv6 action in epithelial cells.

Our findings linking the Trpv6-meiated Ca^{2+} uptake to the cellular quiescence regulation have important biomedical implications. Approximately 90% of human cancers arise in epithelial tissues and over-proliferation is one of the cancer hallmarks (Hanahan and Weinberg, 2011). The IGF signaling pathway is one of the most frequently mutated signaling pathways in epithelial tissue-derived cancers, including colon and prostate cancers (Massoner et al., 2010). The *IGF2* gene and *IRS2* gene are frequently gained in colon cancer (Cancer Genome Atlas, 2012) and have been proposed as a colorectal cancer "driver" oncogenes (Day et al., 2013). TRPV6 gene is frequently up regulated in prostate, colon, and other cancer tissues

(Lehen'kyi et al., 2012; Prevarskaya et al., 2018). At present, it is unclear whether the elevated TRPV6 expression promotes tumor growth or it is an adaptive response (Lehen'kyi et al., 2012; Prevarskaya et al., 2018). Knockdown or overexpression of TRPV6 in cultured cancer cells showed mixed effects in increasing/decreasing proliferation and/or apoptosis (Chow et al., 2007; Lehen'Kyi et al., 2007; Lehen'kyi et al., 2012; Raphael et al., 2014; Skrzypski et al., 2016a). Future studies are needed to clarify the role of TRPV6-$[Ca^{2+}]_i$-PP2A in prostate and colon cancer initiation and progression and its relationship to IGF signaling.

3.5 Materials and methods

Chemicals and reagents

All chemical reagents were purchased from Fisher Scientific (Pittsburgh, PA, USA) unless stated otherwise. Restriction enzymes were bought from New England Bio Labs (Beverly, MA, USA).

Zebrafish husbandry

Fish were raised following standard zebrafish husbandry guideline (Westerfield, 2000a). Embryos were obtained by natural cross and staged following Kimmel at al. (Kimmel et al., 1995b). E3 embryo rearing solution (containing 0.33 mM $[Ca^{2+}]$) was prepared as reported (Westerfield, 2000a). Two additional embryo rearing solutions containing 0.2 mM $[Ca^{2+}]$ (i.e., normal $[Ca^{2+}]$ solution) or 0.001 mM $[Ca^{2+}]$ (i.e., low $[Ca^{2+}]$ solution) were made following previously reported formula (Dai et al., 2014a). To inhibit pigmentation, 0.003% (w/v) N-phenylthiourea (PTU) was added in some experiments. All experiments were conducted in

accordance with the guidelines approved by the University of Michigan Institutional Committee on the Use and Care of Animals.

Generation of *trpv6*$^{-/-}$ fish lines using CRISPR/Cas9

The sgRNA targeting *trpv6* (5'-GGGCTCGTTGATGAGCTCCG-3') was designed using CHOPCHOP (http://chopchop.cbu.uib.no/). The sgRNA (30 ng/µl) was mixed with capped with Cas9 protein (700 ng/µl) and co-injected into *Tg(igfbp5a:GFP)* or wild-type embryos at the 1-cell stage as described (Xin and Duan, 2018). After confirming indels by PCR followed by hetero-duplex assay using a subset of F0 embryos, the remaining F0 embryos were raised to adulthood and crossed with *Tg(igfbp5a:GFP)* or wild-type fish. F1 fish were raised to the adulthood and genotyped. After confirming indels by DNA sequencing, the heterozygous F1 fish were intercrossed to generate F2 fish.

Transient knockdown of *ppp2cs*

Three sgRNAs targeting ppp2cs were designed using CHOPCHOP (http://chopchop.cbu.uib.no/). Their sequences are: ppp2ca-sgRNA: 5'-GTTCCATAAGATCGTGAAAC-3'; ppp2cb-sgRNA: 5'-GAGCGTTCTCACTTGGTTCT-3'; ppp2ca2-sgRNA: 5'-GACGAAGGAGTCGAATGTGC-3'. sgRNAs (30 ng/µl) were mixed with Cas9 protein (700 ng/µl) and co-injected into Tg(igfbp5a:GFP) or wild type embryos at the 1-cell stage as reported (Xin and Duan, 2018). A subset of injected embryos were pooled, DNA isolated, and analyzed by PCR followed by hetero-duplex assays as reported (Liu et al., 2018a). After confirming the indels, the remaining injected embryos were used for experiments.

Genotyping

To isolate genomic DNA, pooled embryos or individual adult caudal fin were incubated in 50 μl NaOH (50 mM) at 95 °C for 10 min and neutralized by adding 5 μl 1 M Tris-HCl (pH 8.0). PCR was performed using the following primers: *trpv6*-gt-f, 5'-TGACATTGTGTGTGTTTGTTGC-3'; *trpv6*-gt-r, 5'-GTGAAGGGCTGTTAAACCTGTC-3'*;* *trpv6*-HMA-f, 5'- GCAGCGGTGGCTTTAATGAAT-3'; *trpv6*-HMA-r, 5'-AAACCTGTCAATCAGAGCACAC-3'; *ppp2ca*-gt-f, 5'- TCACCATCAGTGCATGTCAATA-3'; *ppp2ca*-gt-r, 5'- CTCGATCCACATAGTCTCCCAT-3'; *ppp2cb*-gt-f, 5'-TGGATGATAAAGCGTTTACGAA-3'; *ppp2cb*-gt-r, 5'- ACGTTACACATTGCTTTCATGC-3'; *ppp2ca2*-gt-f, 5'-CTGATGGTTGTGATGCTGTTTT-3'; *ppp2ca2*-gt-r, 5'-CGGTTTCCACAGAGTAATAGCC-3'.

Morphology analysis

Body length, defined as the curvilinear distance from the head to the end of caudal tail, was measured. Alizarin red staining was performed following a published protocol (Du et al., 2001). Images were captured with a stereomicroscope (Leica MZ16F, Leica, Wetzlar, Germany) equipped with a QImaging QICAM camera (QImaging, Surrey, BC, Canada).

Whole-mount *in situ* hybridization, and immunostaining

For whole mount immunostaining or in situ hybridization analysis, zebrafish larvae were fixed in 4% paraformaldehyde, permeabilized in methanol, and analyzed as described previously (Dai et al., 2014a). For double color *in situ* hybridization and immunostaining, mCherry mRNA signal was detected using anti-DIG-POD antibody (Roche), followed by Alexa 488 Tyramide

Signal Amplification (Invitrogen). After in situ hybridization, the stained larvae were washed in 1X PBST and incubated with phosphorylated Akt antibody overnight at 4℃ and then stained with a Cy3-conjugated goat anti-rabbit immunoglobulin G antibody (Jackson ImmunoResearch). Fluorescent images were acquired using a Nikon Eclipse E600 Fluorescence Microscope with PMCapture Pro 6 software.

Plasmid and BAC constructs

The ORF of zebrafish Trpv6 were amplified by PCR and cloned into pEGFPN1 using the following primers: BglII-zftrpv6-F, 5'-atatAGATCTcgccaccATGCCACCCGCCATATC-3'; no stop-zftrpv6-ca-SalI-R, 5'- TACCGTCGACcaGAGAAACTTGAAATTggggcaatc-3'; $Trpv6^{D539A}$ was engineered by site-directed mutagenesis using the following primers: zTrpv6_D539A_f, 5'-GGTCAGATTGCCTTGCCAGTGGA-3'; zTrpv6_D539A_r, 5'-TCCACTGGCAAGGCAATCTGACC-3'. Human TRPV6 ORF was sub-cloned into pEGFPN1 using the following primers: 5'-atatCTCGAGcgccaccATGGGTTTGTCACTG-3'; 5'-TACCGTCGACcaGATCTGATATTCC-3'. EGFP sequence in those vectors was replaced by mCherry sequence from pmCherry-C1 vector using the following primers: AgeI-mCherry-F, 5'-caACCGGTCGCCACCATGGTGAGCAAGGGC-3'; mCherry-NotI-stop-r, 5'-TCGCGGCCGCCTACTTGTACAGCTCGTCC-3'. Wild-type zebrafish Trpv6 and Trpv6D539A tagged with mCherry were then inserted into the *igfbp5aBAC* construct to replace the *igfbp5a* coding sequence from the start codon to the end of the first exon through homologous recombination as reported (Liu et al., 2017a). The primers are: *igfbp5a-zTrpv56*-f, 5'-

GTTTTGCCATTTCAAAGCTGGTGAAATAGGTGTTCTACAGTAGGACGATGCCACCCG

CCATATCTGGTGAA-3’ and igfbp5a_frt-kan-rev, 5′-GTTTACTTTTGTCCCATATAAAACAAATACTACAAGTCAATAAAACATACCCGCGTGTAGGCTGGAGCTGCTTC-3′. The resulted BAC DNA was validated by sequencing. The validated BAC DNA and Tol2 mRNA were mixed and injected into 1-cell stage *trpv6*$^{-/-}$; *Tg(igfbp5a:GFP)* embryos. The embryos were raised and analyzed. Cells co-expressing mCherry and GFP were identified and scored using a reported scoring system (Liu et al., 2018a). PP2Ac^{L199P} and PP2Ac^{H118N} were kind gifts from Dr. George Tsokos, Harvard Medical School. They were subloned into pIRES-mCherry vector using the following primers: EcoRI-PP2A-f: 5’-ccgGAATTCATGGACGAGAAGGTGTTCAC-3’, BamHI-PP2A-r: 5’-cgcGGATCCTTACAGGAAGTAGTCTGGGG-3’ and used in cell transfection.

Generation of the *Tg(igfbp5a:GCaMP7a)* fish line

GCaMP7a DNA was cloned into pEGFPN1 to replace the EGFP sequence using the following primers: BamHI-HA-F, 5’- cgcggatccATGGCATACCCCTACGACG-3’; GCaMP7a-stop-NotI-R, 5’- atttgcggccgcTTACTTAGCGGTCATCATC-3’. *BAC* (*igfbp5a*:*GCaMP7a*) construct was generated following a published protocol (Liu et al., 2017a). The following primers were used to amplify the GCaMP7a cassette sequence: *igfbp5a*_GCaMP7a_fw, 5′-GTTTTGCCATTTCAAAGCTGGTGAAATAGGTGTTCTACAGTAGGACGATGGCATACCCCTACGACGTGCCCGAC -3′ and igfbp5a_frt-kan-rev. The resulted *BAC (igfbp5a:*GCaMP7a*)* was validated by PCR using the following primers: igfbp5a-5UTR-fw, 5’-GAACGCTGTTCGCTTGAT-3’ and GCaMP7a-stop-NotI-R, 5’-ATTTGCGGCCGCTTACTTAGCGGTCATCATC -3’. The *BAC (igfbp5a:GCaMP7a)* DNA and *Tol2* mRNA were mixed and injected into zebrafish embryos at 1-cell stage. The F0 embryos

were screened at 72 hpf by checking GCaMP7a responses to high or low [Ca^{2+}] solutions. GCaMP7a-positive F0 embryos were raised and crossed with wild-type fish to obtain F1 individuals. F2 fish were generated by crossing F1 fish.

Live GCaMP7a imaging

Zebrafish larvae were anesthetized using normal [Ca^{2+}] embryo solution supplemented with 0.168 mg/ml tricaine. They were mounted in 0.3% low-melting agarose gel and immersed in 1 ml normal [Ca^{2+}] solution. A Leica TCS SP8 confocal microscope equipped with the HC PL APO 93X/1.30 GLYC was used for imaging and LAS X and Image J were used for image analysis.

RT-qPCR

Zebrafish larvae raised in E3 embryo rearing solution were transferred to normal or low [Ca^{2+}] embryo solution from at 3 dpf. Two days later, caudal fin was clipped for genotyping. The larvae were pooled and RNA was isolated. Reverse transcription reaction was performed using M-MLV (Invitrogen) oligo$(dT)_{18}$ oligos primer. qPCR was carried out using SYBR Green (Bio-Rad). Primers for qPCR are: *trpv6*-qPCR-F: 5'- GGACCCTACGTCATTGTGATAC-3', *trpv6*-qPCR-R: 5'- GGTACTGCGGAAGTGCTAAG-3', *igf1ra*-qPCR-F: 5'-CGTACCTCAATGCCAACAAG-3', *igf1ra*-qPCR-R: 5'- TAGGGCTGTTCGGCTAATGT-3', *igf1rb*-qPCR-F: 5'- AAACTTGGGACCAGGGAACT-3', *igf1rb*-qPCR-R: 5'-ATCTTCTCCCGCTCCACTTC-3'. *18s*-qPCR-F: 5'- AATCGCATTTGCCATCACCG-3', *18s*-qPCR-R: 5'- TCACCACCCTCTCAACCTCA-3'.

Cell culture

Human embryonal kidney cells (HEK293) and human LoVo conlon cancer cells were obtained from ATCC. HEK293 cells were cultured in DMEM or DMEM/F12 supplemented with 10% FBS, penicillin and streptomycin in a humidified-air atmosphere incubator containing 5% CO2.

Fura-2 imaging and electrophysiology recording

HEK293 cells were plated onto 24 mm cover glass coated with L-polylysine and transfected with 0.3 µg of plasmid DNA using Lipofectamine 2000. Twenty-four hours after the transfection, the cover glass was mounted on an imaging chamber and washed with calcium-free Krebs-Ringer HEPES (KRH) solution (118 mM NaCl, 4.8 mM KCl, 1 mM $MgCl_2$, 5 mM D-glucose, and 10 mM HEPES, pH=7.4). Fura-2 loading was performed following a published method **(**Kovacs et al., 2012**)**. Successfully transfected cells were chosen by mCherry expression. Their cytosolic Ca^{2+} levels were recorded by an EasyRatio Pro system (PTI) at two different wavelengths (340 nm and 380 nm). The Fura-2 ratio (F340 /F380) was used to determine changes in intracellular $[Ca^{2+}]i$. At least 50 cells were measured in each slide. Patch clamp recordings were performed at room temperature (Weissgerber et al., 2012**)**. The internal pipette solution contained (in mM): Aspartate-Cs 145, NaCl 8, $MgCl_2$ 2, HEPES 10, EGTA 10, Mg-ATP 2, pH 7.2. Normal external solution contained (in mM): NaCl 135, KCl 6, $MgCl_2$ 1.2, HEPES 10, Glucose 12, pH 7.4, supplemented with 10 mM $CaCl_2$ or 30 mM $BaCl_2$. For measuring Ca^{2+} currents, cells were perfused with normal external solution at first and then switched to solutions as indicated. DVF solutions contains (in mM): NaCl 150, EDTA 10,

HEPES 10, pH 7.4. Solutions with different concentration of Ca^{2+} contains (in mM): NaCl 150, HEPES 10, Glucose 12, pH 7.4, supplemented with 0 to 10 mM $CaCl_2$ as indicated.

Flowcytometry analysis and MTT assay

Human LoVo cells were washed 3 times with serum-free medium (SFM) and starved in SFM for 12h. The cells were then stimulated with 2% FBS medium with or without inhibitors. Forty-eight hours later, cell cycle analysis was performed using Attune Acoustic Focusing cytometer (Applied Biosystems, Life Technologies) after propidium iodide staining (Liu et al., 2018a). For siRNA transfection, 100 pmol siRNA and 1.5 µl Lipofectamine RNAiMAX (Invitrogen) was used in each well in 24-well tissue culture plates. For plasmid transfection, 2 µg plasmid and 2 µl Lipofectamine 3000 (Invitrogen) were used in in each well in 24-well tissue culture plates. Six hrs post transfection, cells were grown in complete media containing 10% FBS. There were washed 3 times with SFM and synchronized by incubation in SFM for 12h. The synchronized cells were stimulated with 2% FBS-containing medium for 48 hrs and subjected to cell cycle analysis or MTT assay. For MTT assay, 5mg/ml MTT (Invitrogen) stock solution was diluted in 2% FBS-containing medium and cells were stained for 4hr at 37 ℃ before dissolving using DMSO. Absorbance at 540nm was read by microplate reader (Tecan).

Statistical analysis

Values are shown as Mean ± standard error of the mean (SEM). Statistical significance among experimental groups was determined using one-way ANOVA followed by Tukey's multiple comparison test or student t-test. Chi-square test was used to analyze the association between two categorical variables. Statistical significances were accepted at $P < 0.05$ or greater.

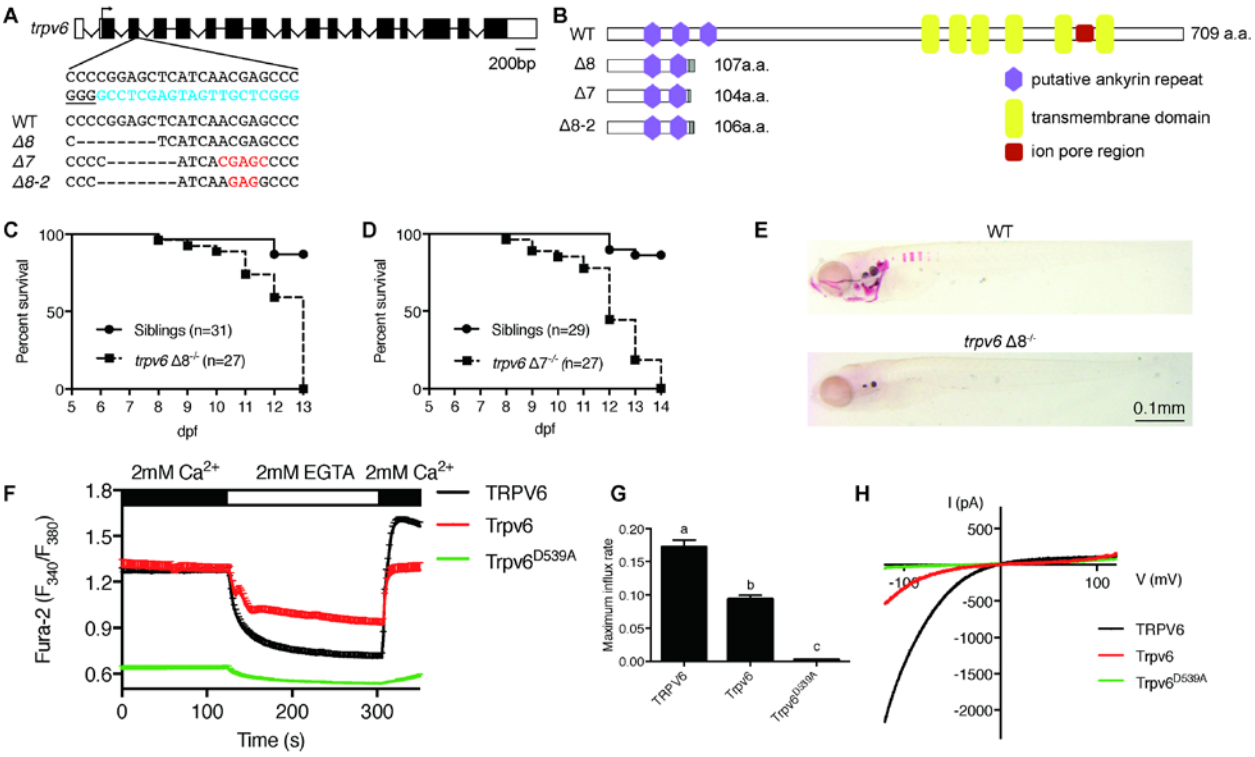

Figure 3.1 Genetic deletion of the conserved epithelial calcium channel Trpv6 results in calcium deficiency and premature death

(A) Schematic diagram showing *trpv6* gene (WT) and various mutant sequences. Filled boxes indicate *trpv6* ORF and open boxes indicate UTRs. Introns are shown as lines. The gRNA targeting site is indicated by blue color and PAM motif is underlined. Deleted and inserted nucleotides are indicated by dash lines and red letters, respectively. (B) Schematic diagram of Trpv6 (WT) and its mutants. Putative function domains are indicated. The grey box indicates altered sequence caused by frame shifts. (C-D) Survival curves of *trpv6Δ8*$^{-/-}$*; Tg(igfbp5a:GFP)* (C) and *trpv6Δ7*$^{-/-}$*; Tg (igfbp5a:GFP)* fish (D) and siblings. The numbers of total fish are indicated. (E) Representative images of Alizarin red stained wild-type and *trpv6Δ8*$^{-/-}$*; Tg(igfbp5a:GFP)* fish at 7 day post fertilization (dpf). (F) Fura-2 Ca^{2+} imaging analysis of HEK293 cells transfected with the indicated plasmids. n > 50 cells from 3 independent experiments. (G) The maximal influx rate. n = 3 independent experiments. (H) Currents evoked

by a RAMP voltage from -120mV to +120 mV in HEK293 cells transfected with the indicated plasmids. In this and all subsequent figures, unless specified otherwise data shown are Mean ± SEM. Different letters indicate significant difference at $P < 0.05$, one-way ANOVA followed by Tukey's multiple comparison test.

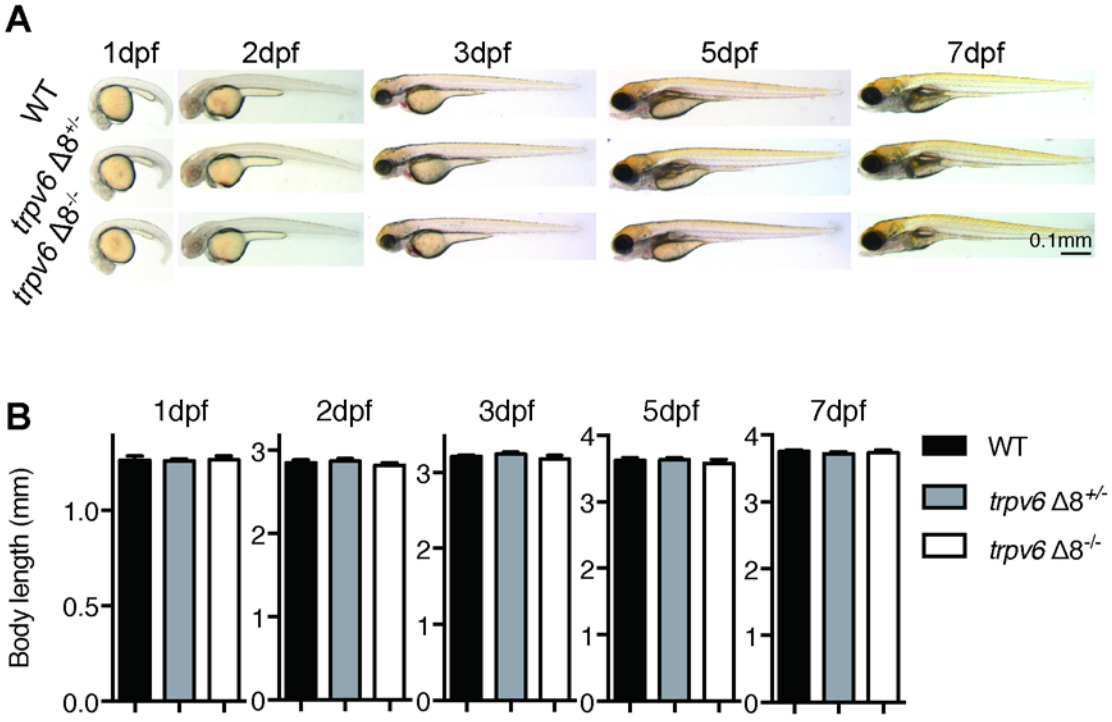

Figure 3.2 Morphology of *trpv6* mutant fish

(A-B) Gross morphology (A) and body size (B) of *trpv6Δ8$^{-/-}$; Tg(igfbp5a:GFP)* fish and siblings.

Values are Mean ± SEM, n=7-23 fish. No statistical significance was found.

```
Trpv6   IFLIGSSAALWIFYMTQEPLALPQYRSFPITLFSQFEVSVGQIDLPVDHTLFTHPVVYWT
TRPV5 VVILGFASAFYIIFQTEDPTSLGQFYDYPMALFTTFELFLTVIDAPANYDVDLPFMFSIV
TRPV6 VVILGFASAFYIIFQTEDPEELGHFYDYPMALFSTFELFLTIIDGPANYNVDLPFMYSIT
      :.::* ::*::*:: *::*  * :: .:*::**: **: :  ** *.:: :    :   .
```

Figure 3.3 Sequence alignment in the pore region of zebrafish Trpv6, human TRPV5, and human TRPV6

Transmembrane domain 5 and 6 are indicated in yellow and orange letters. The ion pore region is indicated by black letters and the critical Asp residue (D) is labeled in red.

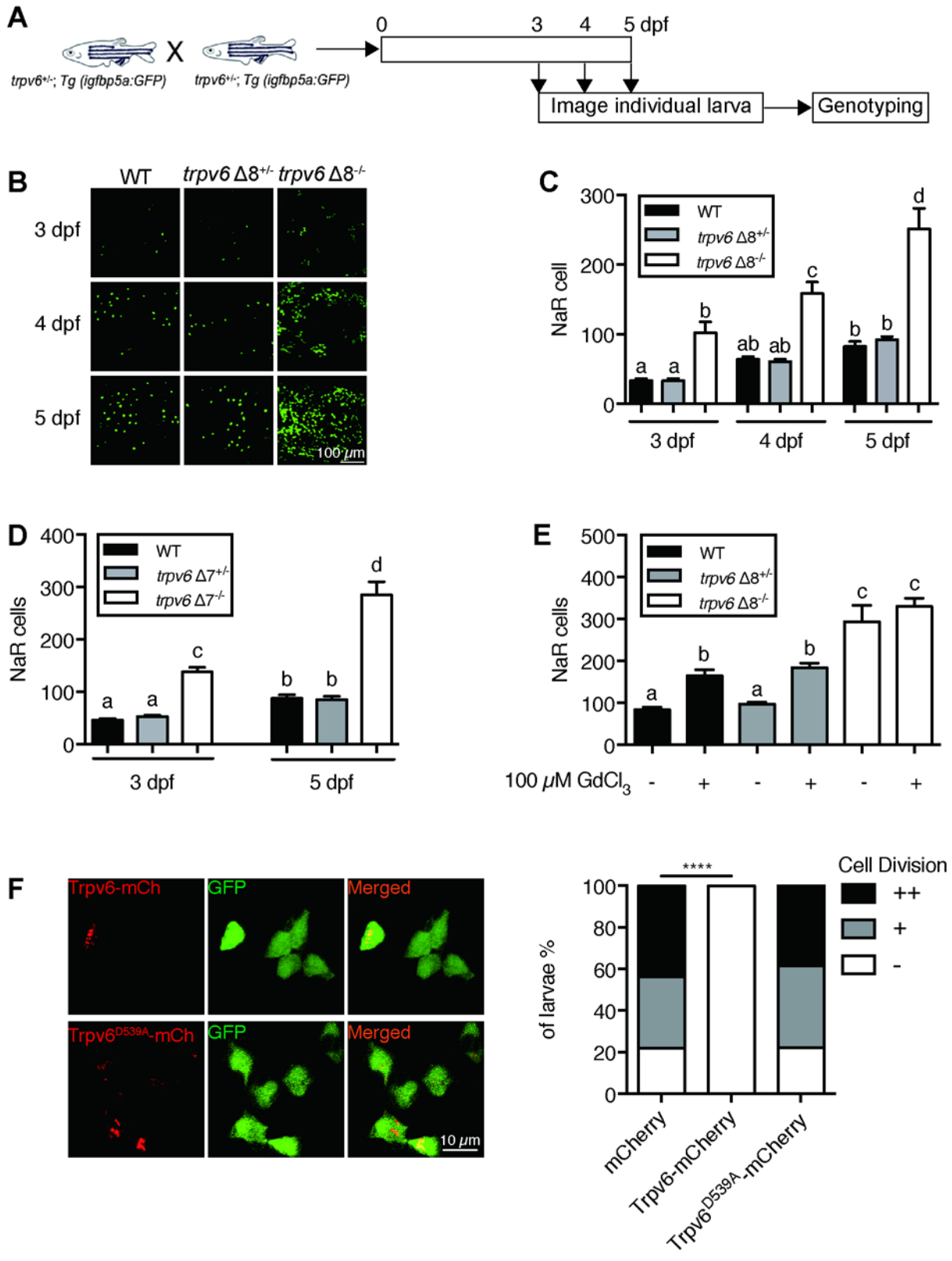

Figure 3.4 Trpv6 regulates epithelial cell quiescence-proliferation decision

(A) Diagram of the experimental design. (B) Representative images. In this and all subsequent larval images, lateral views of the yolk-sac region are shown with dorsal up and anterior to the left. (C-D) Mean NaR cell number/fish of the indicated genotypes. n = 6-9. (E) Progenies of *trpv6 Δ8$^{+/-}$; Tg (igfbp5a:GFP)* intercross were raised to 3 dpf and treated with 100 μM $GdCl_3$ from 3 to 5 dpf. NaR cells in each fish were quantified following individual genotyping. n = 13-22. (F) Progenies of *trpv6Δ8$^{+/-}$;Tg(igfbp5a:GFP)* intercross were injected with the indicated BAC-mCherry DNA at one-cell stage. At 5 dpf, the Trpv6-expressing NaR cells in each fish were scored following a published scoring system (Liu et al., 2018a). Representative images are shown in the left and quantified results in the right panel. ****, P <0.0001 by Chi-Square test, fish n = 12-38.

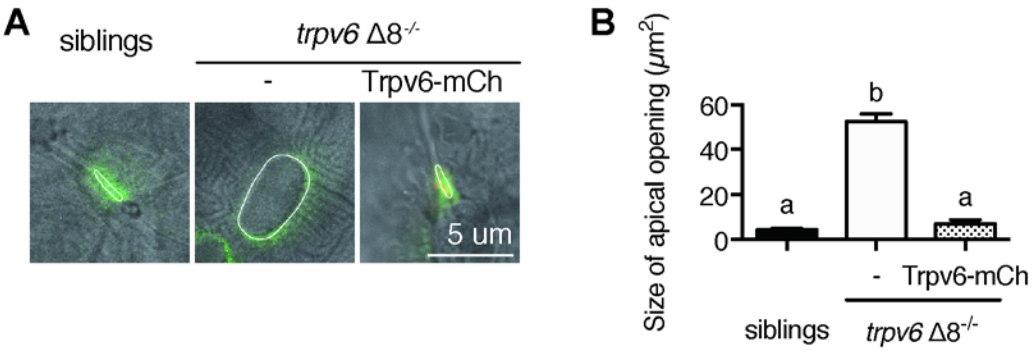

Figure 3.5 Genetic deletion of Trpv6 increases epithelial cell apical opening

(A-B) Progenies of a *trpv6Δ8*$^{+/-}$*;Tg (igfbp5a:GFP)* intercross were injected with or without the *BAC (igfbp5a:Trpv6-mCherry)* DNA. At 3dpf, larvae were photographed followed by individual genotyping. Representative images are shown in (A). The apical opening of NaR cells were quantified and shown in (B). Data are Mean ± SEM, n = 8-42. Different letters indicate significant difference at $P < 0.05$, one-way ANOVA followed by Tukey's multiple comparison test.

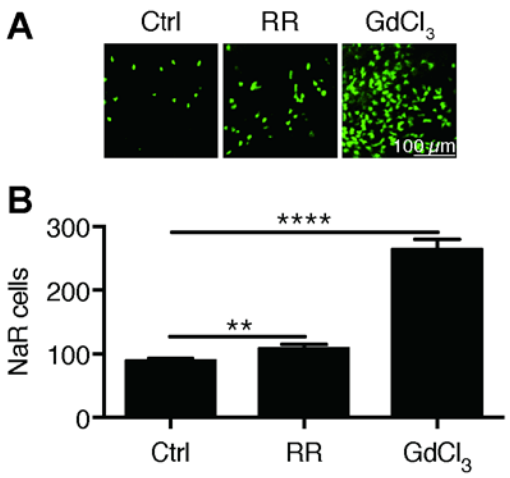

Figure 3.6 Inhibition of Trpv6 increases epithelial cell proliferation

(A-B) *Tg(igfbp5a:GFP)* fish were treated with Ruthenium Red (2 µM) or $GdCl_3$ (100 µM) from 3 to 5 dpf. Representative images are shown in (A). NaR cell numbers were quantified and shown in (B). **, **** indicate $P < 0.01$ and 0.0001 by unpaired t-test.

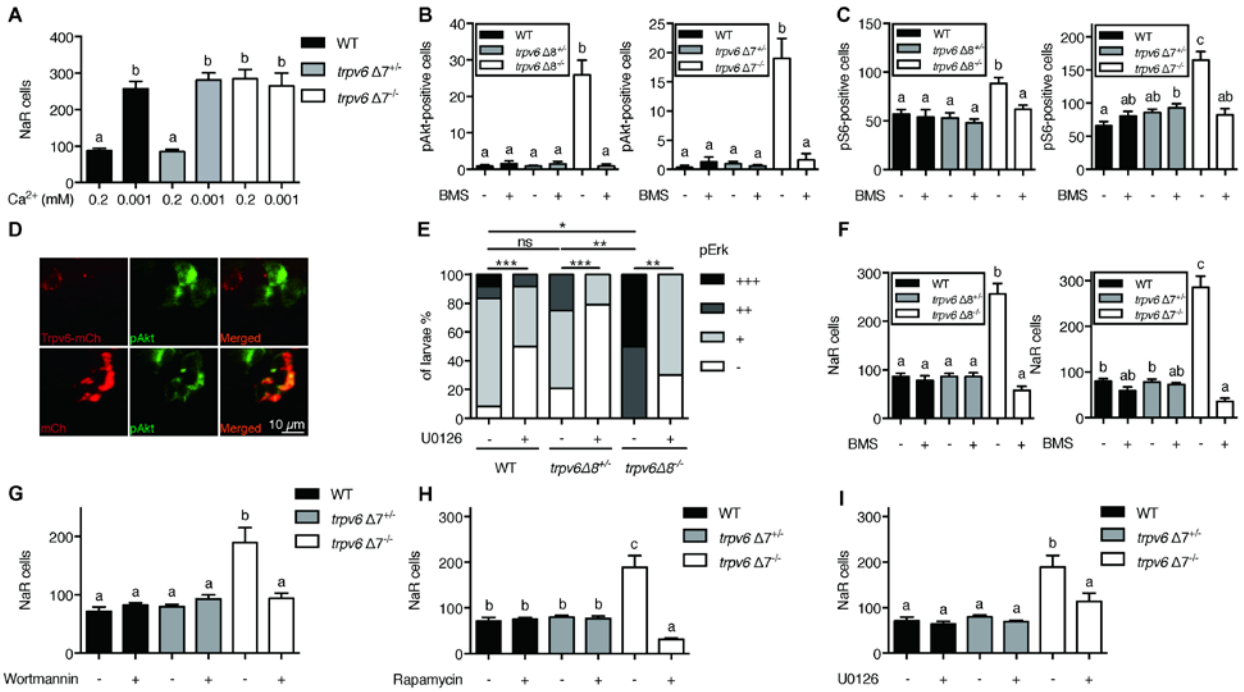

Figure 3.7 Trpv6 prevents the quiescence to proliferation transition via regulating IGF1 receptor-mediated IGF signaling

(A) Progenies of *trpv6*Δ7$^{+/-}$*; Tg(igfbp5a:GFP)* intercrosses were grown in embryo solutions with the indicated Ca^{2+} concentration from 3 dpf to 5 dpf. NaR cells in each fish were quantified followed by individual genotyping. n = 5-17 fish. (B-C) Embryos of the indicated genotypes were raised to 3 dpf and treated with 0.3 μM BMS-754807 or DMSO. At 4 dpf, the treated fish were subjected to immunostaining using an anti-phospho-Akt antibody (B) or an anti-phospho-S6 antibody (C). Representative images are shown in (figure supplement 2A and 2B). n = 5-41. (D) Progenies of a *trpv6Δ8*$^{+/-}$*; Tg (igfbp5a:GFP)* intercross were injected with the indicated BAC-mCherry DNA at one-cell stage. At 4 dpf, the larvae were subjected to phospho-Akt and mCherry double staining. (E) Embryos of the indicated genotypes were raised to 3 dpf and treated with 30 μM U0126 or DMSO. At 4 dpf, the treated fish were subjected to immunostaining using an anti-phospho-Erk antibody. pErk signals were scaled as shown in (Dai

et al., 2014a). n=4-24. (F-I) Progenies of *trpv6*Δ8$^{+/-}$*; Tg(igfbp5a:GFP)* or *trpv6*Δ7$^{+/-}$*; Tg(igfbp5a:GFP)* intercrosses were raised to 3 dpf and treated with BMS-754807 (0. 3 μM), Wortmannin (0. 06 μM), Rapamycin (1 μM), U0126 (10 μM) or DMSO from 3 to 5 dpf. NaR cells in each fish were quantified followed by individual genotyping, n = 6-22.

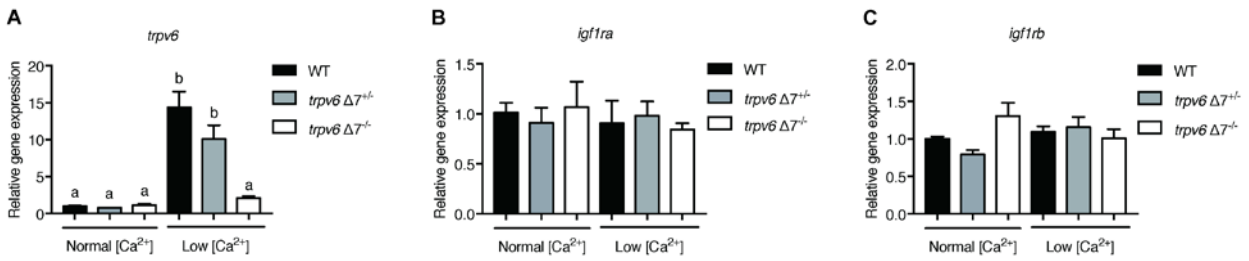

Figure 3.8 *trpv6, igf1ra, igf1rb* expression in *trpv6*$^{-/-}$

(A-C) *trpv6*Δ7$^{+/-}$*; Tg(igfbp5a:GFP)* intercrosses were raised in normal or low [Ca^{2+}] solutions from 3-5 dpf. Caudal fin was clipped for genotyping and 4-6 fish from the same genotype group were pooled for RNA extraction and RT-qPCR. Gene expression level was normalized to *18s*. Values shown are Mean ± SEM, n=3.

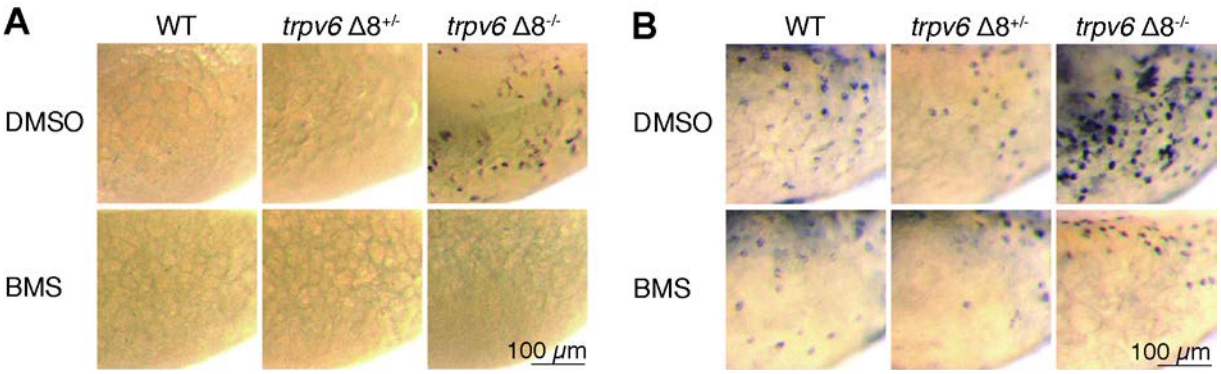

Figure 3.9 Akt-Tor pathway activation in *trpv6*$^{-/-}$

(A-B) *trpv6*Δ8$^{+/-}$*; Tg(igfbp5a:GFP)* intercrosses were treated with 0.3 μM BMS-754807 or DMSO. At 4 dpf, the treated fish were subjected to immunostaining using an anti-phospho-Akt antibody (A) or an anti-phospho-S6 antibody (B).

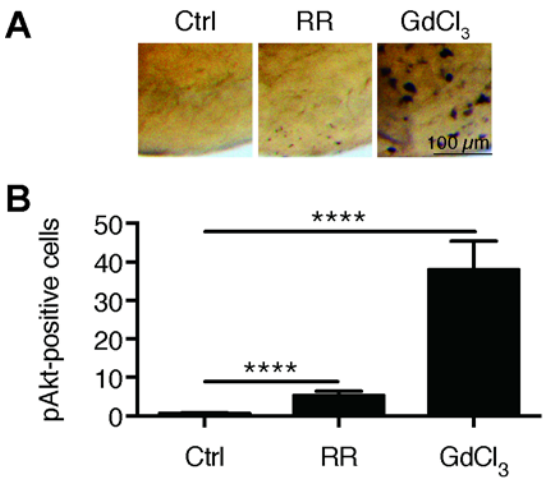

Figure 3.10 Inhibition of Trpv6 increases Akt signaling.

(A-B) Wild type fish were treated with Ruthenium Red (30 µM) or $GdCl_3$ (100 µM) from 3 to 4 dpf and analyzed by immunostaining using an anti-phospho-Akt antibody. Representative images are shown in (A) and quantified results shown in (B). **, **** indicate $P < 0.01$ and 0.0001 by unpaired t-test.

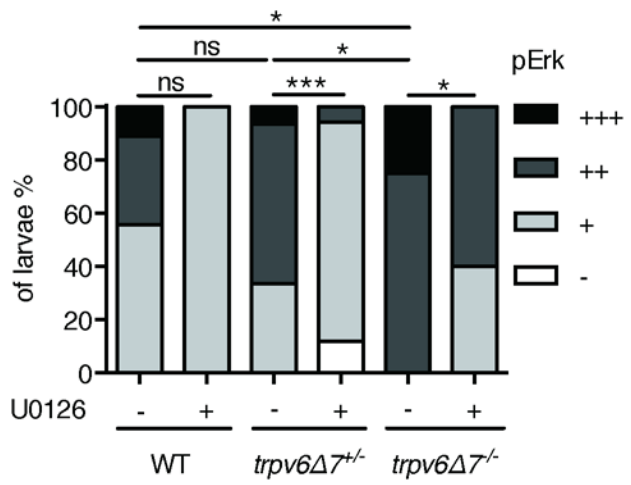

Figure 3.11 pErk level was elevated in in *trpv6*Δ7$^{-/-}$

(A) *trpv6*Δ7$^{+/-}$*; Tg(igfbp5a:GFP)* intercrosses were treated with 30 µM U0126 or DMSO from 3-4 dpf and then stained for phosphorylated-Erk signals. pErk signals were scaled as shown in (Dai et al., 2014a). n=5-17.

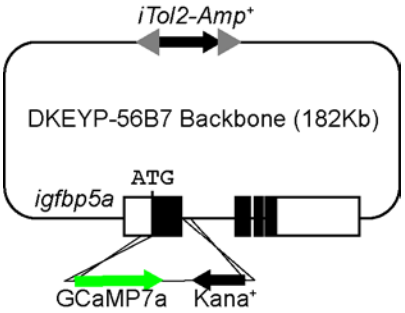

Figure 3.12 Schematic diagram showing the *BAC(igfbp5a:GCaMP7a)* construct

Filled boxes indicate *igfbp5a* ORF and open boxes indicate its UTRs. The *iTol2* cassette and GCaMP7a reporter cassette were introduced into DKEYP-56B7 by homologous recombination. The *igfbp5a* sequence from the start codon to the end of first exon was replaced by the GCaMP7a cassette.

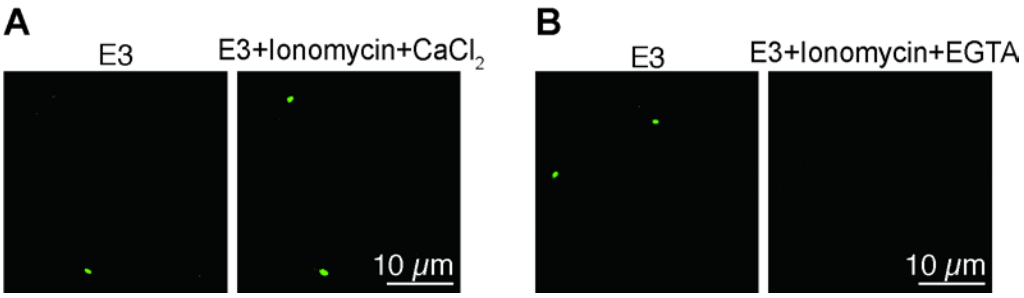

Figure 3.13 Validation of *Tg(igfbp5a:GCaMP7a)* fish

(A-B) Embryos injected with *BAC(igfbp5a:GCaMP7a)* DNA were raised in E3 embryo solution and imaged at 3 dpf before and after the addition of the indicated chemicals (Ionomycin: 5 μM, $CaCl_2$: 10 mM, EGTA: 10 mM).

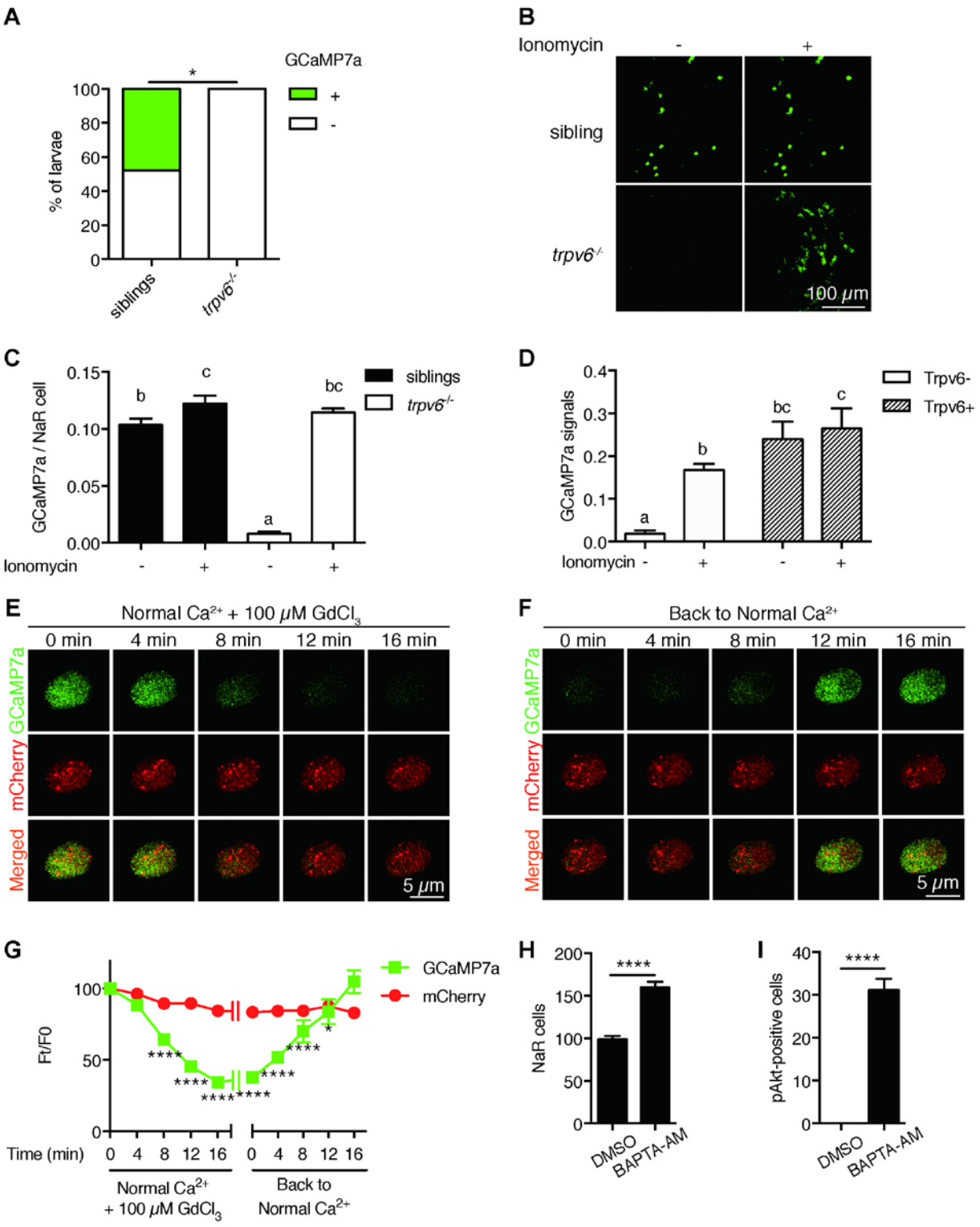

Figure 3.14 Trpv6 is constitutively open and mediates Ca^{2+} influx and maintain high $[Ca^{2+}]_i$ in epithelial cells in vivo

(A) *trpv6Δ8-2*$^{+/-}$*;Tg (igfbp5a:GCaMP7a)*$^{+/-}$ was crossed with *trpv6Δ8-2*$^{+/-}$. The progenies were imaged at 3 dpf followed by individual genotyping. Percentage of GCaMP7a-positive fish is shown. *, $P < 0.05$ by Chi-Square test, n = 21/21. 6 fish in *trpv6*$^{-/-}$ group contain *GCaMP7a* gene indicated by genotyping results. (B-C) Fish described in (A) were imaged before and after the addition of 7.5 µM Ionomycin + 10 mM $CaCl_2$. Representative images are shown in (B) and the quantified results are shown in (C). n = 5-7. (D) Progenies from a *trpv6Δ8-2*$^{+/-}$*;Tg (igfbp5a:GCaMP7a)*$^{+/-}$ and *trpv6Δ8-2*$^{+/-}$ intercross were injected with *BAC (igfbp5a:Trpv6-mCherry)* DNA at 1-cell stage. They were raised to 3 dpf. GCaMP7a signal intensity in Trpv6-mCherry-expressing cells and non-expressing NaR cells were quantified before and after the addition of 7.5 µM Ionomycin+10 mM $CaCl_2$. n = 4. (E-G) Time-lapse images of 3 dpf *Tg (igfbp5a:GCaMP7a)* larvae after the addition of 100 µM $GdCl_3$ (E) or following drug removal (F). Changes in GCaMP7a and mCherry signal intensity ratio were quantified and shown in (G). n = 5. * and **** indicate $P < 0.05$ and < 0.0001 by Two-way ANOVA followed by Dunnett's multiple comparisons test. (H) Wild-type larvae were treated with BAPTA-AM (100 µM) from 3 dpf to 5 dpf. NaR cells were labeled by *in situ* hybridization using a *trpv6* riboprobe and quantified. (I) Larvae described in (H) were stained for phosphorylated Akt after 24 hour treatment. Mean ± SEM. ****, $P<0.0001$, unpaired t-test. n = 15-19.

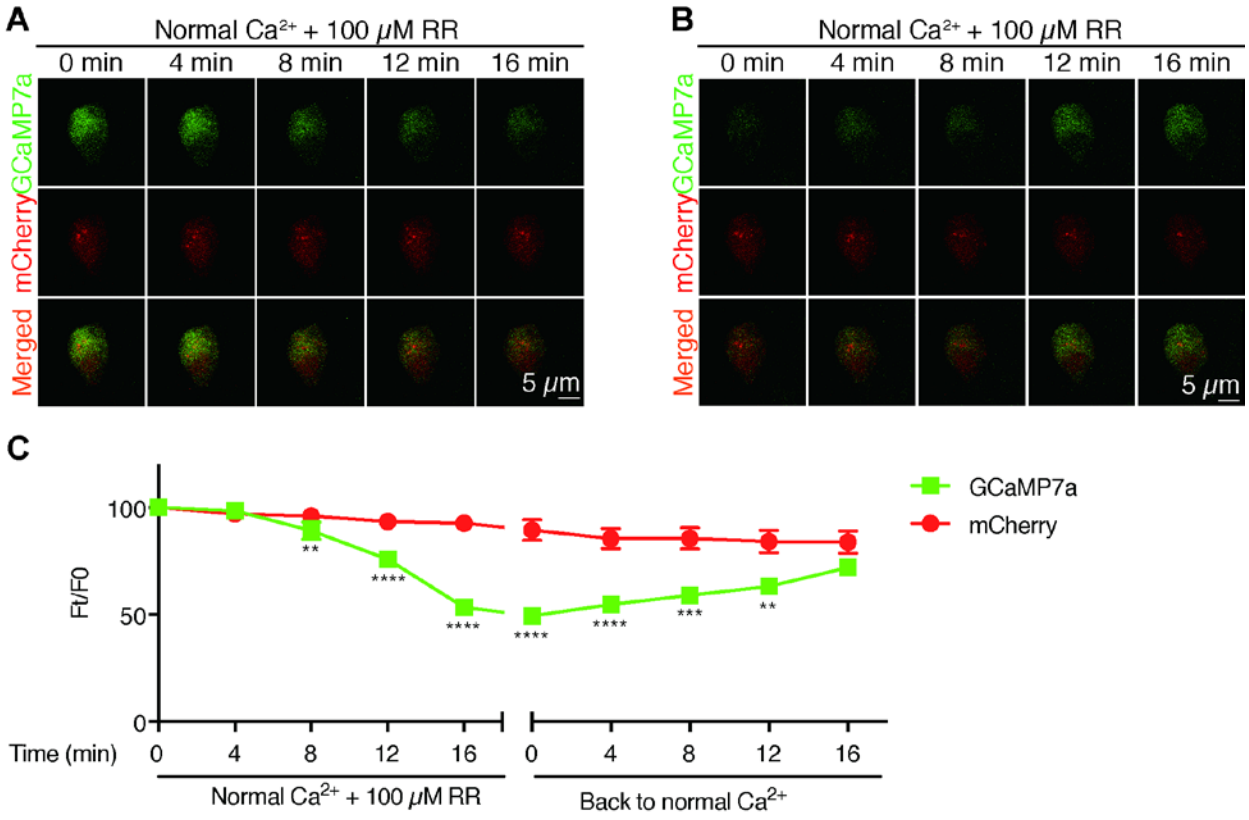

Figure 3.15 Inhibition of Trpv6 decreases $[Ca^{2+}]_i$ in NaR cells

(A-C) Time-lapse images of 3 dpf larvae were taken after the addition (A) and removal (B) of 100 μM Ruthenium red (RR) at the indicated time points. Fluorescence change of GCaMP7a (green) and mCherry (red) were quantified and shown in (C). Mean ± SEM, n = 8. **,***, and **** indicate $P < 0.01$, $P < 0.001$, $P < 0.0001$ by multiple t-tests.

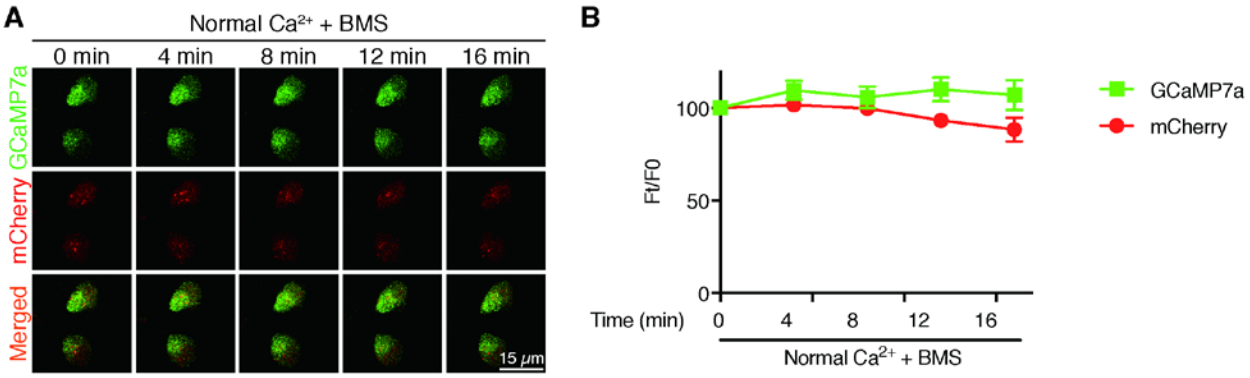

Figure 3.16 Inhibition of IGF1 receptor does not change $[Ca^{2+}]_i$ in NaR cells

Time-lapse images of 3 dpf *Tg (igfbp5a:GCaMP7a)* larvae at the indicated time points after adding 0.3 μM BMS-754807. Changes in GCaMP7a (green) and mCherry (red) signal intensity were quantified. Representative images are shown in (A) and quantified results are shown in (B). Mean ± SEM, n = 3. No significance was found by two-way ANOVA followed by Dunnett's multiple comparisons test.

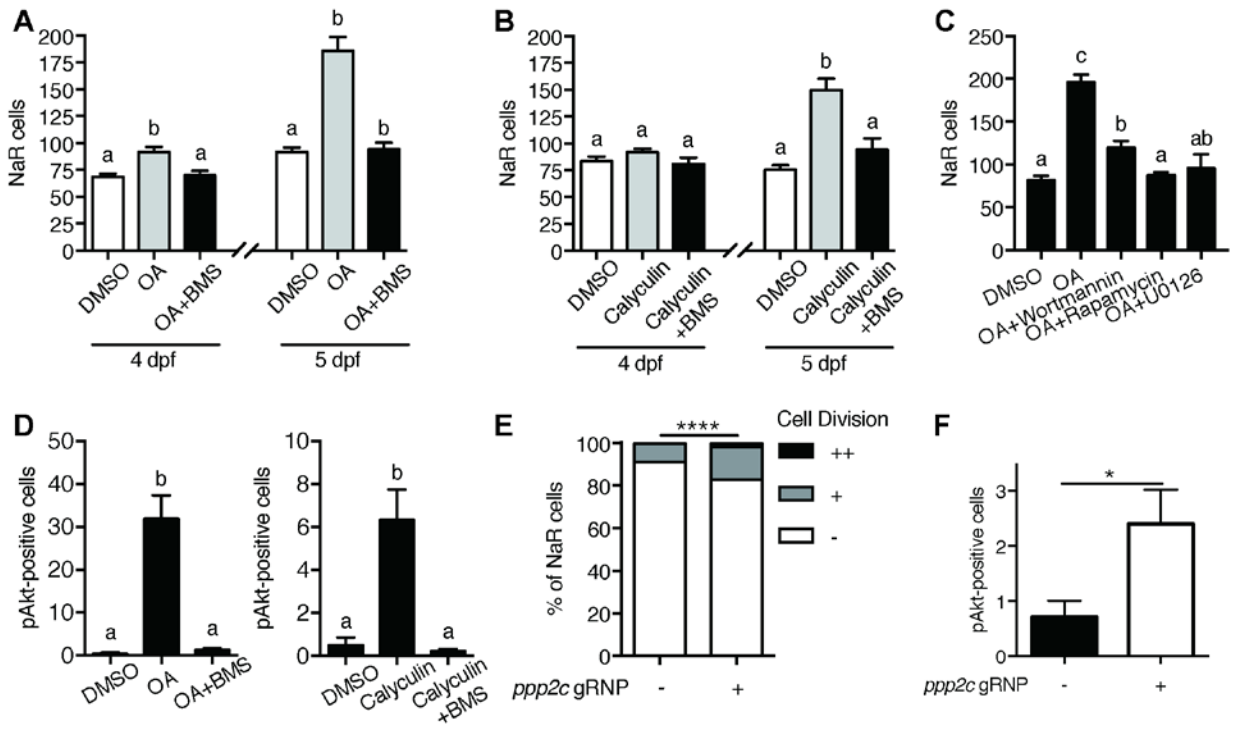

Figure 3.17 PP2A is a downstream effector of Trpv6

(A-B) *Tg(igfbp5a:GFP)* embryos were treated with 1 µM Okadaic acid (OA) or 0.1 µM Calyculin A in the presence or absence of 0.3 µM BMS-754807 from 3 dpf. NaR cells were quantified at 4 and 5 dpf. Data shown are n = 10-38. (C) *Tg(igfbp5a:GFP)* embryos were treated with 1 µM Okadaic acid (OA) in the presence or absence of Wortmannin (0. 06 µM), Rapamycin (1 µM), U0126 (10 µM) or DMSO from 3 to 5 dpf. NaR cells were quantified at 4 and 5 dpf. Data shown are n = 16-19. (D) Wild-type larvae were treated with 1 µM Okadaic acid or 0.1 µM Calyculin in the presence or absence of 0.3 µM BMS-754807 from 3 dpf to 4 dpf. They were analyzed by immunostaining for phospho-Akt. n = 9-16. (E) *Tg(igfbp5a:GFP)* embryos were injected with gRNAs targeting three *ppp2c* genes and Cas9 protein at one-cell stage. They were raised to 5 dpf. NaR cell division was quantified following a published scoring system (Liu et al., 2018a). n = 24-28. ****, $P < 0.0001$ by Chi-Square test. (F) The embryos

treated as in (E) were raised to 4 dpf and analyzed by immunostaining for phospho-Akt signal. n = 20-21. *, $P< 0.05$, unpaired t-test.

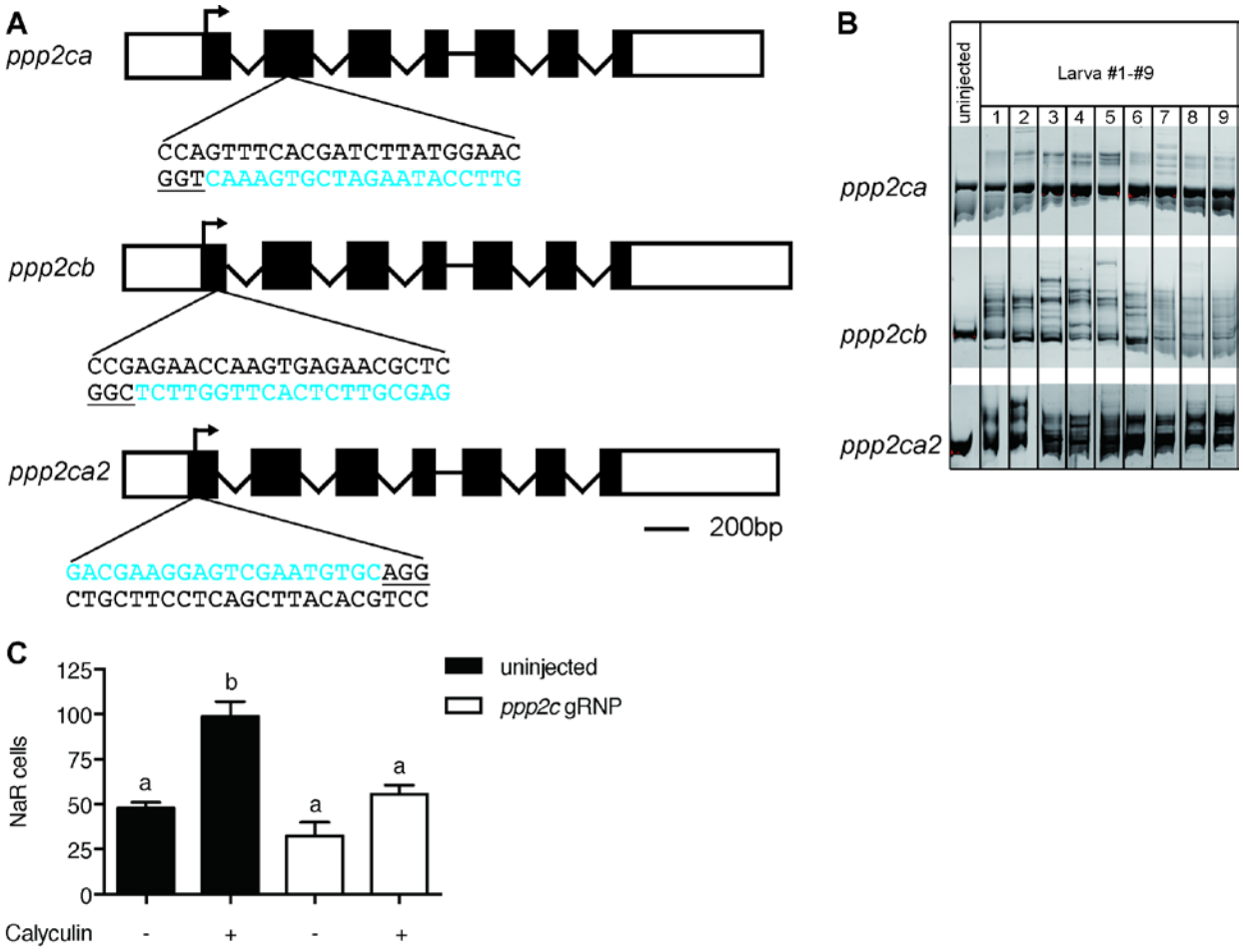

Figure 3.18 Transient knockdown of *pp2a* catalytic subunit genes

(A) Schematic diagram and guide RNA targeting sites. The target sites are labeled by blue letters and the PAM motif is underlined. (B) Embryos injected with gRNAs and Cas9 protein were raised to 1 dpf. Each of them was lysed and analyzed by PCR followed by hetero-duplex motility assay. (C) Embryos injected with gRNAs and Cas9 protein were raised to 3 dpf and treated with Calyculin or vehicle. Values are Mean ± SEM, n = 7-15.

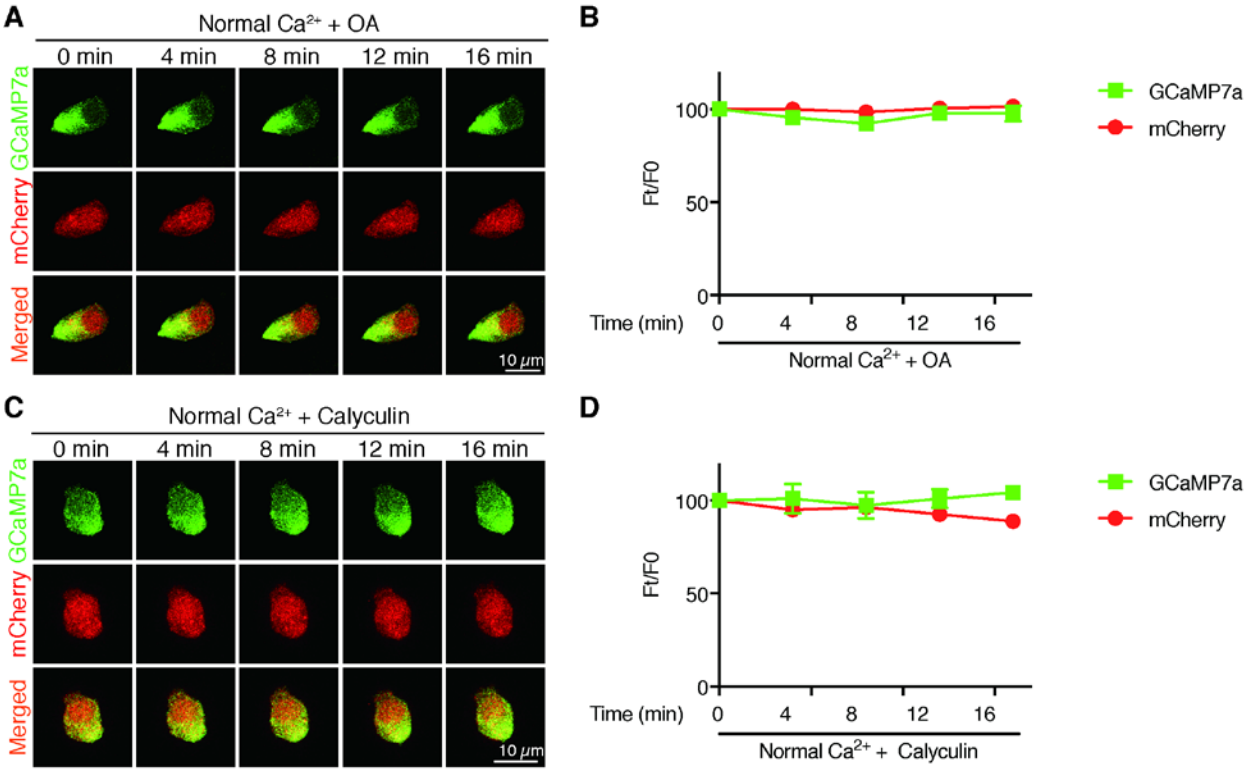

Figure 3.19 Inhibition of PP2A does not change $[Ca^{2+}]_i$ in NaR cells

Time-lapse images of 3 dpf *Tg (igfbp5a:GCaMP7a)* larvae at the indicated time points after adding 1 µM Okadaic acid (OA) (**A, B**) or 0.1 µM Calyculin (**C, D**). Changes in GCaMP7a (green) and mCherry (red) signal intensity were quantified. Representative images are shown in (**A**, **C**) and quantified results are shown in (**B, D**). Mean ± SEM, n = 3. No significance was found by two-way ANOVA followed by Dunnett's multiple comparisons test.

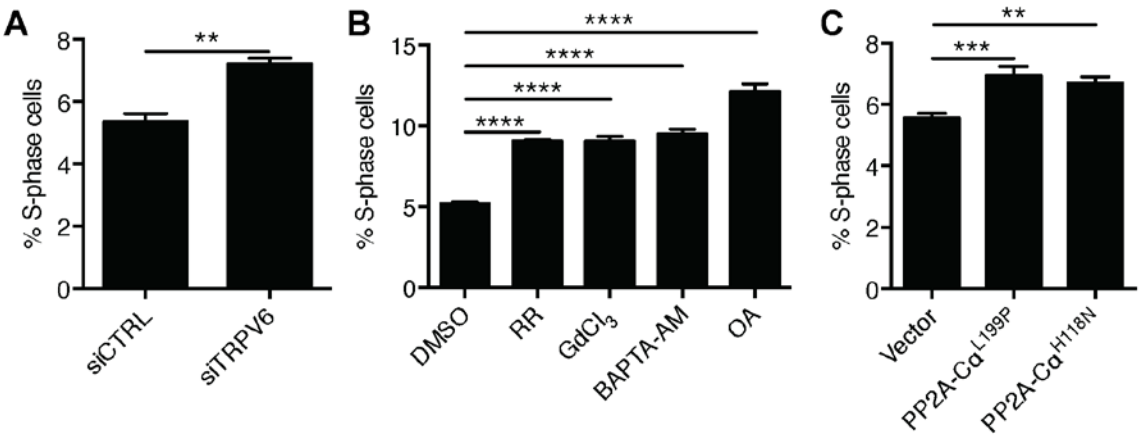

Figure 3.20 Knockdown and inhibition of TRPV6 and PP2A increases human colon carcinoma cell proliferation

(A) LoVo cells transfected with scrambled siRNA or TRPV6 targeting siRNA were synchronized by serum starvation followed with serum re-stimulation. Cells were analyzed by flow cytometry analysis after propidium iodide staining. Percentage of S-phase cells are calculated and shown. Mean ± SEM, n = 3. **, $P<0.01$ by unpaired t-test. (B) LoVo cells were synchronized by serum starvation. They were re-stimulated with 2% FBS medium containing Ruthenium Red (RR, 100 µM), $GdCl_3$ (100 µM), BAPTA-AM (100 µM), Okadaic acid (OA, 20 nM) or DMSO for 48 hours and analyzed by flow cytometry analysis after propidium iodide staining. Percentage of S-phase cells are shown. Mean ± SEM, n = 3. One-way ANOVA followed by Tukey's multiple comparison test was used to analyze data in B and C. ****, ***, ** indicates $P<0.0001$, $P<0.001$, $P<0.01$ respectively. (C) LoVo cells transfected with the indicated DN-PP2A constructs were synchronized by serum starvation followed with serum re-stimulation. Cells were analyzed by flow cytometry analysis after propidium iodide staining. Percentage of S-phase cells are calculated and shown. Mean ± SEM, n = 3

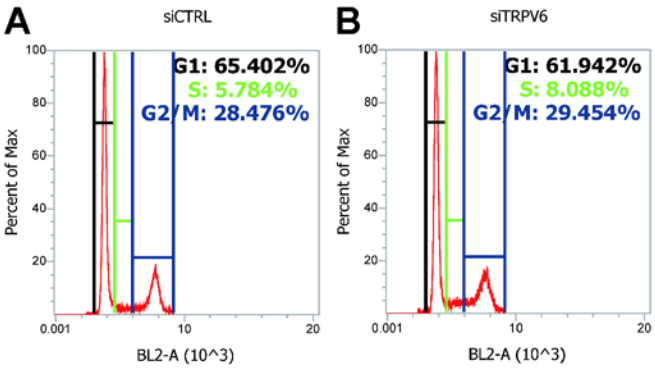

Figure 3.21 Cell cycle analysis results of TRPV6 knockdown

The PI fluorescence intensity is given in arbitrary units (a.u.) on the X-axis, and the Y-axis indicates cell counts normalized to percent of the max as measured by flow cytometry. Knockdown of TRPV6 significantly increased percentage of S phase cells.

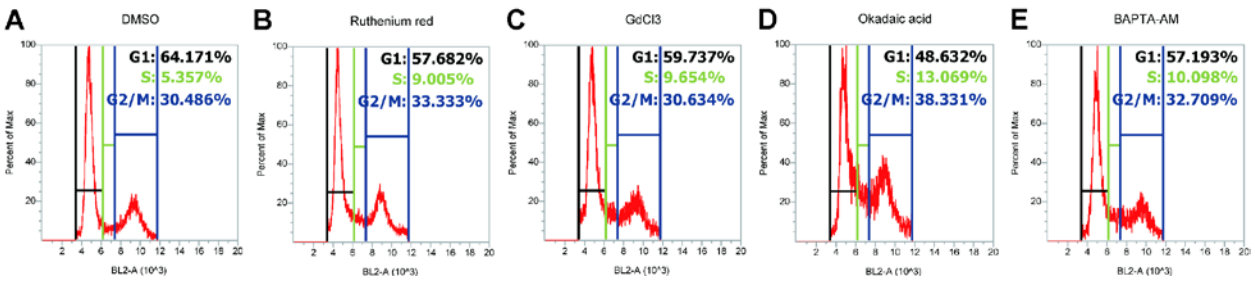

Figure 3.22 Cell cycle analysis results of pharmacological inhibiting TRPV6-Ca^{2+}-PP2A pathway

The PI fluorescence intensity is given in arbitrary units (a.u.) on the X-axis, and the Y-axis indicates cell counts normalized to percent of the max as measured by flow cytometry. Pharmacological inhibition of TRPV6, PP2A or chelating intracellular Ca^{2+} using BAPTA-AM significantly increased percentage of S phase cells.

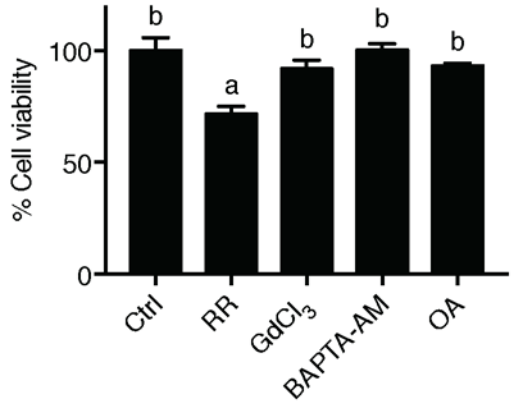

Figure 3.23 LoVo cell viability

LoVo cells were synchronized by serum starvation. They were re-stimulated with 2% FBS medium containing Ruthenium Red (RR, 100 µM), $GdCl_3$ (100 µM), BAPTA-AM (100 µM), Okadaic acid (OA, 20 nM) or DMSO for 48 hours and analyzed by MTT assays. Mean ± SEM, n = 3.

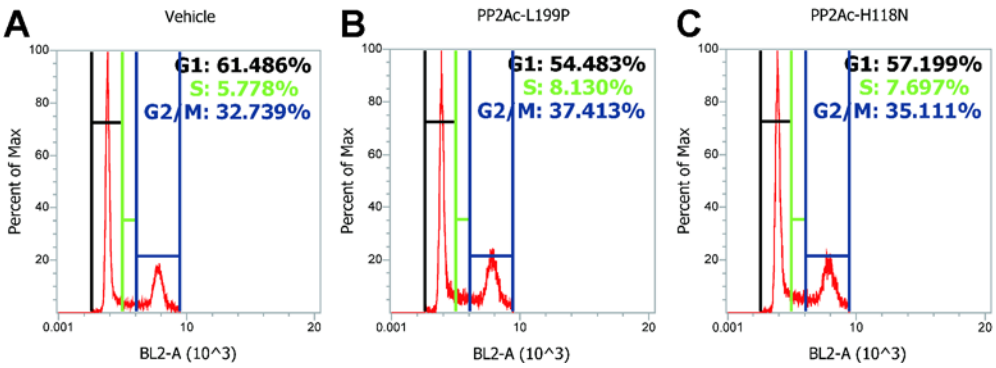

Figure 3.24 Cell cycle analysis results of overexpression dominant-negative PP2A

The PI fluorescence intensity is given in arbitrary units (a.u.) on the X-axis, and the Y-axis indicates cell counts normalized to percent of the max as measured by flow cytometry. Overexpression of dominant-negative PP2A constructs significantly increased percentage of S phase cells.

Table 3-1 Key Resources Table

Reagent type (species) or resource	Designation	Source or reference	Identifiers	Additional information
strain, strain background (Danio rerio)	*Tg(igfbp5a:GFP)*	Pubmed ID: 28515443	RRID:ZFIN_ZDB--TGCONSTRCT-170830-2	
strain, strain background (Danio rerio)	*trpv6*$^{-/-}$; *Tg(igfbp5a:GFP)*	This paper		Crispr/Cas9-mediated knockout
strain, strain background (Danio rerio)	*Tg(igfbp5a:GCaMP7a)*	This paper		Tol2-mediated transgenesis
strain, strain background (Danio rerio)	*trpv6*$^{-/-}$	This paper		Crispr/Cas9-mediated knockout
strain, strain background (Danio rerio)	*trpv6*$^{-/-}$; *Tg(igfbp5a:GCaMP7a)*	This paper		Cross *trpv6*$^{-/-}$ with *Tg (igfbp5a:GCaMP7a)*
genetic reagent (Homo Sapiens)	Human TRPV6 siRNA	Pubmed ID: 19270724		GACUCUCUAUGACCUCACA
genetic reagent ()	Mission siRNA Universal Negative Control #1	Sigma	Catalog no.: SIC001-10nmol	
cell line (Homo Sapiens)	LoVo	ATCC	Catalog no.: CCL-229	
cell line (Homo Sapiens)	HEK293	ATCC	Catalog no.: CRL-1573	
antibody	Phospho-Akt (Ser473)	Cell Signaling Technology	Catalog no.: 4060	
antibody	Phospho-p44/42 MAPK (Erk1/2) (Thr202/Tyr204)	Cell Signaling Technology	Catalog no.: 4370	

antibody	Phospho-S6 Ribosomal Protein (Ser235/236)	Cell Signaling Technology	Catalog no.: 4856	
antibody	Peroxidase-conjugated AffiniPure Donkey Anti-Rabbit IgG (H+L)	Jackson Immuno Research Laboratories	RRID: AB_10015282	
antibody	Cy3 AffiniPure Goat Anti-Rabbit IgG (H+L)	Jackson Immuno Research Laboratories	RRID: AB_2338006	
antibody	Anti-digoxigenin POD-conjugate; from sheep	Roche	Catalog no.: 11207733910	
recombinant DNA reagent	PP2Ac-L199P	Pubmed ID: 16224536		
recombinant DNA reagent	PP2Ac-H118N	Pubmed ID: 16224536		
chemical compound, drug	BMS-754807	Active Biochemicals Co.	Catalog no.: A-1013	
chemical compound, drug	Wortmannin	Cell Signaling Technology	Catalog no.: 9951	
chemical compound, drug	Rapamycin	Calbiochem	Catalog no.: 553210	
chemical compound, drug	U0126	Cell Signaling Technology	Catalog no.: 9903	
chemical compound, drug	Okadaic acid	Santa Cruz Biotechnology	Catalog no.: sc3513	

chemical compound, drug	Calyculin	Alonmone	Catalog no.: C-100	
chemical compound, drug	Gadolinium (III) chloride	Sigma-Aldrich	Catalog no.: 439770	
chemical compound, drug	Ruthenium red	Sigma-Aldrich	Catalog no.: R2751	
peptide, recombinant protein	Cas9 protein with NLS	PNA Bio	CP01	
software, algorithm	GraphPad Prism	RRID:SCR_002798		

Chapter 4 CaMKK Promotes Epithelial Cell Quiescence-Proliferation Transition by Increasing IGF1 Receptor-PI3K-Akt Activity

4.1 Abstract

Epithelial tissues face constant environmental challenges and frequently re-activate a pool of quiescent cells to maintain tissue homeostasis. The molecular mechanisms governing the quiescence-proliferation balance is poorly defined. Using a zebrafish model, here we report that Ca^{2+}/calmodulin-dependent kinase kinase (CaMKK) plays a critical role in promoting the quiescence-proliferation transition in a group of Ca^{2+}-transporting epithelial cells (NaR cells). NaR cells are maintained in the quiescent state by Trpv6-mediated constitutive Ca^{2+} influx. Lowering the intracellular Ca^{2+} ($[Ca^{2+}]_i$) levels by genetic deletion of Trpv6, pharmacological inhibition of Trpv6, competitive blockade of Trpv6-mediated Ca^{2+} influx, or removing Ca^{2+} from the embryo rearing solution all resulted in elevated Akt and Tor activity and NaR cell quiescence-proliferation transition. This action was abolished by inhibition of IGF1 receptor. Chemical biology screens and CRISPR/Cas9 knockdown experiments identified CaMKK as a key link between $[Ca^{2+}]_i$ and IGF-Akt-Tor signaling. Depletion of the ER Ca^{2+} store by inhibiting sarco/endoplasmic reticulum Ca^{2+}-ATPase abolished NaR cell reactivation and Akt signaling. These results suggest that ER Ca^{2+} release in response to the reduction of $[Ca^{2+}]_i$ is important in activating CaMKK and IGF signaling and this in turn promoting quiescent cells to re-enter the cell cycle. Importantly, this $[Ca^{2+}]_i$-CaMKK-Akt signaling mechanism is conserved in human colon carcinoma cells.

4.2 Introduction

Epithelial tissues provide the protective layer against the external environment and play critical role in nutrient absorption, gas exchange, and water-ion balance. As such, epithelia tissues have a very high turnaround rate. Its tissue homeostasis is maintained by re-activating a pool of quiescent cells. The molecular mechanisms governing the quiescence-proliferation transition is poorly defined. Recently, a group of quiescent epithelial cells in zebrafish absorptive epithelia, known as Na^+-K^+-ATPase-rich (NaR) cells have been shown to be reactivated in respond to low environmental Ca^{2+} stress (Dai et al., 2014a). This has been attributed to the activation of the insulin-like growth factor receptor 1 (IGF1R)-mediated phosphoinositide-3-kinases (PI3K)-Akt and target of rapamycin (Tor) signaling (Dai et al., 2014a). These findings made with fish NaR cells resemble previous studies made in the mouse adult hematopoietic stem cells (HSCs) and the fly neural stem cells (Chell and Brand, 2010; Lee et al., 2007; Paik et al., 2009; Siegemund et al., 2015; Wang et al., 2018a), suggesting that the activity of IGF-PI3K-Akt-Tor is critical in cellular quiescence reactivation in multiple cell types across a wide range of species.

In addition to the IGF-PI3K-Akt-Tor signaling, Ca^{2+} signaling has been shown to regulate cellular quiescence in intestinal stem cells (ISCs) (Deng et al., 2015), pluripotency of mouse embryonic stem cells (mESCs) (MacDougall et al., 2019), and mesenchymal stem cell (Lee et al., 2018). In fact, Ca^{2+} is a universal signaling in the cell and it influences many cellular processes (Clapham, 2007). The Ca^{2+} signaling toolkits can be hijacked by cancer cells for unrestrained cell cycle progression (Varghese et al., 2019). In a recent study, we have shown that Trpv6-mediated Ca^{2+} influx establishes the quiescent state of NaR cells by maintaining high intracellular Ca^{2+} concentrations ($[Ca^{2+}]_i$) (Xin et al., 2019). Genetic deletion and

pharmacological inhibition of Trpv6 resulted in reduced $[Ca^{2+}]_i$ levels and this in turn leads to increased IGF signaling and promotes NaR quiescence-proliferation transition. The molecular mechanisms linking the reduction of intracellular Ca^{2+} ($[Ca^{2+}]_i$) levels to the activation of IGF signaling, however, is unclear.

In the present study, we investigated the role of Ca^{2+} signaling in NaR cell recativation and its cross-talk with the IGF-PI3K-Akt-Tor signaling pathway. We found that lowering the intracellular Ca^{2+} ($[Ca^{2+}]_i$) levels by genetic deletion of Trpv6, pharmacological inhibition of Trpv6-mediated Ca2+ influx, or removing Ca2+ from the embryo rearing solution all increased IGF signaling and led to NaR cell quiescence-proliferation transition. We further showed that CaMKK functions as a link between changes in [Ca2+]i to IGF-Akt-Tor signaling activation.

4.3 Results

4.3.1 Reducing $[Ca^{2+}]_i$ stimulates quiescence exit of NaR cells

Treatment of Tg(*igfbp5a*: GCaMP7a) zebrafish larvae with the Trpv6 channel inhibitor lanthanum chloride (Kovacs et al., 2011) resulted in decreased intracellular Ca^{2+} level in NaR cells, while mCherry fluorescence in these cells remained largely unchanged (Figure 4.1A and B). TRPV6 channel permeability is estimated to be about 100 times more selective for Ca^{2+} than for Na^+ (Voets et al., 2004). Increasing environmental Na^+ concentration from 0.5 mM to 100 mM significantly reduced intracellular Ca^{2+} level (Figure 4.1D and E). (NMDG)Cl of the same concentration had no such effect, suggesting osmolarity or Cl^- concentration change does not affect Ca^{2+} influx in NaR cells. When Ca^{2+} influx is restricted through reducing environmental Ca^{2+} (Normal $[Ca^{2+}]_e$ = 0.2 mM, Low $[Ca^{2+}]_e$ = 0.001 mM), intracellular Ca^{2+} level in the NaR cells decreases dramatically as well (Figure 4.1G and H). All those treatments reduced $[Ca^{2+}]_i$ and promoted the reactivation of NaR cells (Figure 4.1C, F, and I).

4.3.2 Depletion of endoplasmic reticulum Ca^{2+} abolished NaR cell reactivation

Ca^{2+} serves as a versatile and universal second messenger controlling a wide range of biological processes. Tight control of intracellular Ca^{2+} concentrations in different compartments is crucial for precisely decoding the Ca^{2+} signals for specific cellular function (Bootman, 2012). To determine whether intracellular Ca^{2+} stores such as ER plays any role, we imaged $[Ca^{2+}]_i$ for a long period. As described before, GCaMP7a fluorescence in NaR cells decreases greatly once extracellular Ca^{2+} is removed, however, after 30 min incubation in low $[Ca2^{+}]_e$, GCaMP7a fluorescence gradually came back, indicating the replenishment of intracellular Ca^{2+} across time (Figure 4.2A). Addition of intracellular Ca^{2+} chelator BAPTA-AM in the low Ca^{2+} solution significantly decreased low Ca^{2+} -induced NaR cell reactivation (Figure 4.2B). These results indicate that when $[Ca^{2+}]_i$ decreased, ER released Ca^{2+} into the cytosol. Chelating extracellular Ca^{2+} using EGTA (2 mM) also induced NaR cell reactivation (Figure 4.2C). The endoplasmic reticulum (ER) is the major intracellular Ca^{2+} reservoir. However, when we measured $[Ca^{2+}]_{ER}$ using a genetically-encoded ER Ca^{2+} indicator ER-LAR-GECO1 (Wu et al., 2014), no major change in $[Ca^{2+}]_{ER}$ was observed during low $[Ca^{2+}]_e$ incubation (Figure 4.2D). But when an inhibitor targeting sarco/endoplasmic reticulum Ca^{2+}-ATPase, thapsigargin (TG) was added into low Ca^{2+} solution, $[Ca^{2+}]_{ER}$ decreased dramatically as Ca^{2+} uptake by ER is blocked (Figure 4.2D), suggesting ER-LAR-GECO1 fluorescence can report a major change of $[Ca^{2+}]_{ER}$ level. Depletion of ER Ca^{2+} store using TG or another SERCA inhibitor cyclopiazonic (CPA) strongly attenuated the low $[Ca^{2+}]_i$ -mediated reactivation of NaR cells (Figure 4.2E and F).

4.3.3 CaMKK activity is required for low $[Ca^{2+}]_i$-mediated NaR cell reactivation

We next tried to identify the molecular link between reduced $[Ca^{2+}]_i$ to the reactivation of NaR cells through screening chemicals targeting Ca^{2+}-sensitive molecules. Among the hits that

inhibited low $[Ca^{2+}]_i$ -induced reactivation of NaR cells, CaMKK inhibitor STO-609 had the strongest inhibitory effects (Figure 4.3A). Loss of Trpv6 in *trpv6*$^{-/-}$ mutant fish induces quiescence exit in NaR cells as reported (Figure 4.3B) and reactivation of NaR cells in the mutant fish can be fully suppressed by CaMKK inhibition. Restricting Ca^{2+} influx through Trpv6 by addition of high $[Na^+]_e$ also resulted in increased NaR cell reactivation and that can be blocked by CaMKK inhibitor as well (Figure 4.3C). Knockdown of *camkk*s through CRISPR/Cas9 also resulted dramatically decreased the low $[Ca^{2+}]_i$ -mediated NaR cell reactivation in F0 larvae (Figure 4.3D). Additionally, CaM inhibitor W-7 and calmidazolium chloride also resulted in reduced NaR cell reactivation (Figure 4.3E).

4.3.4 CaMKK possibly regulates epithelial cell reactivation through phosphorylating Akt

Akt has been known as a low affinity downstream target of CaMKK and can be directly phosphorylated by CaMKK at Thr308 site (Yano et al., 1998). Follow-up studies have shown CaMKK-dependent Akt activation in mouse muscle cells, HEK293 cells, LNCaP cells, human gastric adenocarcinoma cells, and malignant ovarian tissue (Chen et al., 2002; Gocher et al., 2017; Ma et al., 2016; Schmitt et al., 2012; Wang et al., 2015b). Recent studies suggest both CaMKKα and CaMKKβ are involved in Akt phosphorylation (Gocher et al., 2017; Witczak et al., 2007). Therefore, we propose CaMKK promotes NaR cells reactivation through phosphorylating Akt. Akt phosphorylation had been known to be specifically elevated in NaR cells upon low Ca^{2+} acclimation or in the *trpv6*$^{-/-}$ mutants (Dai et al., 2014a; Xin et al., 2019). As anticipated, other ways to reduce $[Ca^{2+}]_i$ resulted in elevated Akt phosphorylation as well (Figure 4.4A and B). And maintaining ER-Ca^{2+} store is also critical for Akt phosphorylation as both SERCA inhibitors TG and CPA strongly suppressed low $[Ca^{2+}]_i$-activated Akt phosphorylation (Figure 4.4C and D).

To further investigate which isoform of Akt is the key player mediating the reactivation of NaR cell, selective Akt isoform inhibitors and pan Akt inhibitor Triciribine were tested. Selective Akt1 inhibitor A-674563 significantly diminished low Ca^{2+}-mediated reactivation of NaR cells while selective inhibitor for Akt2 CCT128930 does not had any effects (Figure 4.4E and F), indicating Akt1 is probably a more critical player for low $[Ca^{2+}]_i$ -triggered activation of IGF signaling pathway. Phosphorylation of both Ser 473 site and Thr 308 site are required for maximal activation of the kinase (Alessi et al., 1996). STO-609 could inhibited phosphorylation at both residues in the low $[Ca^{2+}]_i$ -reactivated NaR cells. Such effects are also evolutionarily conserved from fish to humans as low $[Ca^{2+}]_i$ -amplified Akt phosphorylation in cultured human colon carcinoma cells (Caco2) can also inhibited by CaMKK inhibitor STO-609 (Figure 4.5).

4.4 Discussion

In this study, we uncover an intriguing pathway that regulates epithelial cell quiescence to proliferation transition (Figure 4.6). Using multiple methods reducing Ca^{2+} influx through Trpv6, we showed that reduction in $[Ca^{2+}]_i$ level promotes quiescent NaR cells to reenter the cell cycle and proliferate. We observed a replenishment of $[Ca^{2+}]_i$ after long-term incubation under low Ca^{2+} medium, probably coming from Ca^{2+} release from the ER Ca^{2+} store. Chelation of intracellular Ca^{2+} with BAPTA-AM partially blocked this NaR reactivation. It is thus proposed that local Ca^{2+} microdomains are underlying the quiescence exit of NaR cells under low $[Ca^{2+}]_i$. In further support of this hypothesis, depletion of ER Ca^{2+} store using SERCA inhibitors completely abolished low $[Ca^{2+}]_i$ -triggered NaR cell reactivation.

Ca^{2+} microdomains have long been recognized as critical regulators for Ca^{2+} signaling (Berridge, 2006). The $[Ca^{2+}]_i$ a cell under resting conditions is around 100 nM, while ER $[Ca^{2+}]$ ($[Ca^{2+}]_{ER}$) is maintained around 100 μM. Release of ER Ca^{2+} via a the 1,4,5-triphosphate

receptor (IP3R) or ryanodine receptor (RyR) can result in a sharp increase in $[Ca^{2+}]_i$ locally, creating Ca^{2+} microdomains without changing much of global $[Ca^{2+}]_i$ level (Bagur and Hajnoczky, 2017). Ca^{2+} microdomains can regulate specific cellular processes in different regions of the cell, given that the actions of local Ca^{2+} signals may be restricted to effectors (such as channels, transporters and binding proteins) located within sub-micron distances from the Ca^{2+} source (Carafoli and Krebs, 2016). ER-mitochondria membrane contacts or ER-plasma membrane contacts during store-operated calcium entry (SOCE) are two major interfaces for Ca^{2+} microdomains (Bagur and Hajnoczky, 2017). In this case, SOCE is less likely to be involved as ER Ca^{2+} store depletion induced by SERCA inhibitors inhibited NaR cell reactivation rather than triggered this process. Further studies are required to further determine whether local Ca^{2+} microdomains at ER-mitochondria membrane contacts are critical for the quiescence to proliferation transition of NaR cells.

Next, chemical biology screen revealed that CaMKK is potentially mediating the quiescence exit of NaR cells. Utilizing both pharmacological and genetic approaches, we validated that CaMKK activity is required for reactivating NaR cells. CaM is a ubiquitously expressed, highly -conserved protein with each globular end containing a pair of helix-loop-helix EF-hand Ca^{2+}-binding motifs connected by a flexible α helix (Chin and Means, 2000). Each EF motif allows calmodulin to sense intracellular Ca^{2+} levels by binding one Ca^{2+} ion. Binding of Ca^{2+} produces a conformational change in CaM, exposing hydrophobic residues that promote interactions of the Ca^{2+}/CaM complex to numerous target proteins, thereby regulating their functions (Davis et al., 1989). Ca^{2+}/CaM-dependent kinases include Ca^{2+}/CaM -dependent kinase kinase (CaMKK) as well as its downstream targets CaMKI and the predominantly nuclear CaMKIV (Wayman et al., 2011). CaMKK comprises 1 (α) and 2 (β) isoforms in mammals and 3

isoforms (*camkk1a, camkk1b* and *camkk2*) in zebrafish. They are encoded by different genes and expressed in cells as monomer, containing a catalytic, autoinhibitory, and CaM-binding domain (Swulius and Waxham, 2008). Like all other CaM-dependent kinases, CaMKK is held in an inactive state by its autoinhibitory domain, which interacts with the catalytic domain to prevent kinase activity. Binding of Ca^{2+}/CaM relieves this inhibition by displacing the autoinhibitory domain and exposing the catalytic site. This leads to the activation of CaMKK and the subsequent phosphorylation of its downstream substrates (Tokumitsu and Soderling, 1996). Ca^{2+}/CaM binding is absolutely required for the relief of CaMKK1 autoinhibition, which results in its activation. However, CaMKK2 also exhibits significant activity even in the absence of Ca^{2+}/CaM binding (Tokumitsu et al., 2001). The Ca^{2+}/CaM sensitivity of CaMKK2 is uniquely dependent on phosphorylation of Ser129, Ser133 and Ser137 located within a regulatory sequence N-terminal to the catalytic domain (Green et al., 2011). Phosphorylation of Ser137 by proline-directed kinases (Pro-K) primes CaMKK2 for subsequent phosphorylation on Ser133 and Ser129 by glycogen synthase kinase 3 (GSK3). Without phosphorylation at these sites, CaMKK2 exhibits increased autonomous activity in the absence of Ca^{2+}/CaM. Additionally, once bound to Ca^{2+}/CaM, CaMKK2 undergoes autophosphorylation at Thr85, which generates Ca^{2+}-independent autonomous activity by maintaining CaMKK2 in the activated state after removal of the Ca^{2+} stimulus (Scott et al., 2015).

Ca^{2+} has long been known to drive proliferation in many cell types through direct activation of CaM and CaM-dependent kinases including CaMKK upon Ca^{2+} influx (Berchtold and Villalobo, 2014; Gocher et al., 2017; Kahl and Means, 2003; Olianas et al., 2018). Increasing evidence have shown CaMKKs are involved in cellular quiescence to proliferation regulation. CaMKK2 has been shown to be an important regulator of anabolic pathways downstream of the

androgen receptor in prostate cancer cells (Massie et al., 2011). Pharmacological inhibition of CaMKK2 improves survival and accelerates hematopoietic stem and progenitor cell recovery following hematopoietic radiation injury (Racioppi et al., 2017).

Another interesting finding in this paper is that Ca^{2+} mainly controls NaR cell quiescence exit through Akt1. As AKT controls a plethora of cellular processes, pan-AKT inhibitors could affect the functions of normal cells and may result in severe side effects, which is probably one of the reasons that AKT inhibitors have been less successful than expected in the clinical trials (Molife et al., 2014; Yap et al., 2011). AKT comprises three isoforms (AKT1, AKT2, and AKT3), and the different isoforms are believed to mediate critical non-redundant or even opposing functions in cancer (Wang et al., 2018b). The opposing functions of AKT1 and AKT2 in cell migration and invasion were also demonstrated in vivo in mouse models (Chin and Toker, 2010; Irie et al., 2005; Liu et al., 2006). Moreover, specific AKT isoforms have been demonstrated to be drivers in particular cancers. For example, in PTEN-deficient prostate cancer, AKT2 is required for cancer cell survival and maintenance while AKT1 is dispensable (Chin and Toker, 2010). Therefore, precise inhibition of specific AKT isoforms in particular cancers at specific stages provides a way to overcome the disadvantages of pan-AKT inhibition in terms of toxicity.

Overall, this study reveals a previously uncovered role of active CaMKK under a globally low intracellular Ca^{2+} condition. The initial reduction in $[Ca^{2+}]_i$ might trigger Ca^{2+} release from ER, and the local Ca^{2+} signals activate CaMKK-Akt to reactivate epithelial cells from quiescent state.

4.5 Methods and Materials

Ethics statement

All experiments were conducted in accordance with the guidelines approved by the University of Michigan Institutional Committee on the Use and Care of Animals.

Zebrafish husbandry

Fish were raised according to the standard zebrafish husbandry guidelines (Westerfield, 2000a). Embryos were obtained by natural cross and staged following Kimmel at al. (Kimmel et al., 1995b). Artificial freshwater with different Ca^{2+} and other ion concentrations was prepared using double deionized water generated by Milli-Q Academic System (Millipore) as reported (Dai., et al 2014). In some experiments, 0.003% (w/v) N-phenylthiourea (PTU) was added to prevent pigmentation.

Plasmid construction

ER-LAR-GECO1 cassette was amplified from CMV-ER-LAR-GECO1 and integrated into Kanamycin resistance gene carrying plasmid using the following primers: BglII-ER-F, 5'-gaagatctATGCTGCTGCCCGTCCCCCT-3'; ER-stop-NotI-R, 5'-atttgcggccgcTTACAGCTCGTCCTTCTTCG-3'; ER-LAR-GECO1-Kana cassette was then amplified and integrated into *igfbp5aBAC* as reported (Liu., et al, 2017) using the following primers: igfbp5a-ER-LAR-f, 5'-GTTTTGCCATTTCAAAGCTGGTGAAATAGGTGTTCTACAGTAGGACGATGCTGCTGCCCGTCCCCCT -3'; igfbp5a-pEGFP-C3-kan-R, 5'-

GTTTACTTTTGTCCCATATAAAACAAATACTACAAGTCAATAAAACATACAGAACTC
CAGCATGAGATCCCCGC-3';

GCaMP7a imaging

Tg (igfbp5a:GCaMP7a) was injected with *BAC (igfbp5a:mCherry)* and raised in E3 embryo solution till 3 dpf. Fish were anesthetized and then mounted in 1% low-melting curve agarose gel and later agarose gels on yolk sac regions were removed. Leica SP8 equipped HC PL APO 93X/1.30 GLYC were used for imaging. LAS X and Image J were used for image analysis.

Transient knockout of CaMKKs

Three sgRNAs targeting *camkks* were designed using CHOPCHOP (http://chopchop.cbu.uib.no/). Their sequences are: camkk1a-sgRNA1: 5'-GGACACTCGTTTGGATTCGA-3'; camkk1a-sgRNA2: 5'-GCCAGACAGGTGTGGCCTCT-3'; camkk1b-sgRNA1: 5'-GGTCCTGTACCCGTTTGGTG-3'; camkk1b-sgRNA2: 5'-GCAGCTGGATCTCTCCTGCA-3'; camkk2-sgRNA1: 5'-GTTTGTAGAGCCGTGATGG-3'; camkk2-sgRNA2: 5'-GCAGGTCCTGGAAGTAGAAG-3'; 40 pg sgRNAs and 400 pg Cas9 mRNA were co-injected into *Tg(igfbp5a:GFP)* at the 1-cell stage as reported (Xin and Duan, 2018). A subset of injected embryos was pooled, DNA isolated, and analyzed by PCR followed by hetero-duplex assay as reported (Liu et al., 2018). After confirming the indels, the remaining injected embryos were used for experiments.

Whole mount in situ hybridization and immunostaining

Zebrafish larvae were fixed in 4% paraformaldehyde, permeabilized in methanol, and subjected to immunostaining or in situ hybridization as reported before (Dai., et al 2014).

Cell culture and western blot

Cell culture and flowcytometry analysis. Human colorectal adenocarcinoma (Caco2) cells were cultured in DMEM supplemented with 10% FBS, penicillin, and streptomycin in a humidified air atmosphere incubator containing 5% CO2 at 37℃. Culture media was prepared by adding $CaCl_2$ to DMEM without Ca^{2+} at the desired concentration. After washing three times with these media, Caco2 cells were incubated in low Ca^{2+} SFM containing DMSO or STO-609 for 24 hours before IGF2 treatment. Cells were harvest for western blot analysis 10 min after treatment with 200ng/ml IGF2.

Statistical analysis

Values are shown as Mean ± standard error of the mean (SEM). Statistical significance among experimental groups was determined using one-way ANOVA followed by Tukey's multiple comparison test or student t-test.

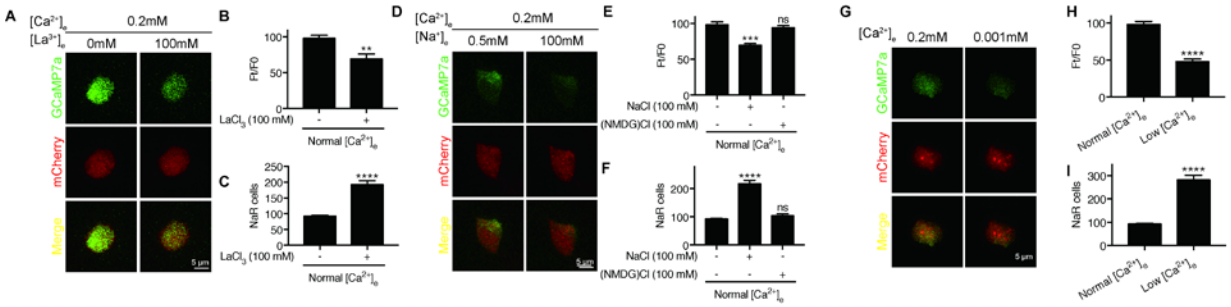

Figure 4.1 Reducing $[Ca^{2+}]_i$ stimulates NaR cell reactivation

(A, B, D, E, G, H) *Tg (igfbp5a:GCaMP7a)* was injected with *BAC(igfbp5a:mCherry)* and raised in E3 till 3 dpf. GCaMP7a and mCherry co-expressing NaR cells were exposed to normal $[Ca^{2+}]$ solution and then switched to different medium as labelled. GCaMP7a intensity at normal $[Ca^{2+}]$ condition and 3 minutes post medium change was shown in and quantified (mean ± SEM) in E. One-way ANOVA followed by Tukey's multiple comparison test was used for statistical analysis, ***P < 0.001, ****P < 0.0001, fish n > 3, cell n > 20. (C, F, I) For measuring NaR cell reactivation under the same condition, *Tg (igfbp5a:GFP)* was subjected to treatment indicated from 3-5 dpf and NaR cells were quantified at 5 dpf. Data shown are mean ± SEM, one-way ANOVA followed by Tukey's multiple comparison test was used for statistical analysis, ****P < 0.0001, fish n > 13.

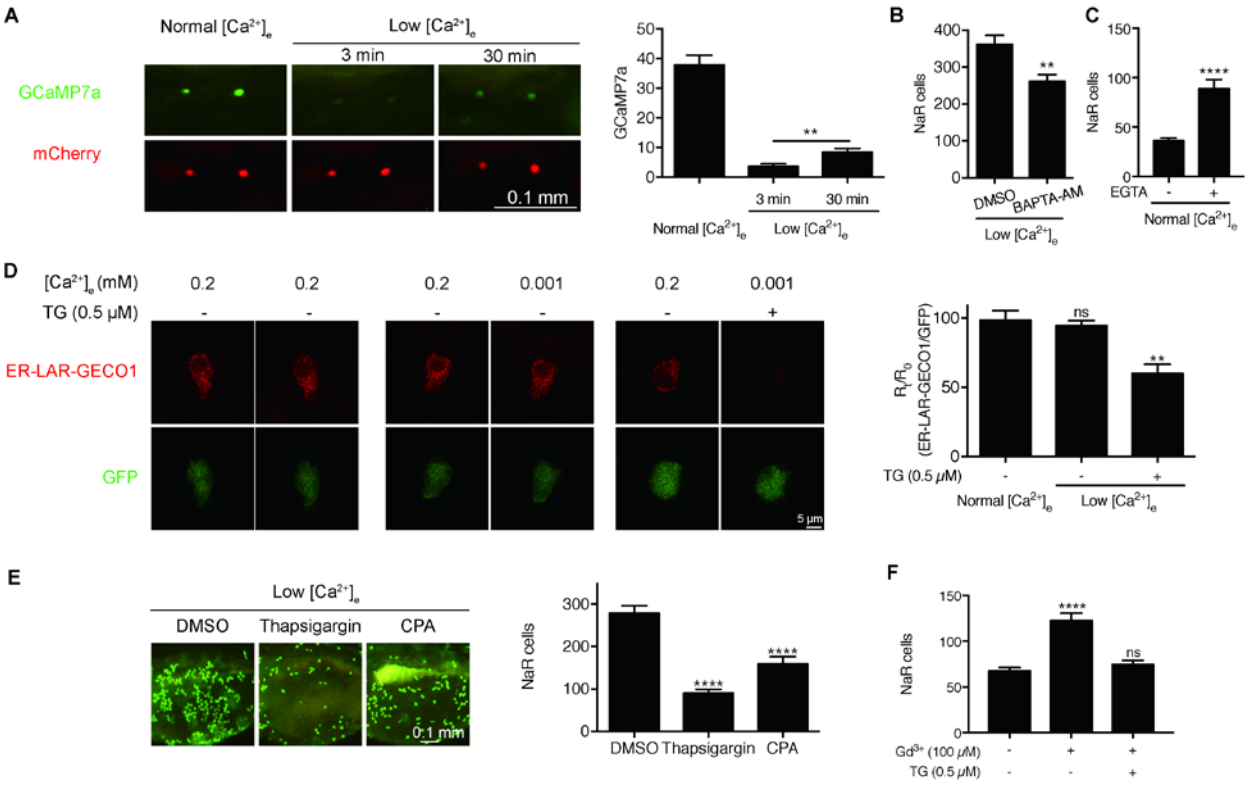

Figure 4.2 ER Ca^{2+} plays a role in NaR cell reactivation

(A) Time course of NaR cell $[Ca^{2+}]_I$ after low Ca^{2+} stress. *BAC (igfbp5a:GCaMP7a)* and *BAC (igfbp5a:mCherry)* constructs were co-injected into 1-cell stage wild-type embryos. The fluorescent intensity change in NaR cells co-expressing GCaMP7a and mCherry were imaged and quantified after transferring to to low Ca^{2+} solution. Representative images were shown in the left panel and quantified results in the right panel. Data shown are mean ± SEM, unpaired t-test, **P < 0.01, n = 42 in 10 fish. (B) BAPTA-AM treatment. wild-type fish were treated with DMSO or 100 µM BAPTA-AM from 3 dpf to 5 dpf and analyzed by in situ hybridization using *trpv6* probe. NaR cell number in each fish was quantified and shown as mean ± SEM. **P < 0.01, unpaired t-test, n=21-22. (C) EGTA treatment. *Tg(igfbp5a:GFP)* fish were treated with normal Ca^{2+} solution with or without 2 mM EGTA between 3-5 dpf. NaR cell number in each fish was quantified and shown (mean ± SEM). ****P < 0.0001, unpaired t-test, fish n= 11-11.

(D) Thapsigargin treatment reduces $[Ca^{2+}]_{ER}$. *BAC(igfbp5a:ER-LAR-GECO1)* was injected into *Tg(igfbp5a:GFP)* embryos at 1-cell stage. At 3 dpf, fish were treated with normal or low Ca^{2+} with/without 0.5 µM Thapsigargin. Maximal projection of z-stack images of ER-LAR-GECO1 and GFP fluorescence at 30 min post treatment are shown in the left panel and quantified results in the right panel. Data shown are mean ± SEM, **P < 0.01, one-way ANOVA followed by Tukey's multiple comparison test, n=3-8. (E) Thapsigargin treatment increases NaR cell reactivation. *Tg(igfbp5a:GFP)* fish were transferred to the low Ca^{2+} solution containing DMSO, 0.25 µM Thapsigargin or 5 µM CPA at 3 dp. Two days later, NaR cell number in each fish was quantified. Datd shown are mean ± SEM. ****P < 0.0001, one-way ANOVA, n= 10-13. (F) Thapsigargin inhibits Gd^{3+}-induced NaR cell activation. *Tg(igfbp5a:GFP)* fish were treated with indicated chemicals (100 mM GdCl3, 0.5 µM Thapsigargin) from 3 to 4 dpf. NaR cell number in each fish was quantified and shown as mean ± SEM. ****P < 0.0001, one-way ANOVA, n= 30-37.

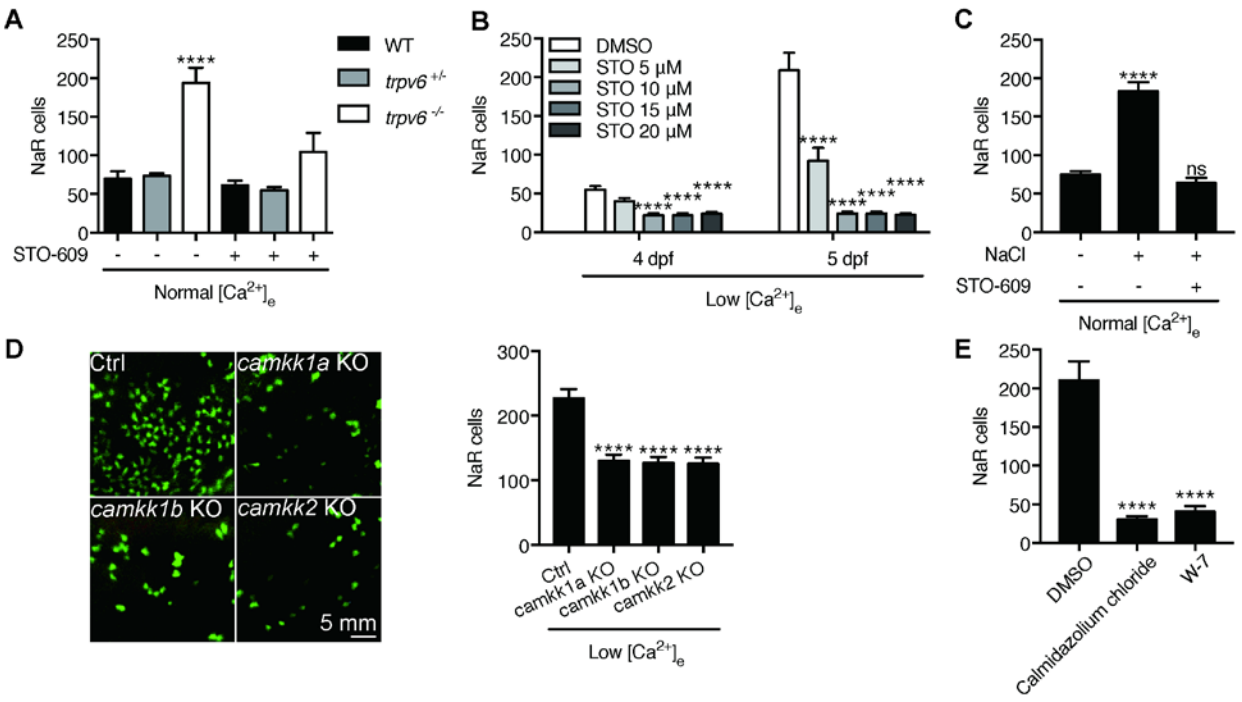

Figure 4.3 CaMKK activity is required for NaR cell reactivation.

(A) STO-609 treatment abolishes elevated NaR cell reactivation in trpv6-/- fish. Progenies of *trpv6Δ7*$^{+/-}$; *Tg(igfbp5a:GFP)* intercrosses were raised in normal Ca^{2+} solutions. 10 µM STO-609 was added at 3 dpf. After NaR cell number in each larva was quantified at 5 dpf, fish were genotyped. Data shown are mean ± SEM. ****P < 0.0001, One-way ANOVA followed by Tukey's multiple comparison test. n= 12-41. (B) STO-609 treatment inhibits low Ca2+ stress-induced NaR cell reactivation. *Tg(igfbp5a:GFP)* fish were transferred to the low Ca^{2+} solutions containing DMSO or STO-609 at 3 dpf. Fish were imaged at 4 dpf and 5 dpf. NaR cell number in each fish was quantified and shown as mean ± SEM. ****P < 0.0001, 2-way ANOVA followed by multiple comparison to the DMSO group, n = 17-20. (C) STO-609 treatment inhibits NaCl-induced NaR cell activation. *Tg(igfbp5a:GFP)* fish were raised in normal Ca^{2+} solution. 100 mM NaCl and/or 10 µM STO-609) were added at 3 dpf. NaR cell number in each

fish was quantified at 5 dpf and shown as mean ± SEM. ****P < 0.0001, one-way ANOVA followed by Tukey's multiple comparison test, n= 22-24. (D) Knockdown of camkk genes inhibits NaR cell reactivation. *Tg(igfbp5a:GFP)* fish were injected with guide RNAs targeting zebrafish *camkks* and Cas9 mRNAs at one-cell stage. The injected embryos were raised. At 3 dpf, they were subjected to the low Ca^{2+} stress test. NaR cell number in each fish was quantified at 5 dpf. Representative images are shown in the left panel and qautified data in the right. Data shown are mean ± SEM. ****P < 0.0001, one-way ANOVA followed by Tukey's multiple comparison test, n= 42-66. (E) Inhibition of calmodulin inhibits NaR cell reactivation NaR cell reactivation. *Tg(igfbp5a:GFP)* fish were transferred to the low Ca^{2+} solutions containing DMSO, 5 µM calmidazolium chloride, or 50 µM W-7 from 3-5 dpf. NaR cell number in each fish was quantified at 5 dpf and shown as mean ± SEM. ****P < 0.0001, One-way ANOVA followed by Tukey's multiple comparison test was used for statistical analysis, n= 5-7.

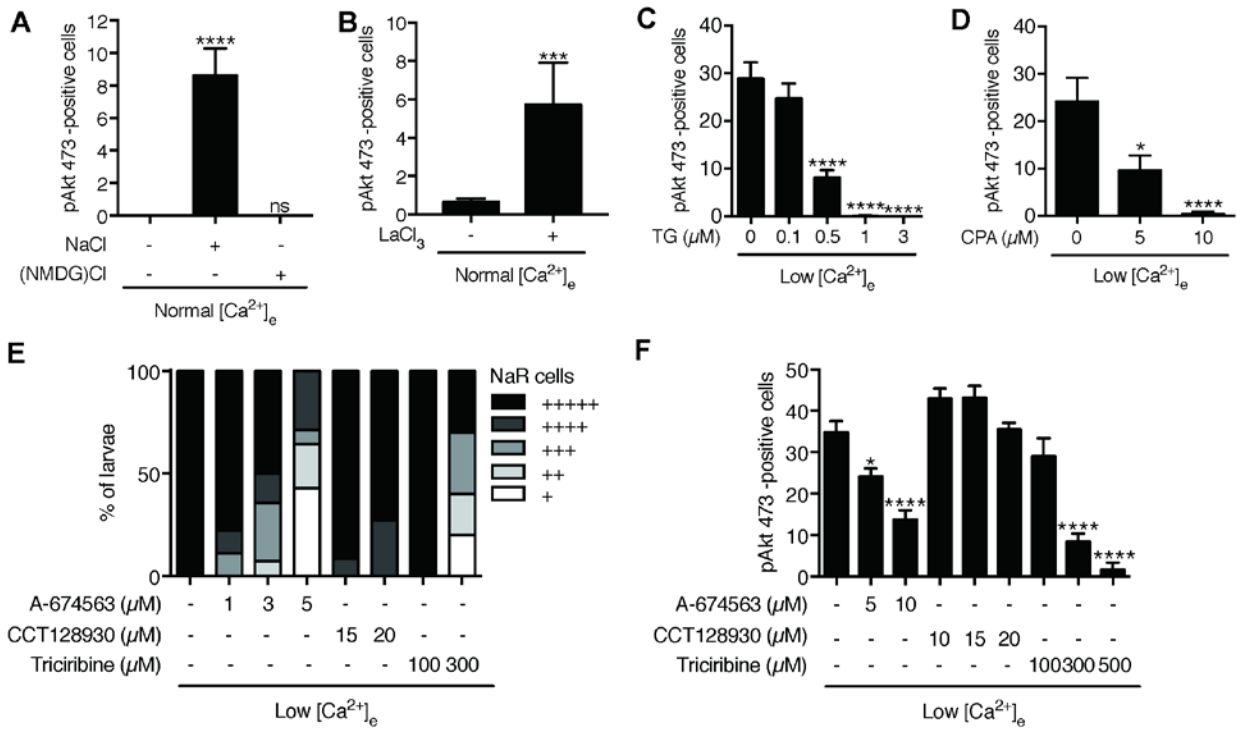

Figure 4.4 Akt1 signaling is required in NaR cell reactivation

(A-D) Wild-type larvae were treated with indicated conditions from 3 dpf to 4 dpf. The larvae were fixed and analyzed by immunostaining using antibody against phosphor-Akt (S473). pAkt 473-positive cells were quantified and shown as mean ± SEM . *P < 0.05, ***P < 0.001, ****P < 0.0001, One-way ANOVA followed by Tukey's multiple comparison test, n= 11-32.

(E) Wild-type larvae were treated with low Ca^{2+} with Akt inhibitors at indicated concentrations from 3 dpf to 5 dpf and then subjected for in situ hybridization using *trpv6* probe for NaR cell number quantification. NaR cell number were categorized according to scales reported before (Dai., et al, 2014). (F) WT larvae were treated from 3-4 dpf with low Ca^{2+} conditions with DMSO or Akt inhibitors at indicated concentrations and then subjected to pAkt-473 immunostaining. pAkt-473-positive cells were quantified (mean ± SEM). One-way ANOVA followed by Tukey's multiple comparison test or unpaired t-test was used for statistical analysis, *P < 0.05, ****P < 0.0001, n= 9-36.

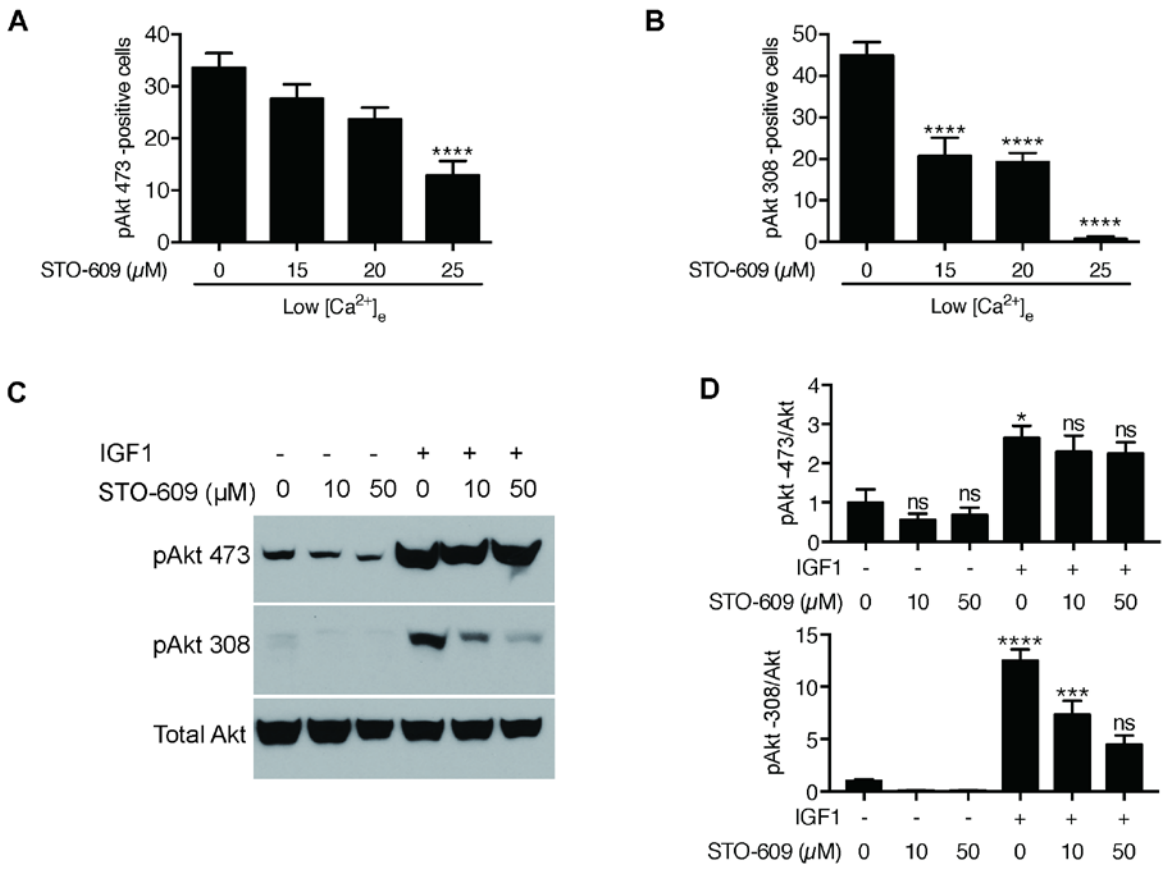

Figure 4.5 STO-609 treatment abolished low Ca^{2+}-mediated AKT signaling activation in zebrafish and in human colon carcinoma cells

(A-B) Wild-type zebrafish larvae were transferred to the low Ca^{2+} containing the indicated concentrations of STO-609 or DMSO from 3 dpf to 4 dpf. They were fixed and analyzed by immunostaining using an antibody against phosphor-Akt (S473) (A) or phospho-pAkt (Thr308). pAk-positive cells were quantified and shown as mean ± SEM, *P < 0.05, ****P < 0.0001, One-way ANOVA ANOVA, n= 11-28. (C-D) Caco2 cells were treated with low Ca^{2+} serum-free medium containing DMSO or STO-609 for 24 hours before adding 200 ng/ml IGF-1. 10 min after the IGF-1 treatment, cells were harvest and subjected to western blot analysis using antibodies against phospho-Akt (Ser473) and phospho-pAkt (Thr308). A representative result is

shown in (A) and quantified results in (B). *P < 0.05, ***P < 0.001, ****P < 0.0001, one-way ANOVA followed by Tukey's multiple comparison test was used for statistical analysis, n= 3.

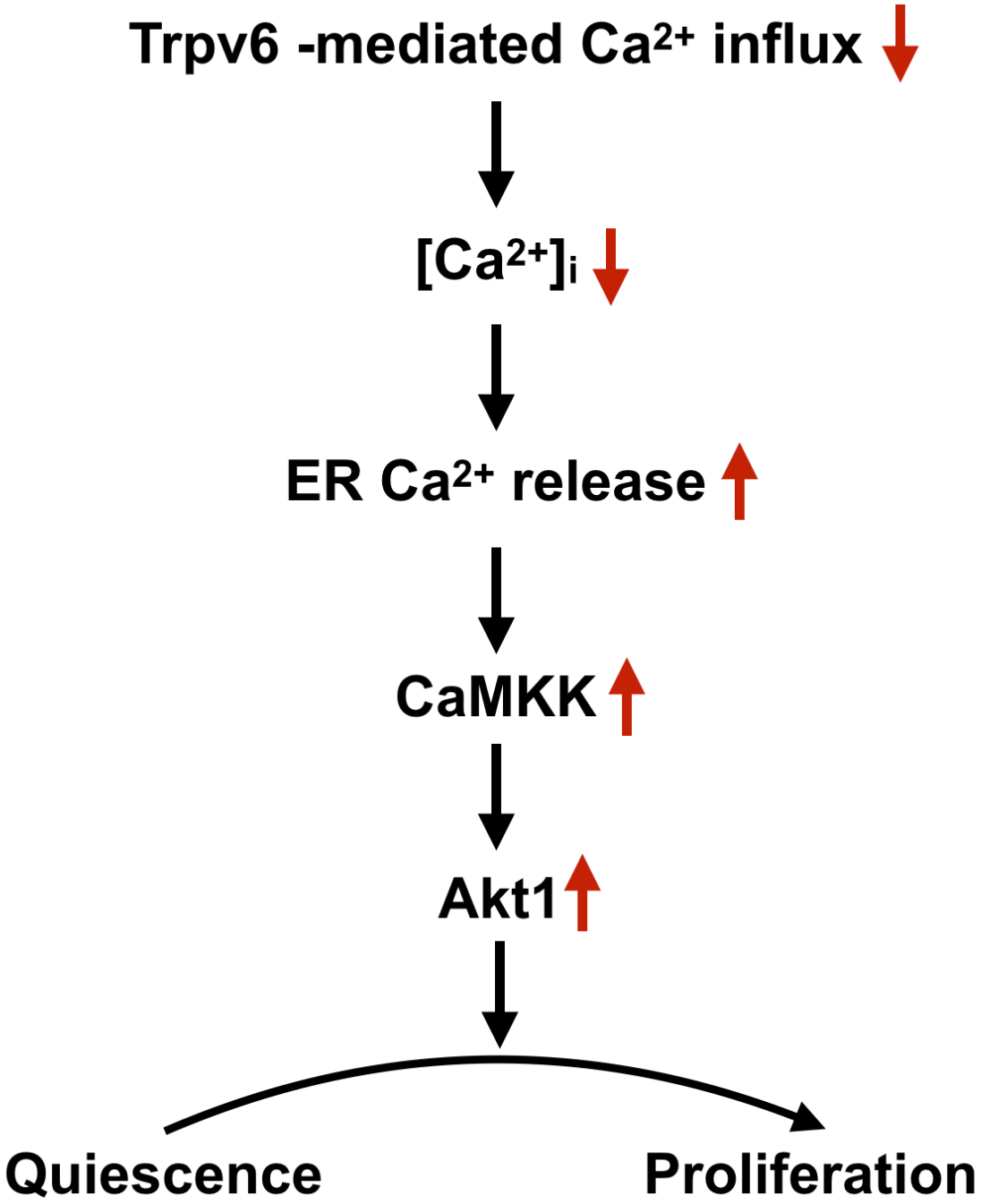

Figure 4.6. Schematic diagram of the proposed model.

Table 4-1 Key Resources Table

Reagent type (species) or resource	Designation	Source or reference	Identifiers
strain, strain background (*Danio rerio*)	*Tg(igfbp5a:GCaMP7a)*	Pubmed ID: 31526479	
strain, strain background (*Danio rerio*)	*Tg(igfbp5a:GFP)*	Pubmed ID: 28515443	
strain, strain background (*Danio rerio*)	*trpv6 Δ7; Tg(igfbp5a:GFP)*	Pubmed ID: 31526479	
strain, strain background (*Danio rerio*)	*Tg(ubi:ASAP1)*	Pubmed ID: 29757272	
chemical compound, drug	Lanthanum(III) chloride	Sigma-Aldrich	Catalog no.: 449830-5G
chemical compound, drug	Thapsigargin	Sigma-Aldrich	Catalog no.: T9033
chemical compound, drug	CPA	Sigma-Aldrich	Catalog no.: C1530
chemical compound, drug	BAPTA-AM	Sigma-Aldrich	Catalog no.: A1076
chemical compound, drug	STO-609	Enzo Life Sciences	Catalog no.: BML-EI389
chemical compound, drug	A674563	Selleck Chemicals	Catalog no.: S2670
chemical compound, drug	CCT128930	Selleck Chemicals	Catalog no.: S2635
chemical compound, drug	H-89 dihydrochloride hydrate	Sigma-Aldrich	Catalog no.: B1427
chemical compound, drug	W-7	Calbiochem	Catalog no.: 681629
chemical compound, drug	Calmidazolium chloride	Tocris Bioscience	Catalog no.: 2561
chemical compound, drug	Gadolinium(III) chloride	Sigma-Aldrich	Catalog no.: 439770

antibody	Phospho-Akt (Ser473)	Cell Signaling Technology	Catalog no.: 4060
antibody	Phospho-Akt (Thr308)	Cell Signaling Technology	Catalog no.: 9275
Cell line	Caco2	ATCC	Catalog no.: HTB-37
Genetic reagent	ER-LAR-GECO1	Addgene	Catalog no.: 61244

Chapter 5 Conclusions and Future Directions

5.1 Conclusions

Previous studies have shown that the IGF/PI3-kinase/Akt/Tor pathway is required for the NaR cell reactivation under low [Ca^{2+}] stress (Dai et al., 2014a). How this activation of IGF signaling under low [Ca^{2+}] stress is regulated was not clear. In Chapter 2, I presented results showing that genetic deletion of *igfbp5a* blunted the low [Ca^{2+}] stress-induced IGF signaling and NaR cell proliferation. Likewise, knockdown of IGFBP5 in human colon carcinoma cells also resulted in reduced IGF-stimulated cell proliferation, suggesting this is an evolutionarily conserved mechanism. These results reveal a conserved mechanism by which a locally expressed Igfbp activates IGF signaling and promoting cell quiescence-proliferation transition under Ca^{2+}-deficient states.

Trpv6 is the epithelial Ca^{2+} channel with high selectivity for Ca^{2+}. Through constructing a NaR cell-specific Ca^{2+} reporter fish, I showed in Chapter 3 that Trpv6 mediates constitutive Ca^{2+} influx and maintains the high $[Ca^{2+}]_i$ in NaR cells. Pharmacological inhibition of Trpv6 activity or genetic knockout of Trpv6 resulted in reduced intracellular Ca^{2+} level and reduced IGF signaling in NaR cells and NaR cell reactivation. Blockage of IGF1 receptor or PI3 kinase or Tor activity retained NaR cells in quiescent state in *trpv6*$^{-/-}$, suggesting Ca^{2+} influx-mediated by Trpv6 suppressed IGF signaling pathway. Using a chemical biology screen, I unraveled a novel player in IGF signaling-mediated regulation of NaR cellular quiescence, protein phosphatase 2A (PP2A). Genetic knockdown or pharmacological inhibition of PP2A elevates Akt

phosphorylation and NaR cell proliferation under normal Ca^{2+} conditions, indicating PP2A actions downstream of Ca^{2+} and upstream of Akt phosphorylation.

Ca^{2+}/calmodulin-dependent kinase kinase (CaMKK) is a calcium-dependent kinase and typically gets activated upon Ca^{2+} influx and increased intracellular Ca^{2+} concentration (Brzozowski and Skelding, 2019). Through chemical biology screening and later validated using CRISPR/Cas9-mediated knockdown of zebrafish *camkk* genes, I found CaMKK activity is required for low $[Ca^{2+}]_i$-triggered NaR cell quiescence exit decision. I propose that Ca^{2+} release from ER Ca^{2+} store can form local Ca^{2+} microdomains and activate CaMKK. In line with this hypothesis, depletion of ER Ca^{2+} store by blocking Ca^{2+} uptake into ER abolished Akt signaling activation as well as NaR cell quiescence exit under low $[Ca^{2+}]_i$. Taken together, these findings reveal a novel role of CaMKK in regulating IGF/PI3K/AKT/TOR pathway upon reduction of $[Ca^{2+}]_i$.

5.2 Future directions

5.2.1 Explore whether Igfbp5a activity is regulated by low $[Ca^{2+}]$ stress

IGFBP5/Igfbp5a has been shown to inhibit and/or potentiate IGF actions in mammalian and zebrafish cells (Dai et al., 2010; Liu et al., 2018a; Ren et al., 2008; Zheng et al., 1998a). How the same protein exerts these opposing biological effects is not completely understood, and the importance of IGFBP5 proteinases has been suggested (Allard and Duan, 2018; Clemmons, 2018; Conover and Oxvig, 2017; Zheng et al., 1998b). In vitro studies suggested that pregnancy-associated plasma protein-A (PAPP-A) is tethered to the cell-surface and it cleaves IGFBP4, IGFBP5, and to a lesser degree IGFBP2, while PAPP-A2 is secreted and mainly cleaves IGFBP3 and IGFBP5 (Gyrup and Oxvig, 2007; Oxvig, 2015). Recently, a hypocalcaemic hormone

stanniocalcin (STC) was identified as a powerful inhibitor of PAPP-A proteolytic activity in mice (Jepsen et al., 2015). Stanniocalcin was initially discovered in corpuscles of Stannius in teleost fish (Wagner et al., 1986) and later identified in mammalians as well (Wagner et al., 1995). In zebrafish, stanniocalcin level was known to be regulated by environmental Ca^{2+} (Chou et al., 2015; Tseng et al., 2009). In a pilot experiment, I found zebrafish stc1 gene expression was positively associated with environmental Ca^{2+} level and is downregulated in *trpv6*$^{-/-}$ knockout (Figure 5.1). It will be interesting to further test if Igfbp5a is cleaved by PAPP-A in zebrafish and whether this process is modulated by Ca^{2+} through stanniocalcin.

5.2.2 Determine whether PP2A or CaMKK activity is altered by Ca^{2+}

Chemical biology screen unravels two novel regulators involved in Ca^{2+}-regulated IGF/PI3K/AKT/TOR pathway, PP2A and CaMKK. The specific PP2A is unclear at present. PP2A has 3 distinct families of regulatory subunits. One family of the regulatory subunits (B'') are known to contain EF motifs and are potentially Ca^{2+}-dependent. In a preliminary experiment, I found that knockdown of the two B'' regulatory subunits of PP2A did not induce NaR cell proliferation (Figure 5.2). Other genes encoding B'' regulatory subunits need to be tested in the future. Additionally, Ca^{2+} may regulate PP2A through other mechanisms. For example, PP2A activity has been reported to be under the regulation of other Ca^{2+}-dependent molecules such as the Ca2+-dependent protease m-calpain (Janssens et al., 2009). It will also be critical to determine whether PP2A or CaMKK enzyme activity is altered by $[Ca^{2+}]_i$. Antibody targeting phosphorylated-PP2A are available but has not been tested in zebrafish (De Palma et al., 2019; Liu et al., 2008). An alternative way is to sort out GFP labelled-NaR cells through FACS and then assay PP2A or CaMKK activity using commercially available kit (Wallace et al., 2012; Yurimoto et al., 2012).

5.2.3 Determine whether local Ca^{2+} microdomains are involved

Based on the CaMKK inhibitor STO-609 results and the fact that intracellular Ca^{2+} chelator BAPTA-AM decreased low Ca^{2+}-mediated NaR cell proliferation. I postulate that Ca^{2+} release from ER is the underlying source for Ca^{2+} microdomains under low $[Ca^{2+}]_i$. Consistent with the proposed model, I found ER Ca^{2+} depletion abolished low Ca^{2+} stress-triggered Akt signaling elevation and NaR cell reactivation. However, preliminary analysis using the ER-targeting Ca^{2+} reporter (ER-LAR-GECO1) did not show a significant reduction of ER Ca^{2+} level in NaR cells under low Ca^{2+} stress. $[Ca^{2+}]_{ER}$ is around 100 μM in the resting state and in the low micromolar range in the depletion state (Suzuki et al., 2014), 5000 to 10000-fold than that of the the cytosol.. LAR-GECO1 is a low affinity Ca^{2+} indicator (Kd = 24 μM) (Wu et al., 2014). A subtle change that is enough to induce a steep increase Ca^{2+} in the cytosol locally may not be captured by this Ca^{2+} indicator. Recently, bioluminescence low-affinity ER Ca^{2+} indicator with disassociation constant around 100 μM (Hossain et al., 2018) or CEPIA family reporters with even lower affinity towards Ca^{2+} (Kd = 500-700 μM) (Suzuki et al., 2014) has been reported and could be used to visualize the ER Ca^{2+} change in our system. These tools can be used in the future. We can also analyze the cytosolic Ca^{2+} signals in the GCaMP7a reporter fish line under higher resolution to detect any aberrant microdomain Ca^{2+} signals in NaR cells. In combination with GFP-tagged IP3R (Thillaiappan et al., 2017) and organelle-specific marker, one can also determine whether the observed local Ca^{2+} microdomain is mediated by IP3R at the specific interorganellar surfaces. Deciphering this subcellular localization will shed new light on our understanding about how AKT signaling is regulated at endomembranes (Jethwa et al., 2015; Siess and Leonard, 2019; Sugiyama et al., 2019).

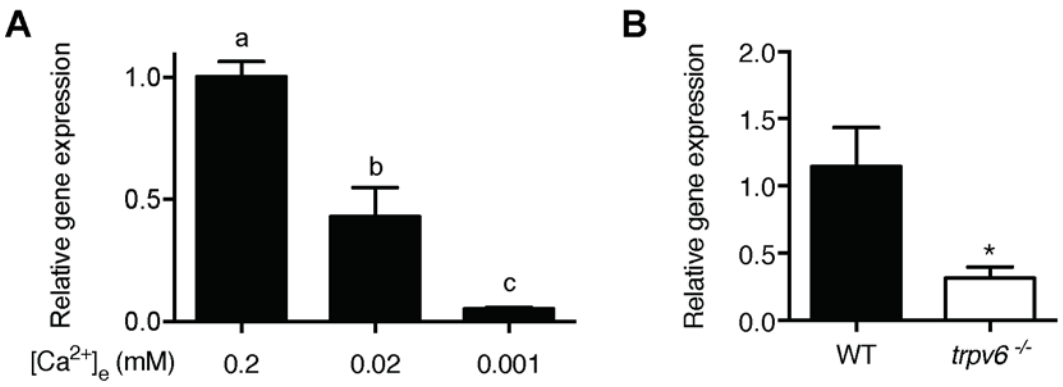

Figure 5.1 *stc1* expression is downregulated in low $[Ca^{2+}]_e$ and *trpv6*$^{-/-}$

(A) Wild-type embryos were acclimated in varying Ca^{2+} solutions from 0-72 hpf. 10-20 embryos were pooled for RNA extraction and RT-qPCR. *stc1* gene expression was normalized to *beta-actin*. Mean ± SEM, n=3. One-way ANOVA followed by Turkey's multiple comparison test was used for statistical analysis and different letter indicates $P < 0.5$. (B) Caudal fin of *trpv6*$^{+/-}$ intercrossed progeny were clipped at 7 dpf for genotyping. 6-10 embryos of the same genotype group were pooled together for RNA extraction and RT-qPCR. *stc1* gene expression was normalized to *beta-actin*. Mean ± SEM, n=4. Unpaired t-test was used for statistical analysis and * indicates $P < 0.5$.

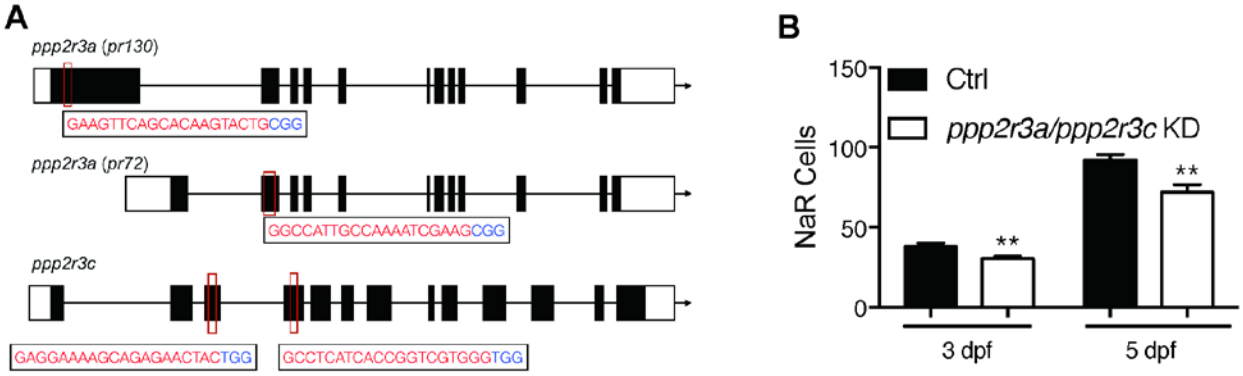

Figure 5.2 Knockdown of *ppp2r3a* and *ppp2r3c* doesn't induce NaR cell proliferation

(A) Schematic diagram of guide RNA targeting sites of *ppp2r3a* and *ppp2r3c*. Target sites are outlined by the red box. Red characters indicate the guide RNA targeting site sequence and blue characters indicate the PAM sequence. (B) *Tg(igfbp5a:GFP)* is injected with guide RNAs targeting *ppp2r3a* and *ppp2r3c* mixed with Cas9 mRNA at 1-cell stage. NaR cells were imaged and quantified at 3 dpf and 5 dpf. Unpaired t-tests suggest slight decrease rather than increase of NaR cell number at both 3 dpf and 5 dpf.

References

Abbas, L., Hajihashemi, S., Stead, L.F., Cooper, G.J., Ware, T.L., Munsey, T.S., Whitfield, T.T., and White, S.J. (2011). Functional and developmental expression of a zebrafish Kir1.1 (ROMK) potassium channel homologue Kcnj1. J Physiol *589*, 1489-1503.

Aberdam, D., Gambaro, K., Rostagno, P., Aberdam, E., de la Forest Divonne, S., and Rouleau, M. (2007). Key role of p63 in BMP-4-induced epidermal commitment of embryonic stem cells. Cell Cycle *6*, 291-294.

Accili, D., Drago, J., Lee, E.J., Johnson, M.D., Cool, M.H., Salvatore, P., Asico, L.D., Jose, P.A., Taylor, S.I., and Westphal, H. (1996). Early neonatal death in mice homozygous for a null allele of the insulin receptor gene. Nat Genet *12*, 106-109.

Acharya, J.K., Jalink, K., Hardy, R.W., Hartenstein, V., and Zuker, C.S. (1997). InsP3 receptor is essential for growth and differentiation but not for vision in Drosophila. Neuron *18*, 881-887.

Akkiprik, M., Hu, L., Sahin, A., Hao, X., and Zhang, W. (2009). The subcellular localization of IGFBP5 affects its cell growth and migration functions in breast cancer. BMC Cancer *9*, 103.

Alessi, D.R., Andjelkovic, M., Caudwell, B., Cron, P., Morrice, N., Cohen, P., and Hemmings, B.A. (1996). Mechanism of activation of protein kinase B by insulin and IGF-1. EMBO J *15*, 6541-6551.

Allard, J.B., and Duan, C. (2018). IGF-Binding Proteins: Why Do They Exist and Why Are There So Many? Front Endocrinol (Lausanne) *9*, 117.

Almasi, S., Sterea, A.M., Fernando, W., Clements, D.R., Marcato, P., Hoskin, D.W., Gujar, S., and El Hiani, Y. (2019). TRPM2 ion channel promotes gastric cancer migration, invasion and tumor growth through the AKT signaling pathway. Sci Rep *9*, 4182.

Anderson, J.L., Mulligan, T.S., Shen, M.C., Wang, H., Scahill, C.M., Tan, F.J., Du, S.J., Busch-Nentwich, E.M., and Farber, S.A. (2017). mRNA processing in mutant zebrafish lines generated by chemical and CRISPR-mediated mutagenesis produces unexpected transcripts that escape nonsense-mediated decay. PLoS Genet *13*, e1007105.

Andjelkovic, M., Jakubowicz, T., Cron, P., Ming, X.F., Han, J.W., and Hemmings, B.A. (1996). Activation and phosphorylation of a pleckstrin homology domain containing protein kinase (RAC-PK/PKB) promoted by serum and protein phosphatase inhibitors. Proc Natl Acad Sci U S A *93*, 5699-5704.

Andress, D.L., and Birnbaum, R.S. (1991). A novel human insulin-like growth factor binding protein secreted by osteoblast-like cells. Biochem Biophys Res Commun *176*, 213-218.

Armbrecht, H.J., Boltz, M.A., and Kumar, V.B. (1999). Intestinal plasma membrane calcium pump protein and its induction by 1,25(OH)(2)D(3) decrease with age. Am J Physiol *277*, G41-47.

Bagur, R., and Hajnoczky, G. (2017). Intracellular Ca(2+) Sensing: Its Role in Calcium Homeostasis and Signaling. Mol Cell *66*, 780-788.

Baker, J., Liu, J.P., Robertson, E.J., and Efstratiadis, A. (1993). Role of insulin-like growth factors in embryonic and postnatal growth. Cell *75*, 73-82.

Bakkers, J., Hild, M., Kramer, C., Furutani-Seiki, M., and Hammerschmidt, M. (2002). Zebrafish DeltaNp63 is a direct target of Bmp signaling and encodes a transcriptional repressor blocking neural specification in the ventral ectoderm. Dev Cell *2*, 617-627.

Balk, S.D. (1971). Calcium as a regulator of the proliferation of normal, but not of transformed, chicken fibroblasts in a plasma-containing medium. Proc Natl Acad Sci U S A *68*, 271-275.

Bantug, G.R., Fischer, M., Grahlert, J., Balmer, M.L., Unterstab, G., Develioglu, L., Steiner, R., Zhang, L., Costa, A.S.H., Gubser, P.M., et al. (2018). Mitochondria-Endoplasmic Reticulum Contact Sites Function as Immunometabolic Hubs that Orchestrate the Rapid Recall Response of Memory CD8(+) T Cells. Immunity *48*, 542-555 e546.

Bartik, L., Whitfield, G.K., Kaczmarska, M., Lowmiller, C.L., Moffet, E.W., Furmick, J.K., Hernandez, Z., Haussler, C.A., Haussler, M.R., and Jurutka, P.W. (2010). Curcumin: a novel nutritionally derived ligand of the vitamin D receptor with implications for colon cancer chemoprevention. J Nutr Biochem *21*, 1153-1161.

Bate, N., Caves, R.E., Skinner, S.P., Goult, B.T., Basran, J., Mitcheson, J.S., and Vuister, G.W. (2018). A Novel Mechanism for Calmodulin-Dependent Inactivation of Transient Receptor Potential Vanilloid 6. Biochemistry *57*, 2611-2622.

Bautista, C.M., Baylink, D.J., and Mohan, S. (1991). Isolation of a novel insulin-like growth factor (IGF) binding protein from human bone: a potential candidate for fixing IGF-II in human bone. Biochem Biophys Res Commun *176*, 756-763.

Baxter, R.C. (2014). IGF binding proteins in cancer: mechanistic and clinical insights. Nat Rev Cancer *14*, 329-341.

Baxter, R.C., Martin, J.L., and Beniac, V.A. (1989). High molecular weight insulin-like growth factor binding protein complex. Purification and properties of the acid-labile subunit from human serum. J Biol Chem *264*, 11843-11848.

Baxter, R.C., and Twigg, S.M. (2009). Actions of IGF binding proteins and related proteins in adipose tissue. Trends Endocrinol Metab *20*, 499-505.

Bayaa, M., Vulesevic, B., Esbaugh, A., Braun, M., Ekker, M.E., Grosell, M., and Perry, S.F. (2009). The involvement of SLC26 anion transporters in chloride uptake in zebrafish (Danio rerio) larvae. J Exp Biol *212*, 3283-3295.

Beaty, M.M., Lee, E.Y., and Glauert, H.P. (1993). Influence of dietary calcium and vitamin D on colon epithelial cell proliferation and 1,2-dimethylhydrazine-induced colon carcinogenesis in rats fed high fat diets. J Nutr *123*, 144-152.

Beauchamp, E.M., and Platanias, L.C. (2013). The evolution of the TOR pathway and its role in cancer. Oncogene *32*, 3923-3932.

Becerra, M., and Anadon, R. (1993). Development of the inner ear of the brown trout (Salmo trutta fario): I. Gross morphology and sensory cell proliferation. J Morphol *216*, 209-223.

Bedell, V.M., Wang, Y., Campbell, J.M., Poshusta, T.L., Starker, C.G., Krug, R.G., 2nd, Tan, W., Penheiter, S.G., Ma, A.C., Leung, A.Y., et al. (2012). In vivo genome editing using a high-efficiency TALEN system. Nature *491*, 114-118.

Berchtold, M.W., and Villalobo, A. (2014). The many faces of calmodulin in cell proliferation, programmed cell death, autophagy, and cancer. Biochim Biophys Acta *1843*, 398-435.

Berra-Romani, R., Mazzocco-Spezzia, A., Pulina, M.V., and Golovina, V.A. (2008). Ca2+ handling is altered when arterial myocytes progress from a contractile to a proliferative phenotype in culture. Am J Physiol Cell Physiol *295*, C779-790.

Berridge, M.J. (2006). Calcium microdomains: organization and function. Cell Calcium *40*, 405-412.

Betz, C., Stracka, D., Prescianotto-Baschong, C., Frieden, M., Demaurex, N., and Hall, M.N. (2013). Feature Article: mTOR complex 2-Akt signaling at mitochondria-associated endoplasmic reticulum membranes (MAM) regulates mitochondrial physiology. Proc Natl Acad Sci U S A *110*, 12526-12534.

Bianco, S.D., Peng, J.B., Takanaga, H., Suzuki, Y., Crescenzi, A., Kos, C.H., Zhuang, L., Freeman, M.R., Gouveia, C.H., Wu, J., et al. (2007). Marked disturbance of calcium homeostasis in mice with targeted disruption of the Trpv6 calcium channel gene. J Bone Miner Res *22*, 274-285.

Binoux, M., and Hossenlopp, P. (1988). Insulin-like growth factor (IGF) and IGF-binding proteins: comparison of human serum and lymph. J Clin Endocrinol Metab *67*, 509-514.

Bodding, M., and Flockerzi, V. (2004). Ca2+ dependence of the Ca2+-selective TRPV6 channel. J Biol Chem *279*, 36546-36552.

Bootman, M.D. (2012). Calcium signaling. Cold Spring Harb Perspect Biol *4*, a011171.

Boynton, A.L., and Whitfield, J.F. (1976). Different calcium requirements for proliferation of conditionally and unconditionally tumorigenic mouse cells. Proc Natl Acad Sci U S A *73*, 1651-1654.

Brahmkhatri, V.P., Prasanna, C., and Atreya, H.S. (2015). Insulin-like growth factor system in cancer: novel targeted therapies. Biomed Res Int *2015*, 538019.

Breves, J.P., Fujimoto, C.K., Phipps-Costin, S.K., Einarsdottir, I.E., Bjornsson, B.T., and McCormick, S.D. (2017). Variation in branchial expression among insulin-like growth-factor binding proteins (igfbps) during Atlantic salmon smoltification and seawater exposure. BMC Physiol *17*, 2.

Brini, M., and Carafoli, E. (2011). The plasma membrane Ca(2)+ ATPase and the plasma membrane sodium calcium exchanger cooperate in the regulation of cell calcium. Cold Spring Harb Perspect Biol *3*.

Britton, J.S., and Edgar, B.A. (1998). Environmental control of the cell cycle in Drosophila: nutrition activates mitotic and endoreplicative cells by distinct mechanisms. Development *125*, 2149-2158.

Brzozowski, J.S., and Skelding, K.A. (2019). The Multi-Functional Calcium/Calmodulin Stimulated Protein Kinase (CaMK) Family: Emerging Targets for Anti-Cancer Therapeutic Intervention. Pharmaceuticals (Basel) *12*.

Burren, C.P., Caswell, R., Castle, B., Welch, C.R., Hilliard, T.N., Smithson, S.F., and Ellard, S. (2018). TRPV6 compound heterozygous variants result in impaired placental calcium transport and severe undermineralization and dysplasia of the fetal skeleton. Am J Med Genet A *176*, 1950-1955.

Butt, A.J., Dickson, K.A., McDougall, F., and Baxter, R.C. (2003). Insulin-like growth factor-binding protein-5 inhibits the growth of human breast cancer cells in vitro and in vivo. J Biol Chem *278*, 29676-29685.

Cahalan, M.D. (2009). STIMulating store-operated Ca(2+) entry. Nat Cell Biol *11*, 669-677.

Cai, X. (2007). Molecular evolution and structural analysis of the Ca(2+) release-activated Ca(2+) channel subunit, Orai. J Mol Biol *368*, 1284-1291.

Cancer Genome Atlas, N. (2012). Comprehensive molecular characterization of human colon and rectal cancer. Nature *487*, 330-337.

Cao, C., Zakharian, E., Borbiro, I., and Rohacs, T. (2013). Interplay between calmodulin and phosphatidylinositol 4,5-bisphosphate in Ca2+-induced inactivation of transient receptor potential vanilloid 6 channels. J Biol Chem *288*, 5278-5290.

Carafoli, E., and Krebs, J. (2016). Why Calcium? How Calcium Became the Best Communicator. J Biol Chem *291*, 20849-20857.

Cermak, T., Doyle, E.L., Christian, M., Wang, L., Zhang, Y., Schmidt, C., Baller, J.A., Somia, N.V., Bogdanove, A.J., and Voytas, D.F. (2011). Efficient design and assembly of custom TALEN and other TAL effector-based constructs for DNA targeting. Nucleic acids research *39*, e82.

Chang, W.J., Horng, J.L., Yan, J.J., Hsiao, C.D., and Hwang, P.P. (2009). The transcription factor, glial cell missing 2, is involved in differentiation and functional regulation of H+-ATPase-rich cells in zebrafish (Danio rerio). Am J Physiol Regul Integr Comp Physiol *296*, R1192-1201.

Charlesworth, A., and Rozengurt, E. (1994). Thapsigargin and di-tert-butylhydroquinone induce synergistic stimulation of DNA synthesis with phorbol ester and bombesin in Swiss 3T3 cells. J Biol Chem *269*, 32528-32535.

Chell, J.M., and Brand, A.H. (2010). Nutrition-responsive glia control exit of neural stem cells from quiescence. Cell *143*, 1161-1173.

Chen, B.C., Wu, W.T., Ho, F.M., and Lin, W.W. (2002). Inhibition of interleukin-1beta -induced NF-kappa B activation by calcium/calmodulin-dependent protein kinase kinase occurs through Akt activation associated with interleukin-1 receptor-associated kinase phosphorylation and uncoupling of MyD88. J Biol Chem *277*, 24169-24179.

Chen, C., Liu, Y., Liu, R., Ikenoue, T., Guan, K.L., Liu, Y., and Zheng, P. (2008). TSC-mTOR maintains quiescence and function of hematopoietic stem cells by repressing mitochondrial biogenesis and reactive oxygen species. J Exp Med *205*, 2397-2408.

Chen, C., Liu, Y., Liu, Y., and Zheng, P. (2009). mTOR regulation and therapeutic rejuvenation of aging hematopoietic stem cells. Sci Signal *2*, ra75.

Chen, C.C., Ke, W.H., Ceng, L.H., Hsieh, C.W., and Wung, B.S. (2010). Calcium- and phosphatidylinositol 3-kinase/Akt-dependent activation of endothelial nitric oxide synthase by apigenin. Life Sci *87*, 743-749.

Chen, F., Ni, B., Yang, Y.O., Ye, T., and Chen, A. (2014). Knockout of TRPV6 causes osteopenia in mice by increasing osteoclastic differentiation and activity. Cell Physiol Biochem *33*, 796-809.

Chen, H.X., and Sharon, E. (2013). IGF-1R as an anti-cancer target--trials and tribulations. Chin J Cancer *32*, 242-252.

Chen, Y.C., Liao, B.K., Lu, Y.F., Liu, Y.H., Hsieh, F.C., Hwang, P.P., and Hwang, S.L. (2019). Zebrafish Klf4 maintains the ionocyte progenitor population by regulating epidermal stem cell proliferation and lateral inhibition. PLoS Genet *15*, e1008058.

Cheng, K.T., Ong, H.L., Liu, X., and Ambudkar, I.S. (2013). Contribution and regulation of TRPC channels in store-operated Ca2+ entry. Curr Top Membr *71*, 149-179.

Cheung, T.H., and Rando, T.A. (2013). Molecular regulation of stem cell quiescence. Nat Rev Mol Cell Biol *14*, 329-340.

Chin, D., and Means, A.R. (2000). Calmodulin: a prototypical calcium sensor. Trends Cell Biol *10*, 322-328.

Chin, Y.R., and Toker, A. (2010). The actin-bundling protein palladin is an Akt1-specific substrate that regulates breast cancer cell migration. Mol Cell *38*, 333-344.

Cho, C.H., Lee, S.Y., Shin, H.S., Philipson, K.D., and Lee, C.O. (2003). Partial rescue of the Na+-Ca2+ exchanger (NCX1) knock-out mouse by transgenic expression of NCX1. Exp Mol Med *35*, 125-135.

Chou, M.Y., Hung, J.C., Wu, L.C., Hwang, S.P., and Hwang, P.P. (2011). Isotocin controls ion regulation through regulating ionocyte progenitor differentiation and proliferation. Cell Mol Life Sci *68*, 2797-2809.

Chou, M.Y., Lin, C.H., Chao, P.L., Hung, J.C., Cruz, S.A., and Hwang, P.P. (2015). Stanniocalcin-1 controls ion regulation functions of ion-transporting epithelium other than calcium balance. Int J Biol Sci *11*, 122-132.

Chow, J., Norng, M., Zhang, J., and Chai, J. (2007). TRPV6 mediates capsaicin-induced apoptosis in gastric cancer cells--Mechanisms behind a possible new "hot" cancer treatment. Biochim Biophys Acta *1773*, 565-576.

Clapham, D.E. (2007). Calcium signaling. Cell *131*, 1047-1058.

Clemmons, D.R. (1993). IGF binding proteins and their functions. Mol Reprod Dev *35*, 368-374; discussion 374-365.

Clemmons, D.R. (2016). Role of IGF Binding Proteins in Regulating Metabolism. Trends Endocrinol Metab *27*, 375-391.

Clemmons, D.R. (2018). Role of IGF-binding proteins in regulating IGF responses to changes in metabolism. J Mol Endocrinol *61*, T139-T169.

Conover, C.A., and Kiefer, M.C. (1993). Regulation and biological effect of endogenous insulin-like growth factor binding protein-5 in human osteoblastic cells. J Clin Endocrinol Metab *76*, 1153-1159.

Conover, C.A., and Oxvig, C. (2017). PAPP-A: a promising therapeutic target for healthy longevity. Aging Cell *16*, 205-209.

Cosens, D.J., and Manning, A. (1969). Abnormal electroretinogram from a Drosophila mutant. Nature *224*, 285-287.

Cross, S.S., Hamdy, F.C., Deloulme, J.C., and Rehman, I. (2005). Expression of S100 proteins in normal human tissues and common cancers using tissue microarrays: S100A6, S100A8, S100A9 and S100A11 are all overexpressed in common cancers. Histopathology *46*, 256-269.

Cui, H., Cruz-Correa, M., Giardiello, F.M., Hutcheon, D.F., Kafonek, D.R., Brandenburg, S., Wu, Y., He, X., Powe, N.R., and Feinberg, A.P. (2003). Loss of IGF2 imprinting: a potential marker of colorectal cancer risk. Science *299*, 1753-1755.

Dai, W., Bai, Y., Hebda, L., Zhong, X., Liu, J., Kao, J., and Duan, C. (2014a). Calcium deficiency-induced and TRP channel-regulated IGF1R-PI3K-Akt signaling regulates abnormal epithelial cell proliferation. Cell Death Differ *21*, 568-581.

Dai, W., Bai, Y., Hebda, L., Zhong, X., Liu, J., Kao, J., and Duan, C. (2014b). Calcium deficiency-induced and TRP channel-regulated IGF1R-PI3K-Akt signaling regulates abnormal epithelial cell proliferation. Cell death and differentiation *21*, 568.

Dai, W., Kamei, H., Zhao, Y., Ding, J., Du, Z., and Duan, C. (2010). Duplicated zebrafish insulin-like growth factor binding protein-5 genes with split functional domains: evidence for evolutionarily conserved IGF binding, nuclear localization, and transactivation activity. FASEB J *24*, 2020-2029.

Danciu, T.E., Adam, R.M., Naruse, K., Freeman, M.R., and Hauschka, P.V. (2003). Calcium regulates the PI3K-Akt pathway in stretched osteoblasts. FEBS Lett *536*, 193-197.

Daughaday, W.H., and Kapadia, M. (1989). Significance of abnormal serum binding of insulin-like growth factor II in the development of hypoglycemia in patients with non-islet-cell tumors. Proc Natl Acad Sci U S A *86*, 6778-6782.

Davis, J.A., Donkaewbua, S., Wagner, J.E., and White, R.G. (1989). Cysticercus fasciolaris infection in a breeding colony of mice. Lab Anim Sci *39*, 250-252.

Day, E., Poulogiannis, G., McCaughan, F., Mulholland, S., Arends, M.J., Ibrahim, A.E., and Dear, P.H. (2013). IRS2 is a candidate driver oncogene on 13q34 in colorectal cancer. International journal of experimental pathology *94*, 203-211.

Daza, D.O., Sundstrom, G., Bergqvist, C.A., Duan, C., and Larhammar, D. (2011). Evolution of the insulin-like growth factor binding protein (IGFBP) family. Endocrinology *152*, 2278-2289.

De Boeck, K., and Amaral, M.D. (2016). Progress in therapies for cystic fibrosis. Lancet Respir Med *4*, 662-674.

De Palma, R.M., Parnham, S.R., Li, Y., Oaks, J.J., Peterson, Y.K., Szulc, Z.M., Roth, B.M., Xing, Y., and Ogretmen, B. (2019). The NMR-based characterization of the FTY720-SET complex reveals an alternative mechanism for the attenuation of the inhibitory SET-PP2A interaction. FASEB J *33*, 7647-7666.

Deliot, N., and Constantin, B. (2015). Plasma membrane calcium channels in cancer: Alterations and consequences for cell proliferation and migration. Biochim Biophys Acta *1848*, 2512-2522.

DeMambro, V.E., Clemmons, D.R., Horton, L.G., Bouxsein, M.L., Wood, T.L., Beamer, W.G., Canalis, E., and Rosen, C.J. (2008). Gender-specific changes in bone turnover and skeletal architecture in igfbp-2-null mice. Endocrinology *149*, 2051-2061.

Demetriades, C., Doumpas, N., and Teleman, A.A. (2014). Regulation of TORC1 in response to amino acid starvation via lysosomal recruitment of TSC2. Cell *156*, 786-799.

Denduluri, S.K., Idowu, O., Wang, Z., Liao, Z., Yan, Z., Mohammed, M.K., Ye, J., Wei, Q., Wang, J., Zhao, L., et al. (2015). Insulin-like growth factor (IGF) signaling in tumorigenesis and the development of cancer drug resistance. Genes Dis *2*, 13-25.

Deng, H., Gerencser, A.A., and Jasper, H. (2015). Signal integration by Ca(2+) regulates intestinal stem-cell activity. Nature *528*, 212-217.

Denley, A., Cosgrove, L.J., Booker, G.W., Wallace, J.C., and Forbes, B.E. (2005). Molecular interactions of the IGF system. Cytokine Growth Factor Rev *16*, 421-439.

Dibble, C.C., and Manning, B.D. (2013). Signal integration by mTORC1 coordinates nutrient input with biosynthetic output. Nat Cell Biol *15*, 555-564.

Ding, M., Bruick, R.K., and Yu, Y. (2016). Secreted IGFBP5 mediates mTORC1-dependent feedback inhibition of IGF-1 signalling. Nature cell biology *18*, 319-327.

Divolis, G., Mavroeidi, P., Mavrofrydi, O., and Papazafiri, P. (2016). Differential effects of calcium on PI3K-Akt and HIF-1alpha survival pathways. Cell Biol Toxicol *32*, 437-449.

Du, S.J., Frenkel, V., Kindschi, G., and Zohar, Y. (2001). Visualizing normal and defective bone development in zebrafish embryos using the fluorescent chromophore calcein. Dev Biol *238*, 239-246.

Duan, C., and Clemmons, D.R. (1998). Differential expression and biological effects of insulin-like growth factor-binding protein-4 and -5 in vascular smooth muscle cells. The Journal of biological chemistry *273*, 16836-16842.

Duan, C., Ren, H., and Gao, S. (2010). Insulin-like growth factors (IGFs), IGF receptors, and IGF-binding proteins: roles in skeletal muscle growth and differentiation. Gen Comp Endocrinol *167*, 344-351.

Duan, C., and Xu, Q. (2005). Roles of insulin-like growth factor (IGF) binding proteins in regulating IGF actions. Gen Comp Endocrinol *142*, 44-52.

Duong Van Huyen, J.P., Cheval, L., Bloch-Faure, M., Belair, M.F., Heudes, D., Bruneval, P., and Doucet, A. (2008). GDF15 triggers homeostatic proliferation of acid-secreting collecting duct cells. J Am Soc Nephrol *19*, 1965-1974.

Durham, A.C., and Walton, J.M. (1982). Calcium ions and the control of proliferation in normal and cancer cells. Biosci Rep *2*, 15-30.

Duvillie, B., Cordonnier, N., Deltour, L., Dandoy-Dron, F., Itier, J.M., Monthioux, E., Jami, J., Joshi, R.L., and Bucchini, D. (1997). Phenotypic alterations in insulin-deficient mutant mice. Proc Natl Acad Sci U S A *94*, 5137-5140.

Ebner, M., Lucic, I., Leonard, T.A., and Yudushkin, I. (2017a). PI(3,4,5)P3 Engagement Restricts Akt Activity to Cellular Membranes. Mol Cell *65*, 416-431 e416.

Ebner, M., Sinkovics, B., Szczygiel, M., Ribeiro, D.W., and Yudushkin, I. (2017b). Localization of mTORC2 activity inside cells. J Cell Biol *216*, 343-353.

El-Brolosy, M.A., and Stainier, D.Y.R. (2017). Genetic compensation: A phenomenon in search of mechanisms. PLoS Genet *13*, e1006780.

Esaki, M., Hoshijima, K., Nakamura, N., Munakata, K., Tanaka, M., Ookata, K., Asakawa, K., Kawakami, K., Wang, W., Weinberg, E.S., et al. (2009). Mechanism of development of ionocytes rich in vacuolar-type H(+)-ATPase in the skin of zebrafish larvae. Dev Biol *329*, 116-129.

Ewen-Campen, B., Mohr, S.E., Hu, Y., and Perrimon, N. (2017). Accessing the Phenotype Gap: Enabling Systematic Investigation of Paralog Functional Complexity with CRISPR. Developmental cell *43*, 6-9.

Facchinetti, V., Ouyang, W., Wei, H., Soto, N., Lazorchak, A., Gould, C., Lowry, C., Newton, A.C., Mao, Y., Miao, R.Q., et al. (2008). The mammalian target of rapamycin complex 2 controls folding and stability of Akt and protein kinase C. EMBO J *27*, 1932-1943.

Fecher-Trost, C., Wissenbach, U., and Weissgerber, P. (2017). TRPV6: From identification to function. Cell Calcium *67*, 116-122.

Feher, J.J., Fullmer, C.S., and Wasserman, R.H. (1992). Role of facilitated diffusion of calcium by calbindin in intestinal calcium absorption. Am J Physiol *262*, C517-526.

Feher, J.J., and Wasserman, R.H. (1979). Calcium absorption and intestinal calcium-binding protein: quantitative relationship. Am J Physiol *236*, E556-561.

Feng, J., Hu, W., Feng, C., Mao, X., Jin, K., and Ye, Y. (2015). Increasing Proliferation of Intrinsic Tubular Cells after Renal Ischemia-reperfusion Injury in Adult Rat. Aging Dis *6*, 228-235.

Ferron, S., Radford, E., Domingo-Muelas, A., Kleine, I., Ramme, A., Gray, D., Sandovici, I., Constancia, M., Ward, A., and Menheniott, T. (2015). Differential genomic imprinting regulates paracrine and autocrine roles of IGF2 in mouse adult neurogenesis. Nature communications *6*, 8265.

Feske, S., Gwack, Y., Prakriya, M., Srikanth, S., Puppel, S.H., Tanasa, B., Hogan, P.G., Lewis, R.S., Daly, M., and Rao, A. (2006). A mutation in Orai1 causes immune deficiency by abrogating CRAC channel function. Nature *441*, 179-185.

Fiore, A., Ribeiro, P.F., and Bruni-Cardoso, A. (2018). Sleeping Beauty and the Microenvironment Enchantment: Microenvironmental Regulation of the Proliferation-Quiescence Decision in Normal Tissues and in Cancer Development. Front Cell Dev Biol *6*, 59.

Firth, S.M., Clemmons, D.R., and Baxter, R.C. (2001). Mutagenesis of basic amino acids in the carboxyl-terminal region of insulin-like growth factor binding protein-5 affects acid-labile subunit binding. Endocrinology *142*, 2147.

Flamini, V., Ghadiali, R.S., Antczak, P., Rothwell, A., Turnbull, J.E., and Pisconti, A. (2018). The Satellite Cell Niche Regulates the Balance between Myoblast Differentiation and Self-Renewal via p53. Stem Cell Reports *10*, 970-983.

Flik, G., Verbost, P.M., and S.E., W.B. (1995). Calcium transport process in fishes. In: Cellular and Molecular Approaches to Fish Ionic Regulation, edited by Wood, C.M. and Shuttleworth, T.J. San Diego, CA: Academic, 317-342.

Frasca, F., Pandini, G., Scalia, P., Sciacca, L., Mineo, R., Costantino, A., Goldfine, I.D., Belfiore, A., and Vigneri, R. (1999). Insulin receptor isoform A, a newly recognized, high-affinity insulin-like growth factor II receptor in fetal and cancer cells. Mol Cell Biol *19*, 3278-3288.

Fu, S., Hirte, H., Welch, S., Ilenchuk, T.T., Lutes, T., Rice, C., Fields, N., Nemet, A., Dugourd, D., Piha-Paul, S., et al. (2017). First-in-human phase I study of SOR-C13, a TRPV6 calcium channel inhibitor, in patients with advanced solid tumors. Invest New Drugs *35*, 324-333.

Furuya, Y., and Isaacs, J.T. (1994). Proliferation-dependent vs. independent programmed cell death of prostatic cancer cells involves distinct gene regulation. Prostate *25*, 301-309.

Gao da, Y., Zhang, B.L., Leung, M.C., Au, S.C., Wong, P.Y., and Shum, W.W. (2016). Coupling of TRPV6 and TMEM16A in epithelial principal cells of the rat epididymis. J Gen Physiol *148*, 161-182.

Gao, T., Furnari, F., and Newton, A.C. (2005). PHLPP: a phosphatase that directly dephosphorylates Akt, promotes apoptosis, and suppresses tumor growth. Mol Cell *18*, 13-24.

Gees, M., Colsoul, B., and Nilius, B. (2010). The role of transient receptor potential cation channels in Ca2+ signaling. Cold Spring Harb Perspect Biol *2*, a003962.

Giacomello, M., and Pellegrini, L. (2016). The coming of age of the mitochondria-ER contact: a matter of thickness. Cell Death Differ *23*, 1417-1427.

Gil-Ranedo, J., Gonzaga, E., Jaworek, K.J., Berger, C., Bossing, T., and Barros, C.S. (2019). STRIPAK Members Orchestrate Hippo and Insulin Receptor Signaling to Promote Neural Stem Cell Reactivation. Cell Rep *27*, 2921-2933 e2925.

Giorgi, C., Marchi, S., and Pinton, P. (2018). The machineries, regulation and cellular functions of mitochondrial calcium. Nat Rev Mol Cell Biol *19*, 713-730.

Giorgi, C., Romagnoli, A., Pinton, P., and Rizzuto, R. (2008). Ca2+ signaling, mitochondria and cell death. Curr Mol Med *8*, 119-130.

Gocher, A.M., Azabdaftari, G., Euscher, L.M., Dai, S., Karacosta, L.G., Franke, T.F., and Edelman, A.M. (2017). Akt activation by Ca(2+)/calmodulin-dependent protein kinase kinase 2 (CaMKK2) in ovarian cancer cells. J Biol Chem *292*, 14188-14204.

Green, M.F., Scott, J.W., Steel, R., Oakhill, J.S., Kemp, B.E., and Means, A.R. (2011). Ca2+/Calmodulin-dependent protein kinase kinase beta is regulated by multisite phosphorylation. J Biol Chem *286*, 28066-28079.

Grupp, K., Jedrzejewska, K., Tsourlakis, M.C., Koop, C., Wilczak, W., Adam, M., Quaas, A., Sauter, G., Simon, R., Izbicki, J.R., et al. (2013). High mitochondria content is associated with prostate cancer disease progression. Mol Cancer *12*, 145.

Guh, Y.J., Lin, C.H., and Hwang, P.P. (2015). Osmoregulation in zebrafish: ion transport mechanisms and functional regulation. EXCLI J *14*, 627-659.

Gyrup, C., and Oxvig, C. (2007). Quantitative analysis of insulin-like growth factor-modulated proteolysis of insulin-like growth factor binding protein-4 and -5 by pregnancy-associated plasma protein-A. Biochemistry *46*, 1972-1980.

Haas, M., and Forbush, B., 3rd (2000). The Na-K-Cl cotransporter of secretory epithelia. Annu Rev Physiol *62*, 515-534.

Hakuno, F., and Takahashi, S.I. (2018). IGF1 receptor signaling pathways. J Mol Endocrinol *61*, T69-T86.

Han, C., Shin, A., Lee, J., Lee, J., Park, J.W., Oh, J.H., and Kim, J. (2015). Dietary calcium intake and the risk of colorectal cancer: a case control study. BMC Cancer *15*, 966.

Hanahan, D., and Weinberg, R.A. (2011). Hallmarks of cancer: the next generation. Cell *144*, 646-674.

Hemmati, S., Sinclair, T., Tong, M., Bartholdy, B., Okabe, R.O., Ames, K., Ostrodka, L., Haque, T., Kaur, I., Mills, T.S., et al. (2019). PI3 kinase alpha and delta promote hematopoietic stem cell activation. JCI Insight *5*.

Hille, B. (1978). Ionic channels in excitable membranes. Current problems and biophysical approaches. Biophys J *22*, 283-294.

Hoenderop, J.G., Nilius, B., and Bindels, R.J. (2005). Calcium absorption across epithelia. Physiol Rev *85*, 373-422.

Hogan, P.G., and Rao, A. (2015). Store-operated calcium entry: Mechanisms and modulation. Biochem Biophys Res Commun *460*, 40-49.

Hossain, M.N., Suzuki, K., Iwano, M., Matsuda, T., and Nagai, T. (2018). Bioluminescent Low-Affinity Ca(2+) Indicator for ER with Multicolor Calcium Imaging in Single Living Cells. ACS Chem Biol *13*, 1862-1871.

Howell, J.J., Ricoult, S.J., Ben-Sahra, I., and Manning, B.D. (2013). A growing role for mTOR in promoting anabolic metabolism. Biochem Soc Trans *41*, 906-912.

Hsiao, C.D., You, M.S., Guh, Y.J., Ma, M., Jiang, Y.J., and Hwang, P.P. (2007). A positive regulatory loop between foxi3a and foxi3b is essential for specification and differentiation of zebrafish epidermal ionocytes. PLoS One *2*, e302.

Huang, G.N., Zeng, W., Kim, J.Y., Yuan, J.P., Han, L., Muallem, S., and Worley, P.F. (2006). STIM1 carboxyl-terminus activates native SOC, I(crac) and TRPC1 channels. Nat Cell Biol *8*, 1003-1010.

Huang, J., and Wang, H. (2018). Hsp83/Hsp90 Physically Associates with Insulin Receptor to Promote Neural Stem Cell Reactivation. Stem Cell Reports *11*, 883-896.

Humeau, J., Bravo-San Pedro, J.M., Vitale, I., Nunez, L., Villalobos, C., Kroemer, G., and Senovilla, L. (2018). Calcium signaling and cell cycle: Progression or death. Cell Calcium *70*, 3-15.

Hwang, P.-P. (2009a). Ion uptake and acid secretion in zebrafish (Danio rerio). Journal of Experimental Biology *212*, 1745-1752.

Hwang, P.P. (2009b). Ion uptake and acid secretion in zebrafish (Danio rerio). J Exp Biol *212*, 1745-1752.

Hwang, P.P., and Chou, M.Y. (2013). Zebrafish as an animal model to study ion homeostasis. Pflugers Arch *465*, 1233-1247.

Ikura, M. (1996). Calcium binding and conformational response in EF-hand proteins. Trends Biochem Sci *21*, 14-17.

Imai, Y., Moralez, A., Andag, U., Clarke, J.B., Busby, W.H., Jr., and Clemmons, D.R. (2000). Substitutions for hydrophobic amino acids in the N-terminal domains of IGFBP-3 and -5 markedly reduce IGF-I binding and alter their biologic actions. J Biol Chem *275*, 18188-18194.

Irie, H.Y., Pearline, R.V., Grueneberg, D., Hsia, M., Ravichandran, P., Kothari, N., Natesan, S., and Brugge, J.S. (2005). Distinct roles of Akt1 and Akt2 in regulating cell migration and epithelial-mesenchymal transition. J Cell Biol *171*, 1023-1034.

Janicke, M., Carney, T.J., and Hammerschmidt, M. (2007). Foxi3 transcription factors and Notch signaling control the formation of skin ionocytes from epidermal precursors of the zebrafish embryo. Dev Biol *307*, 258-271.

Janssens, V., Derua, R., Zwaenepoel, K., Waelkens, E., and Goris, J. (2009). Specific regulation of protein phosphatase 2A PR72/B" subunits by calpain. Biochem Biophys Res Commun *386*, 676-681.

Jean, S., and Kiger, A.A. (2014). Classes of phosphoinositide 3-kinases at a glance. J Cell Sci *127*, 923-928.

Jepsen, M.R., Kloverpris, S., Mikkelsen, J.H., Pedersen, J.H., Fuchtbauer, E.M., Laursen, L.S., and Oxvig, C. (2015). Stanniocalcin-2 inhibits mammalian growth by proteolytic inhibition of the insulin-like growth factor axis. J Biol Chem *290*, 3430-3439.

Jethwa, N., Chung, G.H., Lete, M.G., Alonso, A., Byrne, R.D., Calleja, V., and Larijani, B. (2015). Endomembrane PtdIns(3,4,5)P3 activates the PI3K-Akt pathway. J Cell Sci *128*, 3456-3465.

Jones, J.I., and Clemmons, D.R. (1995). Insulin-like growth factors and their binding proteins: biological actions. Endocr Rev *16*, 3-34.

Jones, J.I., Gockerman, A., Busby, W.H., Jr., Wright, G., and Clemmons, D.R. (1993). Insulin-like growth factor binding protein 1 stimulates cell migration and binds to the alpha 5 beta 1 integrin by means of its Arg-Gly-Asp sequence. Proc Natl Acad Sci U S A *90*, 10553-10557.

Joshi, R.L., Lamothe, B., Cordonnier, N., Mesbah, K., Monthioux, E., Jami, J., and Bucchini, D. (1996). Targeted disruption of the insulin receptor gene in the mouse results in neonatal lethality. EMBO J *15*, 1542-1547.

Kahl, C.R., and Means, A.R. (2003). Regulation of cell cycle progression by calcium/calmodulin-dependent pathways. Endocr Rev *24*, 719-736.

Kalus, W., Zweckstetter, M., Renner, C., Sanchez, Y., Georgescu, J., Grol, M., Demuth, D., Schumacher, R., Dony, C., Lang, K., et al. (1998). Structure of the IGF-binding domain of the insulin-like growth factor-binding protein-5 (IGFBP-5): implications for IGF and IGF-I receptor interactions. EMBO J *17*, 6558-6572.

Kamei, H., Ding, Y., Kajimura, S., Wells, M., Chiang, P., and Duan, C. (2011). Role of IGF signaling in catch-up growth and accelerated temporal development in zebrafish embryos in response to oxygen availability. Development *138*, 777-786.

Karnaky, K.J., Jr., Ernst, S.A., and Philpott, C.W. (1976). Teleost chloride cell. I. Response of pupfish Cyprinodon variegatus gill Na,K-ATPase and chloride cell fine structure to various high salinity environments. J Cell Biol *70*, 144-156.

Katsiari, C.G., Kyttaris, V.C., Juang, Y.T., and Tsokos, G.C. (2005). Protein phosphatase 2A is a negative regulator of IL-2 production in patients with systemic lupus erythematosus. J Clin Invest *115*, 3193-3204.

Kever, L., Cherezova, A., Zenin, V., Negulyaev, Y., Komissarchik, Y., and Semenova, S. (2019). Downregulation of TRPV6 channel activity by cholesterol depletion in Jurkat T cell line. Cell Biol Int *43*, 965-975.

Keys, A., and Willmer, E.N. (1932). "Chloride secreting cells" in the gills of fishes, with special reference to the common eel. J Physiol *76*, 368-378 362.

Kiefer, M.C., Schmid, C., Waldvogel, M., Schlapfer, I., Futo, E., Masiarz, F.R., Green, K., Barr, P.J., and Zapf, J. (1992). Characterization of recombinant human insulin-like growth factor binding proteins 4, 5, and 6 produced in yeast. The Journal of biological chemistry *267*, 12692-12699.

Kim, D.H., Sarbassov, D.D., Ali, S.M., King, J.E., Latek, R.R., Erdjument-Bromage, H., Tempst, P., and Sabatini, D.M. (2002). mTOR interacts with raptor to form a nutrient-sensitive complex that signals to the cell growth machinery. Cell *110*, 163-175.

Kim, E., Cheng, Y., Bolton-Gillespie, E., Cai, X., Ma, C., Tarangelo, A., Le, L., Jambhekar, M., Raman, P., Hayer, K.E., et al. (2017). Rb family proteins enforce the homeostasis of quiescent hematopoietic stem cells by repressing Socs3 expression. J Exp Med *214*, 1901-1912.

Kim, J., and Guan, K.L. (2019). mTOR as a central hub of nutrient signalling and cell growth. Nat Cell Biol *21*, 63-71.

Kimmel, C.B., Ballard, W.W., Kimmel, S.R., Ullmann, B., and Schilling, T.F. (1995a). Stages of embryonic development of the zebrafish. Developmental dynamics : an official publication of the American Association of Anatomists *203*, 253-310.

Kimmel, C.B., Ballard, W.W., Kimmel, S.R., Ullmann, B., and Schilling, T.F. (1995b). Stages of embryonic development of the zebrafish. Developmental Dynamics *203*, 253-310.

Kippin, T.E., Martens, D.J., and van der Kooy, D. (2005). p21 loss compromises the relative quiescence of forebrain stem cell proliferation leading to exhaustion of their proliferation capacity. Genes Dev *19*, 756-767.

Kitaori, T., Ito, H., Schwarz, E.M., Tsutsumi, R., Yoshitomi, H., Oishi, S., Nakano, M., Fujii, N., Nagasawa, T., and Nakamura, T. (2009). Stromal cell-derived factor 1/CXCR4 signaling is critical for the recruitment of mesenchymal stem cells to the fracture site during skeletal repair in a mouse model. Arthritis Rheum *60*, 813-823.

Kok, F.O., Shin, M., Ni, C.W., Gupta, A., Grosse, A.S., van Impel, A., Kirchmaier, B.C., Peterson-Maduro, J., Kourkoulis, G., Male, I., et al. (2015). Reverse genetic screening reveals poor correlation between morpholino-induced and mutant phenotypes in zebrafish. Developmental cell *32*, 97-108.

Kovacs, G., Danko, T., Bergeron, M.J., Balazs, B., Suzuki, Y., Zsembery, A., and Hediger, M.A. (2011). Heavy metal cations permeate the TRPV6 epithelial cation channel. Cell Calcium *49*, 43-55.

Kovacs, G., Montalbetti, N., Simonin, A., Danko, T., Balazs, B., Zsembery, A., and Hediger, M.A. (2012). Inhibition of the human epithelial calcium channel TRPV6 by 2-aminoethoxydiphenyl borate (2-APB). Cell Calcium *52*, 468-480.

Kovalevskaya, N.V., Bokhovchuk, F.M., and Vuister, G.W. (2012). The TRPV5/6 calcium channels contain multiple calmodulin binding sites with differential binding properties. J Struct Funct Genomics *13*, 91-100.

Kraemer, A.M., Saraiva, L.R., and Korsching, S.I. (2008). Structural and functional diversification in the teleost S100 family of calcium-binding proteins. BMC Evol Biol *8*, 48.

Kurimchak, A., Haines, D.S., Garriga, J., Wu, S., De Luca, F., Sweredoski, M.J., Deshaies, R.J., Hess, S., and Graña, X. (2013). Activation of p107 by Fibroblast Growth Factor, Which Is Essential for Chondrocyte Cell Cycle Exit, Is Mediated by the Protein Phosphatase 2A/B55α Holoenzyme. Molecular and Cellular Biology *33*, 3330-3342.

Kusakabe, M., Ishikawa, A., Ravinet, M., Yoshida, K., Makino, T., Toyoda, A., Fujiyama, A., and Kitano, J. (2017). Genetic basis for variation in salinity tolerance between stickleback ecotypes. Mol Ecol *26*, 304-319.

Lallet-Daher, H., Roudbaraki, M., Bavencoffe, A., Mariot, P., Gackiere, F., Bidaux, G., Urbain, R., Gosset, P., Delcourt, P., Fleurisse, L., et al. (2009). Intermediate-conductance Ca2+-activated K+ channels (IKCa1) regulate human prostate cancer cell proliferation through a close control of calcium entry. Oncogene *28*, 1792-1806.

Lambers, T.T., Weidema, A.F., Nilius, B., Hoenderop, J.G., and Bindels, R.J. (2004). Regulation of the mouse epithelial Ca2(+) channel TRPV6 by the Ca(2+)-sensor calmodulin. J Biol Chem *279*, 28855-28861.

Lamprecht, S.A., and Lipkin, M. (2003). Chemoprevention of colon cancer by calcium, vitamin D and folate: molecular mechanisms. Nat Rev Cancer *3*, 601-614.

Langenbacher, A.D., Dong, Y., Shu, X., Choi, J., Nicoll, D.A., Goldhaber, J.I., Philipson, K.D., and Chen, J.N. (2005). Mutation in sodium-calcium exchanger 1 (NCX1) causes cardiac fibrillation in zebrafish. Proc Natl Acad Sci U S A *102*, 17699-17704.

Lanner, J.T., Georgiou, D.K., Joshi, A.D., and Hamilton, S.L. (2010). Ryanodine receptors: structure, expression, molecular details, and function in calcium release. Cold Spring Harb Perspect Biol *2*, a003996.

Laplante, M., and Sabatini, D.M. (2012). mTOR signaling in growth control and disease. Cell *149*, 274-293.

Larsson, D., and Nemere, I. (2002). Vectorial Transcellular Calcium Transport in Intestine: Integration of Current Models. J Biomed Biotechnol *2*, 117-119.

Lau, J.K., Brown, K.C., Dom, A.M., Witte, T.R., Thornhill, B.A., Crabtree, C.M., Perry, H.E., Brown, J.M., Ball, J.G., Creel, R.G., et al. (2014). Capsaicin induces apoptosis in human small cell lung cancer via the TRPV6 receptor and the calpain pathway. Apoptosis *19*, 1190-1201.

Laviola, L., Natalicchio, A., and Giorgino, F. (2007). The IGF-I signaling pathway. Curr Pharm Des *13*, 663-669.

Lawson, N.D., and Weinstein, B.M. (2002). In vivo imaging of embryonic vascular development using transgenic zebrafish. Dev Biol *248*, 307-318.

Le Roith, D. (2003). The insulin-like growth factor system. Exp Diabesity Res *4*, 205-212.

Lee, B.M., Lee, G.S., Jung, E.M., Choi, K.C., and Jeung, E.B. (2009). Uterine and placental expression of TRPV6 gene is regulated via progesterone receptor- or estrogen receptor-mediated pathways during pregnancy in rodents. Reprod Biol Endocrinol *7*, 49.

Lee, H., and Kimelman, D. (2002). A dominant-negative form of p63 is required for epidermal proliferation in zebrafish. Dev Cell *2*, 607-616.

Lee, J., Kanatsu-Shinohara, M., Inoue, K., Ogonuki, N., Miki, H., Toyokuni, S., Kimura, T., Nakano, T., Ogura, A., and Shinohara, T. (2007). Akt mediates self-renewal division of mouse spermatogonial stem cells. Development *134*, 1853-1859.

Lee, M.N., Hwang, H.S., Oh, S.H., Roshanzadeh, A., Kim, J.W., Song, J.H., Kim, E.S., and Koh, J.T. (2018). Elevated extracellular calcium ions promote proliferation and migration of mesenchymal stem cells via increasing osteopontin expression. Exp Mol Med *50*, 142.

Lee, W.H., Choong, L.Y., Jin, T.H., Mon, N.N., Chong, S., Liew, C.S., Putti, T., Lu, S.Y., Harteneck, C., and Lim, Y.P. (2017). TRPV4 plays a role in breast cancer cell migration via Ca(2+)-dependent activation of AKT and downregulation of E-cadherin cell cortex protein. Oncogenesis *6*, e338.

Legrand, G., Humez, S., Slomianny, C., Dewailly, E., Vanden Abeele, F., Mariot, P., Wuytack, F., and Prevarskaya, N. (2001). Ca2+ pools and cell growth. Evidence for sarcoendoplasmic Ca2+-ATPases 2B involvement in human prostate cancer cell growth control. J Biol Chem *276*, 47608-47614.

Lehen'Kyi, V., Flourakis, M., Skryma, R., and Prevarskaya, N. (2007). TRPV6 channel controls prostate cancer cell proliferation via Ca 2+/NFAT-dependent pathways. Oncogene *26*, 7380.

Lehen'kyi, V., Raphael, M., and Prevarskaya, N. (2012). The role of the TRPV6 channel in cancer. J Physiol *590*, 1369-1376.

Lewitt, M.S., Saunders, H., Phuyal, J.L., and Baxter, R.C. (1994). Complex formation by human insulin-like growth factor-binding protein-3 and human acid-labile subunit in growth hormone-deficient rats. Endocrinology *134*, 2404-2409.

Li, M., Zhang, C.S., Zong, Y., Feng, J.W., Ma, T., Hu, M., Lin, Z., Li, X., Xie, C., Wu, Y., et al. (2019). Transient Receptor Potential V Channels Are Essential for Glucose Sensing by Aldolase and AMPK. Cell Metab *30*, 508-524 e512.

Liao, B.K., Chen, R.D., and Hwang, P.P. (2009). Expression regulation of Na+-K+-ATPase alpha1-subunit subtypes in zebrafish gill ionocytes. Am J Physiol Regul Integr Comp Physiol *296*, R1897-1906.

Liao, B.K., Deng, A.N., Chen, S.C., Chou, M.Y., and Hwang, P.P. (2007). Expression and water calcium dependence of calcium transporter isoforms in zebrafish gill mitochondrion-rich cells. BMC Genomics *8*, 354.

Lieben, L., Benn, B.S., Ajibade, D., Stockmans, I., Moermans, K., Hediger, M.A., Peng, J.B., Christakos, S., Bouillon, R., and Carmeliet, G. (2010). Trpv6 mediates intestinal calcium absorption during calcium restriction and contributes to bone homeostasis. Bone *47*, 301-308.

Lin, C.H., and Hwang, P.P. (2016). The Control of Calcium Metabolism in Zebrafish (Danio rerio). Int J Mol Sci *17*.

Lin, L.Y., Horng, J.L., Kunkel, J.G., and Hwang, P.P. (2006). Proton pump-rich cell secretes acid in skin of zebrafish larvae. Am J Physiol Cell Physiol *290*, C371-378.

Liou, J., Fivaz, M., Inoue, T., and Meyer, T. (2007). Live-cell imaging reveals sequential oligomerization and local plasma membrane targeting of stromal interaction molecule 1 after Ca2+ store depletion. Proc Natl Acad Sci U S A *104*, 9301-9306.

Liou, J., Kim, M.L., Heo, W.D., Jones, J.T., Myers, J.W., Ferrell, J.E., Jr., and Meyer, T. (2005). STIM is a Ca2+ sensor essential for Ca2+-store-depletion-triggered Ca2+ influx. Curr Biol *15*, 1235-1241.

Liu, C., Dai, W., Bai, Y., Chi, C., Xin, Y., He, G., Mai, K., and Duan, C. (2017a). Development of a Whole Organism Platform for Phenotype-Based Analysis of IGF1R-PI3K-Akt-Tor Action. Sci Rep *7*, 1994.

Liu, C., Luan, J., Bai, Y., Li, Y., Lu, L., Liu, Y., Hakuno, F., Takahashi, S., Duan, C., and Zhou, J. (2014). Aspp2 negatively regulates body growth but not developmental timing by modulating IRS signaling in zebrafish embryos. Gen Comp Endocrinol *197*, 82-91.

Liu, C., Xin, Y., Bai, Y., Lewin, G., He, G., Mai, K., and Duan, C. (2018a). Ca2+ concentration–dependent premature death of igfbp5a−/− fish reveals a critical role of IGF signaling in adaptive epithelial growth. Sci. Signal. *11*, eaat2231.

Liu, H., Radisky, D.C., Nelson, C.M., Zhang, H., Fata, J.E., Roth, R.A., and Bissell, M.J. (2006). Mechanism of Akt1 inhibition of breast cancer cell invasion reveals a protumorigenic role for TSC2. Proc Natl Acad Sci U S A *103*, 4134-4139.

Liu, J.P., Baker, J., Perkins, A.S., Robertson, E.J., and Efstratiadis, A. (1993). Mice carrying null mutations of the genes encoding insulin-like growth factor I (Igf-1) and type 1 IGF receptor (Igf1r). Cell *75*, 59-72.

Liu, P., Gan, W., Chin, Y.R., Ogura, K., Guo, J., Zhang, J., Wang, B., Blenis, J., Cantley, L.C., Toker, A., et al. (2015). PtdIns(3,4,5)P3-Dependent Activation of the mTORC2 Kinase Complex. Cancer Discov *5*, 1194-1209.

Liu, R., Zhou, X.W., Tanila, H., Bjorkdahl, C., Wang, J.Z., Guan, Z.Z., Cao, Y., Gustafsson, J.A., Winblad, B., and Pei, J.J. (2008). Phosphorylated PP2A (tyrosine 307) is associated with Alzheimer neurofibrillary pathology. J Cell Mol Med *12*, 241-257.

Liu, S.L., Wang, Z.G., Hu, Y., Xin, Y., Singaram, I., Gorai, S., Zhou, X., Shim, Y., Min, J.H., Gong, L.W., et al. (2018b). Quantitative Lipid Imaging Reveals a New Signaling Function of Phosphatidylinositol-3,4-Bisphophate: Isoform- and Site-Specific Activation of Akt. Mol Cell *71*, 1092-1104 e1095.

Liu, Y., Elf, S.E., Miyata, Y., Sashida, G., Liu, Y., Huang, G., Di Giandomenico, S., Lee, J.M., Deblasio, A., Menendez, S., et al. (2009). p53 regulates hematopoietic stem cell quiescence. Cell Stem Cell *4*, 37-48.

Liu, Y., Tang, H., Xie, R., Li, S., Liu, X., Lin, H., Zhang, Y., and Cheng, C.H. (2017b). Genetic Evidence for Multifactorial Control of the Reproductive Axis in Zebrafish. Endocrinology *158*, 604-611.

Luchsinger, L.L., Strikoudis, A., Danzl, N.M., Bush, E.C., Finlayson, M.O., Satwani, P., Sykes, M., Yazawa, M., and Snoeck, H.W. (2019). Harnessing Hematopoietic Stem Cell Low Intracellular Calcium Improves Their Maintenance In Vitro. Cell Stem Cell *25*, 225-240 e227.

Lucic, I., Rathinaswamy, M.K., Truebestein, L., Hamelin, D.J., Burke, J.E., and Leonard, T.A. (2018). Conformational sampling of membranes by Akt controls its activation and inactivation. Proc Natl Acad Sci U S A *115*, E3940-E3949.

Ma, Z., Wen, D., Wang, X., Yang, L., Liu, T., Liu, J., Zhu, J., and Fang, X. (2016). Growth inhibition of human gastric adenocarcinoma cells in vitro by STO-609 is independent of calcium/calmodulin-dependent protein kinase kinase-beta and adenosine monophosphate-activated protein kinase. Am J Transl Res *8*, 1164-1171.

MacDougall, M.S., Clarke, R., and Merrill, B.J. (2019). Intracellular Ca(2+) Homeostasis and Nuclear Export Mediate Exit from Naive Pluripotency. Cell Stem Cell *25*, 210-224 e216.

Magenta, A., Fasanaro, P., Romani, S., Di Stefano, V., Capogrossi, M.C., and Martelli, F. (2008). Protein phosphatase 2A subunit PR70 interacts with pRb and mediates its dephosphorylation. Mol Cell Biol *28*, 873-882.

Malli, R., and Graier, W.F. (2017). The Role of Mitochondria in the Activation/Maintenance of SOCE: The Contribution of Mitochondrial Ca(2+) Uptake, Mitochondrial Motility, and Location to Store-Operated Ca(2+) Entry. Adv Exp Med Biol *993*, 297-319.

Manning, B.D., and Toker, A. (2017). AKT/PKB Signaling: Navigating the Network. Cell *169*, 381-405.

Marchi, S., Corricelli, M., Branchini, A., Vitto, V.A.M., Missiroli, S., Morciano, G., Perrone, M., Ferrarese, M., Giorgi, C., Pinotti, M., et al. (2019). Akt-mediated phosphorylation of MICU1 regulates mitochondrial Ca(2+) levels and tumor growth. EMBO J *38*.

Marchi, S., Marinello, M., Bononi, A., Bonora, M., Giorgi, C., Rimessi, A., and Pinton, P. (2012). Selective modulation of subtype III IP(3)R by Akt regulates ER Ca(2)(+) release and apoptosis. Cell Death Dis *3*, e304.

Marchi, S., Rimessi, A., Giorgi, C., Baldini, C., Ferroni, L., Rizzuto, R., and Pinton, P. (2008). Akt kinase reducing endoplasmic reticulum Ca2+ release protects cells from Ca2+-dependent apoptotic stimuli. Biochem Biophys Res Commun *375*, 501-505.

Marshall, W.S. (2011). Mechanosensitive signalling in fish gill and other ion transporting epithelia. Acta Physiol (Oxf) *202*, 487-499.

Massie, C.E., Lynch, A., Ramos-Montoya, A., Boren, J., Stark, R., Fazli, L., Warren, A., Scott, H., Madhu, B., Sharma, N., et al. (2011). The androgen receptor fuels prostate cancer by regulating central metabolism and biosynthesis. EMBO J *30*, 2719-2733.

Massoner, P., Ladurner-Rennau, M., Eder, I.E., and Klocker, H. (2010). Insulin-like growth factors and insulin control a multifunctional signalling network of significant importance in cancer. Br J Cancer *103*, 1479-1484.

Matson, J.P., and Cook, J.G. (2017). Cell cycle proliferation decisions: the impact of single cell analyses. FEBS J *284*, 362-375.

Matsumoto, A., Takeishi, S., Kanie, T., Susaki, E., Onoyama, I., Tateishi, Y., Nakayama, K., and Nakayama, K.I. (2011). p57 is required for quiescence and maintenance of adult hematopoietic stem cells. Cell Stem Cell *9*, 262-271.

Matthews, E.A., Schoch, S., and Dietrich, D. (2013). Tuning local calcium availability: cell-type-specific immobile calcium buffer capacity in hippocampal neurons. J Neurosci *33*, 14431-14445.

Maures, T., Chan, S.J., Xu, B., Sun, H., Ding, J., and Duan, C. (2002). Structural, biochemical, and expression analysis of two distinct insulin-like growth factor I receptors and their ligands in zebrafish. Endocrinology *143*, 1858-1871.

Maures, T.J., and Duan, C. (2002). Structure, developmental expression, and physiological regulation of zebrafish IGF binding protein-1. Endocrinology *143*, 2722-2731.

McCormick, S.D., Hasegawa, S., and Hirano, T. (1992). Calcium uptake in the skin of a freshwater teleost. Proc Natl Acad Sci U S A *89*, 3635-3638.

McCubrey, J.A., Steelman, L.S., Chappell, W.H., Abrams, S.L., Wong, E.W., Chang, F., Lehmann, B., Terrian, D.M., Milella, M., Tafuri, A., et al. (2007). Roles of the Raf/MEK/ERK pathway in cell growth, malignant transformation and drug resistance. Biochim Biophys Acta *1773*, 1263-1284.

McGoldrick, L.L., Singh, A.K., Saotome, K., Yelshanskaya, M.V., Twomey, E.C., Grassucci, R.A., and Sobolevsky, A.I. (2018). Opening of the human epithelial calcium channel TRPV6. Nature *553*, 233-237.

Melle, C., Ernst, G., Schimmel, B., Bleul, A., Mothes, H., Kaufmann, R., Settmacher, U., and Von Eggeling, F. (2006). Different expression of calgizzarin (S100A11) in normal colonic epithelium, adenoma and colorectal carcinoma. Int J Oncol *28*, 195-200.

Meng, D., Frank, A.R., and Jewell, J.L. (2018a). mTOR signaling in stem and progenitor cells. Development *145*.

Meng, Y., Sun, J., Yu, J., Wang, C., and Su, J. (2018b). Dietary Intakes of Calcium, Iron, Magnesium, and Potassium Elements and the Risk of Colorectal Cancer: a Meta-Analysis. Biol Trace Elem Res.

Menon, S., Dibble, C.C., Talbott, G., Hoxhaj, G., Valvezan, A.J., Takahashi, H., Cantley, L.C., and Manning, B.D. (2014). Spatial control of the TSC complex integrates insulin and nutrient regulation of mTORC1 at the lysosome. Cell *156*, 771-785.

Mignen, O., Constantin, B., Potier-Cartereau, M., Penna, A., Gautier, M., Gueguinou, M., Renaudineau, Y., Shoji, K.F., Felix, R., Bayet, E., et al. (2017). Constitutive calcium entry and cancer: updated views and insights. Eur Biophys J *46*, 395-413.

Miled, N., Yan, Y., Hon, W.C., Perisic, O., Zvelebil, M., Inbar, Y., Schneidman-Duhovny, D., Wolfson, H.J., Backer, J.M., and Williams, R.L. (2007). Mechanism of two classes of cancer mutations in the phosphoinositide 3-kinase catalytic subunit. Science *317*, 239-242.

Mita, K., Zhang, Z., Ando, Y., Toyama, T., Hamaguchi, M., Kobayashi, S., Hayashi, S., Fujii, Y., Iwase, H., and Yamashita, H. (2007). Prognostic significance of insulin-like growth factor binding protein (IGFBP)-4 and IGFBP-5 expression in breast cancer. Jpn J Clin Oncol *37*, 575-582.

Mohan, S., Nakao, Y., Honda, Y., Landale, E., Leser, U., Dony, C., Lang, K., and Baylink, D.J. (1995). Studies on the mechanisms by which insulin-like growth factor (IGF) binding protein-4 (IGFBP-4) and IGFBP-5 modulate IGF actions in bone cells. The Journal of biological chemistry *270*, 20424-20431.

Mokady, E., Schwartz, B., Shany, S., and Lamprecht, S.A. (2000). A protective role of dietary vitamin D3 in rat colon carcinogenesis. Nutr Cancer *38*, 65-73.

Molife, L.R., Yan, L., Vitfell-Rasmussen, J., Zernhelt, A.M., Sullivan, D.M., Cassier, P.A., Chen, E., Biondo, A., Tetteh, E., Siu, L.L., et al. (2014). Phase 1 trial of the oral AKT inhibitor MK-2206 plus carboplatin/paclitaxel, docetaxel, or erlotinib in patients with advanced solid tumors. J Hematol Oncol *7*, 1.

Montoro, D.T., Haber, A.L., Biton, M., Vinarsky, V., Lin, B., Birket, S.E., Yuan, F., Chen, S., Leung, H.M., Villoria, J., et al. (2018). A revised airway epithelial hierarchy includes CFTR-expressing ionocytes. Nature *560*, 319-324.

Moore, S.F., Hunter, R.W., and Hers, I. (2011). mTORC2 protein complex-mediated Akt (Protein Kinase B) Serine 473 Phosphorylation is not required for Akt1 activity in human platelets [corrected]. J Biol Chem *286*, 24553-24560.

Moreau, B., Nelson, C., and Parekh, A.B. (2006). Biphasic regulation of mitochondrial Ca2+ uptake by cytosolic Ca2+ concentration. Curr Biol *16*, 1672-1677.

Motiani, R.K., Tanwar, J., Raja, D.A., Vashisht, A., Khanna, S., Sharma, S., Srivastava, S., Sivasubbu, S., Natarajan, V.T., and Gokhale, R.S. (2018). STIM1 activation of adenylyl cyclase 6 connects Ca(2+) and cAMP signaling during melanogenesis. EMBO J *37*.

Muto, A., and Kawakami, K. (2013). Prey capture in zebrafish larvae serves as a model to study cognitive functions. Frontiers in Neural Circuits *7*, 110.

Nilius, B., and Flockerzi, V. (2014). Mammalian transient receptor potential (TRP) cation channels. Preface. Handb Exp Pharmacol *223*, v - vi.

Nilius, B., Prenen, J., Hoenderop, J.G., Vennekens, R., Hoefs, S., Weidema, A.F., Droogmans, G., and Bindels, R.J. (2002). Fast and slow inactivation kinetics of the Ca2+ channels ECaC1

and ECaC2 (TRPV5 and TRPV6). Role of the intracellular loop located between transmembrane segments 2 and 3. J Biol Chem *277*, 30852-30858.

Nilius, B., Vennekens, R., Prenen, J., Hoenderop, J.G., Bindels, R.J., and Droogmans, G. (2000). Whole-cell and single channel monovalent cation currents through the novel rabbit epithelial Ca2+ channel ECaC. J Physiol *527 Pt 2*, 239-248.

Ning, Y., Hoang, B., Schuller, A.G., Cominski, T.P., Hsu, M.S., Wood, T.L., and Pintar, J.E. (2007). Delayed mammary gland involution in mice with mutation of the insulin-like growth factor binding protein 5 gene. Endocrinology *148*, 2138-2147.

Nixon, G.F., Mignery, G.A., and Somlyo, A.V. (1994). Immunogold localization of inositol 1,4,5-trisphosphate receptors and characterization of ultrastructural features of the sarcoplasmic reticulum in phasic and tonic smooth muscle. J Muscle Res Cell Motil *15*, 682-700.

Nunez, L., Valero, R.A., Senovilla, L., Sanz-Blasco, S., Garcia-Sancho, J., and Villalobos, C. (2006). Cell proliferation depends on mitochondrial Ca2+ uptake: inhibition by salicylate. J Physiol *571*, 57-73.

O'Connor, R. (2003). Regulation of IGF-I receptor signaling in tumor cells. Horm Metab Res *35*, 771-777.

O'Gorman, D.B., Weiss, J., Hettiaratchi, A., Firth, S.M., and Scott, C.D. (2002). Insulin-like growth factor-II/mannose 6-phosphate receptor overexpression reduces growth of choriocarcinoma cells in vitro and in vivo. Endocrinology *143*, 4287-4294.

Olianas, M.C., Dedoni, S., and Onali, P. (2018). Muscarinic Acetylcholine Receptors Potentiate 5'-Adenosine Monophosphate-Activated Protein Kinase Stimulation and Glucose Uptake Triggered by Thapsigargin-Induced Store-Operated Ca(2+) Entry in Human Neuroblastoma Cells. Neurochem Res *43*, 245-258.

Otsu, K., Willard, H.F., Khanna, V.K., Zorzato, F., Green, N.M., and MacLennan, D.H. (1990). Molecular cloning of cDNA encoding the Ca2+ release channel (ryanodine receptor) of rabbit cardiac muscle sarcoplasmic reticulum. J Biol Chem *265*, 13472-13483.

Oxvig, C. (2015). The role of PAPP-A in the IGF system: location, location, location. J Cell Commun Signal *9*, 177-187.

Paik, J.H., Ding, Z., Narurkar, R., Ramkissoon, S., Muller, F., Kamoun, W.S., Chae, S.S., Zheng, H., Ying, H., Mahoney, J., et al. (2009). FoxOs cooperatively regulate diverse pathways governing neural stem cell homeostasis. Cell Stem Cell *5*, 540-553.

Palacios, J., Regadera, J., Nistal, M., and Paniagua, R. (1991). Apical mitochondria-rich cells in the human epididymis: an ultrastructural, enzymohistochemical, and immunohistochemical study. Anat Rec *231*, 82-88.

Pan, T.C., Liao, B.K., Huang, C.J., Lin, L.Y., and Hwang, P.P. (2005). Epithelial Ca(2+) channel expression and Ca(2+) uptake in developing zebrafish. Am J Physiol Regul Integr Comp Physiol *289*, R1202-1211.

Pandini, G., Frasca, F., Mineo, R., Sciacca, L., Vigneri, R., and Belfiore, A. (2002). Insulin/insulin-like growth factor I hybrid receptors have different biological characteristics depending on the insulin receptor isoform involved. J Biol Chem *277*, 39684-39695.

Pathak, T., and Trebak, M. (2018). Mitochondrial Ca(2+) signaling. Pharmacol Ther *192*, 112-123.

Payan, P., Mayer-Gostan, N., and Pang, P.K. (1981). Site of calcium uptake in the fresh water trout gill. J Exp Zool *216*, 345-347.

Peleg, S., Sellin, J.H., Wang, Y., Freeman, M.R., and Umar, S. (2010). Suppression of aberrant transient receptor potential cation channel, subfamily V, member 6 expression in hyperproliferative colonic crypts by dietary calcium. Am J Physiol Gastrointest Liver Physiol *299*, G593-601.

Peng, J.B., Chen, X.Z., Berger, U.V., Vassilev, P.M., Tsukaguchi, H., Brown, E.M., and Hediger, M.A. (1999). Molecular cloning and characterization of a channel-like transporter mediating intestinal calcium absorption. J Biol Chem *274*, 22739-22746.

Peng, J.B., Chen, X.Z., Berger, U.V., Weremowicz, S., Morton, C.C., Vassilev, P.M., Brown, E.M., and Hediger, M.A. (2000). Human calcium transport protein CaT1. Biochem Biophys Res Commun *278*, 326-332.

Peng, J.B., Zhuang, L., Berger, U.V., Adam, R.M., Williams, B.J., Brown, E.M., Hediger, M.A., and Freeman, M.R. (2001). CaT1 expression correlates with tumor grade in prostate cancer. Biochem Biophys Res Commun *282*, 729-734.

Perrotti, D., and Neviani, P. (2013). Protein phosphatase 2A: a target for anticancer therapy. Lancet Oncol *14*, e229-238.

Peterlik, M., and Cross, H.S. (2005). Vitamin D and calcium deficits predispose for multiple chronic diseases. Eur J Clin Invest *35*, 290-304.

Peterlik, M., Grant, W.B., and Cross, H.S. (2009). Calcium, vitamin D and cancer. Anticancer Res *29*, 3687-3698.

Peters, A.A., Simpson, P.T., Bassett, J.J., Lee, J.M., Da Silva, L., Reid, L.E., Song, S., Parat, M.O., Lakhani, S.R., Kenny, P.A., et al. (2012). Calcium channel TRPV6 as a potential therapeutic target in estrogen receptor-negative breast cancer. Mol Cancer Ther *11*, 2158-2168.

Plasschaert, L.W., Zilionis, R., Choo-Wing, R., Savova, V., Knehr, J., Roma, G., Klein, A.M., and Jaffe, A.B. (2018). A single-cell atlas of the airway epithelium reveals the CFTR-rich pulmonary ionocyte. Nature *560*, 377-381.

Pollak, M. (2008a). Insulin and insulin-like growth factor signalling in neoplasia. Nat Rev Cancer *8*, 915-928.

Pollak, M. (2008b). Insulin, insulin-like growth factors and neoplasia. Best Pract Res Clin Endocrinol Metab *22*, 625-638.

Powell-Braxton, L., Hollingshead, P., Warburton, C., Dowd, M., Pitts-Meek, S., Dalton, D., Gillett, N., and Stewart, T.A. (1993). IGF-I is required for normal embryonic growth in mice. Genes Dev *7*, 2609-2617.

Prevarskaya, N., Skryma, R., and Shuba, Y. (2018). Ion Channels in Cancer: Are Cancer Hallmarks Oncochannelopathies? Physiological reviews *98*, 559-621.

Racioppi, L., Lento, W., Huang, W., Arvai, S., Doan, P.L., Harris, J.R., Marcon, F., Nakaya, H.I., Liu, Y., and Chao, N. (2017). Calcium/calmodulin-dependent kinase kinase 2 regulates hematopoietic stem and progenitor cell regeneration. Cell Death Dis *8*, e3076.

Raphael, M., Lehen'kyi, V., Vandenberghe, M., Beck, B., Khalimonchyk, S., Vanden Abeele, F., Farsetti, L., Germain, E., Bokhobza, A., Mihalache, A., et al. (2014). TRPV6 calcium channel translocates to the plasma membrane via Orai1-mediated mechanism and controls cancer cell survival. Proc Natl Acad Sci U S A *111*, E3870-3879.

Ren, H., Yin, P., and Duan, C. (2008). IGFBP-5 regulates muscle cell differentiation by binding to IGF-II and switching on the IGF-II auto-regulation loop. J Cell Biol *182*, 979-991.

Rievaj, J., Pan, W., Cordat, E., and Alexander, R.T. (2013). The Na(+)/H(+) exchanger isoform 3 is required for active paracellular and transcellular Ca(2)(+) transport across murine cecum. Am J Physiol Gastrointest Liver Physiol *305*, G303-313.

Rimessi, A., Pedriali, G., Vezzani, B., Tarocco, A., Marchi, S., Wieckowski, M.R., Giorgi, C., and Pinton, P. (2019). Interorganellar calcium signaling in the regulation of cell metabolism: A cancer perspective. Semin Cell Dev Biol.

Rossi, A., Kontarakis, Z., Gerri, C., Nolte, H., Holper, S., Kruger, M., and Stainier, D.Y. (2015). Genetic compensation induced by deleterious mutations but not gene knockdowns. Nature *524*, 230-233.

Sakipov, S., Sobolevsky, A.I., and Kurnikova, M.G. (2018). Ion Permeation Mechanism in Epithelial Calcium Channel TRVP6. Sci Rep *8*, 5715.

Sancak, Y., Thoreen, C.C., Peterson, T.R., Lindquist, R.A., Kang, S.A., Spooner, E., Carr, S.A., and Sabatini, D.M. (2007). PRAS40 is an insulin-regulated inhibitor of the mTORC1 protein kinase. Mol Cell *25*, 903-915.

Santoni, G., Farfariello, V., and Amantini, C. (2011). TRPV channels in tumor growth and progression. Adv Exp Med Biol *704*, 947-967.

Saotome, K., Singh, A.K., Yelshanskaya, M.V., and Sobolevsky, A.I. (2016). Crystal structure of the epithelial calcium channel TRPV6. Nature *534*, 506-511.

Saxton, R.A., and Sabatini, D.M. (2017). mTOR Signaling in Growth, Metabolism, and Disease. Cell *169*, 361-371.

Schauberger, C.W., and Pitkin, R.M. (1979). Maternal-perinatal calcium relationships. Obstet Gynecol *53*, 74-76.

Schenck, A., Goto-Silva, L., Collinet, C., Rhinn, M., Giner, A., Habermann, B., Brand, M., and Zerial, M. (2008). The endosomal protein Appl1 mediates Akt substrate specificity and cell survival in vertebrate development. Cell *133*, 486-497.

Schlueter, P.J., Royer, T., Farah, M.H., Laser, B., Chan, S.J., Steiner, D.F., and Duan, C. (2006). Gene duplication and functional divergence of the zebrafish insulin-like growth factor 1 receptors. FASEB journal : official publication of the Federation of American Societies for Experimental Biology *20*, 1230-1232.

Schmid, C., Schlapfer, I., Gosteli-Peter, M.A., Froesch, E.R., and Zapf, J. (1996). Effects and fate of human IGF-binding protein-5 in rat osteoblast cultures. Am J Physiol *271*, E1029-1035.

Schmitt, J.M., Smith, S., Hart, B., and Fletcher, L. (2012). CaM kinase control of AKT and LNCaP cell survival. J Cell Biochem *113*, 1514-1526.

Schneider, M.R., Zhou, R., Hoeflich, A., Krebs, O., Schmidt, J., Mohan, S., Wolf, E., and Lahm, H. (2001). Insulin-like growth factor-binding protein-5 inhibits growth and induces differentiation of mouse osteosarcoma cells. Biochem Biophys Res Commun *288*, 435-442.

Schwarz, E.C., Kummerow, C., Wenning, A.S., Wagner, K., Sappok, A., Waggershauser, K., Griesemer, D., Strauss, B., Wolfs, M.J., Quintana, A., et al. (2007). Calcium dependence of T cell proliferation following focal stimulation. Eur J Immunol *37*, 2723-2733.

Schwindling, C., Quintana, A., Krause, E., and Hoth, M. (2010). Mitochondria positioning controls local calcium influx in T cells. J Immunol *184*, 184-190.

Scott, J.W., Park, E., Rodriguiz, R.M., Oakhill, J.S., Issa, S.M., O'Brien, M.T., Dite, T.A., Langendorf, C.G., Wetsel, W.C., Means, A.R., et al. (2015). Autophosphorylation of CaMKK2 generates autonomous activity that is disrupted by a T85S mutation linked to anxiety and bipolar disorder. Sci Rep *5*, 14436.

Seshacharyulu, P., Pandey, P., Datta, K., and Batra, S.K. (2013). Phosphatase: PP2A structural importance, regulation and its aberrant expression in cancer. Cancer Lett *335*, 9-18.

Shao, Y., Guan, Y., Wang, L., Qiu, Z., Liu, M., Chen, Y., Wu, L., Li, Y., Ma, X., Liu, M., et al. (2014). CRISPR/Cas-mediated genome editing in the rat via direct injection of one-cell embryos. Nat Protoc *9*, 2493-2512.

Shim, J., Mukherjee, T., and Banerjee, U. (2012). Direct sensing of systemic and nutritional signals by haematopoietic progenitors in Drosophila. Nat Cell Biol *14*, 394-400.

Short, A.D., Klein, M.G., Schneider, M.F., and Gill, D.L. (1993). Inositol 1,4,5-trisphosphate-mediated quantal Ca2+ release measured by high resolution imaging of Ca2+ within organelles. J Biol Chem *268*, 25887-25893.

Shuch, B., Vourganti, S., Friend, J.C., Zehngebot, L.M., Linehan, W.M., and Srinivasan, R. (2012). Targeting the mTOR pathway in Chromophobe Kidney Cancer. J Cancer *3*, 152-157.

Shull, G.E. (2000). Gene knockout studies of Ca2+-transporting ATPases. Eur J Biochem *267*, 5284-5290.

Siddle, K. (2012). Molecular basis of signaling specificity of insulin and IGF receptors: neglected corners and recent advances. Front Endocrinol (Lausanne) *3*, 34.

Siddle, K., Urso, B., Niesler, C.A., Cope, D.L., Molina, L., Surinya, K.H., and Soos, M.A. (2001). Specificity in ligand binding and intracellular signalling by insulin and insulin-like growth factor receptors. Biochem Soc Trans *29*, 513-525.

Siegemund, S., Rigaud, S., Conche, C., Broaten, B., Schaffer, L., Westernberg, L., Head, S.R., and Sauer, K. (2015). IP3 3-kinase B controls hematopoietic stem cell homeostasis and prevents lethal hematopoietic failure in mice. Blood *125*, 2786-2797.

Siess, K.M., and Leonard, T.A. (2019). Lipid-dependent Akt-ivity: where, when, and how. Biochem Soc Trans *47*, 897-908.

Singh, A.K., McGoldrick, L.L., Twomey, E.C., and Sobolevsky, A.I. (2018a). Mechanism of calmodulin inactivation of the calcium-selective TRP channel TRPV6. Sci Adv *4*, eaau6088.

Singh, A.K., Saotome, K., McGoldrick, L.L., and Sobolevsky, A.I. (2018b). Structural bases of TRP channel TRPV6 allosteric modulation by 2-APB. Nat Commun *9*, 2465.

Skrzypski, M., Kolodziejski, P.A., Mergler, S., Khajavi, N., Nowak, K.W., and Strowski, M.Z. (2016a). TRPV6 modulates proliferation of human pancreatic neuroendocrine BON-1 tumour cells. Biosci Rep *36*.

Skrzypski, M., Kołodziejski, P.A., Mergler, S., Khajavi, N., Nowak, K.W., and Strowski, Mathias Z. (2016b). TRPV6 modulates proliferation of human pancreatic neuroendocrine BON-1 tumour cells. Bioscience Reports *36*, e00372.

Sobradillo, D., Hernandez-Morales, M., Ubierna, D., Moyer, M.P., Nunez, L., and Villalobos, C. (2014). A reciprocal shift in transient receptor potential channel 1 (TRPC1) and stromal interaction molecule 2 (STIM2) contributes to Ca2+ remodeling and cancer hallmarks in colorectal carcinoma cells. J Biol Chem *289*, 28765-28782.

Sood, A., McClain, D., Maitra, R., Basu-Mallick, A., Seetharam, R., Kaubisch, A., Rajdev, L., Mariadason, J.M., Tanaka, K., and Goel, S. (2012). PTEN gene expression and mutations in the PIK3CA gene as predictors of clinical benefit to anti-epidermal growth factor receptor antibody therapy in patients with KRAS wild-type metastatic colorectal cancer. Clinical colorectal cancer *11*, 143-150.

Sooy, K., Kohut, J., and Christakos, S. (2000). The role of calbindin and 1,25dihydroxyvitamin D3 in the kidney. Curr Opin Nephrol Hypertens *9*, 341-347.

Sousa-Nunes, R., Yee, L.L., and Gould, A.P. (2011). Fat cells reactivate quiescent neuroblasts via TOR and glial insulin relays in Drosophila. Nature *471*, 508-512.

Spencer, S.L., Cappell, S.D., Tsai, F.C., Overton, K.W., Wang, C.L., and Meyer, T. (2013). The proliferation-quiescence decision is controlled by a bifurcation in CDK2 activity at mitotic exit. Cell *155*, 369-383.

Sprekeler, N., Kowalewski, M.P., and Boos, A. (2012). TRPV6 and Calbindin-D9k-expression and localization in the bovine uterus and placenta during pregnancy. Reprod Biol Endocrinol *10*, 66.

Steele-Perkins, G., Turner, J., Edman, J.C., Hari, J., Pierce, S.B., Stover, C., Rutter, W.J., and Roth, R.A. (1988). Expression and characterization of a functional human insulin-like growth factor I receptor. J Biol Chem *263*, 11486-11492.

Storkel, S., Steart, P.V., Drenckhahn, D., and Thoenes, W. (1989). The human chromophobe cell renal carcinoma: its probable relation to intercalated cells of the collecting duct. Virchows Arch B Cell Pathol Incl Mol Pathol *56*, 237-245.

Sugiyama, M.G., Fairn, G.D., and Antonescu, C.N. (2019). Akt-ing Up Just About Everywhere: Compartment-Specific Akt Activation and Function in Receptor Tyrosine Kinase Signaling. Front Cell Dev Biol *7*, 70.

Sun, D., and Buttitta, L. (2015). Protein phosphatase 2A promotes the transition to G0 during terminal differentiation in Drosophila. Development *142*, 3033-3045.

Sun, D., and Buttitta, L. (2017). States of G0 and the proliferation-quiescence decision in cells, tissues and during development. Int J Dev Biol *61*, 357-366.

Suzuki, J., Kanemaru, K., Ishii, K., Ohkura, M., Okubo, Y., and Iino, M. (2014). Imaging intraorganellar Ca2+ at subcellular resolution using CEPIA. Nat Commun *5*, 4153.

Suzuki, Y., Chitayat, D., Sawada, H., Deardorff, M.A., McLaughlin, H.M., Begtrup, A., Millar, K., Harrington, J., Chong, K., Roifman, M., et al. (2018). TRPV6 Variants Interfere with Maternal-Fetal Calcium Transport through the Placenta and Cause Transient Neonatal Hyperparathyroidism. Am J Hum Genet *102*, 1104-1114.

Swulius, M.T., and Waxham, M.N. (2008). Ca(2+)/calmodulin-dependent protein kinases. Cell Mol Life Sci *65*, 2637-2657.

Tang, H., Liu, Y., Luo, D., Ogawa, S., Yin, Y., Li, S., Zhang, Y., Hu, W., Parhar, I.S., Lin, H., et al. (2015). The kiss/kissr systems are dispensable for zebrafish reproduction: evidence from gene knockout studies. Endocrinology *156*, 589-599.

Taylor, C.W., and Machaca, K. (2018). IP3 receptors and store-operated Ca(2+) entry: a license to fill. Curr Opin Cell Biol *57*, 1-7.

Thillaiappan, N.B., Chavda, A.P., Tovey, S.C., Prole, D.L., and Taylor, C.W. (2017). Ca(2+) signals initiate at immobile IP3 receptors adjacent to ER-plasma membrane junctions. Nat Commun *8*, 1505.

Thoppil, R.J., Adapala, R.K., Cappelli, H.C., Kondeti, V., Dudley, A.C., Gary Meszaros, J., Paruchuri, S., and Thodeti, C.K. (2015). TRPV4 channel activation selectively inhibits tumor endothelial cell proliferation. Sci Rep *5*, 14257.

Thorpe, L.M., Yuzugullu, H., and Zhao, J.J. (2015). PI3K in cancer: divergent roles of isoforms, modes of activation and therapeutic targeting. Nat Rev Cancer *15*, 7-24.

Tokumitsu, H., Iwabu, M., Ishikawa, Y., and Kobayashi, R. (2001). Differential regulatory mechanism of Ca2+/calmodulin-dependent protein kinase kinase isoforms. Biochemistry *40*, 13925-13932.

Tokumitsu, H., and Soderling, T.R. (1996). Requirements for calcium and calmodulin in the calmodulin kinase activation cascade. J Biol Chem *271*, 5617-5622.

Tripathi, G., Salih, D.A., Drozd, A.C., Cosgrove, R.A., Cobb, L.J., and Pell, J.M. (2009). IGF-independent effects of insulin-like growth factor binding protein-5 (Igfbp5) in vivo. FASEB J *23*, 2616-2626.

Tseng, D.Y., Chou, M.Y., Tseng, Y.C., Hsiao, C.D., Huang, C.J., Kaneko, T., and Hwang, P.P. (2009). Effects of stanniocalcin 1 on calcium uptake in zebrafish (Danio rerio) embryo. Am J Physiol Regul Integr Comp Physiol *296*, R549-557.

Tu, C.L., Oda, Y., Komuves, L., and Bikle, D.D. (2004). The role of the calcium-sensing receptor in epidermal differentiation. Cell Calcium *35*, 265-273.

Twigg, S.M., and Baxter, R.C. (1998). Insulin-like growth factor (IGF)-binding protein 5 forms an alternative ternary complex with IGFs and the acid-labile subunit. J Biol Chem *273*, 6074-6079.

Ueki, I., Ooi, G.T., Tremblay, M.L., Hurst, K.R., Bach, L.A., and Boisclair, Y.R. (2000). Inactivation of the acid labile subunit gene in mice results in mild retardation of postnatal growth

despite profound disruptions in the circulating insulin-like growth factor system. Proc Natl Acad Sci U S A *97*, 6868-6873.

Ullrich, A., Gray, A., Tam, A.W., Yang-Feng, T., Tsubokawa, M., Collins, C., Henzel, W., Le Bon, T., Kathuria, S., Chen, E., et al. (1986). Insulin-like growth factor I receptor primary structure: comparison with insulin receptor suggests structural determinants that define functional specificity. EMBO J *5*, 2503-2512.

Vadas, O., Burke, J.E., Zhang, X., Berndt, A., and Williams, R.L. (2011). Structural basis for activation and inhibition of class I phosphoinositide 3-kinases. Sci Signal *4*, re2.

Vadas, O., Dbouk, H.A., Shymanets, A., Perisic, O., Burke, J.E., Abi Saab, W.F., Khalil, B.D., Harteneck, C., Bresnick, A.R., Nurnberg, B., et al. (2013). Molecular determinants of PI3Kgamma-mediated activation downstream of G-protein-coupled receptors (GPCRs). Proc Natl Acad Sci U S A *110*, 18862-18867.

Valcourt, J.R., Lemons, J.M., Haley, E.M., Kojima, M., Demuren, O.O., and Coller, H.A. (2012). Staying alive: metabolic adaptations to quiescence. Cell Cycle *11*, 1680-1696.

Valero, R.A., Senovilla, L., Nunez, L., and Villalobos, C. (2008). The role of mitochondrial potential in control of calcium signals involved in cell proliferation. Cell Calcium *44*, 259-269.

van de Graaf, S.F., Hoenderop, J.G., Gkika, D., Lamers, D., Prenen, J., Rescher, U., Gerke, V., Staub, O., Nilius, B., and Bindels, R.J. (2003). Functional expression of the epithelial Ca(2+) channels (TRPV5 and TRPV6) requires association of the S100A10-annexin 2 complex. EMBO J *22*, 1478-1487.

Van der Eerden, B.C., Weissgerber, P., Fratzl-Zelman, N., Olausson, J., Hoenderop, J.G., Schreuders-Koedam, M., Eijken, M., Roschger, P., De Vries, T.J., and Chiba, H. (2012). The transient receptor potential channel TRPV6 is dynamically expressed in bone cells but is not crucial for bone mineralization in mice. Journal of cellular physiology *227*, 1951-1959.

van der Flier, L.G., and Clevers, H. (2009). Stem cells, self-renewal, and differentiation in the intestinal epithelium. Annu Rev Physiol *71*, 241-260.

Vander Haar, E., Lee, S.I., Bandhakavi, S., Griffin, T.J., and Kim, D.H. (2007). Insulin signalling to mTOR mediated by the Akt/PKB substrate PRAS40. Nat Cell Biol *9*, 316-323.

Vanoevelen, J., Janssens, A., Huitema, L.F., Hammond, C.L., Metz, J.R., Flik, G., Voets, T., and Schulte-Merker, S. (2011). Trpv5/6 is vital for epithelial calcium uptake and bone formation. FASEB J *25*, 3197-3207.

Varghese, E., Samuel, S.M., Sadiq, Z., Kubatka, P., Liskova, A., Benacka, J., Pazinka, P., Kruzliak, P., and Busselberg, D. (2019). Anti-Cancer Agents in Proliferation and Cell Death: The Calcium Connection. Int J Mol Sci *20*.

Vassiliadis, J., Bracken, C., Matthews, D., O'Brien, S., Schiavi, S., and Wawersik, S. (2011). Calcium mediates glomerular filtration through calcineurin and mTORC2/Akt signaling. J Am Soc Nephrol *22*, 1453-1461.

Venkatachalam, K., and Montell, C. (2007). TRP channels. Annu Rev Biochem *76*, 387-417.

Venkatraman, A., He, X.C., Thorvaldsen, J.L., Sugimura, R., Perry, J.M., Tao, F., Zhao, M., Christenson, M.K., Sanchez, R., and Jaclyn, Y.Y. (2013a). Maternal imprinting at the H19–Igf2 locus maintains adult haematopoietic stem cell quiescence. Nature *500*, 345.

Venkatraman, A., He, X.C., Thorvaldsen, J.L., Sugimura, R., Perry, J.M., Tao, F., Zhao, M., Christenson, M.K., Sanchez, R., Yu, J.Y., et al. (2013b). Maternal imprinting at the H19-Igf2 locus maintains adult haematopoietic stem cell quiescence. Nature *500*, 345-349.

Vennekens, R., Hoenderop, J.G., Prenen, J., Stuiver, M., Willems, P.H., Droogmans, G., Nilius, B., and Bindels, R.J. (2000). Permeation and gating properties of the novel epithelial Ca(2+) channel. J Biol Chem *275*, 3963-3969.

Villalobos, C., Nunez, L., Chamero, P., Alonso, M.T., and Garcia-Sancho, J. (2001). Mitochondrial [Ca(2+)] oscillations driven by local high [Ca(2+)] domains generated by spontaneous electric activity. J Biol Chem *276*, 40293-40297.

Virshup, D.M., and Shenolikar, S. (2009). From promiscuity to precision: protein phosphatases get a makeover. Mol Cell *33*, 537-545.

Voets, T., Janssens, A., Droogmans, G., and Nilius, B. (2004). Outer pore architecture of a Ca2+-selective TRP channel. J Biol Chem *279*, 15223-15230.

Vogetseder, A., Palan, T., Bacic, D., Kaissling, B., and Le Hir, M. (2007). Proximal tubular epithelial cells are generated by division of differentiated cells in the healthy kidney. Am J Physiol Cell Physiol *292*, C807-813.

Vogetseder, A., Picard, N., Gaspert, A., Walch, M., Kaissling, B., and Le Hir, M. (2008). Proliferation capacity of the renal proximal tubule involves the bulk of differentiated epithelial cells. Am J Physiol Cell Physiol *294*, C22-28.

Volkers, M., Dolatabadi, N., Gude, N., Most, P., Sussman, M.A., and Hassel, D. (2012). Orai1 deficiency leads to heart failure and skeletal myopathy in zebrafish. J Cell Sci *125*, 287-294.

Wacquier, B., Combettes, L., and Dupont, G. (2019). Cytoplasmic and Mitochondrial Calcium Signaling: A Two-Way Relationship. Cold Spring Harb Perspect Biol *11*.

Wagner, G.F., Guiraudon, C.C., Milliken, C., and Copp, D.H. (1995). Immunological and biological evidence for a stanniocalcin-like hormone in human kidney. Proc Natl Acad Sci U S A *92*, 1871-1875.

Wagner, G.F., Hampong, M., Park, C.M., and Copp, D.H. (1986). Purification, characterization, and bioassay of teleocalcin, a glycoprotein from salmon corpuscles of Stannius. Gen Comp Endocrinol *63*, 481-491.

Wallace, A.M., Hardigan, A., Geraghty, P., Salim, S., Gaffney, A., Thankachen, J., Arellanos, L., D'Armiento, J.M., and Foronjy, R.F. (2012). Protein phosphatase 2A regulates innate immune and proteolytic responses to cigarette smoke exposure in the lung. Toxicol Sci *126*, 589-599.

Wang, G., Zhu, H., Situ, C., Han, L., Yu, Y., Cheung, T.H., Liu, K., and Wu, Z. (2018a). p110alpha of PI3K is necessary and sufficient for quiescence exit in adult muscle satellite cells. EMBO J *37*.

Wang, H., Arun, B.K., Wang, H., Fuller, G.N., Zhang, W., Middleton, L.P., and Sahin, A.A. (2008). IGFBP2 and IGFBP5 overexpression correlates with the lymph node metastasis in T1 breast carcinomas. Breast J *14*, 261-267.

Wang, J., Zhao, W., Guo, H., Fang, Y., Stockman, S.E., Bai, S., Ng, P.K., Li, Y., Yu, Q., Lu, Y., et al. (2018b). AKT isoform-specific expression and activation across cancer lineages. BMC Cancer *18*, 742.

Wang, J.Y., Sun, J., Huang, M.Y., Wang, Y.S., Hou, M.F., Sun, Y., He, H., Krishna, N., Chiu, S.J., Lin, S., et al. (2015a). STIM1 overexpression promotes colorectal cancer progression, cell motility and COX-2 expression. Oncogene *34*, 4358-4367.

Wang, N., Yao, M., Xu, J., Quan, Y., Zhang, K., Yang, R., and Gao, W.Q. (2015b). Autocrine Activation of CHRM3 Promotes Prostate Cancer Growth and Castration Resistance via CaM/CaMKK-Mediated Phosphorylation of Akt. Clin Cancer Res *21*, 4676-4685.

Wang, Y.F., Tseng, Y.C., Yan, J.J., Hiroi, J., and Hwang, P.P. (2009). Role of SLC12A10.2, a Na-Cl cotransporter-like protein, in a Cl uptake mechanism in zebrafish (Danio rerio). Am J Physiol Regul Integr Comp Physiol *296*, R1650-1660.

Wasilewska, I., Gupta, R.K., Palchevska, O., and Kuznicki, J. (2019). Identification of Zebrafish Calcium Toolkit Genes and their Expression in the Brain. Genes (Basel) *10*.

Wayman, G.A., Tokumitsu, H., Davare, M.A., and Soderling, T.R. (2011). Analysis of CaM-kinase signaling in cells. Cell Calcium *50*, 1-8.

Weissgerber, P., Kriebs, U., Tsvilovskyy, V., Olausson, J., Kretz, O., Stoerger, C., Mannebach, S., Wissenbach, U., Vennekens, R., Middendorff, R., et al. (2012). Excision of Trpv6 gene leads to severe defects in epididymal Ca2+ absorption and male fertility much like single D541A pore mutation. J Biol Chem *287*, 17930-17941.

Weissgerber, P., Kriebs, U., Tsvilovskyy, V., Olausson, J., Kretz, O., Stoerger, C., Vennekens, R., Wissenbach, U., Middendorff, R., Flockerzi, V., et al. (2011). Male fertility depends on Ca(2)+ absorption by TRPV6 in epididymal epithelia. Sci Signal *4*, ra27.

Welsh-Bacic, D., Nowik, M., Kaissling, B., and Wagner, C.A. (2011). Proliferation of acid-secretory cells in the kidney during adaptive remodelling of the collecting duct. PLoS One *6*, e25240.

Weroha, S.J., and Haluska, P. (2012). The insulin-like growth factor system in cancer. Endocrinol Metab Clin North Am *41*, 335-350, vi.

Westerfield, M. (2000a). The zebrafish book: a guide for the laboratory use of zebrafish. http://zfin. org/zf_info/zfbook/zfbk. html.

Westerfield, M. (2000b). The zebrafish book. A guide for the laboratory use of zebrafish (Danio rerio). (Eugene: Univ. of Oregon Press).

Wetterau, L.A., Moore, M.G., Lee, K.W., Shim, M.L., and Cohen, P. (1999). Novel aspects of the insulin-like growth factor binding proteins. Mol Genet Metab *68*, 161-181.

Wissenbach, U., Niemeyer, B.A., Fixemer, T., Schneidewind, A., Trost, C., Cavalie, A., Reus, K., Meese, E., Bonkhoff, H., and Flockerzi, V. (2001). Expression of CaT-like, a novel calcium-

selective channel, correlates with the malignancy of prostate cancer. J Biol Chem *276*, 19461-19468.

Witczak, C.A., Fujii, N., Hirshman, M.F., and Goodyear, L.J. (2007). Ca2+/calmodulin-dependent protein kinase kinase-alpha regulates skeletal muscle glucose uptake independent of AMP-activated protein kinase and Akt activation. Diabetes *56*, 1403-1409.

Wood, T.L., Rogler, L.E., Czick, M.E., Schuller, A.G., and Pintar, J.E. (2000). Selective alterations in organ sizes in mice with a targeted disruption of the insulin-like growth factor binding protein-2 gene. Mol Endocrinol *14*, 1472-1482.

Woudenberg-Vrenken, T.E., Lameris, A.L., Weissgerber, P., Olausson, J., Flockerzi, V., Bindels, R.J., Freichel, M., and Hoenderop, J.G. (2012). Functional TRPV6 channels are crucial for transepithelial Ca2+ absorption. Am J Physiol Gastrointest Liver Physiol *303*, G879-885.

Wu, J., Prole, D.L., Shen, Y., Lin, Z., Gnanasekaran, A., Liu, Y., Chen, L., Zhou, H., Chen, S.R., Usachev, Y.M., et al. (2014). Red fluorescent genetically encoded Ca2+ indicators for use in mitochondria and endoplasmic reticulum. Biochem J *464*, 13-22.

Xin, Y., and Duan, C. (2018). Microinjection of Antisense Morpholinos, CRISPR/Cas9 RNP, and RNA/DNA into Zebrafish Embryos. In Hypoxia: Methods and Protocols. L.E. Huang, ed. (New York, NY: Springer New York), pp. 205-211.

Xin, Y., Malick, A., Hu, M., Liu, C., Batah, H., Xu, H., and Duan, C. (2019). Cell-autonomous regulation of epithelial cell quiescence by calcium channel Trpv6. Elife *8*.

Xu, K., Chen, G., Li, X., Wu, X., Chang, Z., Xu, J., Zhu, Y., Yin, P., Liang, X., and Dong, L. (2017). MFN2 suppresses cancer progression through inhibition of mTORC2/Akt signaling. Sci Rep *7*, 41718.

Xu, Q., Li, S., Zhao, Y., Maures, T.J., Yin, P., and Duan, C. (2004). Evidence that IGF binding protein-5 functions as a ligand-independent transcriptional regulator in vascular smooth muscle cells. Circ Res *94*, E46-54.

Xue, H., Wang, Y., MacCormack, T.J., Lutes, T., Rice, C., Davey, M., Dugourd, D., Ilenchuk, T.T., and Stewart, J.M. (2018). Inhibition of Transient Receptor Potential Vanilloid 6 channel, elevated in human ovarian cancers, reduces tumour growth in a xenograft model. J Cancer *9*, 3196-3207.

Yamashita, S., Mizumoto, H., Sawada, H., Suzuki, Y., and Hata, D. (2019). TRPV6 Gene Mutation in a Dizygous Twin With Transient Neonatal Hyperparathyroidism. J Endocr Soc *3*, 602-606.

Yan, J.-J., and Hwang, P.-P. (2019a). Novel Discoveries in Acid-base Regulation and Osmoregulation: A Review of Selected Hormonal Actions in Zebrafish and Medaka. General and comparative endocrinology.

Yan, J.J., and Hwang, P.P. (2019b). Novel discoveries in acid-base regulation and osmoregulation: A review of selected hormonal actions in zebrafish and medaka. Gen Comp Endocrinol *277*, 20-29.

Yang, K., Shrestha, S., Zeng, H., Karmaus, P.W., Neale, G., Vogel, P., Guertin, D.A., Lamb, R.F., and Chi, H. (2013). T cell exit from quiescence and differentiation into Th2 cells depend on Raptor-mTORC1-mediated metabolic reprogramming. Immunity *39*, 1043-1056.

Yang, S., Zhang, J.J., and Huang, X.Y. (2009). Orai1 and STIM1 are critical for breast tumor cell migration and metastasis. Cancer Cell *15*, 124-134.

Yano, S., Tokumitsu, H., and Soderling, T.R. (1998). Calcium promotes cell survival through CaM-K kinase activation of the protein-kinase-B pathway. Nature *396*, 584-587.

Yao, G. (2014). Modelling mammalian cellular quiescence. Interface Focus *4*, 20130074.

Yao, G., Lee, T.J., Mori, S., Nevins, J.R., and You, L. (2008). A bistable Rb-E2F switch underlies the restriction point. Nat Cell Biol *10*, 476-482.

Yap, T.A., Yan, L., Patnaik, A., Fearen, I., Olmos, D., Papadopoulos, K., Baird, R.D., Delgado, L., Taylor, A., Lupinacci, L., et al. (2011). First-in-man clinical trial of the oral pan-AKT inhibitor MK-2206 in patients with advanced solid tumors. J Clin Oncol *29*, 4688-4695.

Yeromin, A.V., Zhang, S.L., Jiang, W., Yu, Y., Safrina, O., and Cahalan, M.D. (2006). Molecular identification of the CRAC channel by altered ion selectivity in a mutant of Orai. Nature *443*, 226-229.

Yi, S., Cui, C., Huang, X., Yin, X., Li, Y., Wen, J., and Luan, Q. (2019). MFN2 silencing promotes neural differentiation of embryonic stem cells via the Akt signaling pathway. J Cell Physiol.

Yin, P., Xu, Q., and Duan, C. (2004). Paradoxical actions of endogenous and exogenous insulin-like growth factor-binding protein-5 revealed by RNA interference analysis. The Journal of biological chemistry *279*, 32660-32666.

Yue, L., Peng, J.B., Hediger, M.A., and Clapham, D.E. (2001). CaT1 manifests the pore properties of the calcium-release-activated calcium channel. Nature *410*, 705-709.

Yumoto, N., Yu, X., and Hatakeyama, M. (2006). Expression of the ErbB4 receptor causes reversal regulation of PP2A in the Shc signal transduction pathway in human cancer cells. Mol Cell Biochem *285*, 165-171.

Yurimoto, S., Fujimoto, T., Magari, M., Kanayama, N., Kobayashi, R., and Tokumitsu, H. (2012). In vitro substrate phosphorylation by Ca(2)(+)/calmodulin-dependent protein kinase kinase using guanosine-5'-triphosphate as a phosphate donor. BMC Biochem *13*, 27.

Zhang, C., Lu, L., Li, Y., Wang, X., Zhou, J., Liu, Y., Fu, P., Gallicchio, M.A., Bach, L.A., and Duan, C. (2012). IGF binding protein-6 expression in vascular endothelial cells is induced by hypoxia and plays a negative role in tumor angiogenesis. Int J Cancer *130*, 2003-2012.

Zhang, L., Zhou, W., Velculescu, V.E., Kern, S.E., Hruban, R.H., Hamilton, S.R., Vogelstein, B., and Kinzler, K.W. (1997). Gene expression profiles in normal and cancer cells. Science *276*, 1268-1272.

Zhang, P., Bai, Y., Lu, L., Li, Y., and Duan, C. (2016). An oxygen-insensitive Hif-3alpha isoform inhibits Wnt signaling by destabilizing the nuclear beta-catenin complex. Elife *5*.

Zhang, Y., Zhang, T., Wu, C., Xia, Q., and Xu, D. (2017). ASIC1a mediates the drug resistance of human hepatocellular carcinoma via the Ca(2+)/PI3-kinase/AKT signaling pathway. Lab Invest *97*, 53-69.

Zhao, M., Song, B., Pu, J., Wada, T., Reid, B., Tai, G., Wang, F., Guo, A., Walczysko, P., Gu, Y., et al. (2006a). Electrical signals control wound healing through phosphatidylinositol-3-OH kinase-gamma and PTEN. Nature *442*, 457-460.

Zhao, Y., Yin, P., Bach, L.A., and Duan, C. (2006b). Several acidic amino acids in the N-domain of insulin-like growth factor-binding protein-5 are important for its transactivation activity. J Biol Chem *281*, 14184-14191.

Zheng, B., Clarke, J.B., Busby, W.H., Duan, C., and Clemmons, D.R. (1998a). Insulin-like growth factor-binding protein-5 is cleaved by physiological concentrations of thrombin. Endocrinology *139*, 1708-1714.

Zheng, B., Duan, C., and Clemmons, D.R. (1998b). The effect of extracellular matrix proteins on porcine smooth muscle cell insulin-like growth factor (IGF) binding protein-5 synthesis and responsiveness to IGF-I. J Biol Chem *273*, 8994-9000.

Zhong, Y., Lu, L., Zhou, J., Li, Y., Liu, Y., Clemmons, D.R., and Duan, C. (2011). IGF binding protein 3 exerts its ligand-independent action by antagonizing BMP in zebrafish embryos. Journal of cell science *124*, 1925-1935.

Zhu, X., Xu, Y., Yu, S., Lu, L., Ding, M., Cheng, J., Song, G., Gao, X., Yao, L., Fan, D., et al. (2014). An efficient genotyping method for genome-modified animals and human cells generated with CRISPR/Cas9 system. Scientific reports *4*, 6420.

Zhuang, L., Peng, J.B., Tou, L., Takanaga, H., Adam, R.M., Hediger, M.A., and Freeman, M.R. (2002). Calcium-selective ion channel, CaT1, is apically localized in gastrointestinal tract epithelia and is aberrantly expressed in human malignancies. Lab Invest *82*, 1755-1764.

Ziegler, A.N., Feng, Q., Chidambaram, S., Testai, J.M., Kumari, E., Rothbard, D.E., Constancia, M., Sandovici, I., Cominski, T., and Pang, K. (2019). Insulin-like Growth Factor II: An Essential Adult Stem Cell Niche Constituent in Brain and Intestine. Stem cell reports.

Ziegler, A.N., Levison, S.W., and Wood, T.L. (2015). Insulin and IGF receptor signalling in neural-stem-cell homeostasis. Nature Reviews Endocrinology *11*, 161.

Zimmer, D.B., Wright Sadosky, P., and Weber, D.J. (2003). Molecular mechanisms of S100-target protein interactions. Microsc Res Tech *60*, 552-559.

Zou, S., Kamei, H., Modi, Z., and Duan, C. (2009). Zebrafish IGF genes: gene duplication, conservation and divergence, and novel roles in midline and notochord development. PloS one *4*, e7026.